# Palaeoclimate reconstruction of the last 200 ka in south-eastern Spain, based on proxies of speleothems from Cueva Victoria

Dissertation
zur Erlangung des akademischen Grades
„Doktor der Naturwissenschaften“
im Promotionsfach Geologie/Paläontologie

Fachbereich 09 für Chemie, Pharmazie und Geowissenschaften
Institut für Geowissenschaften
Johannes Gutenberg-Universität, Mainz

Alexander Budsky
geb. in Weinheim

Mainz, 2019

Dekan: [redacted]
1. Berichterstatter: Prof. Dr. Denis Scholz
2. Berichterstatter: [redacted]

# Eidesstattliche Erklärung

Ich versichere hiermit die vorliegende Arbeit eigenständig und nur mit den angegebenen Hilfsmitteln und Quellen verfasst zu haben. Die Dissertation ist weder komplett noch in Teilen an einer anderen Universität oder Fakultät als wissenschaftliche Arbeit oder zu einer Prüfung vorgelegt worden.

Mainz, den: _____ _____

(Alexander Budsky)

## Zusammenfassung

In den letzten Jahrzehnten haben sich Speläotheme zu einem wichtigen terrestrischen Paläoklimaarchiv etabliert. Durch hochpräzise Uran-Ungleichgewichtsdatierungen ist es möglich, akkurate und unabhängige Alters-Tiefenmodelle zu erstellen. Mit der Kombination von der Datierungsmethode und einer hohen räumlichen Auflösung von Proxy-Messungen sind Speläotheme ein wichtiges Paläoklimaarchiv mit hoher zeitlicher Auflösung. Die Proxys, z.B. stabile Isotope ($\delta^{13}$C, $\delta^{18}$O) und Spurenelemente, lassen Rückschlüsse auf Veränderungen des vergangenen Klimas, der Vegetation, sowie des Bodens zu.

Einen großen Vorteil der Speläotheme gegenüber anderen Klimaarchiven bietet die $^{230}$Th/U-Datierung mittels Multikollektor-Massenspektrometrie mit induktiv gekoppeltem Plasma (MC-ICP-MS) an. Diese Methode der präzisen Altersdatierung wurde für die Speläotheme aus der Cueva Victoria angewandt. Zusätzlich wurden Proben für die Kohlenstoff- und Sauerstoffisotopenmessungen ($\delta^{13}$C, $\delta^{18}$O) gebohrt und mit einem Isotopenverhältnis Massenspektrometer (IRMS) gemessen. Spurenelemente wurden mit der Laser Ablation (LA)-ICP-MS in hoher räumlichen Auflösung gemessen.

Paläoklimaarchive aus Südost-Spanien, einer der trockensten Regionen Europas, fehlen bisher, obwohl sie wichtige neue Informationen über hydrologische Veränderungen zwischen Warm- und Kaltzeiten liefern können. Die $^{230}$Th/U-Datierungen der Speläotheme aus der Cueva Victoria zeigen ein bevorzugtes Wachstum während der Warmzeiten, dies deutet auf humide Bedingungen während höherer Temperaturen hin. Die $\delta^{18}$O-Werte spiegeln Temperatur, Mengeneffekt des Niederschlags und die Isotopie der Ozeane als Quelle des Niederschlages wider. Die $\delta^{13}$C-Werte hingegen, geben Aufschluss über die Vegetation, sowie der mikrobiologischen Bodenaktivität über der Höhle, welche in der Regel mit den Warmzeiten zunimmt und ebenfalls auf humidere Bedingungen hinweist. Eine Ausnahme bildet ein Abschnitt im Holozän (9.7 - 7.8 ka) in dem, übereinstimmend mit anderen mediterranen Klimaarchiven, positivere $\delta^{13}$C-Werte eine Reduktion der Vegetation durch eine erhöhte Saisonalität mit verlängerter und intensiver Trockenperiode im Frühling und Sommer aufzeigen.

Ausgehend von der letzten Warmzeit gab es in den Marinen Isotopenstadien 5 bis 3 eine starke Temperaturvariabilität auf der Nordhemisphäre bedingt durch die warmen Dansgaard/Oeschger (DO) und kalten Heinrich-Events. Viele DO-Events gehen mit humideren Bedingungen und einer Zunahme der Vegetation einher. Dies spiegelt sich in deutlich negativeren $\delta^{13}$C- und $\delta^{18}$O-Werten wider, während die Kaltphasen einen Rückgang der Vegetation (erhöhte $\delta^{13}$C- und $\delta^{18}$O-Werte) oder gar das Unterbrechen des Speläothemwachstums hervorrufen.

Aufgrund der semi-ariden Klimabedingungen reagieren Speläotheme aus der Cueva Victoria sehr sensitiv auf Klimaveränderungen und sind damit für Paläoklimarekonstruktionen, vor allem der Warmzeiten, ideal geeignet. Klimatische Veränderungen auf der Nordhemisphäre werden durch die stabilen Isotope der Speläotheme präzise aufgezeichnet, und bieten damit ein großes Potential für Paläoklimarekonstruktion des westlichen Mittelmeeres.

## Abstract

In the last decades speleothems have been established as a robust palaeoclimate archive using the U-disequilibrium dating method to construct accurate age-depth models. Advantages in dating methods and high spatial resolution of proxy measurements promote speleothems as an important palaeoclimate archive in high temporal resolution. Proxies such as stable isotopes ($\delta^{13}$C, $\delta^{18}$O) and trace elements can provide new insights into palaeoclimatological changes and changes in vegetation and soil. In addition to other palaeoclimate archives, speleothems occur worldwide in carbonate host rocks can add important information to local and regional palaeoclimate.

Several precise $^{230}$Th/U-datings on Cueva Victoria speleothems were performed using a multi-collector inductively coupled plasma mass spectrometer (MC-ICP-MS). In addition, samples for stable carbon and oxygen isotopes ($\delta^{13}$C, $\delta^{18}$O) were micro milled with high spatial resolution using an isotope ratio mass spectrometer (IRMS). Laser ablation (LA)-ICP-MS technique was used to perform trace element measurements in very high spatial resolution.

South-eastern Spain is one of the driest regions in Europe and high temporal resolution palaeoclimate archives are absent in this region, although they could provide important new information on hydrological changes from glacials to interglacials. $^{230}$Th/U-dating of Cueva Victoria speleothems shows preferred growth phases during interglacial phases. This indicates more humid conditions in combination with higher temperatures and is also displayed by more negative $\delta^{18}$O values in speleothems. These $\delta^{18}$O values are mainly influenced by temperature, amount effect and the source for rainwater, the proximate sea. Another important speleothem proxy is the carbon isotope composition ($\delta^{13}$C) reflecting vegetation type and microbiological soil activity above the cave. Concordant with $\delta^{18}$O values, $\delta^{13}$C values are more negative within warm phases as a result of a vegetation increase. However, during the Holocene, elevated $\delta^{13}$C values indicate less favourable conditions for the vegetation. High summer insolation during the Holocene (9.7 - 7.8 ka) enhances seasonality and, as a result, summer drought is prolonged and extended to the growing season in springtime, which is in agreement to other Mediterranean palaeoclimate archives.

Since the end of the last interglacial during Marine Isotope Stages 5 to 3, climate is strongly influenced by millennial Northern Hemisphere temperature changes by the warm Dansgaard/-Oeschger (DO) and cool Heinrich events. Warm DO events are accompanied by humid conditions and an increase in vegetation density, which is reflected by very negative speleothem $\delta^{13}$C and $\delta^{18}$O values. Cold phases, however, show less negative speleothem isotope values or even growth interruptions, which indicate very dry conditions.

Cueva Victoria speleothems provide the first robust terrestrial palaeoclimate archive in this semi-arid region and they respond sensitively to changes in palaeoclimate, predominantly during warm phases. Fast changes in stable isotopes ($\delta^{13}$C, $\delta^{18}$O) with respect to Northern Hemisphere climate changes highlight their potential as a proxy for palaeoclimate reconstruction in the semi-arid south-eastern Spain.

# Contents

# List of Figures

# List of Tables

# 1 Introduction

Regarding climate change, the Intergovernmental Panel on Climate Change report (Intergovernmental Panel on Climate Change, 2014) emphasises increasing heat waves and droughts in the future. Especially the Mediterranean with increasing warming is one important hot-spot of climate change (Giorgi, 2006). Although difficult to disentangle and calculate, Coupled Model Intercomparison Project phase five (CMIP5) runs calculate with future warming consistent less mean annual precipitation over the Mediterranean region (Figure 1.1; Fischer et al., 2015). However, in particular future precipitation is still difficult to predict by climate models and palaeoclimate reconstructions, for example on speleothems, can support these models by providing new insights on past climate variability.

In the last decades, speleothems (secondary cave carbonates) have been established as an important terrestrial climate archive, providing information of the palaeoclimate from all latitudes and altitudes within abundant carbonate host rock appearance (Fairchild & Baker, 2012). Their huge advantage towards marine sediment or ice core records is the potential of accurate dating beyond the $^{14}$C-dating limit ($< 50$ ka) up to 600 ka using the U-series disequilibrium method (Henderson, 2006; Richards & Dorale, 2003; Scholz & Hoffmann, 2008). On the basis of the precise dating method, proxies such as stable carbon ($\delta^{13}$C) and oxygen ($\delta^{18}$O) isotopes, as well as trace elements provide the possibility to reconstruct palaeoclimate conditions with high temporal resolution (Fairchild & Treble, 2009; Genty et al., 2006; Lachniet, 2009) in respect of palaeohydrology (Bard et al., 2002; Rozanski et al., 1992), palaeovegetation and microbiological soil activity (Breecker et al., 2012; Genty et al., 2006, 2003; Meyer et al., 2014) or monsoon activity across several terminations (Cheng et al., 2016; Wang et al., 2001).

Based on marine records from the Alboran Sea and the Iberian Margin, there is a broad knowledge about the ocean circulation and general vegetation changes from glacial to interglacial climate around the Iberian Peninsula (Martrat et al., 2007, 2004), as well as the response to warm Dansgaard/Oeschger and cold Heinrich events (Cacho et al., 1999; Moreno et al., 2005; Naughton et al., 2009). However, only a few terrestrial palaeoclimate records covering the last 200 ka are known for southern Spain in particular and their temporal resolution is limited (Camuera et al., 2019; Hodge et al., 2008). A Portuguese speleothem stack emphasizes the imprint of proximate sea surface temperatures (SST) of the North Atlantic/Iberian Margin to terrestrial climate conditions for this region with warm and humid vegetated interglacial and interstadial (Denniston et al., 2018). This is in agreement with circum-Mediterranean pollen records (Allen et al., 1999; Camuera et al., 2019; Tzedakis, 1993; Tzedakis et al., 2006).

Cueva Victoria is located in south-eastern Spain, in one of the driest regions in Europe, with

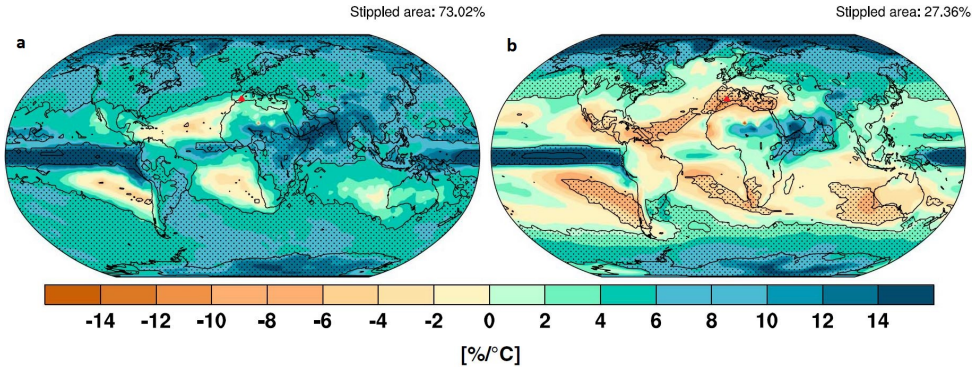


Figure 1.1: Multimodel mean for changes in future precipitation extremes (**a**) and mean annual precipitation (**b**) out of 15 CMIP5 models (Fischer et al., 2015). Stippled areas indicate an agreement sign of change of 12 out of 15 models for a linear regression model from 1901 to 2100. They concordant calculate less annual mean precipitation in the Mediterranean with climate change towards 2100. The red triangle indicates the location of Cueva Victoria.

a mean annual precipitation between 200 and 300 mm. The climate is characterized by strong seasonality with hot and dry summers ($<$ 10 mm/month), and humid autumns ($\approx$50 mm/month) and the vegetation is limited by the low mean annual precipitation. The scope of this thesis addresses changes in climate on orbital and millennial time scale of this climatic sensitive region. In particular, the main focus is on Cueva Victoria speleothem $\delta^{13}$C and $\delta^{18}$O values. These proxies enable a palaeohydroclimatic reconstruction for south-eastern Spain with respect to distant Atlantic influences such as the atmospheric North Atlantic Oscillation (NAO, Hurrell & Loon, 1997) and the Western Mediterranean Oscillation (WeMO, Martin-Vide & Lopez-Bustins, 2006). Precisely dated speleothems ($^{230}$Th/U-dating) using multi-collector inductively coupled plasma mass spectrometry (MC-ICP-MS) in combination with high spatial resolution, stable isotope measurements provide the possibility of a paleoclimate reconstruction.

Using the $^{230}$Th/U-dating method, multiple growth phases in several analysed flowstones from Cueva Vitoria can be detected. The obtained ages indicate a preferred speleothem growth during interglacial phases and/or Dansgaard/Oeschger events. Compared to pollen records, these phases coincide with high arboreal pollen amount during interglacials in the Mediterranean region and high SST at the Iberian Margin as presented in Manuscript I (Chapter 3). These $^{230}$Th/U-datings display the occurrences of more humid climate conditions in south-eastern Spain providing the basis for further investigations.

Starting chronologically, the youngest flowstone deposition records the onset of the present interglacial including the Bølling/Allerød warming and the Younger Dryas towards the Holocene climate optimum. Whereas $\delta^{18}$O values follow the pattern of the proximate SSTs of the Alboran Sea, $\delta^{13}$C values indicate an important shift in vegetation to much drier climate conditions between 9.7 and 7.8 ka. To understand past hydroclimate changes, we investigate in Manuscript II (Chapter 4) present day climate in terms of atmospheric settings leading to precipitation in

south-eastern Spain. The comparison of circum-Western Mediterranean early Holocene palaeoclimate archives partly support the hypothesis of reduced vegetation by enhanced and prolonged spring/summer drought reflected by the $\delta^{13}$C excursion, which can only be triggered by enhanced seasonality.

As elaborated in Manuscript I (Chapter 3), flowstones at Cueva Victoria grew predominantly during interglacial phases. However, after the last interglacial (MIS 5), climate in Europe is strongly dominated by warm Dansgaard/Oeschger and cold Heinrich events, even during MIS 3, as an intermediate interglacial. Manuscript III (Chapter 5) addresses the fast palaeoclimate variability due to North Atlantic instabilities. Higher North Atlantic and Mediterranean SST control significantly the precipitation during warm Dansgaard/Oeschger events, which led to increased precipitation in the whole Mediterranean. This can rarely be explained by modern atmospheric circulation patterns such as NAO or WeMO.

Comparing the Holocene with the last interglacial (MIS 5), based on Cueva Victora flowstones, we elaborate differences in the setting of the interglacials (Manuscript IV, Chapter 6). Indicated by the deposition of organic-rich anoxic sediment layers (sapropels) in the Eastern Mediterranean, a strong and enhanced seasonality with increased freshwater input can be assumed in the Mediterranean during peak interglacial conditions (Eemian). Thus, it also potentially increases precipitation in the Western Mediterranean during winter. However, exceeding Holocene temperatures (Manuscript I, Chapter 3), we assume for the Eemian a negative precipitation – evapotranspiration balance due to extended summer drought, prohibiting the propagation of vegetation and speleothem growth. Whereas, during glacial sapropel deposition (MIS 6, S6) or phases of reduced temperatures of an interglacial (MIS 5, S3 & S4), speleothem $\delta^{13}$C values reach their minimum, indicating favourable vegetation conditions and a positive precipitation – evapotranspiration balance. Its position and in general restricted mean annual precipitation, Cueva Victoria seems to be even more sensitive to precipitation variability, than other sites (e.g., Italy).

# 2 Basics

## 2.1 Karst processes and speleothem formation

Carbonate rocks are in contrast to most other rock types prone to dissolution by even weak acids and are therefore (besides gypsum) favourable to karstification. Through microbiological activities in the soil and root respiration $CO_2$ accumulates within the soil zone up to several percent and can subsequently form carbonic acid in combination with rainwater (Eqn. 2.1). The rainwater equilibrates with soil-$CO_2$ and the $CO_2$-saturated solution seeps through the host rock via fissures and cracks into the epikarst. The karst can be divided by the water table into a vadose and a phreatic zone. The vadose zone is located above the water table, where caves with speleothem growth exist. It is an important zone for water storage and via vertical shafts water can seep into the underlying phreatic zone. Dominated by continuous presence of water, the phreatic (water saturated) zone undergoes constant dissolution within geological time scales of several thousand to million years resulting predominantly in horizontal cavities. If the water table drops and cavities in the vadose zone are linked to the outside, they interact with the atmosphere and gas exchange takes place. In temperate climate regions with different winter and summer temperature, air transport is driven by temperature differences to the outside by fissures and cracks. In case of one cave entrance, ventilation of the cave occurs predominantly in wintertimes, when cold heavy air enters the cave and replaces the warmer $CO_2$-rich cave atmosphere. Meanwhile during summertime, ventilation is reduced and dependent on the outside minimum temperature. Two cave entrances at different altitudes lead to persistent ventilation throughout the whole year with ascending air during summer on one hand and ventilation from the higher to the lower entrance in winter on the other. In many cases, a slight ventilation is also possible via fissures and cracks.

$$CO_2(g) + H_2O \longleftrightarrow H_2CO_3 \tag{2.1}$$

The formation of speleothems in caves is predominantly controlled by the differences of the $pCO_2$ of the drip water and the cave atmosphere, which itself is dependent on cave ventilation. When $CO_2$ rich water enters a cave with low $pCO_2$, $CO_2$ degasses immediately (Hansen et al., 2013) by shifting the equation 2.2 to the left side resulting in the precipitation of $CaCO_3$. These secondary carbonates form, depending on the residence time of the water film, as stalactites on the cave ceiling, or as stalagmites and flowstones on the cave floor. Stalagmite morphology strongly varies depending on drip rate, drip height and drip water chemistry itself (Dreybrodt,

1999; Hansen et al., 2013). In contrast to stalagmites, flowstones are built up by precipitation of $CaCO_3$ under more continuous (laminar) flowing thin water films. They in general require a higher water throughput and are often related to fissures in the host rock.

$$CO_2 + H_2O + CaCO_3 \longleftrightarrow Ca^{2+} + 2HCO_3^- \tag{2.2}$$

Speleothems at Cueva Victoria are mainly represented by flowstones, stalagmites are less present, which might be a relict of ancient mining activities and the destruction of the original cave floor (Pérez de Perceval et al., 2015). Though, the inhomogeneous dolomite and limestone host rock is cross-cutted by several faults and cracks (Manteca Martínez & Pina, 2015; Ros & Llamusí, 2015), which enables, if available, a high water throughput in the karst system and the predominant formation of flowstones. However, the ancient small cave profile might reduce the ventilation and the $CO_2$ degassing as well. This might accumulate $CO_2$ in the cave air and suppresses $CO_2$ degassing of the solution, which might promote the formation of flowstones at Cueva Victoria.

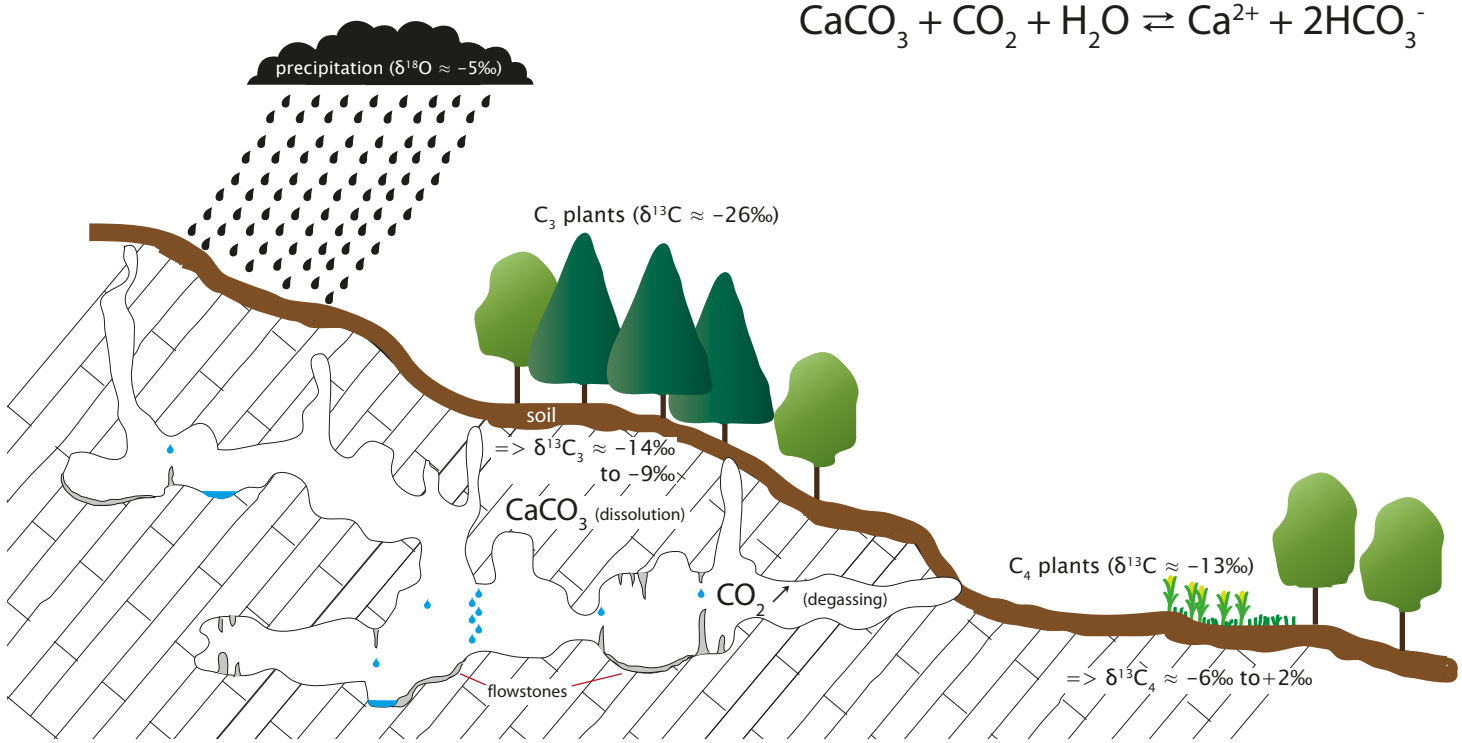


Figure 2.1: Processes in and above the cave and appropriate isotope values. Rainwater passes the soil while uptaking $CO_2$ and dissolving the carbonate host rock. Soil $\delta^{13}C$ values depending on plant type ($C_3$, $C_4$) get mixed with host rock $\delta^{13}C$ values of about 0 ‰ resulting in the displayed values for speleothems.

## 2.2 Dating of speleothem samples

Precise dating of palaeoclimate archives is one of the main issue in palaeoclimatology. Marine and terrestrial archives can easily be dated with $^{14}C$ dating up to $\approx 55\,ka$. Beyond the limit of $^{14}C$ dating method, precise age depth models are, depending on the archive substrate, challenging. One option for lacustrine sediments is varve counting, but this limited to lakes with continuous sedimentation of predominant fine grained material. To some extent, layer counting can be also applied to the youngest parts of ice cores. In addition to that, it is very precise to use interbedded tephra layers as anchor points for the chronology. These can be linked chemically and petrographically to other tephra layers, or in case of unaltered minerals, the $^{40}K/^{40}Ar$ or more state of the art the $^{40}Ar/^{39}Ar$ dating method can be applied to K-rich and Ar-retentive minerals as sanidine or hornblende (Wulf et al., 2004). However, the interpolation can be done linear or, more common, tuned on the NGRIP ice core (North Greenland Ice Core Project members, 2004) or on even longer time scales over several terminations tuned to orbital parameters, like the insolation. Subsequently, the uncertainties of the age depth-models are in the order of the reference record and temporal discrepancies to orbital parameters cannot be resolved.

In contrast to most other climate archives, speleothems are formed in isolated environments, which were not exposed to weathering and alteration. Diagenesis, like recrystallization of the $CaCO_3$ can easily be identified by looking into crystal fabrics (Frisia, 2015) or the growth structure of the speleothem itself and may lead to significant age inversions (Scholz et al., 2014). Several dating methods have been applied to speleothems, in the beginning of the speleothem science, the radiocarbon $^{14}C$ method was applied. However, there are some major issues with the radiocarbon method addressing the infiltration time, soil processes and the dead carbon fraction (Genty et al., 2001). Especially the old dead carbon fraction from the soil can alter the signal, and a monitoring site to measure the dead carbon percentage is required to correct for $^{14}C$ dating (Fohlmeister et al., 2011; Genty et al., 2001). In addition $^{14}C$ dating on speleothems is limited by its short half-life time of $\approx 5730\,ka$ (Godwin, 1962). However, nuclear bomb tests in the late 60's enriched $^{14}C$ in the atmosphere and can be used to detect the bomb peak in recent growing speleothems (Hodge et al., 2011; Mattey et al., 2008).

First U-series dating on speleothems were done with $\alpha$-spectrometry, followed by thermal ionization mass spectrometry (TIMS). Both require high sample amounts compared to the more recent method with multi-collector inductively coupled plasma mass spectrometry (MC-ICP-MS, Hellstrom, 2006; Hoffmann, 2008). With the advantage of chemical separation and MC-ICP-MS measurements, the age uncertainty is about 1 % (Fairchild & Baker, 2012) and could reduced by further improvements to some permile even for samples of several hundred ka (Cheng et al., 2016).

Due to the fact, that U and Th behave geochemically different, speleothems are perfect for the $^{230}Th/U$ disequilibrium dating method. While U is transported as dissolved uranyl ion $(UO_2)^{2+}$ in water in the aquifer and into the cave, Th is particle reactant and therefore adsorbed by

particles and not further transported, at least not as ion in water (Ivanovich & Harmon, 1992). The uranyl $(UO_2)^{2+}$ is incorporated into the carbonate crystal and ranges from close to zero in calcite up to some 100 µg/g in aragonite (Ford & Williams, 2010). Once U ($^{234}$U, $^{235}$U, $^{238}$U) is incorporated, it decays within the calcite. Due to transportation and incongruent dissolution, fractionation occurs in the decay chain of $^{238}$U with the radioactive daughter $^{234}$U ($\lambda = 2.826 * 10^{-6}$; Cheng et al., 2000) disturbing the ($^{234}$U/$^{238}$U) ratio. Thus, the initial ($^{234}$U/$^{238}$U) has to be corrected by the constant $^{235}$U/$^{238}$U ratio of 0.007. $^{234}$U decays by an $\alpha$-decay to $^{230}$Th and with a half life of $\approx 75$ ka it further decays finally to $^{206}$Pb. Due to chemical separation of U and Th in the solution during transport, only U isotopes should be incorporated into speleothems and Th should be zero during calcite precipitation. To prove this assumption, $^{232}$Th is measured additionally to estimate the initial detrital Th amount. It is recommended to correct for the initial detrital $^{230}$Th and the most commonly used value for detrital ($^{230}$Th/$^{232}$Th) correction in literature is given by Wedepohl (1995), ($^{232}$Th/$^{238}$U) = 1.25. However, depending on host rock initial U and Th concentration, this value is highly variable. For Cueva Victoria speleothems, the approach of a factor minimizing the age inversions over the whole sample has been applied (Budsky et al., 2019; Chapter 3).

Older speleothems, which are too old for the $^{230}$Th/U disequilibrium dating method can be dated with the traditional U/Pb dating method (Richards et al., 1998). Thus, a minimum of initial common Pb is required for Pleistocene samples, due to the very low amount of radiogenic Pb produced by the radioactive decay within the short time compared to the long half life of radioactive mother isotope ($t_{1/2}(^{238}U) = 4.468 * 10^9 a$).

## 2.3 Stable oxygen isotopes in speleothems

The most important proxy of palaeoclimate archives is the stable oxygen isotope composition, reflecting the water composition during the time of deposition. Samples for stable isotope measurements can easily be taken from the central growth axis of speleothem slabs with a MicroMill device in µm-distances and are routinely analysed with isotope ratio mass spectrometers (IRMS; Spötl & Vennemann, 2003). Carbonate sample measurements are in $\delta$-notation as per mile deviation compared to a carbonate reference material (Eqn. 2.3), the Vienna PeeDee Belemnite (VPDB). $\delta^{18}$O-data of fluids and water is compared to Standard Mean Ocean Water (SMOW $\delta^{18}$O = 0 ‰; Coplen, 1996).

$$\delta^{18}O = \frac{\frac{^{18}O}{^{16}O\,sample} - \frac{^{18}O}{^{16}O\,ref.mat}}{\frac{^{18}O}{^{16}O\,sample}} * 1000‰ \tag{2.3}$$

Speleothem $\delta^{18}$O values are influenced by several processes: the $\delta^{18}$O composition of the hydrological cycle (e.g., rainwater, seawater, etc.) and fractionation processes inside the cave and the karst aquifer. Depending on the isotopic composition of the moisture source, the oceans (LeGrande & Schmidt, 2006), seawater evaporates and fractionation of oxygen isotopes prefers

$^{16}O$ over $^{18}O$ and the air moisture $\delta^{18}O$ is negative. Fractionation processes (equilibrium and kinetic) are strongly influenced by temperature and water vapor of the air. Within the atmosphere the air parcel underlies the Rayleigh distillation. Further $^{18}O$ depletion occur during precipitation and cooling on the way towards higher latitudes and crossing continents (Lachniet, 2009; McDermott et al., 2011; McDermott, 2004; Rozanski et al., 1993). Finally, precipitation/snow at high latitudes is very depleted in $^{18}O$, indicated by strong negative $\delta^{18}O$ values ($\approx$-30 ‰; Bowen & Wilkinson, 2002), which built up the ice sheets. However, it is worth mentioning, that especially in the tropics and the Mediterranean, the so called "amount effect" the isotope fractionation with heavy rainfall events might be changed to more negative values (Bar-Matthews et al., 2003; Celle-Jeanton et al., 2004; Dansgaard, 1964). Each region has its own isotopic signature in precipitation, which can diverge over a year, influenced by seasonality (intra-annual temperature and rainfall variation; Araguas-Araguas & Diaz Teijeiro, 2005; Budsky et al., 2019) and the atmospheric circulation pattern (Comas-Bru et al., 2016; Moreno et al., 2014).

Once precipitation with a distinct isotopic signature infiltrating the soil, evaporation fractionation can influence the $\delta^{18}O$ to higher values in arid to semiarid regions, depending on soil moisture (Dansgaard, 1964; Rozanski et al., 1993). The recharging seepage water will be mixed and while entering the cave also be affected by fractionation processes, depending on cave temperature and relative humidity (water vapor exchange with the air) disequilibrium and/or equilibrium fractionation will occur prior to calcite precipitation (Coplen, 2007; Hansen et al., 2019; Hendy, 1971; Mühlinghaus et al., 2009; Scholz et al., 2009; Tremaine et al., 2011).

The climatic interpretation of speleothem $\delta^{18}O$ values is challenging (Budsky et al., 2019; Hodge et al., 2008; Mischel et al., 2017; Weber et al., 2018), but can be interpreted as an indicator for rainfall amount (Ayalon et al., 2002; Bar-Matthews et al., 2003), monsoon activity for East Asian cave locations (Cheng et al., 2016; Wang et al., 2008) or as temperature at higher altitudes (Boch et al., 2011; Moseley et al., 2015). There is no simple interpretation for speleothem $\delta^{18}O$ values, it varies for each study site and intra-cave processes. This often requires a cave monitoring over several years (Baldini et al., 2010; Mischel et al., 2015; Moreno et al., 2014). Nevertheless, with a multiproxy-approach it is possible to disentangle different processes and provide more insights into past climate variability.

Despite the non-existing monitoring at Cueva Victoria, speleothem $\delta^{18}O$ values are assumed to reflect predominantly a combination of temperature, moisture source of rainfall and to some extent an amount effect on millennial scale. In addition, on orbital scale, speleothem $\delta^{18}O$ values follow the influence of solar forcing.

## 2.4 Stable carbon isotopes in speleothems

In addition to $\delta^{18}O$ values, stable carbon isotopes ($^{12}C$, $^{13}C$) can be measured concurrently. Similar to carbonate $\delta^{18}O$ values, $\delta^{13}C$ values of carbonates are given with respect to VPDB ($\delta^{13}C = 0$ ‰). Whereas $\delta^{18}O$ values reflect the hydrological cycle, $\delta^{13}C$ is related to soil processes, mainly as $\delta^{13}C$ of the soil $CO_2$. Soil $CO_2$ is predominantly formed by root respiration and

microbiological activity (Genty et al., 2005). Seeping rainwater is in chemical and isotopic equilibrium with soil $pCO_2$. Due to the $CO_2$-uptake, it is capable to dissolve the carbonate host rock subsequently. The carbon isotope composition in soil strongly depends on the vegetation type. While most trees, shrub and crops belong to $C_3$ plants, grasses in warm arid regions belong to the $C_4$ plant classification due to different types of photosynthesis. This leads to a different way of incorporation of $CO_2$ (Cerling et al., 1993; Edwards et al., 2010; Kauwe et al., 2015). Crassulacean acid metabolism (CAM) plants can combine the photosynthesis of both $C_3$ and $C_4$ plants depending on the availability of water. Different types of photosynthesis cause different fractionation of the stable carbon isotopes take place, resulting in very negative $\delta^{13}C$ values of $C_3$ plants ($\approx$-26 ‰) and higher $\delta^{13}C$ values for $C_4$ of around -13 ‰ (Figure 2.1). Thus, this reflects the isotopic signature of the released plant $CO_2$ in the soil and by dissolution and consumption of one carbon of the host rock ($CaCO_3$; 0 to +3 ‰), $\delta^{13}C$ values of the drip water increase (Eqn. 2.2; Figure 2.1).

Higher precipitation in semiarid regions or higher temperatures in temperate regions can increase microbiological soil activity as well as the vegetation density or plant type (Cerling et al., 1993; Denniston et al., 2000; Hall & Penner, 2013), resulting in lower $\delta^{13}C$ values of the seepage water. However, several processes in the aquifer and the cave can alter the isotopic signal of speleothems. For semiarid regions, increased precipitation leads to intense dissolution of the host rock, which dilutes the soil $CO_2$ signal and enhances the $\delta^{13}C$ values of the carbonate host rock resulting in elevated speleothem $\delta^{13}C$ values (Bar-Matthews et al., 2003, 1996). In addition, elevated speleothem $\delta^{13}C$ values are often indicative for prior calcite precipitation (PCP). Within the host rock, small air filled cavities connected to the atmosphere, enable a PCP of the $CO_2$ saturated solution, before it enters the cave to form speleothems. PCP is favoured during drier periods, when cavities in the vadose zone are no longer completely filled with water (Fairchild & Treble, 2009; Johnson et al., 2006). Disequilibrium fractionation processes occur even on flowstones by progressive calcite precipitation on the way to the sample site (Hansen et al., 2017, 2019; Johnson et al., 2006; Mattey et al., 2010; Mühlinghaus et al., 2009). Speleothem $\delta^{13}C$ values increase during these processes and might restrict the palaeoclimatic interpretation. Due to the fact that vegetation at Cueva Victoria is limited by low precipitation, speleothem $\delta^{13}C$ values are not only interpreted as vegetation density but also as an indicator for palaeohydrological conditions in south-eastern Spain.

## 2.5 Trace elements in speleothems

Trace elements are another important proxy in speleothem sciences and the application of Laser ablation (LA)-ICP-MS enables high spatial resolution measurements (several µm) within a short time. Despite the easy application set-up, the interpretation of trace elements is challenging and not straightforward. However, elements with the same ionic charge as Calcium ($Mg^{2+}, Sr^{2+}, Ba^{2+}$) are commonly used in addition to stable isotopes. As proxies in speleothems, they could disentangle potential fractionation processes observed in stable isotopes. For example,

Mg/Ca, Sr/Ca and Ba/Ca ratios are immediately influenced by PCP, due the different, smaller partition coefficients of the ions ($Mg^{2+}$, $Sr^{2+}$, $Ba^{2+}$) in calcite. PCP results in higher Mg, Sr, Ba contents of the speleothem, due to an ongoing increase of the trace element/Ca ratio in the solution with PCP (Johnson et al., 2006; Stoll et al., 2012; Wassenburg et al., 2012). Elements, which do not fit into the carbonate crystal lattice like Al, Si and Y can be used as detrital indicators transported as colloids originating from soil or intra-cave sediments (Fairchild & Treble, 2009). They can give further insights into soil processes and environmental changes (e.g., Zn for deforestation, Borsato et al., 2007). In terms of trace elements, Cueva Victoria speleothems are challenging to interpret, which might be related to the complex Mn-mineralization and the presence of sulphates in the cave (Manteca Martínez & Pina, 2015).

## 2.6 Mediterranean climate

The Mediterranean (subtropical) climate can be characterized according to the Köppen-Geiger classification (Kottek et al., 2006) to warm temperate, summer dry and hot (Csa) to fully humid with hot summer (humid summer months, Cfa) and in parts to cold arid, steppe (BSk) climate, all with substantial winter rainfall. These climate conditions occur at around 40°N and 40°S due to the most northern/southern position of the Intertropical Convergence Zone (ITCZ) during boreal summer/winter and the associated northward/southward shift of the subtropical high (Hadley Cell). During boreal winter, the subtropical high pressure belt follows the southward movement of the ITCZ and enables cyclones to enter the Mediterranean regions, causing the winter rain. Especially in the Mediterranean autumn, rainfall events are prone to result in devastating flash-flood events, due to the high amount of precipitable water caused by high SST and energy, which is stored by the Mediterranean Sea in combination with first autumn cold fronts (Araguas-Araguas & Diaz Teijeiro, 2005). The vegetation is, however, adapted to summer droughts and among others specialized with waxed leaves for reduced water loss by evapotranspiration.

Recent climate conditions in the Western Mediterranean are predominantly influenced by westerlies over the North Atlantic in the winter and the subtropical (Azores) high in the summer. Especially in autumn, cold air from the northern latitudes in combination with high SSTs induces intensive cyclogenesis in the Western Mediterranean basin leading to maximum precipitation. Due to high altitude mountain ranges in the West and associated lee-effects, precipitation from the West is strongly limited at Cueva Victoria. This results in predominantly easterly winds during precipitation events (Budsky et al., 2019). In contrast to main parts of Europe, precipitation in south-eastern Spain is not significantly influenced by the North Atlantic Oscillation (Budsky et al., 2019; Comas-Bru & McDermott, 2014; Hurrell & Loon, 1997). Precipitation is rather triggered by the more regional Western Mediterranean Oscillation with a low pressure system in the Gulf of Cadiz (Martin-Vide & Lopez-Bustins, 2006) resulting in easterly winds and more local moisture uptake over the Mediterranean Sea (Budsky et al., 2019).

## 2.7 Sapropels and circulation of the Mediterranean Sea

The term sapropel is derived from the greek name *sapros*, which means rotten. Sapropels form in (semi-)closed stratified water basins with anoxic bottom water conditions and are built of organic rich, black mud, by definition with organic carbon concentrations ($C_{org}$) above 2 %. Modern sapropel formation takes place in unconnected or partly connected basins with stratified water bodies (e.g. Black Sea), where no deep ocean circulation like the Atlantic Meridional Overturning Circulation (AMOC; Böhm et al., 2015; Boyle & Keigwin, 1987) or the Mediterranean Circulation (Millot & Taupier-Letage, 2005) convey dense oxygen-rich surface water into deep ocean water. For the Eastern Mediterranean, several quaternary sapropel layers have been found in marine cores and some are exposed at the surface (Rohling et al., 2015). Instead of sapropels, organic rich layers (ORL, high $C_{org}$, but no anoxic conditions) were deposited in the Western Mediterranean basin (Ausín et al., 2015; Emeis et al., 1991; Rogerson et al., 2008). This indicates changes in Mediterranean deep water circulation and a strong stratification of the deep water at least in the Eastern Mediterranean.

### 2.7.1 Circulation of the Mediterranean Sea

Modern circulation in the Mediterranean Sea can be divided into three major processes. **1.** Atlantic surface water enters the Alboran Sea via the Strait of Gibraltar and gets mixed with upwelling and outflowing Mediterranean water. This happens within anticyclonic gyres of the Alboran Sea (Millot, 1999; Pinardi et al., 2015) resulting in Modified Atlantic Water (MAW) of ca. 100 - 150 m thickness, with slightly increased salinity compared to fresh Atlantic water (Figure 2.2a). On the way eastward, it splits into one current directed towards the Balearics and into several metastable gyres along the Algerian coast (Figure 2.2b). **2.** In the Gulf of Lions surface water is transformed to Western Mediterranean Deep Water (WMDW) by a strong Mistral (Smith et al., 2008) resulting in a water layer influenced by strong evaporation (cold winds) and SST cooling in winter on top of warmer and more saline water. Chimneys or plumes can develop and exchange water masses between these layers. Subsequently, at the end of winter, fresh water flows into deep parts of the Balearic and Tyrrhenian Sea forming oxygen rich bottom water (Rohling et al., 2015; Smith et al., 2008).

Another current of the MAW is along the Algerian cost with several weak eddys (**1**). Under increased current, the constriction between Sardinia and Tunesia and the Strait of Sicily are passed into the Eastern Mediterranean, the Levantine basin. **3.** Cold winter SST in combination with high salinity favours vertical convection and the formation of an intermediate water, the saline Levantine Intermediate Water (LIW) at depths between 150 and 600 m (Marino, 2008; Rohling et al., 2015; Figure 2.2a). On the way westward, it forms a halocline with die upper MAW. Similarly to the Western Mediterranean basin, a deep water formation also occurs in the eastern part. The formation of Eastern Mediterranean Deep Water (EMDW) is mainly built up by cool and freshwater from the Adriatic Sea. On the way, it gets mixed to some extent with LIW and due to lower temperature and subsequently flows under the LIG (Rohling et al.,

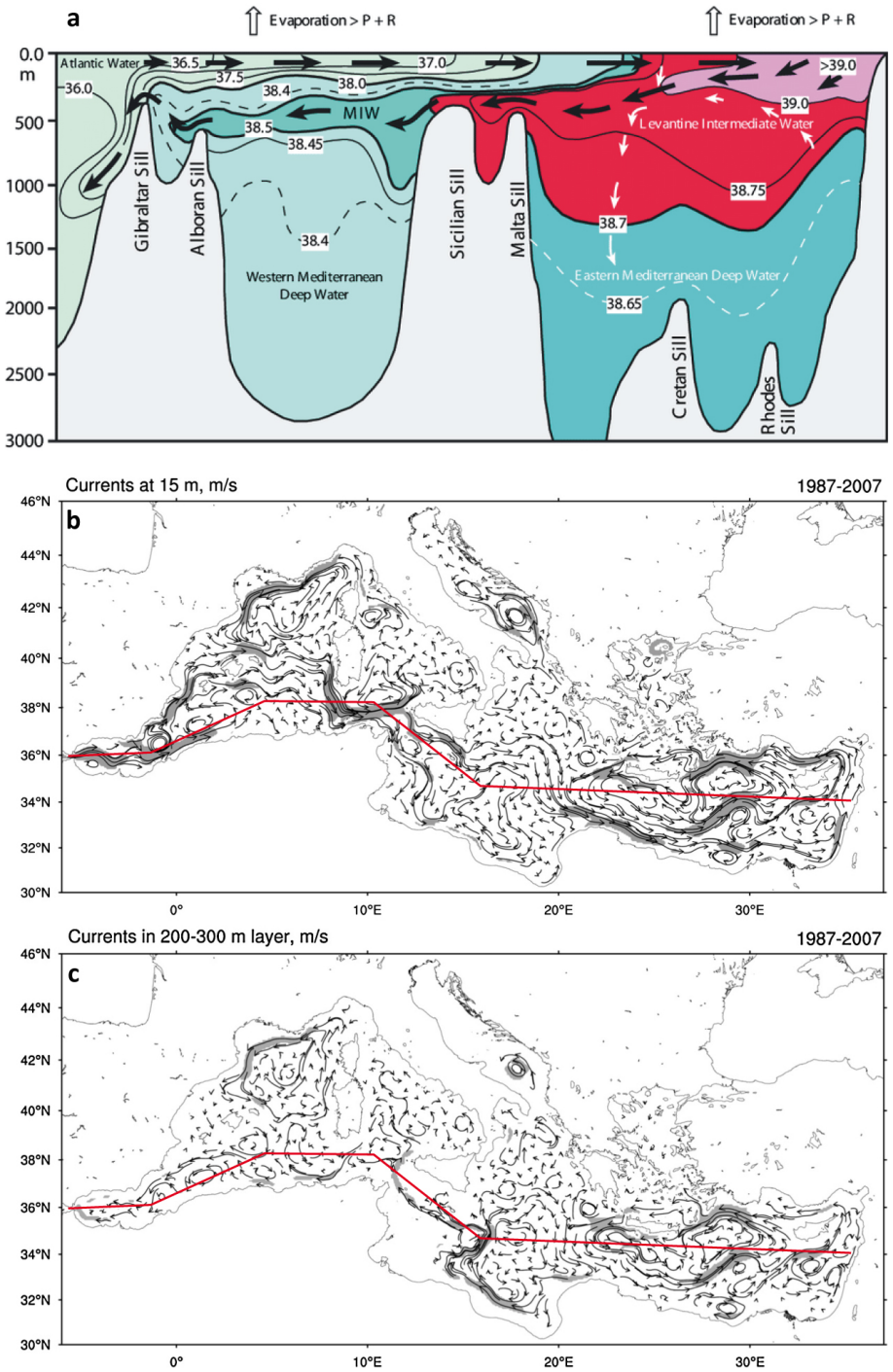


Figure 2.2: Schematic transect across the Mediterranean Sea with sea-floor topography and main water domains (**a**) and their salinity (colorcode and numbers in psu) from Marino (2008). The most dominant circulation is indicated by black arrows and shows the Modified Atlantic Water (MAW), which turns into Levantine Intermediate Water (LIW) due to strong evaporation and the increase of salinity. Mean surface currents (MAW) in the Mediterranean Sea (**b**) display several gyres on the way across the Mediterranean Sea (Reanalysis data, Pinardi et al., 2015). Similar to **b**, the mean currents in 250 m depth (**c**) indicate the circulation of LIW. Shaded areas indicate velocity amplitudes greater than 0.1 m/s (**b**) and 0.05 m/s (**c**), respectively. The red line displays the transect of **a**. During sapropel deposition the circulation is reduced to the upper 300 m.

2015). There also seems to be a contribution of deep water formation from the Aegean Sea to the EMDW (Wüst, 1961).

Especially LIW flows over the Strait of Sicily (below 200 m) to the West into the Western Mediterranean Sea separating the upper eastward flowing MAW from the bottom WMDW (Figure 2.2a). Due to the very shallow depth of the Strait of Sicily, the exit of EMDW to the Western Mediterranean basin and via cascades into the Tyrrhenian Sea is limited (Rohling et al., 2015). Subsequently, Tyrrhenian deep water is mixed with WMDW by flowing into the Western Mediterranean basin. In ≈250 m depth, LIW crosses with several gyres in the Tyrrhenian Sea and Gulf of Lions, the Western Mediterranean basin and flows into the Atlantic over the Strait of Gibraltar (Figure 2.2c). Close to the Strait of Gibraltar, the base of LIW (700 m depth) is elevated by Bernoulli aspiration, which enables the WMDW to exit the Western Mediterranean as well (Stommel et al., 1973).

### 2.7.2 Sapropel formation

Since the late Miocene, many sapropels in the Eastern Mediterranean Sea were known during precision minima and maximum summer insolation (Larrasoaña et al., 2013; Rohling et al., 2015). This sequence is only interrupted by the Messinian Salinity Crisis (MSC; Duggen et al., 2003; Larrasoaña et al., 2013). Sapropels, determined by high $C_{org}$, cannot be dated directly, so Pleistocene to Pliocene sapropels were placed in context to orbital forcing and high insolation (Rossignol-Strick & Paterne, 1999), although they can occur offset to the orbital parameters by some thousand years (Grant et al., 2016). Though, by subsequent oxidation after sapropel deposition, they can be geochemical oxidized and altered; even more indicative is the Ba/Al or Mn/Al-ratio reflecting palaeoproductivity (e.g., Gallego-Torres et al., 2010). Simultaneously, shallow marine carbonate shells of planktonic foraminifera display very negative $\delta^{18}O$ values with sapropel formation. Low $\delta^{18}O$ values indicate a strong influence of freshwater by heavy rainfalls due to the amount effect (see section 2.3; Rohling et al., 2002). The most important source of freshwater is the North African Nile river, which drains the monsoon influenced areas (east/northeast Africa). Increased Nile river discharge occurred, when the African monsoon reached its northernmost position during insolation maximum (Rohling et al., 2002; Tisserand et al., 2009; Tjallingii et al., 2008). However, there is also an input from the northern African borderlands suggested by palaeolakes and the greening of the Sahara (Drake et al., 2011; Larrasoaña et al., 2013), which cannot be merely a result by shifting the monsoon northwards. For the Holocene, Tierney et al. (2017) rather suggest a semi-stationary low pressure area in summer over northwestern Africa, leading to enhanced moisture transport from the North Atlantic towards the African continent. This leads to strongly enhanced freshwater input from northern Africa into the Mediterranean Sea during insolation maxima.

While the summer precipitation over North Africa was enhanced, the northern Mediterranean borderland obtained an increase in precipitation during winter via the westerlies from the North Atlantic, due to the very southern position of the ITCZ and Hadley Cell caused by high Southern

Hemisphere insolation (Toucanne et al., 2015). Several pollen records indicate a distinct increase in deciduous and woody pollen taxa (Allen & Huntley, 2009; Camuera et al., 2019; Tzedakis et al., 2006; Wagner et al., 2019) and carbonate sediments with low $\delta^{13}C$ values indicate soil development by vegetation with enhanced precipitation in general (Bard et al., 2002; Regattieri et al., 2017, 2014; Chapter 6). Thus, during the deposition of sapropels, pronounced summer aridity is reflected by expansion of sclerophyllous vegetation in the Eastern Mediterranean (Milner et al., 2012, 2016; Tzedakis, 2007) and the position of the Hadley cell over the Western Mediterranean (Xoplaki et al., 2003) also recorded in palaeoclimate records (Budsky et al., 2019; Frisia et al., 2006; González-Sampériz et al., 2017; Piqué et al., 2018).

The moisture source for precipitation in the borderland is mainly the Mediterranean itself, nevertheless high freshwater input decreases salinity in the Eastern Mediterranean prohibiting the displacement of old denser EMDW. Subsequently, the LIW is also less saline causing a strong salinity gradient to the EMDW and an ocean stratification. High velocities of the outflowing LIW leads to decreased or disabled Bernoulli aspiration of EMDW at the sill of the Strait of Sicily and amplify the anoxic stratification below 300 m (Rogerson et al., 2008; Rohling et al., 2015).

For the Western Mediterranean, ORL deposited mainly due to sea level increase and density gradients (Rohling et al., 2015). During sea level rise, fresh Atlantic water input increases, while older cold and saline WMDW is denser than newly built deep-water leading to a stratification. However, calculations indicate even then a Bernoulli aspiration over the sill of the Strait of Gibraltar (Rogerson et al., 2008), resulting in missing sapropels in the Western Mediterranean. In conclusion, the sapropel formation is strongly dependent on climate forcing and deep water formation, which is controlled completely by salinity gradient over the Mediterranean Sea.

In summary, sapropels display changes of the Mediterranean Sea circulation, which is strongly affected by climate conditions. Hence, sapropels indicate high freshwater input by North African river systems and therewith the position and strength of atmospheric pressure systems such as the ITCZ and associated Hadley cell. Therefore, it is important to understand the processes of deep water formation and their behaviour to changes in palaeohydrology.

# Bibliography


Allen, J. R. M., U. Brandt, A. Brauer, B. Huntley, J. Keller, M. Kraml, A. Mackensen, J. Mingram, J. F. W. Negendank, N. R. Nowaczyk, H. Oberhänsli, W. A. Watts, S. Wulf, & B. Zolitschka (1999). Rapid environmental changes in southern Europe during the last glacial period. *Nature* **400** (6746), pp. 740–743.

Allen, J. R. & B. Huntley (2009). Last Interglacial palaeovegetation, palaeoenvironments and chronology: A new record from Lago Grande di Monticchio, southern Italy. *Quaternary Science Reviews* **28** (15-16), pp. 1521–1538.

Araguas-Araguas, L. & M. Diaz Teijeiro (2005). "Isotope composition of precipitation and water vapour in the Iberian Peninsula: First results of the Spanish Network of Isotopes in Precipitation". In: *Isotopic composition of precipitation in the Mediterranean Basin in relation to air circulation patterns and climate*. IAEA-TECDOC. Vienna: International Atomic Energy Agency, pp. 173–190. ISBN: 92-0-105305-3.

Ausín, B., J.-A. Flores, F.-J. Sierro, M.-A. Bárcena, I. Hernández-Almeida, G. Francés, E. Gutiérrez-Arnillas, B. Martrat, J. O. Grimalt, & I. Cacho (2015). Coccolithophore productivity and surface water dynamics in the Alboran Sea during the last 25 kyr. *Palaeogeography, Palaeoclimatology, Palaeoecology* **418**, pp. 126–140.

Ayalon, A., M. Bar-Matthews, & A. Kaufman (2002). Climatic conditions during marine oxygen isotope stage 6 in the eastern Mediterranean region from the isotopic composition of speleothems of Soreq Cave, Israel. *Geology* **30** (4), pp. 303–306.

Baldini, L. M., F. McDermott, J. U. L. Baldini, M. J. Fischer, & M. Möllhoff (2010). An investigation of the controls on Irish precipitation d18O values on monthly and event timescales. *Climate Dynamics* **35** (6), pp. 977–993.

Bar-Matthews, M., A. Ayalon, M. Gilmour, A. Matthews, & C. J. Hawkesworth (2003). Sea–land oxygen isotopic relationships from planktonic foraminifera and speleothems in the Eastern Mediterranean region and their implication for paleorainfall during interglacial intervals. *Geochimica et Cosmochimica Acta* **67** (17), pp. 3181–3199.

Bar-Matthews, M., A. Ayalon, A. Matthews, E. Sass, & L. Halicz (1996). Carbon and oxygen isotope study of the active water-carbonate system in a karstic Mediterranean cave: Implications for paleoclimate research in semiarid regions. *Geochimica et Cosmochimica Acta* **60** (2), pp. 337–347.

Bard, E., G. Delaygue, F. Rostek, F. Antonioli, S. Silenzi, & D. P. Schrag (2002). Hydrological conditions over the western Mediterranean basin during the deposition of the cold Sapropel 6 (ca. 175 kyr BP). *Earth and Planetary Science Letters* **202** (2), pp. 481–494.

Boch, R., H. Cheng, C. Spötl, R. L. Edwards, X. Wang, & P. Häuselmann (2011). NALPS: a precisely dated European climate record 120–60 ka. *Climate of the Past* **7** (4), pp. 1247–1259.

Böhm, E., J. Lippold, M. Gutjahr, M. Frank, P. Blaser, B. Antz, J. Fohlmeister, N. Frank, M. B. Andersen, & M. Deininger (2015). Strong and deep Atlantic meridional overturning circulation during the last glacial cycle. *Nature* **517** (7532), p. 73.

Borsato, A., S. Frisia, I. J. Fairchild, A. Somogyi, & J. Susini (2007). Trace element distribution in annual stalagmite laminae mapped by micrometer-resolution X-ray fluorescence: Implications for incorporation of environmentally significant species. *Geochimica et Cosmochimica Acta* **71** (6), pp. 1494–1512.

Bowen, G. J. & B. Wilkinson (2002). Spatial distribution of d18O in meteoric precipitation. *Geology* **30** (4), p. 315.

Boyle, E. A. & L. Keigwin (1987). North Atlantic thermohaline circulation during the past 20,000 years linked to high-latitude surface temperature. *Nature* **330** (6143), pp. 35–40.

Breecker, D. O., A. E. Payne, J. Quade, J. L. Banner, C. E. Ball, K. W. Meyer, & B. D. Cowan (2012). The sources and sinks of CO2 in caves under mixed woodland and grassland vegetation. *Geochimica et Cosmochimica Acta* **96**, pp. 230–246.

Budsky, A., D. Scholz, J. A. Wassenburg, R. Mertz-Kraus, C. Spötl, D. F. C. Riechelmann, L. Gibert, K. P. Jochum, & M. O. Andreae (2019). Speleothem d13C record suggests enhanced spring/summer drought in south-eastern Spain between 9.7 and 7.8 ka – A circum-Western Mediterranean anomaly? *The Holocene* **29** (7), pp. 1113–1133.

Cacho, I., J. O. Grimalt, C. Pelejero, M. Canals, F. J. Sierro, J. A. Flores, & N. Shackleton (1999). Dansgaard-Oeschger and Heinrich event imprints in Alboran Sea paleotemperatures. *Paleoceanography* **14** (6), pp. 698–705.

Camuera, J., G. Jiménez-Moreno, M. J. Ramos-Román, A. García-Alix, J. L. Toney, R. S. Anderson, F. Jiménez-Espejo, J. Bright, C. Webster, Y. Yanes, & J. S. Carrión (2019). Vegetation and climate changes during the last two glacial-interglacial cycles in the western Mediterranean: A new long pollen record from Padul (southern Iberian Peninsula). *Quaternary Science Reviews* **205**, pp. 86–105.

Celle-Jeanton, H., R. Gonfiantini, Y. Travi, & B. Sol (2004). Oxygen-18 variations of rainwater during precipitation: Application of the Rayleigh model to selected rainfalls in Southern France. *Journal of Hydrology* **289** (1-4), pp. 165–177.

Cerling, T. E., Y. Wang, & J. Quade (1993). Expansion of C4 ecosystems as an indicator of global ecological change in the late Miocene. *Nature* **361** (6410), pp. 344–345.

Cheng, H., R. Edwards, J. Hoff, C. Gallup, D. Richards, & Y. Asmerom (2000). The half-lives of uranium-234 and thorium-230. *Chemical Geology* **169** (1–2), pp. 17–33.

Cheng, H., R. L. Edwards, A. Sinha, C. Spötl, L. Yi, S. Chen, M. Kelly, G. Kathayat, X. Wang, X. Li, X. Kong, Y. Wang, Y. Ning, & H. Zhang (2016). The Asian monsoon over the past 640,000 years and ice age terminations. *Nature* **534** (7609), pp. 640–646.

Comas-Bru, L., F. McDermott, & M. Werner (2016). The effect of the East Atlantic pattern on the precipitation d18O-NAO relationship in Europe. *Climate Dynamics* **47** (7-8), pp. 1–11.

Comas-Bru, L. & F. McDermott (2014). Impacts of the EA and SCA patterns on the European twentieth century NAO-winter climate relationship. *Quarterly Journal of the Royal Meteorological Society* **140** (679), pp. 354–363.

Coplen, T. B. (1996). New guidelines for reporting stable hydrogen, carbon, and oxygen isotope-ratio data. *Geochimica et Cosmochimica Acta* **60** (17), pp. 3359–3360.

– (2007). Calibration of the calcite–water oxygen-isotope geothermometer at Devils Hole, Nevada, a natural laboratory. *Geochimica et Cosmochimica Acta* **71** (16), pp. 3948–3957.

Dansgaard, W. (1964). Stable isotopes in precipitation. *Tellus* **16** (4), pp. 436–468.

Denniston, R. F., L. A. González, Y. Asmerom, M. K. Reagan, & H. Recelli-Snyder (2000). Speleothem carbon isotopic records of Holocene environments in the Ozark Highlands, USA. *Quaternary International* **67** (1), pp. 21–27.

Denniston, R. F., A. N. Houts, Y. Asmerom, A. D. Wanamaker Jr., J. A. Haws, V. J. Polyak, D. L. Thatcher, S. Altan-Ochir, A. C. Borowske, S. F. M. Breitenbach, C. C. Ummenhofer, F. T. Regala, M. M. Benedetti, & N. F. Bicho (2018). A stalagmite test of North Atlantic SST and Iberian hydroclimate linkages over the last two glacial cycles. *Climate of the Past* **14** (12), pp. 1893–1913.

Drake, N. A., R. M. Blench, S. J. Armitage, C. S. Bristow, & K. H. White (2011). Ancient watercourses and biogeography of the Sahara explain the peopling of the desert. *Proceedings of the National Academy of Sciences* **108** (2), pp. 458–462.

Dreybrodt, W. (1999). Chemical kinetics, speleothem growth and climate. *Boreas* **28** (3), pp. 347–356.

Duggen, S., K. Hoernle, P. van den Bogaard, L. Rüpke, & J. P. Morgan (2003). Deep roots of the Messinian salinity crisis. *Nature* **422** (6932), pp. 602–606.

Edwards, E. J., C. P. Osborne, C. A. E. Strömberg, S. A. Smith, W. J. Bond, P.-A. Christin, A. B. Cousins, M. R. Duvall, D. L. Fox, R. P. Freckleton, O. Ghannoum, J. Hartwell, Y. Huang, C. M. Janis, J. E. Keeley, E. A. Kellogg, A. K. Knapp, A. D. B. Leakey, D. M. Nelson, J. M. Saarela, R. F. Sage, O. E. Sala, N. Salamin, C. J. Still, & B. Tipple (2010). The origins of C4 grasslands: Integrating evolutionary and ecosystem science. *Science (New York, N.Y.)* **328** (5978), pp. 587–591.

Emeis, K.-C., A. Camerlenghi, J. A. McKenzie, D. Rio, & R. Sprovieri (1991). The occurrence and significance of Pleistocene and Upper Pliocene sapropels in the Tyrrhenian Sea. *Marine Geology* **100** (1-4), pp. 155–182.

Fairchild, I. J. & A. Baker (2012). *Speleothem science: From process to past environments*. Oxford et al.: Wiley. ISBN: 978-1-4051-9620-8.

Fairchild, I. J. & P. C. Treble (2009). Trace elements in speleothems as recorders of environmental change. *Quaternary Science Reviews* **28** (5-6), pp. 449–468.

Fischer, E. M., J. Sedláček, E. Hawkins, & R. Knutti (2015). Models agree on forced response pattern of precipitation and temperature extremes. *Geophysical Research Letters* **41** (23), pp. 8554–8562.

Fohlmeister, J., D. Scholz, B. Kromer, & A. Mangini (2011). Modelling carbon isotopes of carbonates in cave drip water. *Geochimica et Cosmochimica Acta* **75** (18), pp. 5219–5228.

Ford, D. & P. W. Williams (2010). *Karst hydrogeology and geomorphology.* [Rev. ed.] Chichester, England & A Hoboken, NJ: John Wiley & Sons. ISBN: 1118684982.

Frisia, S. (2015). Microstratigraphic logging of calcite fabrics in speleothems as tool for palaeoclimate studies. *International Journal of Speleology* **44** (1), pp. 1–16.

Frisia, S., A. Borsato, A. Mangini, C. Spötl, G. Madonia, & U. Sauro (2006). Holocene climate variability in Sicily from a discontinuous stalagmite record and the Mesolithic to Neolithic transition. *Quaternary Research* **66** (3), pp. 388–400.

Gallego-Torres, D., F. Martinez-Ruiz, G. J. de Lange, F. J. Jimenez-Espejo, & M. Ortega-Huertas (2010). Trace-elemental derived paleoceanographic and paleoclimatic conditions for Pleistocene Eastern Mediterranean sapropels. *Palaeogeography, Palaeoclimatology, Palaeoecology* **293** (1-2), pp. 76–89.

Genty, D., D. Blamart, B. Ghaleb, V. Plagnes, C. Causse, M. Bakalowicz, K. Zouari, N. Chkir, J. Hellstrom, & K. Wainer (2006). Timing and dynamics of the last deglaciation from European and North African d13C stalagmite profiles—comparison with Chinese and South Hemisphere stalagmites. *Quaternary Science Reviews* **25** (17-18), pp. 2118–2142.

Genty, D., D. Blamart, R. Ouahdi, M. Gilmour, A. Baker, J. Jouzel, & S. Van-Exter (2003). Precise dating of Dansgaard–Oeschger climate oscillations in western Europe from stalagmite data. *Nature* **421** (6925), pp. 833–837.

Genty, D., A. Baker, M. Massault, C. Proctor, M. Gilmour, E. Pons-Branchu, & B. Hamelin (2001). Dead carbon in stalagmites: carbonate bedrock paleodissolution vs. ageing of soil organic matter. Implications for 13C variations in speleothems. *Geochimica et Cosmochimica Acta* **65** (20), pp. 3443–3457.

Genty, D., N. Combourieu Nebout, C. Hatté, D. Blamart, B. Ghaleb, & L. Isabello (2005). Rapid climatic changes of the last 90 kyr recorded on the European continent. *Comptes Rendus Geoscience* **337** (10-11), pp. 970–982.

Giorgi, F. (2006). Climate change hot-spots. *Geophysical Research Letters* **33** (8), p. 89.

Godwin, H. (1962). Half-life of Radiocarbon. *Nature* **195** (4845), p. 984.

González-Sampériz, P., J. Aranbarri, A. Pérez-Sanz, G. Gil-Romera, A. Moreno, M. Leunda, M. Sevilla-Callejo, J. P. Corella, M. Morellón, B. Oliva, & B. Valero-Garcés (2017). Environmental and climate change in the southern Central Pyrenees since the Last Glacial Maximum: A view from the lake records. *CATENA* **149**, pp. 668–688.

Grant, K. M., R. Grimm, U. Mikolajewicz, G. Marino, M. Ziegler, & E. J. Rohling (2016). The timing of Mediterranean sapropel deposition relative to insolation, sea-level and African monsoon changes. *Quaternary Science Reviews* **140**, pp. 125–141.

Hall, S. A. & W. L. Penner (2013). Stable carbon isotopes, C3–C4 vegetation, and 12,800 years of climate change in central New Mexico, USA. *Palaeogeography, Palaeoclimatology, Palaeoecology* **369**, pp. 272–281.

Hansen, M., W. Dreybrodt, & D. Scholz (2013). Chemical evolution of dissolved inorganic carbon species flowing in thin water films and its implications for (rapid) degassing of CO2 during speleothem growth. *Geochimica et Cosmochimica Acta* **107**, pp. 242–251.

Hansen, M., D. Scholz, M.-L. Froeschmann, B. R. Schöne, & C. Spötl (2017). Carbon isotope exchange between gaseous CO2 and thin solution films: Artificial cave experiments and a complete diffusion-reaction model. *Geochimica et Cosmochimica Acta* **211**, pp. 28–47.

Hansen, M., D. Scholz, B. R. Schöne, & C. Spötl (2019). Simulating speleothem growth in the laboratory: Determination of the stable isotope fractionation (d13C and d18O) between H2O, DIC and CaCO3. *Chemical Geology* **509**, pp. 20–44.

Hellstrom, J. (2006). U–Th dating of speleothems with high initial 230Th using stratigraphical constraint. *Quaternary Geochronology* **1** (4), pp. 289–295.

Henderson, G. M. (2006). Caving In to New Chronologies. *Science* **313** (5787), pp. 620–622.

Hendy, C. (1971). The isotopic geochemistry of speleothems—I. The calculation of the effects of different modes of formation on the isotopic composition of speleothems and their applicability as palaeoclimatic indicators. *Geochimica et Cosmochimica Acta* **35** (8), pp. 801–824.

Hodge, E., J. McDonald, M. Fischer, D. Redwood, Q. Hua, V. Levchenko, R. Drysdale, C. Waring, & D. Fink (2011). Using the 14C Bomb Pulse to Date Young Speleothems. *Radiocarbon* **53** (2), pp. 345–357.

Hodge, E. J., D. A. Richards, P. L. Smart, B. Andreo, D. L. Hoffmann, D. P. Mattey, & A. González-Ramón (2008). Effective precipitation in southern Spain (˜266 to 46 ka) based on a speleothem stable carbon isotope record. *Quaternary Research* **69** (3), pp. 447–457.

Hoffmann, D. L. (2008). 230Th isotope measurements of femtogram quantities for U-series dating using multi ion counting (MIC) MC-ICPMS. *International Journal of Mass Spectrometry* **275** (1-3), pp. 75–79.

Hurrell, J. W. & H. V. Loon (1997). Decadal Variations in climate associated with the North Atlantic Oscillation. *Climatic Change* **36** (3), pp. 301–326.

Intergovernmental Panel on Climate Change (2014). *Climate Change 2013: The Physical Science Basis: Working Group I Contribution to the IPCC Fifth Assessment Report*. Cambridge: Cambridge University Press. ISBN: 978-1-107-66182-0.

Ivanovich, M. & R. Harmon, eds. (1992). *Uranium-series disequilibrium: Applications to earth, marine, and environmental sciences*. Oxford: Clarendon Press. ISBN: 019854278X.

Johnson, K., C. Hu, N. Belshaw, & G. Henderson (2006). Seasonal trace-element and stable-isotope variations in a Chinese speleothem: The potential for high-resolution paleomonsoon reconstruction. *Earth and Planetary Science Letters* **244** (1-2), pp. 394–407.

Kauwe, M. G. de, J. Kala, Y.-S. Lin, A. J. Pitman, B. E. Medlyn, R. A. Duursma, G. Abramowitz, Y.-P. Wang, & D. G. Miralles (2015). A test of an optimal stomatal conductance scheme within the CABLE land surface model. *Geoscientific Model Development* **8** (2), pp. 431–452.

Kottek, M., J. Grieser, C. Beck, B. Rudolf, & F. Rubel (2006). World Map of the Köppen-Geiger climate classification updated. *Meteorologische Zeitschrift* **15** (3), pp. 259–263.

Lachniet, M. S. (2009). Climatic and environmental controls on speleothem oxygen-isotope values. *Quaternary Science Reviews* **28** (5-6), pp. 412–432.

Larrasoaña, J. C., A. P. Roberts, & E. J. Rohling (2013). Dynamics of green Sahara periods and their role in hominin evolution. *PloS one* **8** (10), e76514.

LeGrande, A. N. & G. A. Schmidt (2006). Global gridded data set of the oxygen isotopic composition in seawater. *Geophysical Research Letters* **33** (12), n/a.

Manteca Martínez, J. I. & R. Pina (2015). "Las mineralizaciones ferro-manganesíferas de la mina-cueva Victoria y su contexto geológico: Fe-Mn mineralizations of the mine-cave Victoria and their geological context". In: *Geología y Paleontología de Cueva Victoria*. Ed. by L. Gibert & C. Ferràndez-Canadell. Vol. 11-12-13. Mastia. Cartagena, pp. 59–74. ISBN: 1579-3303.

Marino, G. (2008). "Palaeoceanography of the interglacial eastern Mediterranean Sea". PhD thesis. Utrecht: Utrecht University.

Martin-Vide, J. & J.-A. Lopez-Bustins (2006). The Western Mediterranean Oscillation and rainfall in the Iberian Peninsula. *International Journal of Climatology* **26** (11), pp. 1455–1475.

Martrat, B., J. O. Grimalt, N. J. Shackleton, L. de Abreu, M. A. Hutterli, & T. F. Stocker (2007). Four Climate Cycles of Recurring Deep and Surface Water Destabilizations on the Iberian Margin. *Science* **317** (5837), pp. 502–507.

Martrat, B., J. O. Grimalt, C. Lopez-Martinez, I. Cacho, F. J. Sierro, J. A. Flores, R. Zahn, M. Canals, J. H. Curtis, & D. A. Hodell (2004). Abrupt Temperature Changes in the Western Mediterranean over the Past 250,000 Years. *Science* **306** (5702), pp. 1762–1765.

Mattey, D. P., I. J. Fairchild, T. C. Atkinson, J.-P. Latin, M. Ainsworth, & R. Durell (2010). Seasonal microclimate control of calcite fabrics, stable isotopes and trace elements in modern speleothem from St Michaels Cave, Gibraltar. *Geological Society, London, Special Publications* **336** (1), pp. 323–344.

Mattey, D., D. Lowry, J. Duffet, R. Fisher, E. Hodge, & S. Frisia (2008). A 53 year seasonally resolved oxygen and carbon isotope record from a modern Gibraltar speleothem: Reconstructed drip water and relationship to local precipitation. *Earth and Planetary Science Letters* **269** (1-2), pp. 80–95.

McDermott, F., T. Atkinson, I. Fairchild, L. Baldini, & D. Mattey (2011). A first evaluation of the spatial gradients in d18O recorded by European Holocene speleothems. *Global and Planetary Change* **79** (3-4), pp. 275–287.

McDermott, F. (2004). Palaeo-climate reconstruction from stable isotope variations in speleothems: a review. *Quaternary Science Reviews* **23** (7-8), pp. 901–918.

Meyer, K. W., W. Feng, D. O. Breecker, J. L. Banner, & A. Guilfoyle (2014). Interpretation of speleothem calcite d13C variations: Evidence from monitoring soil CO2, drip water, and modern speleothem calcite in central Texas. *Geochimica et Cosmochimica Acta* **142**, pp. 281–298.

Millot, C. (1999). Circulation in the Western Mediterranean Sea. *Journal of Marine Systems* **20** (1-4), pp. 423–442.

Millot, C. & I. Taupier-Letage (2005). "Circulation in the Mediterranean Sea". In: *Mediterranean Sea, The. The Handbook of Enviornmental Chemistry*. Ed. by A. Saliot. Handbook of Environmental Chemistry. Berlin: Springer, pp. 29–66. ISBN: 354031492X.

Milner, A. M., R. E. Collier, K. H. Roucoux, U. C. Müller, J. Pross, S. Kalaitzidis, K. Christanis, & P. C. Tzedakis (2012). Enhanced seasonality of precipitation in the Mediterranean during the early part of the Last Interglacial. *Geology* **40** (10), pp. 919–922.

Milner, A. M., K. H. Roucoux, R. Collier, U. C. Müller, J. Pross, & P. C. Tzedakis (2016). Vegetation responses to abrupt climatic changes during the Last Interglacial Complex (Marine Isotope Stage 5) at Tenaghi Philippon, NE Greece. *Quaternary Science Reviews* **154**, pp. 169–181.

Mischel, S. A., D. Scholz, & C. Spötl (2015). d18O values of cave drip water: A promising proxy for the reconstruction of the North Atlantic Oscillation? *Climate Dynamics* **45** (11-12), pp. 3035–3050.

Mischel, S. A., D. Scholz, C. Spötl, K. P. Jochum, A. Schröder-Ritzrau, & S. Fiedler (2017). Holocene climate variability in Central Germany and a potential link to the polar North Atlantic: A replicated record from three coeval speleothems. *The Holocene* **27** (4), pp. 509–525.

Moreno, A., I. Cacho, M. Canals, J. O. Grimalt, M. F. Sánchez-Goñi, N. Shackleton, & F. J. Sierro (2005). Links between marine and atmospheric processes oscillating on a millennial time-scale. A multi-proxy study of the last 50,000 yr from the Alboran Sea (Western Mediterranean Sea). *Quaternary Land-ocean Correlation Quaternary Land-ocean Correlation* **24** (14–15), pp. 1623–1636.

Moreno, A., C. Sancho, M. Bartolomé, B. Oliva-Urcia, A. Delgado-Huertas, M. J. Estrela, D. Corell, J. I. López-Moreno, & I. Cacho (2014). Climate controls on rainfall isotopes and their effects on cave drip water and speleothem growth: the case of Molinos cave (Teruel, NE Spain). *Climate Dynamics* **43** (1-2), pp. 221–241.

Moseley, G. E., C. Spötl, H. Cheng, R. Boch, A. Min, & R. L. Edwards (2015). Termination-II interstadial/stadial climate change recorded in two stalagmites from the north European Alps. *Quaternary Science Reviews* **127**, pp. 229–239.

Mühlinghaus, C., D. Scholz, & A. Mangini (2009). Modelling fractionation of stable isotopes in stalagmites. *Geochimica et Cosmochimica Acta* **73** (24), pp. 7275–7289.

Naughton, F., M. F. Sánchez Goñi, M. Kageyama, E. Bard, J. Duprat, E. Cortijo, S. Desprat, B. Malaizé, C. Joly, F. Rostek, & J.-L. Turon (2009). Wet to dry climatic trend in north-western Iberia within Heinrich events. *Earth and Planetary Science Letters* **284** (3-4), pp. 329–342.

North Greenland Ice Core Project members (2004). High-resolution record of Northern Hemisphere climate extending into the last interglacial period. *Nature* **431** (7005), pp. 147–151.

Pérez de Perceval, M. A., J. I. Manteca Martínez, & M. A. López-Morell (2015). "Historia de la minería de Cueva Victoria". In: *Geología y Paleontología de Cueva Victoria*. Ed. by L. Gibert & C. Ferràndez-Canadell. Mastia. Cartagena, pp. 47–58. ISBN: 1579-3303.

Pinardi, N., M. Zavatarelli, M. Adani, G. Coppini, C. Fratianni, P. Oddo, S. Simoncelli, M. Tonani, V. Lyubartsev, S. Dobricic, & A. Bonaduce (2015). Mediterranean Sea large-scale low-frequency ocean variability and water mass formation rates from 1987 to 2007: A retrospective analysis. *Progress in Oceanography* **132**, pp. 318–332.

Piqué, R., J. Revelles, F. Burjachs, L. Caruso Fermé, & R. Pérez-Obiol (2018). Interdisciplinary approach to the landscape and firewood exploitation during the Holocene at La Garrotxa (Girona, NE Iberia). *Quaternary International* **463**, pp. 401–413.

Regattieri, E., B. Giaccio, S. Nomade, A. Francke, H. Vogel, R. N. Drysdale, N. Perchiazzi, B. Wagner, M. Gemelli, I. Mazzini, C. Boschi, P. Galli, & E. Peronace (2017). A Last Interglacial record of environmental changes from the Sulmona Basin (central Italy). *Palaeogeography, Palaeoclimatology, Palaeoecology* **472**, pp. 51–66.

Regattieri, E., G. Zanchetta, R. N. Drysdale, I. Isola, J. C. Hellstrom, & A. Roncioni (2014). A continuous stable isotope record from the penultimate glacial maximum to the Last Interglacial (159–121 ka) from Tana Che Urla Cave (Apuan Alps, central Italy). *Quaternary Research* **82** (02), pp. 450–461.

Richards, D. A. & J. A. Dorale (2003). Uranium-series Chronology and Environmental Applications of Speleothems. *Reviews in Mineralogy and Geochemistry* **52** (1), pp. 407–460.

Richards, D. A., S. H. Bottrell, R. A. Cliff, K. Ströhle, & P. J. Rowe (1998). U-Pb dating of a speleothem of Quaternary age. *Geochimica et Cosmochimica Acta* **62** (23-24), pp. 3683–3688.

Rogerson, M., I. Cacho, F. Jimenez–Espejo, M. I. Reguera, F. J. Sierro, F. Martinez–Ruiz, J. Frigola, & M. Canals (2008). A dynamic explanation for the origin of the western Mediterranean organic–rich layers. *Geochemistry, Geophysics, Geosystems* **9** (7).

Rohling, E. J., T. R. Cane, S. Cooke, M. Sprovieri, I. Bouloubassi, K. C. Emeis, R. Schiebel, D. Kroon, F. J. Jorissen, A. Lorre, & A. Kemp (2002). African monsoon variability during the previous interglacial maximum. *Earth and Planetary Science Letters* **202** (1), pp. 61–75.

Rohling, E. J., G. Marino, & K. M. Grant (2015). Mediterranean climate and oceanography, and the periodic development of anoxic events (sapropels). *Earth-Science Reviews* **143**, pp. 62–97.

Ros, A. & J. L. Llamusí (2015). "Reconsrucción y génesis del karst de Cueva Victoria: Reconstruction and genesis of the Cueva Victoria karst". In: *Geología y Paleontología de Cueva Victoria*. Ed. by L. Gibert & C. Ferràndez-Canadell. Mastia. Cartagena, pp. 111–125. ISBN: 1579-3303.

Rossignol-Strick, M. & M. Paterne (1999). A synthetic pollen record of the eastern Mediterranean sapropels of the last 1 Ma: implications for the time-scale and formation of sapropels. *Marine Geology* **153** (1-4), pp. 221–237.

Rozanski, K., L. Araguás-Araguás, & R. Gonfiantini (1992). Relation between long-term trends of oxygen-18 isotope composition of precipitation and climate. *Science* **258** (5084), pp. 981–985.

– (1993). "Isotopic Patterns in Modern Global Precipitation". In: *Climate Change in Continental Isotopic Records*. Ed. by P. K. Swart, K. C. Lohmann, J. McKenzie, & S. Savin. American Geophysical Union, pp. 1–36. ISBN: 9781118664025.

Scholz, D. & D. Hoffmann (2008). 230Th/U-dating fossil corals and speleothems. *Eiszeitalter und Gegenwart Quaternary Science Journal* **57** (1/2), pp. 52–76.

Scholz, D., C. Mühlinghaus, & A. Mangini (2009). Modelling d13C and d18O in the solution layer on stalagmite surfaces. *Geochimica et Cosmochimica Acta* **73** (9), pp. 2592–2602.

Scholz, D., J. Tolzmann, D. L. Hoffmann, K. P. Jochum, C. Spötl, D. F. Riechelmann, & D. F. Riechelmann (2014). Diagenesis of speleothems and its effect on the accuracy of 230Th/U-ages. *Chemical Geology* **387**, pp. 74–86.

Smith, R. O., H. L. Bryden, & K. Stansfield (2008). Observations of new western Mediterranean deep water formation using Argo floats 2004 - 2006. *Ocean Science* **4** (2), pp. 133–149.

Spötl, C. & T. W. Vennemann (2003). Continuous-flow isotope ratio mass spectrometric analysis of carbonate minerals. *Rapid Communications in Mass Spectrometry* **17** (9), pp. 1004–1006.

Stoll, H. M., W. Müller, & M. Prieto (2012). I-STAL, a model for interpretation of Mg/Ca, Sr/Ca and Ba/Ca variations in speleothems and its forward and inverse application on seasonal to millennial scales. *Geochemistry, Geophysics, Geosystems* **13** (9), n/a.

Stommel, H., H. Bryden, & P. Mangelsdorf (1973). Does some of the Mediterranean outflow come from great depth? *pure and applied geophysics* **105** (4), pp. 879–889.

Tierney, J. E., F. S. R. Pausata, & P. B. deMenocal (2017). Rainfall regimes of the Green Sahara. *Science Advances* **3** (1), e1601503.

Tisserand, A., B. Malaizé, E. Jullien, S. Zaragosi, K. Charlier, & F. Grousset (2009). African monsoon enhancement during the penultimate glacial period (MIS 6.5 $\sim$ 170 ka) and its atmospheric impact. *Paleoceanography* **24** (2), PA2220.

Tjallingii, R., M. Claussen, J.-B. W. Stuut, J. Fohlmeister, A. Jahn, T. Bickert, F. Lamy, & U. Röhl (2008). Coherent high- and low-latitude control of the northwest African hydrological balance. *Nature Geoscience* **1** (10), pp. 670–675.

Toucanne, S., C. M. Angue Minto'o, C. Fontanier, M.-A. Bassetti, S. J. Jorry, & G. Jouet (2015). Tracking rainfall in the northern Mediterranean borderlands during sapropel deposition. *Quaternary Science Reviews* **129**, pp. 178–195.

Tremaine, D. M., P. N. Froelich, & Y. Wang (2011). Speleothem calcite farmed in situ: Modern calibration of d18O and d13C paleoclimate proxies in a continuously-monitored natural cave system. *Geochimica et Cosmochimica Acta* **75** (17), pp. 4929–4950.

Tzedakis, P. C. (1993). Long-term tree populations in northwest Greece through multiple Quaternary climatic cycles. *Nature* **364** (6436), pp. 437–440.

– (2007). Seven ambiguities in the Mediterranean palaeoenvironmental narrative. *Quaternary Science Reviews* **26** (17-18), pp. 2042–2066.

Tzedakis, P., H. Hooghiemstra, & H. Pälike (2006). The last 1.35 million years at Tenaghi Philippon: revised chronostratigraphy and long-term vegetation trends. *Quaternary Science Reviews* **25** (23-24), pp. 3416–3430.

Wagner, B., H. Vogel, A. Francke, T. Friedrich, T. Donders, J. H. Lacey, M. J. Leng, E. Regattieri, L. Sadori, T. Wilke, G. Zanchetta, C. Albrecht, A. Bertini, N. Combourieu-Nebout, A. Cvetkoska, B. Giaccio, A. Grazhdani, T. Hauffe, J. Holtvoeth, S. Joannin, E. Jovanovska,

J. Just, K. Kouli, I. Kousis, A. Koutsodendris, S. Krastel, M. Lagos, N. Leicher, Z. Levkov, K. Lindhorst, A. Masi, M. Melles, A. M. Mercuri, S. Nomade, N. Nowaczyk, K. Panagiotopoulos, O. Peyron, J. M. Reed, L. Sagnotti, G. Sinopoli, B. Stelbrink, R. Sulpizio, A. Timmermann, S. Tofilovska, P. Torri, F. Wagner-Cremer, T. Wonik, & X. Zhang (2019). Mediterranean winter rainfall in phase with African monsoons during the past 1.36 million years. *Nature* **573** (7773), pp. 256–260.

Wang, Y. J., H. Cheng, R. L. Edwards, Z. S. An, J. Y. Wu, C.-C. Shen, & J. A. Dorale (2001). A High-Resolution Absolute-Dated Late Pleistocene Monsoon Record from Hulu Cave, China. *Science* **294** (5550), pp. 2345–2348.

Wang, Y., H. Cheng, R. L. Edwards, X. Kong, X. Shao, S. Chen, J. Wu, X. Jiang, X. Wang, & Z. An (2008). Millennial- and orbital-scale changes in the East Asian monsoon over the past 224,000 years. *Nature* **451** (7182), pp. 1090–1093.

Wassenburg, J. A., A. Immenhauser, D. K. Richter, K. P. Jochum, J. Fietzke, M. Deininger, M. Goos, D. Scholz, & A. Sabaoui (2012). Climate and cave control on Pleistocene/Holocene calcite-to-aragonite transitions in speleothems from Morocco: Elemental and isotopic evidence. *Geochimica et Cosmochimica Acta* **92**, pp. 23–47.

Weber, M., D. Scholz, A. Schröder-Ritzrau, M. Deininger, C. Spötl, F. Lugli, R. Mertz-Kraus, K. P. Jochum, J. Fohlmeister, C. F. Stumpf, & D. F. Riechelmann (2018). Evidence of warm and humid interstadials in central Europe during early MIS 3 revealed by a multi-proxy speleothem record. *Quaternary Science Reviews* **200**, pp. 276–286.

Wedepohl, H. K. (1995). The composition of the continental crust. *Geochimica et Cosmochimica Acta* **59** (7), pp. 1217–1232.

Wulf, S., M. Kraml, A. Brauer, J. Keller, & J. F. Negendank (2004). Tephrochronology of the 100 ka lacustrine sediment record of Lago Grande di Monticchio (southern Italy). *Quaternary International* **122** (1), pp. 7–30.

Wüst, G. (1961). On the vertical circulation of the Mediterranean Sea. *Journal of Geophysical Research* **66** (10), pp. 3261–3271.

Xoplaki, E., J. F. González-Rouco, J. Luterbacher, & H. Wanner (2003). Mediterranean summer air temperature variability and its connection to the large-scale atmospheric circulation and SSTs. *Climate Dynamics* **20** (7-8), pp. 723–739.

# 3 $^{230}$Th/U-dating of the Cueva Victoria flowstone sequence: Preliminary results and paleoclimate implications

Budsky, A.[1, 2], Scholz, D.[2], Gibert, L.[3], and Mertz-Kraus, R.[2]

[1]Biogeochemistry Department, Max Planck Institute for Chemistry, P. O. Box 3060, 55020 Mainz, Germany
[2]Institute for Geosciences, Johannes Gutenberg University Mainz, Johann-Joachim-Becher-Weg 21, 55128 Mainz, Germany
[3]Universitat de Barcelona, Facultat de Geologia, Departament de Geoquímica, Petrologia i Prospecció Geològica, Martí Franquès s/n, 02028, Barcelona, Spain.

**Abstract** Here we present preliminary multi-collector inductively coupled plasma mass spectrometry (MC-ICPMS) $^{230}$Th/U-ages for one drill core from a flowstone sequence from Cueva Victoria, south-east Spain. The ages suggest several humid phases during the last 450 ka in the cave region, which is today one of the driest areas in southern Europe. Flowstone growth at this cave site is very sensitive to the availability of precipitation and probably only occurred during periods with higher precipitation than today. Dated growth periods mainly coincide with global warm phases (interglacial periods). This probably results from a northward shift of the ITCZ during interglacial periods and increasing convection over the Mediterranean Sea due to higher SSTs. However, we also observe speleothem growth during the globally cold MIS 6, which correlates well with the occurrence of arboreal pollen in the Mediterranean region at this time period, which is an indicator for wetter climate and established forests.

**Keywords:** speleothem, flowstone, $^{230}$Th/U-dating, interglacial period

**Resumen** En este trabajo se presentan resultados preliminares de dataciones por el método $^{230}$Th/U de un testigo recogido en una secuencia de espeleotemas de Cueva Victoria, en el SE de España. Las muestras del testigo se analizaron mediante MC-ICP-MS (espectrometría de masas

con fuente de plasma de acoplamiento inductivo multicolector). Las edades obtenidas sugieren distintas fases húmedas durante los últimos 450 ka en esta región, que actualmente es de las más áridas del sur de Europa. El crecimiento de espeleotemas en esta cueva es muy sensible a la precipitación y probablemente sólo tuvo lugar durante periodos con una precipitación mayor que la actual. Los periodos de crecimiento datados coinciden mayoritariamente con fases cálidas globales (periodos interglaciares). Ésto probablemente fue resultado del desplazamiento hacia el norte de la ITCZ (Zona de Convergencia Intertropical) durante periodos interglaciares y a un incremento de la convección en el Mediterráneo debido a temperaturas más altas de las aguas superficiales. Sin embargo, también se observa un crecimiento de espeleotema durante el periodo frío MIS 6, el cual se correlaciona bien con la presencia de polen arbóreo en la región Mediterránea, indicando un clima húmedo y el desarrollo de zonas boscosas.

**Palabras Clave:** espeleotema, flowstone, datación $^{230}$Th/U, periodo interglacial

## 3.1 Introduction

Speleothems are secondary calcite precipitates growing in caves, such as stalagmites or flowstones. They are increasingly used as paleoclimate archives because they are found worldwide, provide long, continuous climate records, and offer a variety of paleoclimate proxies, which can be measured at high temporal resolution (Fairchild and Baker, 2012). Their major advantage compared to other paleoclimate archives, such as lacustrine or marine sediment or ice cores, which are often difficult to date beyond the limits of the $^{14}$C-dating method, is that they can be precisely dated applying the $^{230}$Th/U dating method for material <600 ka (Richards and Dorale, 2003; Scholz and Hoffmann, 2008). Older samples (>800 ka) can be dated with the U-Pb-dating method (e.g., Bajo et al., 2012; Cliff et al., 2010). Speleothem growth can be summarized as follows: Rain water percolating through the soil above the cave equilibrates with the high soil pCO2 produced by root respiration and microbial activity (Fig. 1). This results in the formation of carbonic acid, which then dissolves the calcareous host rock until the water is saturated with respect to calcite. Inside the cave or cavities along the flow path, where pCO2 is usually lower than in the soil zone, CO2 degasses, the solution becomes supersaturated with respect to calcite, calcite precipitates and speleothems form (Dreybrodt and Scholz, 2011). During growth, speleothems incorporate a variety of climate proxies, which can be measured at high temporal resolution. The most commonly used proxies are stable oxygen and carbon isotope ratios ($\delta^{18}$Oand $\delta^{13}$C, e.g., McDermott, 2004; Lachniet, 2009). In the Mediterranean region, the $\delta^{18}$Ovalues of precipitation correlate with the amount of rainfall (e.g., Ayalon et al., 1998), whereas $\delta^{13}$Cvalues reflect changes in vegetation allowing to distinguish, for instance, between C3 and C4 plant cover (Cerling et al., 1993). Trace elements are also increasingly used as climate proxies in speleothems (Jochum et al., 2012). For instance, Mg/Ca and Sr/Ca ratios have been

shown to reflect the amount of precipitation above the cave (e.g., Fairchild and Treble, 2009). Speleothems also incorporate ferromagnetic iron oxides preserving the inclination and direction of the Earth's magnetic field (Bosák et al., 2003). Here we present preliminary $^{230}$Th/U-ages for a flowstone sequence from Cueva Victoria (south-east Spain), which shows a wide distribution of ages. Our data indicate that the flowstone mainly grew during warm and wet interglacial phases, whereas almost no growth occurred during cold and dry glacial phases. The growth periods of the Cueva Victoria flowstone may, thus, represent a useful archive to reconstruct the timing and duration of past interglacial periods, which are usually reconstructed using benthic $\delta^{18}$Ovalues in deep sea sediment cores.

## 3.2 Geological setting and material

Cueva Victoria is located near Cartagena in south-east Spain, which is one of the driest regions in southern Europe with an annual precipitation between 200 and 300 mm/a (Agencia Estatal de Meteorología, 2011). The cave is situated within calcareous Triassic lime- and dolostones of the inner Betic System (Nevado-Filabride, López-Gómez et al., 2002), which are exposed in this area. Close to the cave, Neogene basaltic rocks are exposed (Bellon et al., 1983). Cueva Victoria is well-known for the spectacular occurrence of Pleistocene fauna including early humans and African species (Gibert et al., 2008; Gibert, 1993). The galleries of the cave that were connected with the surface are filled with three stratigraphic units: basal red clay with Manganese nodules and layers, a heterometric breccia, rich in vertebrate fossils, and a capping flowstone on top (Gibert et al., 1999) with a thickness of approximately 10 cm. Other flowstones occur in deeper galleries of the cave that were not connected with the surface. These flowstones usually are up to 60 cm thick, grow on top of decalcified clay or intrakarst breccias and cover large areas of the cave. In some parts of the cave, the flowstone sequence is interrupted by sediment layers. Mertz-Kraus et al. (2011) recognized a polarity change in the lowest part of the flowstone, which might correspond to the Brunhes-Matuyama reversal (Love and Mazaud, 1997).

We collected different drill core samples of several flowstones in different galleries of Cueva Victoria (Figure 3.2), with a width of 5 cm and a length of up to 50 cm (Figure 3.2). In addition, we sampled a stalagmite and the flowstone CV09, which grows on top of the fossiliferous breccia (Mertz-Kraus et al., 2011). The drill cores were obtained using a mobile drilling machine, usually used for sampling concrete. From these drill cores, ca. 1 cm thick slabs were prepared at the University of Mainz using a diamond slab saw.

## 3.3 Methods

Preliminary $^{230}$Th/U-dating of the flowstone was performed by multi-collector inductively coupled plasma mass spectrometry (MC-ICP-MS) at the Max Planck Institute for Chemistry (MPIC), Mainz, Germany, using a Nu Plasma MC-ICP-MS (Nu Instruments, Wrexham, United Kingdom). Small samples of ca. 0.3 g were cut from the obtained drill cores and dissolved in $HNO_3$.

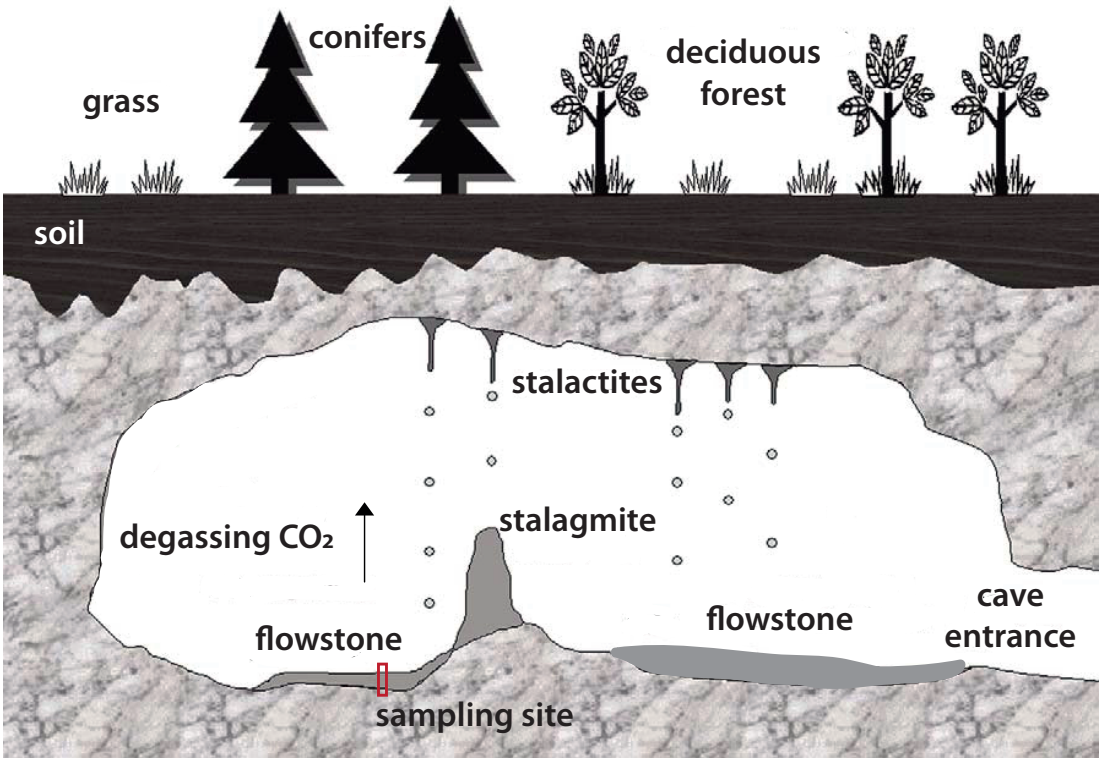


Figure 3.1: Sketch of a cave summarizing the principles of speleothem growth (modified from Frisia and Borsato, 2010). The red rectangle indicates a drill core taken from a flowstone.

Then one droplet of a mixed $^{233}U/^{236}U/^{229}Th$-spike was added. Uranium and Th were separated from the calcite matrix by conventional ion exchange column chemistry (e.g., Hoffmann, 2008). Uranium and Th isotopes were then measured separately as described elsewhere (Hoffmann et al., 2007; Zak et al., 2012; Jochum et al, 2011; Scholz et al., 2014). The $^{230}Th/U$-ages and corresponding errors were calculated by solving the age equation (Eqn.3.1; see e.g., Ivanovich and Harmon, 1992) and a Monte-Carlo simulation (Ludwig, 2003).

$$\left(\frac{^{230}Th}{^{238}U}\right)(t) = (1 - e^{-\lambda_{230}t}) + \left(\left(\frac{^{234}U}{^{238}U}\right)(t) - 1\right)\frac{\lambda_{230}}{\lambda_{230} - \lambda_{234}}(1 - e^{-(\lambda_{230}-\lambda_{234})t}) \qquad (3.1)$$

where ($^{230}Th/^{238}U$) and ($^{234}U/^{238}U$) are the measured activity ratios, and the li's are the decay constants for $^{230}Th$, $^{234}U$, and $^{238}U$ respectively (Cheng et al., 2000; Jaffey et al., 1971). In order to account for potential detrital contamination, we calculated corrected ages applying the standard procedure for correction for detrital U and Th isotopes assuming a bulk Earth $^{232}Th/^{238}U$ weight ratio of 3.8 for the detritus and $^{230}Th$, $^{234}U$ and $^{238}U$ in secular equilibrium.

Figure 3.2: (Left panel) Sampling of the Cueva Victoria flowstone sequence using a mobile drilling machine (picture courtesy of C. Rossi). (Right panel) The obtained cores have a length of ca. 50 cm and a width of 5 cm.

## 3.4 Results

Analytical results and calculated ages are given in Table 3.1 and Figures 3.3 and 3.4. The hitherto available results of drill core Vic-III-2 show several distinct growth phases between 73.2 ±1.0 kaand 411.6 +34.9 -25.5 ka (Figure 3.3). In general, the U concentrations are relatively low, ranging from 0.09 µg/g at the top to 0.17 µg/g at ca. 15 cm distance from the top. Consequently, precise dating of the Cueva Victoria flowstone is challenging. The effect detrital correction is insignificant for all ages (Table 3.1).

## 3.5 Discussion

Flowstone growth strongly depends on the availability and storage of water in the karst aquifer. Our preliminary results indicate that the Cueva Victoria flowstone preferentially grew during interglacial periods (Figure 3.4), probably because climate conditions were too dry for speleothem growth during glacial periods. This is consistent with results from sea surface temperature (SST) records from the Iberian Margin (Martrat et al., 2007) and the amount of arboreal pollen in Greece (Figure 3.3). Our flowstone sequence should, thus, present a valuable archive to reconstruct the transitions from cold to warm phases and consequently the timing and duration of past interglacial periods in south-east Spain. For instance, the three warm episodes corresponding to Marine Isotope Stage (MIS) 5 are well represented in our record and can be clearly distinguished

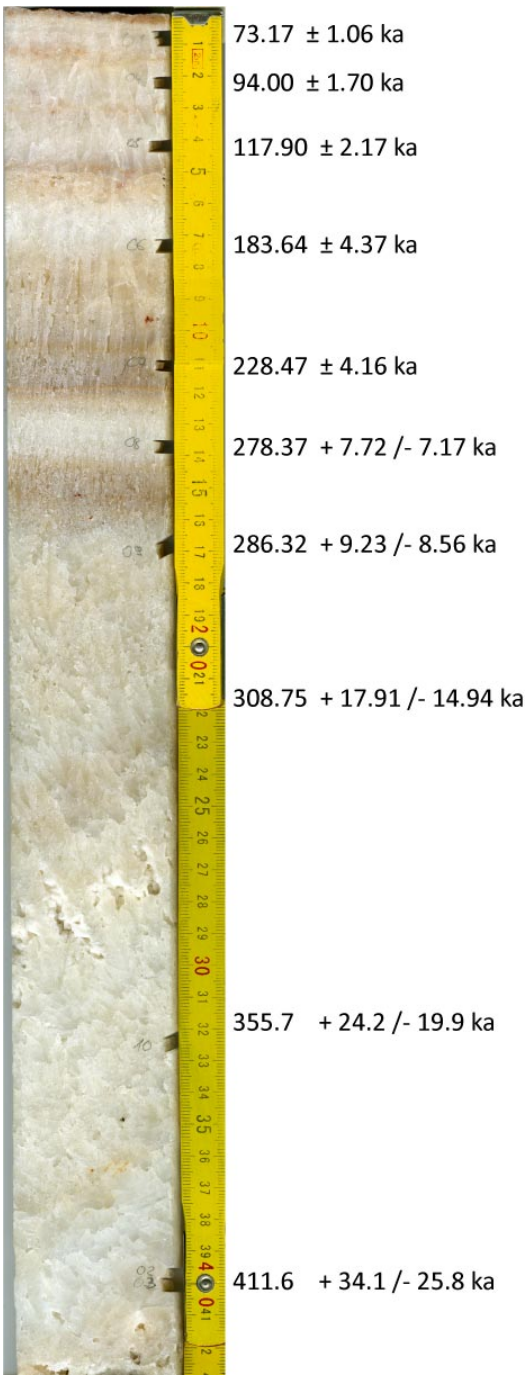


Figure 3.3: Drill core Vic-III-2. The obtained $^{230}$Th/U ages are indicated.

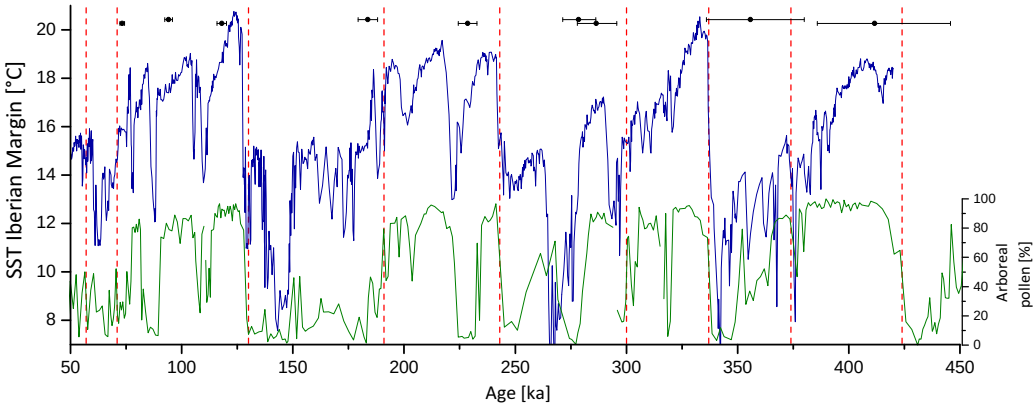


Figure 3.4: Compilation of the $^{230}$Th/U-ages (black). All errors are shown at the 2s-level. Also shown are a sea surface temperature (SST) record from the Iberian Margin (Martrat et al., 2007) and the amount of arboreal pollen from Greece (Tzedakis et al., 2006; Tzedakis et al., 2003). The division into interglacial (yellow shading) and glacial periods as well as the Marine Isotope Stages (MIS) has been adapted from Lisiecki and Raymo (2005).

from each other by a brown layer. However, one age (183.6 ± 4.4 ka, Vic-III-2-06) suggests speleothem growth during the cold MIS 6, confirming previous results from other studies in the Mediterranean region (Argentarola cave, Italy, Bard et al., 2002 and Soreq cave, Israel, Ayalon et al., 2002), also identifying a wet period around 170 ka. Flowstone growth also occurs during MIS 8 (Figures 3.3 and 3.4).

In general, growth of the Cueva Victoria flowstone seems to be strongly related to wetter conditions in this region, which mainly correspond to interglacial periods. A potential mechanism would be a northward shift of the Inner Tropical Convergence Zone (ITCZ, Tisserand et al., 2009) during interglacial periods, which would result in an increase of the amount of precipitation. Additionally, increasing convection over the Mediterranean Sea with higher SSTs is supposed to increase precipitation in coastal regions significantly. During glacial periods, when SST in the Alboran Sea was only 8 °C, convection is supposed to have been suppressed (Cacho et al., 2000; Martrat et al., 2007; 2014).

## 3.6 Conclusions

Preliminary $^{230}$Th/U-dating of the Cueva Victoria flowstone sequence suggests several humid phases during the last 450 ka in south-east Spain, which is today one of the driest regions in southern Europe. Flowstone growth at this cave site is very sensitive to precipitation and only occurred during periods with higher precipitation than today. Growth periods mainly coincide with global warm phases (interglacial periods). This probably results from a northward shift of

Table 3.1: $^{230}$Th/U analytical data and ages for drill core Vic-III-2

| Sample | dft [mm] | $^{238}$U [µg/g] | ± | ($^{230}$Th/$^{232}$Th) | ± | ($^{234}$U/$^{238}$U) | ± | ($^{230}$Th/$^{238}$U) | ± | age uncorrected [ka] | ± | age corrected [ka] | ± |
|---|---|---|---|---|---|---|---|---|---|---|---|---|---|
| Vic-III-2-01 | 7 | 0.0906 | 0.0006 | 581.7 | 8.5 | 1.0743 | 0.0045 | 0.5282 | 0.0047 | 73.2 | 1.0 | 73.2 | 1.1 |
| Vic-III-2-04 | 20 | 0.1001 | 0.0006 | 1444.3 | 26.7 | 1.0597 | 0.0019 | 0.6159 | 0.0072 | 94.0 | 1.7 | 94.0 | 1.7 |
| Vic-III-2-05 | 40 | 0.1155 | 0.0008 | 3213.1 | 67.3 | 1.0554 | 0.0016 | 0.7024 | 0.0071 | 117.9 | 2.2 | 117.9 | 2.2 |
| Vic-III-2-06 | 72 | 0.0973 | 0.0006 | 1161.0 | 19.3 | 1.0573 | 0.0016 | 0.8709 | 0.0080 | 183.7 | 4.3 | 183.6 | 4.4 |
| Vic-III-2-07 | 109 | 0.169 | 0.001 | 445.0 | 4.4 | 1.0450 | 0.0016 | 0.9264 | 0.0048 | 228.6 | 4.2 | 228.5 | 4.2 |
| Vic-III-2-08 | 135 | 0.169 | 0.001 | 1705.1 | 17.5 | 1.0423 | 0.0018 | 0.9726 | 0.0055 | 278.4 | 7.2 | 278.4 | +7.7/ -7.2 |
| Vic-III-2-09 | 165 | 0.1344 | 0.0009 | 675.7 | 7.6 | 1.0513 | 0.0018 | 0.9894 | 0.0063 | 286.4 | +9.0/ -8.3 | 286.3 | +9.2/ -8.6 |
| Vic-III-2-11 | 215 | 0.1211 | 0.0009 | 1433.6 | 23.0 | 1.0422 | 0.0041 | 0.9932 | 0.0086 | 308.8 | +18.2/ -14.9 | 308.8 | +17.9/ -14.9 |
| Vic-III-2-10 | 320 | 0.1530 | 0.0010 | 2775.8 | 38.1 | 1.0420 | 0.0015 | 1.0159 | 0.0083 | 355.7 | +25.1/ -19.7 | 355.7 | +24.2/ -19.9 |
| Vic-III-2-03 | 399 | 0.1161 | 0.0007 | 576.6 | 6.6 | 1.0420 | 0.0021 | 1.0332 | 0.0064 | 411.7 | +34.9/ -25.5 | 411.6 | +34.1/ -25.8 |

All isotope ratios are given as activity ratios. Uncertainties are stated at the 2$\sigma$ level.

the ITCZ during interglacial periods and increasing convection over the Mediterranean Sea due to higher SSTs. However, we also observe speleothem growth during the globally cold MIS 6, which correlates well with the occurrence of arboreal pollen in the Mediterranean region at this time period, which is an indicator for wetter climate and established forests. In future studies, we will expand $^{230}$Th/U-dating to other cores to obtain precise age models for each drill core. Furthermore, we will reconstruct past climate and vegetation changes in this currently particularly dry region by measuring paleoclimate proxies, such as trace elements and stable isotopes, at high temporal resolution.

## 3.7 Acknowledgements

We thank K. P. Jochum and M. O. Andreae (MPIC, Mainz) for their ongoing interest in our work and their support. Our special thanks go to the members of the Centro de Estudios de la Naturaleza y el Mar (CENM) for their valuable technical support during sampling at Cueva Victoria. The City of Cartagena is thanked for administrative support. AB acknowledges funding by the Research Centre Geocycles (University of Mainz) and the MPIC, Mainz.

### References

Agencia Estatal de Meteorología (2011) Atlas climático ibérico: Temperatura del aire y precipitación (1971-2000) [Iberian climate atlas air temperature and precipitation (1971-2000)], Madrid: Instituto Nacional de Meteorología, 79 pp.

Ayalon, A., Bar-Matthews, M., Kaufman, A., 2002. Climatic conditions during marine oxygen isotope stage 6 in the eastern Mediterranean region from the isotopic composition of speleothems of

Soreq Cave, Israel. Geol 30 (4), 303–306.

Ayalon, A., Bar-Matthews, M., Sass, E., 1998. Rainfall-recharge relationships within a karstic terrain in the Eastern Mediterranean semi-arid region, Israel: ? 18O and ?D characteristics. Journal of Hydrology 207 (1-2), 18–31.

Bajo, P., Drysdale, R., Woodhead, J., Hellstrom, J., Zanchetta, G., 2012. High-resolution U–Pb dating of an Early Pleistocene stalagmite from Corchia Cave (central Italy). Quaternary Geochronology 14, 5–17.

Bard, E., Antonioli, F., Silenzi, S., 2002. Sea-level during the penultimate interglacial period based on a submerged stalagmite from Argentarola Cave (Italy). Earth and Planetary Science Letters 196 (3-4), 135–146.

Bellon, H., Bordet, P., Montenat, C., 1983. Chronologie du magmatisme néogène des Cordillières bétiques (Espagne méridionale). Bulletin de la Société Géologique de France 25 (7), 205–217.

Bosák, P., Pruner, P., Kadlec, J., 2003. Magnetostratigraphy of cave sediments: Application and limits. Studia Geophysica et Geodaetica 47 (2), 301–330.

Cacho, I., Grimalt, J.O., Sierro, F.J., Shackleton, N., Canals, M., 2000. Evidence for enhanced Mediterranean thermohaline circulation during rapid climatic coolings. Earth and Planetary Science Letters 183 (3-4), 417–429.

Cerling, T.E., Wang, Y., Quade, J., 1993. Expansion of C4 ecosystems as an indicator of global ecological change in the late Miocene. Nature 361 (6410), 344–345.

Cheng H., Edwards R. L., Hoff J., Gallup C. D., Richards D. A., and Asmerom Y., 2000. The half-lives of uranium-234 and thorium-230. Chemical Geology 169, 17-33.

Cliff, R.A., Spötl, C., Mangini, A., 2010. U–Pb dating of speleothems from Spannagel Cave, Austrian Alps: A high resolution comparison with U–series ages. Quaternary Geochronology 5 (4), 452–458.

Dreybrodt, W., Scholz, D., 2011. Climatic dependence of stable carbon and oxygen isotope signals recorded in speleothems: From soil water to speleothem calcite. Geochimica et Cosmochimica Acta 75 (3), 734–752.

Fairchild, I.J., Treble, P.C., 2009. Trace elements in speleothems as recorders of environmental change. Quaternary Science Reviews 28 (5-6), 449–468.

Fairchild, I.J., Baker, A., 2012. Speleothem science: From process to past environments. Wiley, Oxford, U.K, Hoboken, N.J, 1 online resource (xiv, 432.

Frisia, S., Borsato, A., 2010. Karst, in: van Loon, A.J. (Ed.), Carbonates in continental settings. Facies, environments, and processes. Developments in sedimentology 61. Elsevier Science, Amsterdam, London, pp. 269–318.

Gibert, J., 1993. Significado de la faunade Cueva Victoria. Memorias de Arqueologia 8, 26–32.

Gibert, J., Gibert, L., Canyadell, C.F., Robot, F., Iglesias, A., Gibert, P., 1999. Cueva Victoria: Geología, paleontología, restos humanos y edades. Memorias de Arqueologia 14, 37–62.

Gibert, J., Gibert, L., Ribot, F., Ferràndez-Canadell, C., Sánchez, F., Iglesias, A., Walker, M., 2008.

CV-0, an early Pleistocene human phalanx from Cueva Victoria (Cartagena, Spain). Journal of Human Evolution 54 (1), 150–156.

Hoffmann, D.L., 2008. $^{230}$Th isotope measurements of femtogram quantities for U-series dating using multi ion counting (MIC) MC-ICPMS. International Journal of Mass Spectrometry 275 (1-3), 75–79.

Hoffmann, D.L., Prytulak, J., Richards, D.A., Elliott, T., Coath, C.D., Smart, P.L., Scholz, D., 2007. Procedures for accurate U and Th isotope measurements by high precision MC-ICPMS. International Journal of Mass Spectrometry 264 (2-3), 97–109.

Ivanovich, M., Harmon, R. (Eds.), 1992. Uranium-series disequilibrium: Applications to earth, marine, and environmental sciences. Clarendon Press, Oxford, 910 pp.

Jaffey A. H., Flynn K. F., Glendenin L. E., Bentley W. C., and Essling A. M., 1971. Precision Measurement of Half-Lives and Specific Activities of 235U and $^{238}$U. Physical Reviews C4, 1889-1906.

Jochum, K.P., Wilson, S.A., Abouchami, W., Amini, M., Chmeleff, J., Eisenhauer, A., Hegner, E., Iaccheri, L.M., Kieffer, B., Krause, J., McDonough, W.F., Mertz-Kraus, R., Raczek, I., Rudnick, R.L., Scholz, D., Steinhoefel, G., Stoll, B., Stracke, A., Tonarini, S., Weis, D., Weis, U., Woodhead, J.D., 2011. GSD-1G and MPI-DING Reference Glasses for In Situ and Bulk Isotopic Determination. Geostandards and Geoanalytical Research 35 (2), 193–226.

Jochum, K. P., Scholz, D., Stoll, B., Weis, U., Wilson, S. A., Yang, Q., Schwalb, A., Börner, N., Jacob, D. E., and Andreae, M. O., 2012. Accurate trace element analysis of speleothems and biogenic calcium carbonates by LA-ICP-MS. Chemical Geology 318-319, 31-44.

Lachniet, M.S., 2009. Climatic and environmental controls on speleothem oxygen-isotope values. Quaternary Science Reviews 28 (5-6), 412–432.

Lisiecki, L.E., Raymo, M.E., 2005. A Pliocene-Pleistocene stack of 57 globally distributed benthic $\delta^{18}$Orecords. Paleoceanography 20 (1), PA1003.

López-Gómez, J., Arche, A., Pérez-López, A., 2002. Permian and Triassic, in: Gibbons, W., Moreno, T. (Eds.), The geology of Spain. Geological Society, London, pp. 185–212.

Love, J., Mazaud, A., 1997. A database for the Matuyama-Brunhes magnetic reversal. Physics of the Earth and Planetary Interiors 103 (3-4), 207–245.

Ludwig, K.R., 2003. Mathematical-statistical treatment of data and errors for $^{230}$Th/U geochronology, in: Bourdon, B., Henderson, G.M., Lundstrom, C.C., Turner, S.P. (Eds.), Uranium-series geochemistry. Reviews in mineralogy and geochemistry 52. Geochemical Society; Mineralogical Society of America, [St. Louis, Mo.], Washington, DC, pp. 631–656.

Martrat, B., Grimalt, J.O., Shackleton, N.J., Abreu, L. de, Hutterli, M.A., Stocker, T.F., 2007. Four Climate Cycles of Recurring Deep and Surface Water Destabilizations on the Iberian Margin. Science 317 (5837), 502–507.

Martrat, B., Jimenez-Amat, P., Zahn, R., Grimalt, J.O., 2014. Similarities and dissimilarities between the last two deglaciations and interglaciations in the North Atlantic region. Quaternary Science Reviews 99, 122–134.

McDermott, F., 2004. Palaeo-climate reconstruction from stable isotope variations in speleothems: a review. Quaternary Science Reviews 23 (7-8), 901–918.

Mertz-Kraus, R., Kocot, Y., Gibert, L., Scott, G.R., Jochum, K.P., 2011. Changing environmental conditions during a geomagnetic reversal: Evidence from trace element and isotope variations on Pleistocene flowstone sequences from Cueva Victoria (SE Spain). AGU Fall Meeting Abstracts, C1892.

Richards, D.A., Dorale, J.A., 2003. Uranium-series Chronology and Environmental Applications of Speleothems. Reviews in Mineralogy and Geochemistry 52 (1), 407–460.

Scholz, D., Hoffmann, D., 2008. $^{230}$Th/U-dating fossil corals and speleothems. Special issue: Recent progress in Quaternary dating methods 57 (1/2), 52–76.

Scholz, D., Tolzmann, J., Hoffmann, D.L., Jochum, K.P., Spötl, C., Riechelmann, D.F., 2014. Diagenesis of speleothems and its effect on the accuracy of $^{230}$Th/U-ages. Chemical Geology 387, 74–86.

Tisserand, A., Malaizé, B., Jullien, E., Zaragosi, S., Charlier, K., Grousset, F., 2009. African monsoon enhancement during the penultimate glacial period (MIS 6.5 $\approx$ 170 ka) and its atmospheric impact. Paleoceanography 24 (2), n/a.

Tzedakis, P., Hooghiemstra, H., Pälike, H., 2006. The last 1.35 million years at Tenaghi Philippon: revised chronostratigraphy and long-term vegetation trends. Quaternary Science Reviews 25 (23-24), 3416–3430.

Tzedakis, P., McManus, J., Hooghiemstra, H., Oppo, D., Wijmstra, T., 2003. Comparison of changes in vegetation in northeast Greece with records of climate variability on orbital and suborbital frequencies over the last 450 000 years. Earth and Planetary Science Letters 212 (1-2), 197–212.

Žák, K., Richter, D.K., Filippi, M., Živor, R., Deininger, M., Mangini, A., Scholz, D., 2012. Coarsely crystalline cryogenic cave carbonate – a new archive to estimate the Last Glacial minimum permafrost depth in Central Europe. Clim. Past 8 (6), 1821–1837.

# 4 Speleothem $\delta^{13}$C record suggests enhanced spring/summer drought in south-eastern Spain between 9.7 and 7.8 ka – a circum-Western Mediterranean anomaly?

Budsky, Alexander[1], Scholz, Denis[1], Wassenburg, Jasper A.[2], Mertz-Kraus, Regina[1], Spötl, Christoph[3], Riechelmann, Dana F.C.[1], Gibert, Luis[4], Jochum, Klaus Peter[3], Andreae, Meinrat O.[2, 5]

[1]Institute for Geosciences, Johannes Gutenberg University Mainz, Mainz, Germany
[2]Climate Geochemistry Department, Max Planck Institute for Chemistry, Mainz, Germany
[3]Institute of Geology, University of Innsbruck, Innsbruck, Austria
[4]Departament de Mineralogia, Petrologia i Geologia aplicada, Universitat de Barcelona, Barcelona, Spain
[5]Geology and Geophysics Department, King Saud University, Riyadh, Saudi Arabia

Corresponding author:
Alexander Budsky, Institute for Geosciences, Johannes Gutenberg University Mainz,
Johann-Joachim-Becher-Weg 21, 55128 Mainz, Germany
Phone: 0049 (0)6131-39-23173
Email: albudsky@students.uni-mainz.de

**Abstract** South-eastern Spain is one of the driest regions in Europe and thus, prone to drought. Terrestrial climate records covering the Late Glacial and Holocene from this area are sparse. Here we present a flowstone record from Cueva Victoria, south-eastern Spain, which covers the Late Glacial (15 ka) to the mid-Holocene (7 ka) including the Younger Dryas (YD). Between the onset of the Bølling/Allerød (B/A) and the Early Holocene, flowstone $\delta^{18}$O values progressively decrease in accordance with sea-surface temperatures in the Alboran Sea, indicating an increase in precipitation in south-eastern Spain and a supra-regional signal of North Atlantic temperature change. At the same time, decreasing $\delta^{13}$C values suggest progressively increasing precipitation and vegetation density. This trend is interrupted by both colder and drier conditions during the YD. Between $9.7 \pm 0.3$ and $7.8 \pm 0.2$ ka, a large positive excursion of the $\delta^{13}$C values indicates

a strong reduction in vegetation density, probably as a consequence of very dry spring/summer conditions. In combination with the continuously low speleothem $\delta^{18}O$ values and a nearly unchanged growth rate, this suggests increased seasonality (i.e., drier spring/summer conditions, but not a strong reduction in annual precipitation). This is consistent with several other climate records from the Western Mediterranean region, showing that the Western Mediterranean realm (Spain, Italy) experienced pronounced spring/summer drought during this time interval. Interestingly, the timing of this dry period coincided with the African Humid Period. This may be part of a teleconnection with the North African Monsoon via the Hadley cell circulation.

**Keywords** U-series dating; Holocene; stable oxygen isotopes; stable carbon isotopes; southeastern Spain; drought

## 4.1 Introduction

In the last decades, speleothems (secondary carbonates in caves) have been established as important terrestrial paleoclimate archives (Fairchild and Baker, 2012; Henderson, 2006). Their greatest advantage compared to other terrestrial archives, such as lake sediments, is that they can be very precisely dated by the $^{230}Th/U$-dating method, even beyond the limit of $^{14}C$ dating (>50 ka) (Scholz and Hoffmann, 2008; Richards and Dorale, 2003). In addition, speleothems occur worldwide and are usually well preserved in the sheltered cave environment. Several climate proxies, such as stable oxygen ($\delta^{18}O$, e.g., McDermott, 2004; Lachniet, 2009) and carbon isotope values ($\delta^{13}C$, e.g., Rudzka et al., 2011; Ridley et al., 2015; Genty et al., 2005) as well as trace element concentrations (e.g., Fairchild and Treble, 2009), can be measured at high temporal resolution. The $\delta^{18}O$ values in speleothems from the Mediterranean region are commonly interpreted as a proxy for changes in precipitation (e.g., Ayalon et al., 1998; Ayalon et al., 2002; Bard et al., 2002), while at higher latitudes and altitudes, they are assumed to be more sensitive to temperature changes (e.g., Boch et al., 2009; Fohlmeister et al., 2012; McDermott et al., 2011). However, speleothem $\delta^{18}O$ values can also be affected by several other processes (Lachniet, 2009; McDermott, 2004). Speleothem $\delta^{13}C$ values can be interpreted as a proxy for changes in the composition (Cerling et al., 1993; Denniston et al., 2000; Dorale et al., 1998) and density (Fohlmeister et al., 2011) of the vegetation above the cave and microbiological activity in the soil (Genty et al., 2003; Genty et al., 2006; Breecker et al., 2012; Meyer et al., 2014). Since effective meteoric precipitation directly influences vegetation density and soil microbiological activity, it has an effect on soil $pCO_2$ and the $\delta^{13}C$ value of the drip water (Ridley et al., 2015; Meyer et al., 2014). In general, lower $\delta^{13}C$ values correspond to higher vegetation density and microbiological activity in the soil (Fohlmeister et al., 2011). Thus, $\delta^{13}C$ values should increase in case of decreasing precipitation and vegetation density and vice versa. Currently, only a few terrestrial climate reconstructions from the Mediterranean region are available, and these are mainly based on pollen records (Allen et al., 1999; Tzedakis et al., 2004; Tzedakis et al., 2006;

Brauer et al., 2007), near-shore sediments (Mauz et al., 2012; Zazo et al., 2013; Bardají et al., 2009), and speleothems covering glacial-interglacial timescales (Bar-Matthews et al., 2003; Bard et al., 2002; Hodge et al., 2008). In the Western Mediterranean, climate archives covering the onset of the Holocene are even more sparse and mainly limited to pollen sequences (Carrión et al., 2010; Tinner et al., 2009; Pérez-Sanz et al., 2013), lake-level reconstructions (Magny et al., 2011; Magny et al., 2012; Peyron et al., 2013), and speleothem records from Sicily (Frisia et al., 2006), central and northern Italy (Zanchetta et al., 2007; Scholz et al., 2012). The pollen records have a relatively low temporal resolution (e.g. Carrión, 2002) and often do not cover the onset of the Holocene. The speleothem data, in contrast, have a higher temporal resolution (e.g., Genty et al., 2006; Moreno et al., 2017). However, paleoclimate information from speleothems covering the Pleistocene/Holocene transition is not available yet for south-eastern Spain, which is one of the driest regions in southern Europe with a strong seasonality in precipitation. Thus, this is a key area to study past climate variability and changes in seasonality during the Holocene in southern Europe, which are poorly understood. Here we present a high-resolution flowstone stable isotope record from Cueva Victoria, south-eastern Spain, covering the period from 15 to 7 ka. A previous investigation of flowstones from Cueva Victoria showed that they cover at least the last 1 Ma (Gibert et al., 2016) and mainly grew during warm and humid interglacials (Budsky et al., 2015). This demonstrates that the flowstones from Cueva Victoria represent a sensitive hydroclimate archive in this currently semiarid region.

## 4.2 Regional setting

Cueva Victoria (CV) is located in south-eastern Spain between Cartagena and Mar Menor (37.6°N, 0.82°W, 40 m asl, Figure 4.1). The area is one of the driest regions in Europe with an annual precipitation between 200 and 300 mm (Agencia Estatal de Meteorología, 2011). The climate is characterized by a strong seasonality with moderate precipitation during winter and spring (<30 mm/month), followed by a hot and dry summer (<10 mm/month) and a more humid autumn (≈50 mm/month, Figure S2). It is classified as BSk climate according to the Köppen-Geiger classification, which reflects arid cold steppe climate with a mean annual temperature (MAT) <18°C (Kottek et al., 2006). September to November rainfall is transported to the area by cold air masses entering the warm Mediterranean Sea from the north-west (Araguas-Araguas and Diaz Teijeiro, 2005). During the rainy season, most of the rainfall occurs within 20 to 30 days, and 10 to 15 % of the annual precipitation falls during flash flood events (Araguas-Araguas and Diaz Teijeiro, 2005). This rainfall does not penetrate the thin soil cover, but runs off superficially and is, therefore, not available for the vegetation. The annual precipitation pattern is negatively correlated with the Western Mediterranean Oscillation Index (WeMO), the pressure difference between the Gulf of Cadiz (Spain, San Fernando) and Padua (Italy, Po basin; Martin-Vide and Lopez-Bustins, 2006). This is the result of low pressure entering the Western Mediterranean through the Strait of Gibraltar and moisture transported to eastern Spain, whereas Italy is under the influence of high pressure. A positive WeMO index leads to enhanced precipitation

in the eastern Western Mediterranean and reduced precipitation in eastern Spain. There is no significant influence on precipitation by the North Atlantic Oscillation (NAO, Comas-Bru and McDermott, 2014), which has a strong influence in many other parts of Europe (Hurrell and Loon, 1997; Deininger et al., 2016). The annual temperature pattern in south-eastern Spain shows a stronger relationship with the East Atlantic pattern (EA, Ríos-Cornejo et al., 2015). Cueva Victoria formed in Triassic limestones and dolostones of the Inner Betic Cordillera. These rocks belong to the Alpujarride metamorphic complex (San Ginés unit) and are partly karstified (Manteca Martínez and Pina, 2015). In these zones, manganese ore occurs associated with reddish clay, silt and sand linked to south-west striking faults (Manteca Martínez and Pina, 2015). The cave system extends over 3 km laterally and 155 m vertically (Ros and Llamusí, 2015) and consists of several chambers. The original cave system was widened during the last century due to mining for the underlying manganese ore (Manteca Martínez and Pina, 2015). Ventilation of the original cave system was probably lower compared to the very well ventilated situation today ($pCO_2$ <500 ppmV, data provided by the local caving group, CENM-naturaleza), which results from several artificial openings related to mining. The part, where the flowstone core was recovered, is less well ventilated, as is reflected by the high present-day relative humidity (>90 %). Mean annual cave air temperature at the sampling site of the flowstone is 17 °C (CENM-naturaleza).

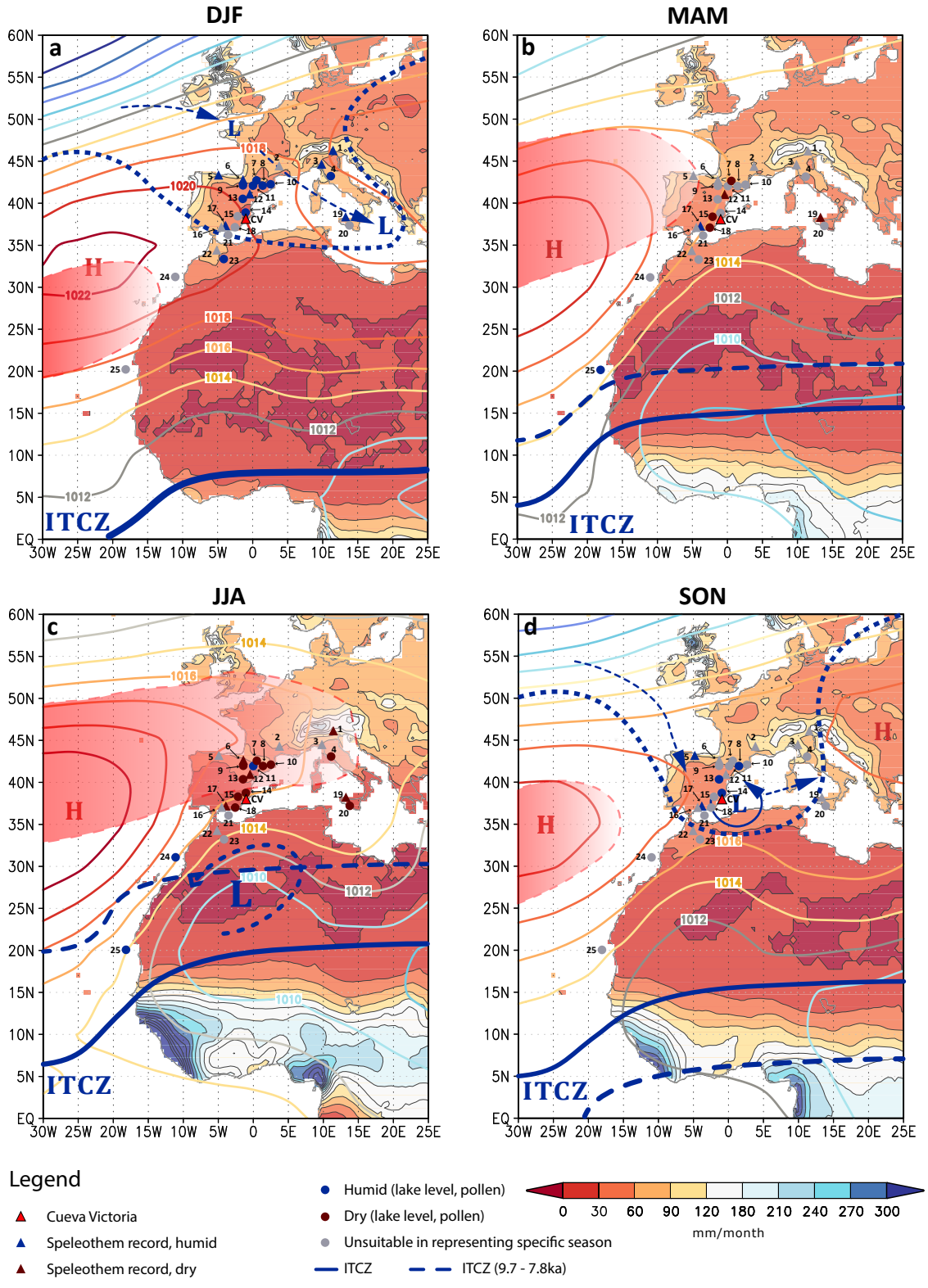


Figure 4.1: Continued.

▲ Figure 4.1 (continued): (a) Modern precipitation (CRU TS 4.01 1901-2016; Harris et al., 2014) and mean sea-level pressure (contour lines; HadSLP 2r, 1850-2018; Allan and Ansell 2006) and the estimated situation for the interval between 9.7 ± 0.3 and 7.8 ± 0.2 ka (dashed lines, see text). For winter (a), spring (b), summer (c) and autumn (d), the estimated northernmost position of the ITCZ (blue lines) is shown. In addition, several records discussed in the text are shown: 1. Ernesto Cave (Scholz et al., 2012); 2. Chauvet Cave (not covering the time interval, Genty et al., 2006); 3. Corchia Cave (Zanchetta et al., 2007); 4. Lake Accesa (Drescher-Schneider et al., 2007; Finsinger et al., 2010; Peyron et al., 2011); 5. Speleothem records from multiple cave sites from northern Spain (Stoll et al., 2013); 6. Kaite Cave (Domínguez-Villar et al., 2017); 7. Basa de la Mora (Pérez-Sanz et al., 2013); 8. Marcelino tufa deposits (Pellicer et al., 2016); 9. Ebro Basin sediments (Bastida et al., 2013); 10. Pollen record, La Garrotxa (Piqué et al., 2018); 11. Lake Estanya (González-Sampériz et al., 2017; Morellón et al., 2009); 12. Molinos Cave (Moreno et al., 2017), 13. Lake Villarquemado (Aranbarri et al., 2014); 14. Lake Salines (Burjachs et al., 2016) and Villena Lake (Jones et al., 2018); 15. Lake Siles (Carrión, 2002); 16. Nerja Cave (McMillan, 2006); 17. Refugio Cave (Walczak et al., 2015); 18. Sediments, San Rafael (Pantaléon-Cano et al., 2003); 19.Grotta di Carburangeli (Frisia et al., 2006); 20. Gorgo Basso (Tinner et al., 2009); 21. Alboran Sea sediment cores MD95-2043 (Cacho et al., 1999; Fletcher et al., 2010; Fletcher and Sánchez Goñi, 2008); ODP161-976 (Combourieu Nebout et al., 2009; Martrat et al., 2014); 22. Grotte de Piste (Wassenburg et al., 2016); 23. Lake Sidi Ali (Zielhofer et al., 2017); 24. GC27 (Tierney et al., 2017); 25. GeoB790-2 (Tjallingii et al., 2008). (For interpretation of the colour-codes, the reader is referred to the online version of this article.)

Cueva Victoria is well known as an Early Pleistocene fossil site with excellently preserved bones of a diverse fauna (Gibert et al., 2016; Gibert and Ferràndez-Canadell, 2015; Ferràndez-Cañadell et al., 2014), including hominin bones (Gibert et al., 2008; Ribot et al., 2015). The fossil-bearing red breccia is covered by a flowstone unit, which occurs throughout the cave and preserves a change in magnetic polarity (Gibert et al., 2016), presumably related to the Brunhes/Matuyama reversal (0.78 Ma). Flowstone thickness is typically between 5 and 15 cm, but may partly exceed 50 cm in the deeper parts of the cave (Gibert et al., 2016).

## 4.3 Material and methods

**Sample collection and preparation** Several flowstone cores were collected from chamber Victoria III (Ros and Llamusí, 2015) using a mobile core drilling device with a diameter of 5 cm. Vic-III-4 has a length of 31 cm, whereas Vic-III-1 and Vic-III-3 are 41.5 and 40.5 cm long, respectively. All cores were embedded in gypsum and cut into slabs (thickness ≈1 cm). One half of the slab was used for polished thin sections (70 µm) to study the crystal fabric (Figure 4.2). Here we focus on the upper 12 cm of Vic-III-4 (Figure 4.2), which correspond to the Holocene (section 4.2). The other two cores mainly grew during older interglacials, and the Holocene is only contained in the upper few millimetres (Figure 4.9).

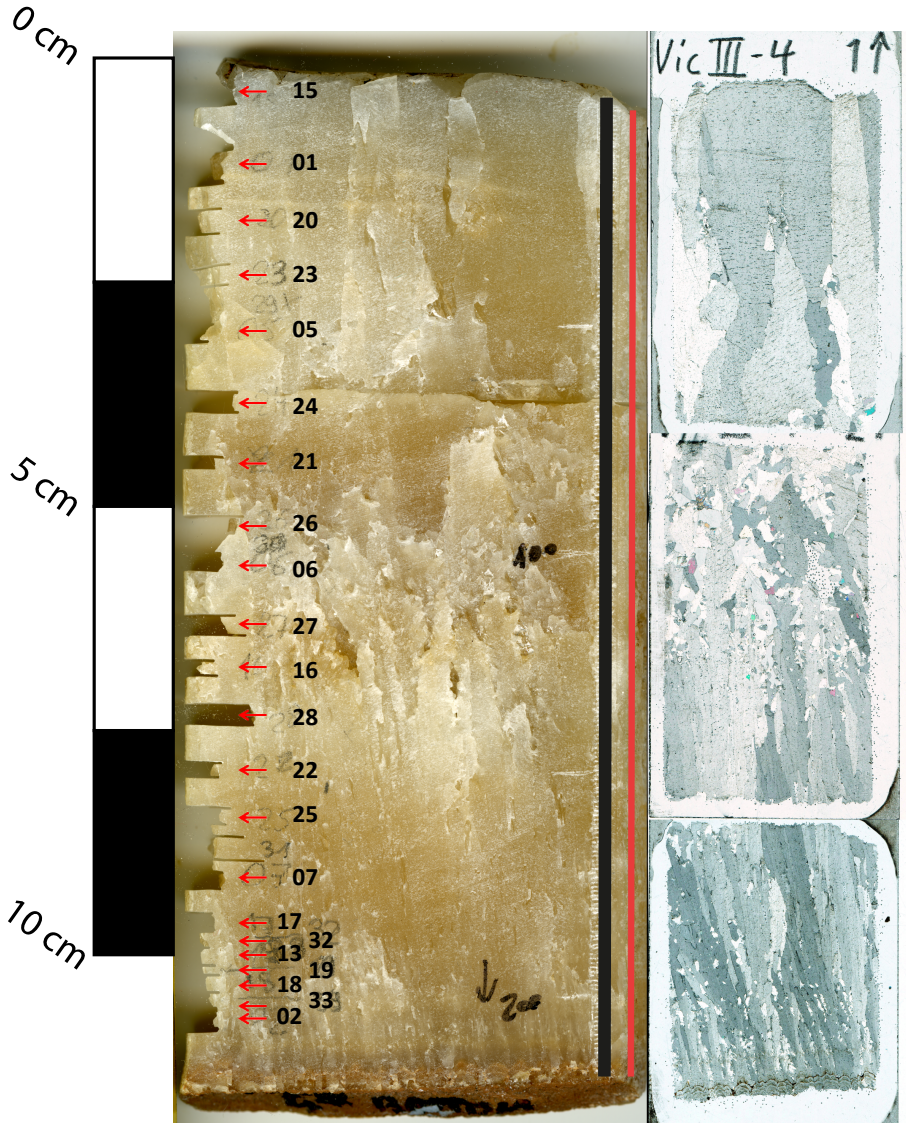


Figure 4.2: (Left) Scan of sample Vic-III-4 with red arrows indicating the positions of $^{230}$Th/U-dating samples. The black line on the right side of the slab marks the stable isotope traverse, and the red line represents the profile for trace-element analysis. (Right) The corresponding thin sections in cross-polarised light prepared from the opposite slab.

**$^{230}$Th/U dating** Twenty-two samples (100 – 300 mg) were cut from the upper 12 cm section of sample Vic-III-4 with a diamond-coated bandsaw following visible growth bands (Figure 4.2). In addition, one sample was obtained from the top of Vic-III-1 (Figure 4.9). The samples were dissolved in 7N $HNO_3$, and a mixed $^{233}$U–$^{236}$U–$^{229}$Th spike (Gibert et al., 2016) was added to the solution. Chemical separation of U and Th was carried out by ion exchange chemistry as described by Yang et al. (2015). U and Th isotope ratios were determined with a Nu instruments multi-collector inductively coupled plasma mass spectrometer (MC-ICP-MS) at the

Max Planck Institute for Chemistry, Mainz. Samples were measured by a standard-sample bracketing procedure as described by Obert et al. (2016). Activity ratios and ages were calculated using the half-lives of Cheng et al. (2000) for $^{230}$Th and $^{234}$U, Le Roux and Glendenin (1963) for $^{232}$Th, and Jaffey et al. (1971) for $^{238}$U.

## 4.4 Trace element measurements

Trace element concentrations were determined by laser ablation inductively coupled plasma mass spectrometry (LA-ICP-MS) in line scan mode at the Institute for Geosciences, University of Mainz. Line scans extended from the bottom of the flowstone drill core parallel to the growth axis (Figure 4.2). Analyses were performed using the ESI NWR193 ArF Excimer laser ablation system equipped with a TwoVol2 sample chamber coupled to an Agilent 7500ce quadrupole ICP-MS. The laser was operated at a repetition rate of 10 Hz with a laser energy at the sample site of $\approx$3 J/m$^2$. The line scans were carried out after pre-ablation of the sample surface with a beam diameter of 100 µm and a scan speed of 10 µm/s. Backgrounds were measured for 20 s prior to each ablation. NIST SRM 612 was used for calibration using the preferred values reported in the GeoReM database (http://georem.mpch-mainz.gwdg.de/, Application Version 21, January 2017, Jochum et al., 2005; Jochum et al., 2011) to calculate the element concentrations in the samples. During each run, basaltic USGS BCR-2G (n = 6) and synthetic carbonate USGS MACS-3 (n = 6) were analysed as a quality control material (QCM) to monitor accuracy and reproducibility of the analyses. For all materials, $^{43}$Ca was used as an internal standard: For the reference materials, the Ca concentration reported in the GeoReM database, and for the samples, a Ca concentration of 39 wt% (Mertz-Kraus et al., 2009) was used. Data processing was performed using Microsoft Excel following the data reduction scheme of Longerich et al. (1996) and Jochum et al. (2007). Details of the calculations are given in Mischel et al. (2017a). The limit of detection (LOD) was calculated according to Kaiser and Specker (1956) for each element as:

$$LOD = I_{background} + 3 * SD_{background} \tag{4.1}$$

where $I_{background}$ is the mean intensity of the signal recorded during the background measurement, and $SD_{background}$ is the standard deviation of the corresponding signal interval (Table S1). We report element concentrations for Mg, Sr and Ba. The measured Mg concentrations of the QCMs agree within 10 % with the reference values, i.e., the preferred values of the GeoReM database for USGS BCR-2G and the preliminary reference values for USGS MACS-3 (personal communication S. Wilson, USGS, in Jochum et al., 2012, Table 4.1). For Sr and Ba, the measured values of both QCMs deviate less than 5 % from the reference values.

### 4.4.1 Stable isotope measurements

Stable isotope samples of samples Vic-III-1 and -4 were milled at a spatial resolution of 0.5 mm using a NWR MicroMill. For Vic-III-3, the sampling resolution was 0.25 mm. Stable isotope measurements were performed at the Institute of Geology, University of Innsbruck, using a Thermo Fisher DeltaplusXL isotope ratio mass spectrometer linked to a Gasbench II as described in Spötl and Vennemann (2003) and Spötl (2011). Long-term analytical precision ($1\sigma$) of the $\delta^{18}$O and $\delta^{13}$C measurements is 0.08 and 0.06 ‰, respectively. Stable isotope values are reported relative to the VPDB standard.

### 4.4.2 Moisture source modelling

Speleothem $\delta^{18}$O values often reflect the $\delta^{18}$O values of precipitation at the cave site, which depend on various parameters, such as latitude, temperature, rainfall amount, and moisture source (Lachniet, 2009; McDermott, 2004). In order to determine the major moisture sources for the precipitation at CV, we performed trajectory analysis using the HYSPLIT (Hybrid Single-Particle Lagrangian Integrated Trajectories) trajectory model of the Air Resources Laboratory of the National Oceanic and Atmospheric Administration (Stein et al., 2015) for three altitudes (1000, 1500, and 2000 m). We used data from a meteorological station located 20 km NNW (San Javier, 37°46'48N, 0°48'36W) of the cave, which provides an almost complete daily-resolution dataset since the late 1940s (KNMI Climate Explorer; Klein Tank et al., 2002). Following the method of Krklec and Domínguez-Villar (2014), we analysed all days since 1950 AD with precipitation >0.5 mm at the San Javier meteorological station, which is considered to be sufficient to contribute to karst aquifer recharge. For each of these days, we calculated the trajectories five days backwards (Gimeno et al., 2010). Effective moisture uptake is defined by a change of specific humidity >0.5 g/kg within 6 hours (Rozanski et al., 1993; Baldini et al., 2010). In order to account for the boundary layer elevation (Sodemann et al., 2008), we assumed a constant level of 900 hPa (Baldini et al., 2010) and only considered values of the trajectories >900 hPa. It is important to consider that along the pathway of a trajectory, several locations of moisture uptake and loss (precipitation) at different elevations can be defined for each day, month and year. To calculate the contribution (i.e., the importance) of the individual moisture sources to total rainfall at CV for specific time periods (e.g., season, year, decade), the corresponding rainfall events were weighted according to their amount in the trajectory analysis. In order to explore the relationship between common atmospheric patterns in Europe and precipitation at the study site, we calculated the correlation between precipitation and the indices of the North Atlantic Oscillation (NAO, Iceland-Gibraltar, Jones et al., 1997), the East Atlantic pattern (EA, Barnston and Livezey, 1987; Rodriguez-Puebla et al., 1998), the Scandinavian pattern (SCA, Barnston and Livezey, 1987) and the Western Mediterranean Oscillation (WeMO, Martin-Vide and Lopez-Bustins, 2006, Table S3).

## 4.5 Results

### 4.5.1 Petrography

The fabrics of flowstone Vic-III-4 (Figure 4.4) were classified according to Frisia (2015). The flowstone exhibits columnar calcite crystals with increasing crystal size towards the top of the sample. In detail, the flowstone is composed of an elongated columnar fabric (Frisia, 2015) with small crystals at the bottom, which become progressively larger up to 6.5 cm distance from top (dft). The section between 6.5 and 3 cm dft is characterized by open columnar fabric. However, there is no evidence of dissolution and/or recrystallization in this section. At 3 cm dft, the open columnar fabric changes to columnar fabric. There is no petrographic evidence of a hiatus within the upper 1 cm dft as revealed by $^{230}$Th/U-dating (next section, Figure 4.3). The crystal fabric of flowstones Vic-III-1 and -3 is columnar and shows no indication of dissolution or recrystallization. Vic-III-1 shows clear evidence for a hiatus at 0.3 cm dft (Figure 4.9). In Vic-III-3, a hiatus is present at ca. 0.25 cm dft, indicated by a detrital layer.

### 4.5.2 $^{230}$Th/U dating

Twenty-two $^{230}$Th/U-ages were determined for Vic-III-4. The $^{238}$U concentration ranges from 0.1 to 0.3 µg/g (Table 4.2) and shows decreasing values from the bottom to the top of the sample. The uncorrected $^{230}$Th/U-ages range from 13.70 ka at the bottom (10.3 cm dft) to 2.78 ka at the top (Table 4.2 and Figure 4.3). At ca. 9 cm dft, the $^{230}$Th/U-ages suggest a large change in growth rate. Between the two uppermost ages of Vic-III-4, we detected a 4 ka-long hiatus (Figure 4.3). Not all ages are in stratigraphic order (Figure 4.3). The samples contain moderate amounts of $^{232}$Th (0.03 to 2.3 ng/g, mean 0.9 ng/g). The corresponding ($^{230}$Th/$^{232}$Th) activity ratios range from 18.8 to 185.7 (Table 4.2). The effect of detrital contamination on $^{230}$Th/U-ages is considered to be significant if ($^{230}$Th/$^{232}$Th) $< 200$ (Richards and Dorale 2003). Thus, detrital contamination should have a significant impact on all $^{230}$Th/U-ages of sample Vic-III-4. We applied the conventional correction for detrital Th assuming a $^{232}$Th/$^{238}$U weight ratio of 3.8 (i.e., a ($^{232}$Th/$^{238}$U) activity ratio of 1.25) for the detritus (Wedepohl, 1995) and $^{230}$Th, $^{234}$U and $^{238}$U in secular equilibrium. This results in a shift towards younger ages by 0.04 ka (sample Vic-III-4-02) to 0.33 ka (sample Vic-III-4-22; Figure 4.3). The largest correction is observed for samples Vic-III-4-01, -22, and -27, which have ($^{230}$Th/$^{232}$Th) ratios lower than 30 (Table 4.2). The larger uncertainties for the corrected ages are due to the assumed 50 % uncertainty of the ($^{232}$Th/$^{238}$U) activity of the detrital material. Obviously, the conventional detrital correction does not eliminate all age inversions (Figure 4.3). The uncorrected $^{230}$Th/U-age at the top of Vic-III-1 is 14.37 ± 0.14 ka (Table S2). This sample has a low ($^{230}$Th/$^{232}$Th) activity ratio of 2.9 resulting in a relatively large conventional correction of 3.7 ka (10.6 ± 1.8 ka). Below the hiatus at 0.3 cm dft, the $^{230}$Th/U-ages are $> 45$ ka (not shown in this paper). Thus, only the section above the hiatus corresponds to the Holocene. Similarly, in Vic-III-3, the ages below 0.25 cm dft are $> 50$ ka. Since the flowstones from this cave mainly grew during interglacials

and interstadials (Budsky et al., 2015), we assume that the upper 0.25 cm correspond to the Holocene, even if direct dating is not possible.

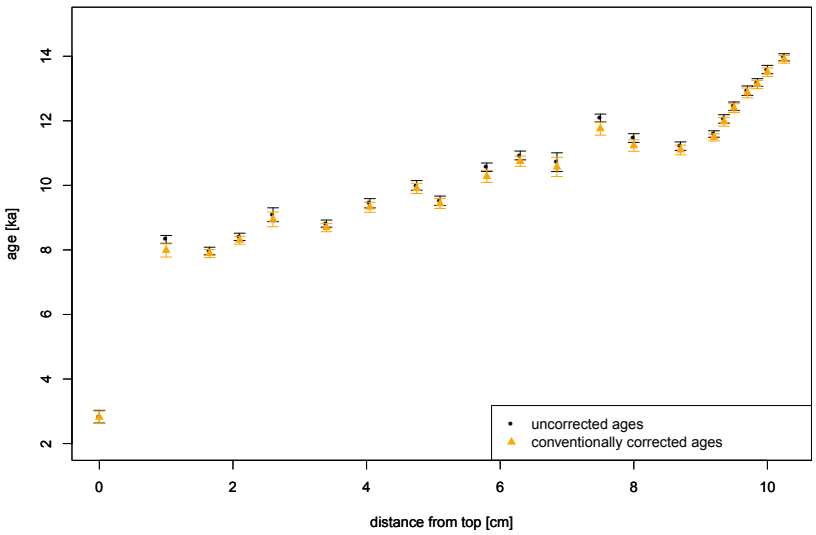


Figure 4.3: Uncorrected (black) and conventionally corrected (i.e., ($^{232}$Th/$^{238}$U) = 1.25; orange) $^{230}$Th/U-ages vs. distance from the top of the flowstone core Vic-III-4.

### 4.5.3 Proxy data

Stable oxygen and carbon isotope values of Vic-III-4 show a decreasing trend from the bottom to the middle of the sample (6 cm dft; $\delta^{18}$O: -4 to -6 ‰, $\delta^{13}$C: -7 to -11 ‰; Figure 4.4). Between 6 and 1.7 cm dft, the $\delta^{13}$C values show a large positive excursion from ca. -11 to ca. -4 ‰, while the $\delta^{18}$O values remain at a constant level of about -6 ‰. At 1.7 cm dft, the $\delta^{13}$C values return to lower values of around $\approx$ 10 ‰. The position of the $\delta^{13}$C excursion is in broad agreement with the observed change from columnar to open columnar fabric (Figure 4.4). In the lower part of the flowstone, the $\delta^{18}$O and $\delta^{13}$C values show a strong positive correlation ($R^2 = 0.93$; Figure 4.4). Samples Vic-III-1 and -3 show a similar increase in $\delta^{13}$C values from ca. -9 to ca. -4 ‰ at 0.25 and 0.2 cm dft, respectively (Figure 4.9). Subsequently, the $\delta^{13}$C values in both cores return to ca. -10 ‰ (Figure 4.9). The $\delta^{18}$O values show a decrease from ca. -4 to ca. -6 ‰ in both cores (Figure 4.9). Due to the large amount of water with very negative $\delta^{18}$O values stored in ice sheets, the $\delta^{18}$O values of the ocean were higher during the Late Glacial compared to the Holocene. Therefore, we corrected the $\delta^{18}$O values of the speleothem record for the corresponding changes in ice volume (Lambeck et al., 2014; Grant et al., 2012). Sea level is directly linked to ice volume and can be used to estimate the ice volume correction (Waelbroeck et al., 2002). To calculate past sea level, we follow the approach of Waelbroeck et al. (2002) using the $\delta^{18}$O values of benthic foraminifera from the Red Sea (Siddall et al., 2003). The ice volume correction shifts the $\delta^{18}$O values in the Late Glacial section of our speleothem

record by ca. ≈1 ‰ (Figure 4.7c). For the youngest part of the flowstone, the correction is negligible (Figure 4.7c). Magnesium concentration in Vic-III-4 displays a trend from high values (≈6000 µg/g) at the bottom (10.5 cm dft) to lower values (2000 µg/g) at around 6 cm dft and then remains at a constant level (Figure 4.4). Strontium concentration shows the same decreasing long-term trend, although it is not correlated with the Mg concentration on shorter time scales. Barium concentration varies between 20 and 160 µg/g, displays no long-term trend and shows peaks at similar dft as Sr.

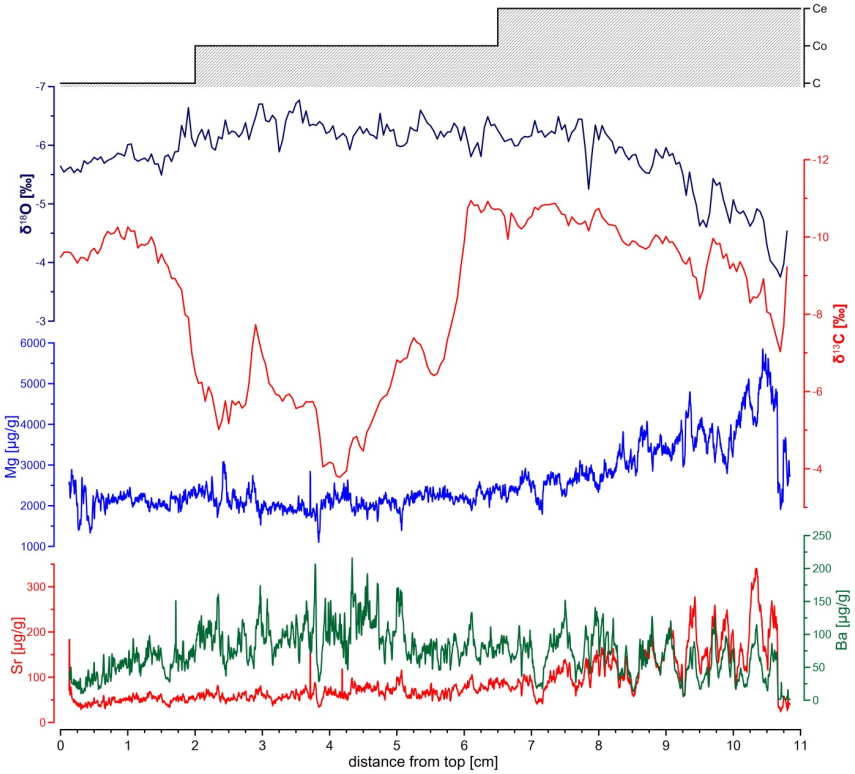


Figure 4.4: Proxy data and petrographic log (according to Frisia 2015, C: columnar, Co: open columnar, Ce: elongated columnar) vs. distance from the top of Vic-III-4. Y-axes are inverted for $\delta^{13}$C and $\delta^{18}$O values.

### 4.5.4 Trajectory analysis

Figure 4.12 shows back-calculated trajectories (120 h, Gimeno et al., 2010) for selected days with precipitation events at the San Javier meteorological station. These examples indicate various pathways of trajectories for CV. The results of the trajectory analysis for the complete rainfall data set from San Javier show that the major sources of precipitation in south-eastern Spain are the Alboran Sea and the surrounding landmasses (N Morocco, Spain) as well as the Iberian Margin (Figure 4.5). Moisture uptake over the more distant Atlantic Ocean also plays a role. In general, the contribution of the Atlantic Ocean is more pronounced during winter and spring. During summer months, regional moisture sources dominate. In order to assess whether recent rainfall amount or air temperature has a significant effect on the $\delta^{18}$O values

of precipitation, we examined $\delta^{18}O$ values of modern precipitation from nearby meteorological stations. The weighted mean annual $\delta^{18}O$ values of modern precipitation (GNIP data, Rozanski et al., 1992, http://www-naweb.iaea.org/napc/ih/index.html) in south-eastern Spain (Almeria, Murcia and Valencia) do not show a significant correlation with the amount of annual precipitation (Figure 4.10). Very high $\delta^{18}O$ values during summer correspond to dry conditions at all stations, whereas lower $\delta^{18}O$ values are observed during the rainy season from October to March (Figure 4.9). Similarly, no significant correlation with mean annual temperature is observed (Figure 4.11). Thus, modern $\delta^{18}O$ values of precipitation reflect neither precipitation amount nor temperature on the inter-annual scale.

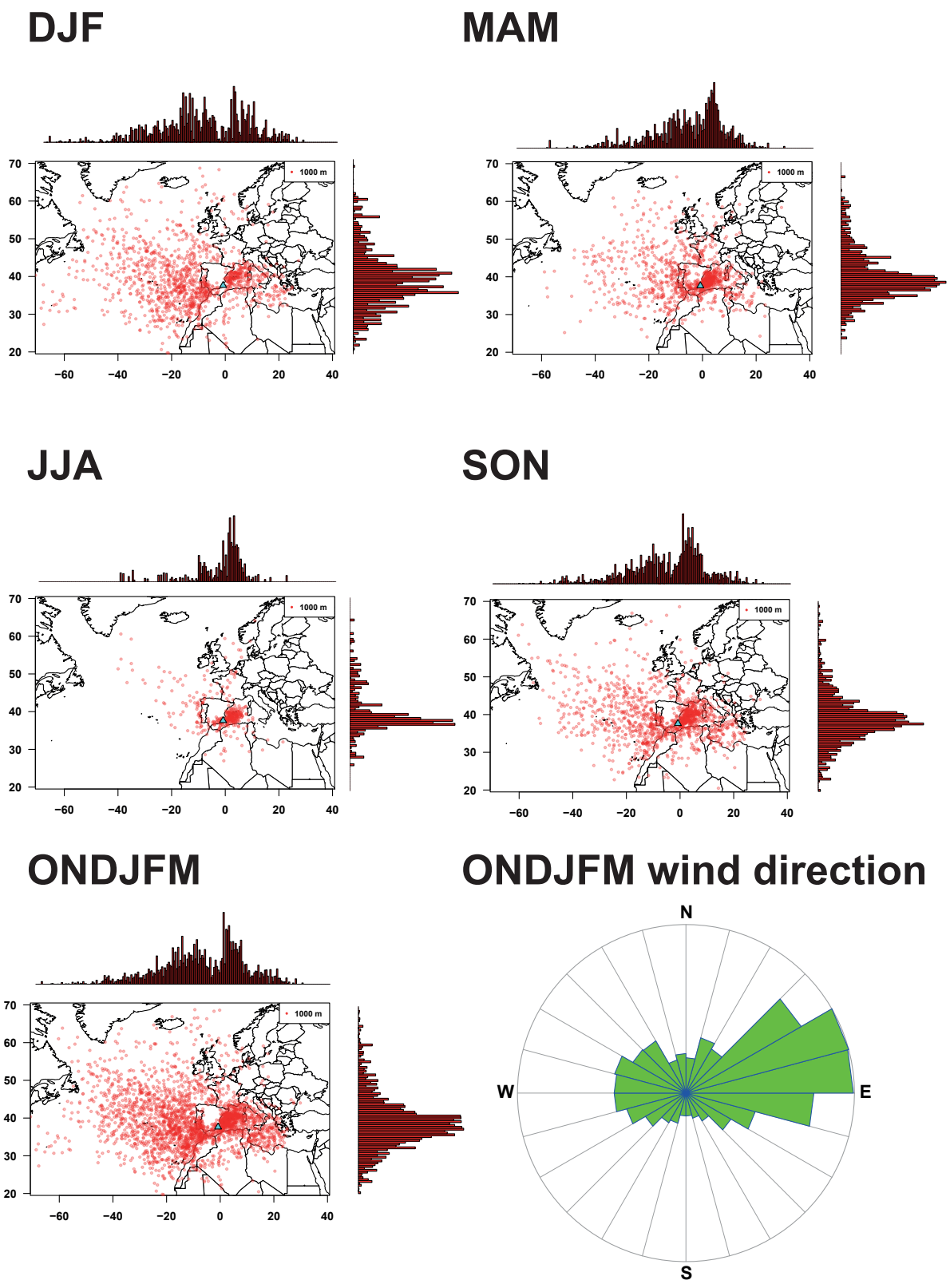


Figure 4.5: Continued.

▲ Figure 4.5 (continued): Moisture uptake for rainy days at the San Javier meteorological station for the period AD 1950 – 2010. Winter (DJF), spring (MAM), summer (JJA), autumn (SON) as well as the rainy season (October to March) are shown in the first five maps. The bar plots on the x- and y-axes show the summarised moisture uptake on a 0.5°× 0.5°grid with respect of the total amount of precipitation. The bottom right panel shows the wind direction (1500 m a.s.l.) transporting moisture to the cave site during the rainy season for the last 6 h before reaching the cave site.

Correlation analysis of winter precipitation (October to March) at San Javier (precip) with the Western Mediterranean Oscillation (WeMO), the Scandinavian pattern (SCA), the North Atlantic Oscillation (NAO) and the East Atlantic pattern (EA, Table 4.3) shows that the WeMO (Martin-Vide and Lopez-Bustins, 2006) has the largest impact on the amount of winter precipitation in the region of CV, followed by the EA pattern (Barnston and Livezey, 1987). These two patterns are not correlated with each other. The NAO (Hurrell and Loon, 1997) and the Scandinavian pattern (SCA, Barnston and Livezey, 1987) show no significant correlation with winter rainfall at San Javier. During summertime, no significant correlation with any circulation pattern is observed (Table 4.3).

## 4.6 Discussion

### 4.6.1 Chronology

The $^{230}$Th/U-ages display several age inversions despite of the correction for detrital Th (Figure 4.3). This suggests that detrital contamination is not completely accounted for by the conventional correction. Several studies have shown that the conventionally used $^{232}$Th/$^{238}$U ratio is not uniformly appropriate for speleothems and that substantially different values have to be used (Roy-Barman and Pons-Branchu, 2016; Rivera-Collazo et al., 2015; Fensterer et al., 2010; Hellstrom, 2006; Hoffmann et al., 2010). In order to constrain the $^{232}$Th/$^{238}$U ratio of the detrital material, the stratigraphic order of the samples can be used (Roy-Barman and Pons-Branchu, 2016; Hellstrom, 2006; Drysdale et al., 2006). Here we apply a similar approach. We used several $(^{232}\mathrm{Th}/^{238}\mathrm{U})_d$ activity ratios for the detritus (i.e., 0.08 to 4, separated by an interval of 0.01) and calculated corrected activity ratios, $(^{234}\mathrm{U}/^{238}\mathrm{U})_{corr}$ and $(^{230}\mathrm{Th}/^{238}\mathrm{U})_{corr}$, assuming secular equilibrium between detrital $^{230}$Th, $^{234}$U and $^{238}$U. Based on the corrected activity ratios, we then solved the age equation to obtain corrected $^{230}$Th/U-ages. To determine the appropriate correction factor for the CV flowstone, we calculated the sum of all inversions (in years) for each correction factor. For this purpose, each age was compared with all other ages, and age inversions (without taking into account the uncertainties) were summed up. Figure 4.6b shows an example for three data points. The conventional correction factor ($(^{232}\mathrm{Th}/^{238}\mathrm{U})_d$ = 1.25, orange) leads to two inversions, whereas the red one only leads to one inversion. Finally, the

blue dots indicate the correction factor leading to no age inversions. Unfortunately, for the whole data set, no correction factor removing all age inversions was found (Figure 4.6a), and the lowest value that can be achieved leads to six age inversions in total. For example, the age at 7.5 cm dft generates two inversions, one with the next age and another inversion with the subsequent one (Figure 4.6b). Due to its relatively large amount of detritus, this sample is very sensitive to changes in the correction factor and is strongly shifted towards younger ages with a decreasing correction factor (Figure 4.6b). Using the correction factor leading to the minimum sum of all inversions ($(^{232}\mathrm{Th}/^{238}\mathrm{U})_d = 0.3$) results in a total amount of about 1200 a of inversions over the complete sample (Figure 4.6c). This is only half of the sum of inversions observed using the conventional correction factor. In addition, it is 500 a less than for the approach minimizing the total number of inversions (Figure 4.6c). Therefore, $(^{232}\mathrm{Th}/^{238}\mathrm{U})_d = 0.3$ was used for all further calculations. The effect of the detrital correction is generally stronger in the upper part of the flowstone ($< 9.5$ cm dft, Figure 4.6a). To account for the potential uncertainties of our approach, we assumed a conservative uncertainty of $\pm 50$ % for the determined $(^{232}\mathrm{Th}/^{238}\mathrm{U})_d$ activity ratio (i.e., $(^{232}\mathrm{Th}/^{238}\mathrm{U})_d = 0.3 \pm 0.15$), which was propagated to the corrected $^{230}$Th/U-ages. This results in relatively large uncertainties of the individual corrected ages (Table S3). Taking into account these uncertainties, the final data set does not show any significant age inversions (Figure 4.6d). Some studies showed that diagenesis and post-depositional mobilisation of U can also occur in speleothems both with (Scholz et al., 2014) and without (Bajo et al., 2016) visible changes in the crystal fabric. Since our approach to account for detrital Th eliminates all age inversions within uncertainty and the crystal fabrics show no evidence of dissolution or recrystallization, we consider post-depositional remobilisation of U as very unlikely.

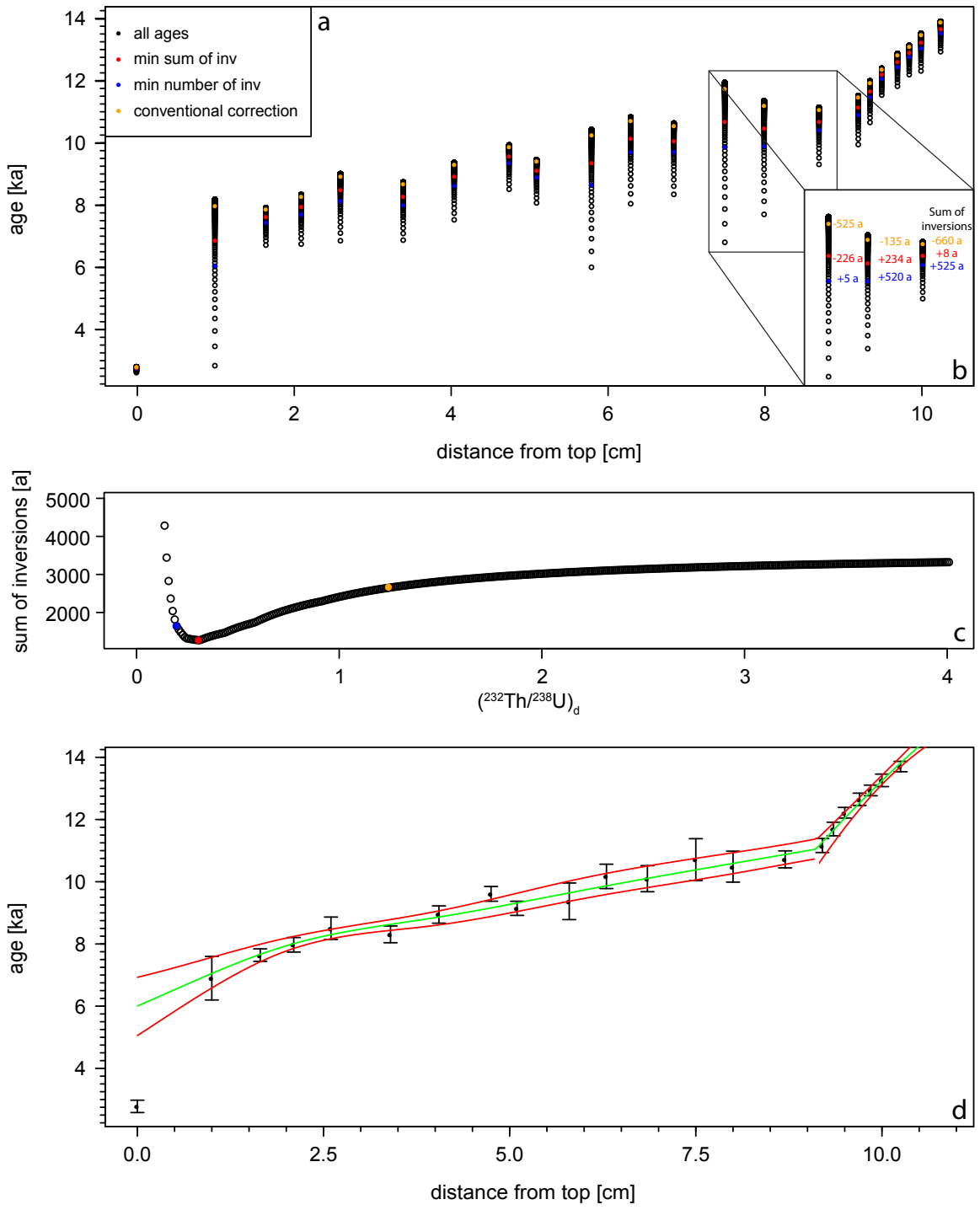


Figure 4.6: Continued.

▲ Figure 4.6 (continued): (a) $^{230}$Th/U-ages calculated assuming different detrital correction factors for the 22 analysed samples. $(^{232}\text{Th}/^{238}\text{U})_d$ ratios were varied from 0.08 to 4 with an increment of 0.01. Blue dots correspond to the correction factor resulting in the smallest number of age inversions, whereas red dots indicate the correction factor yielding the minimum sum of age inversions in years. For comparison, the orange dots display the ages calculated using the conventional correction factor ($(^{232}\text{Th}/^{238}\text{U})_d = 1.25$). (b) Example for three ages. The conventional correction (orange) leads to three age inversions. The first age is 525 a older than the second age, and the second age is 135 a older than the third age, although both should be younger than the third age according to the stratigraphy. The third age is 660 a younger than the first age. The red model minimises the sum of age inversions for the whole data set leading to only one inversion of 226 a for the three ages shown. The blue model results in no inversions between the three data points. (c) Relation between the sum of age inversions and the $(^{232}\text{Th}/^{238}\text{U})_d$ ratio assumed for the detritus. The red dot highlights the value resulting in the lowest value for the sum of inversions, which was used for all further calculations. The orange dot indicates the conventionally used ($^{232}$Th/$^{238}$U) correction factor of 1.25. (d) Age model calculated with StalAge (Scholz and Hoffmann, 2011). The youngest age was excluded due to the long hiatus. The individual age uncertainties include the effect of the detrital correction with $(^{232}\text{Th}/^{238}\text{U})_d = 0.3 \pm 0.15$ and are substantially larger than for the uncorrected and conventionally corrected ages (Figure 4.3; Table 4.2).

The StalAge algorithm (Scholz and Hoffmann, 2011) was then used to construct an age-depth model (Figure 4.6d). We excluded the youngest age from the age model because of the hiatus of approximately 4 ka at the top of the sample (Figures 4.3 and 4.7) and calculated the age model only to 1 cm dft (uppermost used age). In addition, we calculated two separate age models (from the bottom to 9.1 cm dft and from 9.1 cm dft to 1 cm dft) because of the large change in growth rate. The final age model shows a large change in growth rate at 9.1 cm dft (Figure 4.6d). This change is neither represented in the crystal fabric nor in the stable isotope and trace element data (Figure 4.4). All age uncertainties reported in the following sections are based on this age model and are below 500 a. For flowstones Vic-III-1 and -3, it was not possible to construct a chronology for the thin Holocene growth sections based on the $^{230}$Th/U-data. The decrease in $\delta^{18}$O values from -4 to -6 ‰, which is observed in both cores and similar in magnitude with the $\delta^{18}$O signal of Vic-III-4, suggests that these sections of the flowstones correspond to the transition from the Late Glacial to the Holocene. Similarly, the positive excursion in the $\delta^{13}$C values observed in both cores, which is comparable in magnitude and shape to the large excursion recorded in Vic-III-4, can reasonably be interpreted to be related to this phase. Thus, although we cannot independently establish the timing of the two stable isotope records, comparison with

the Vic-III-4 record allows assigning them to the Holocene.

### 4.6.2 Speleothem $\delta^{13}$C values and trace elements

Speleothem $\delta^{13}$C values depend on various parameters, such as the concentration and $\delta^{13}$C value of soil $CO_2$, the $\delta^{13}$C value of the host rock, prior calcite precipitation (PCP), drip rate and cave ventilation. For flowstones, which are fed by water flowing long distances inside the cave, geochemical effects occurring inside the cave, such as variable degassing of $CO_2$ induced by strong cave ventilation (Spötl et al., 2005; Johnson et al., 2006), progressive precipitation of $CaCO_3$ along the flow path (Hansen et al., 2017; Mattey et al., 2010) and disequilibrium stable isotope fractionation (Mühlinghaus et al., 2009), may be of particular importance. In the epikarst, dissolved $CO_2$ may degas and trigger prior calcite precipitation (PCP). Similarly, PCP may occur inside the cave en route to the flowstone. This process may strongly influence the $\delta^{13}$C values of the solution and result in increasing $\delta^{13}$C values (Fairchild and Treble, 2009; Scholz et al., 2009; Dreybrodt and Scholz, 2011). Thus, PCP and processes inside the cave may further amplify the general relationship of higher $\delta^{13}$C values during spring/summer drought conditions. Increased PCP also leads to increased Mg/Ca, Sr/Ca, and sometimes Ba/Ca ratios in the drip water because Mg, Sr and Ba incorporation into calcite is suppressed in comparison to Ca (Fairchild et al., 2000; Stoll et al., 2012). This may lead to positive correlations between speleothem $\delta^{13}$C and Mg/Ca, Sr/Ca and Ba/Ca ratios (Stoll et al., 2012). Except for the millennial-scale trend in Mg and Sr from the Late Glacial to the Early Holocene, we do not observe a positive correlation between Mg, Sr, and $\delta^{13}$C (Figure 4.4). We thus exclude that PCP had a strong effect on our flowstone $\delta^{13}$C record (Sinclair et al., 2012; Treble et al., 2015). Most recharge at CV occurs during the rainy season from October to March. The vegetation growth period in eastern Spain depends on the plant species, but generally ranges from early spring to early summer and may be longer in case of summer rainfall (Camarero et al., 2015; Pasho et al., 2011). In case of long and dry summers and reduced precipitation in spring, vegetation density is negatively affected (Linares et al., 2011). This process is partly associated with long-term effects (Gazol et al., 2017). A prolonged reduction in spring and summer rainfall over several decades will thus result in a decrease in soil $pCO_2$ and soil microbial activity and be reflected in higher $\delta^{13}$C values. Thus, the $\delta^{13}$C values of the CV flowstone should be a sensitive proxy for past spring and summer drought even if aquifer recharge and flowstone growth predominantly occur during the autumn and winter season (Carrasco et al., 2006). Therefore, we interpret the $\delta^{13}$C values as a proxy for soil microbial activity and vegetation density reflecting changes in the length of the vegetation period and, thus, spring/summer drought. The long-term trend in Mg and Sr from the Late Glacial to the Early Holocene (Figure 4.4) was observed in several speleothem records from Central Europe and attributed to glacial aeolian deposits, which are then progressively dissolved and washed into the cave (Fohlmeister et al., 2012; Mischel et al., 2017b). This interpretation may also be valid for south-eastern Spain and CV because loess deposits are present in the region, for instance in the Granada basin, Andalusia, and on littoral plains of the eastern side of the country

(Calvo et al., 2016; Coudé-Gaussen, 1990; Günster et al., 2001). In particular, Pleistocene dunes occur ca. 7 km SE of CV (geological map, Llano del Beal, map sheet 978, Espinosa-Godoy et al., 1972). However, the long-term trend in Mg and Sr may also be related to incongruent dolomite dissolution of the host rock (Fairchild et al., 2000) during the drier glacial phase, when water residence times were longer. Due to increasing precipitation during the Bølling/Allerød (B/A, Figure 4.7 ), the karst aquifer was reactivated and the Mg and Sr concentration of the recharge water was progressively diluted. Unfortunately, we are not able to distinguish between the two processes (leaching of loess deposits vs. incongruent dissolution of dolomite), and it cannot be excluded that the observed signal represents a mixture of both processes. The $\delta^{13}C$ values of the CV flowstone decrease from the bottom of the flowstone (B/A) until the onset of the YD (Figures 4.7 and 4.8). As for the $\delta^{18}O$ values, the YD is indicated by a peak of 1.5 ‰ more positive $\delta^{13}C$ values and more negative $\delta^{18}O$ values, presumably reflecting both drier and colder climate conditions on the Iberian Peninsula (Baldini et al., 2015; Moreno et al., 2010) with reduced vegetation density. Subsequent to the YD, the $\delta^{13}C$ values further decrease until 11 ka and then remain on a constant level of -10.5 ‰ indicating a well-developed $C_3$ vegetation above the cave and enough precipitation to maintain a permanent vegetation cover (Figure 4.8). At $9.7 \pm 0.3$ ka, the $\delta^{13}C$ values show a sharp shift towards higher values (Figure 4.8g) suggesting a strong decrease in precipitation during the vegetation period, which resulted in a decrease in vegetation density above the cave, lower soil $pCO_2$ and reduced microbiological activity. Since the growth rate of the flowstone remained at a similar level as before and after the $\delta^{13}C$ excursion (Figure 4.6), a strong reduction in total annual recharge is unlikely. This is also supported by the two additional flowstone cores, which record calcite deposition – albeit very slowly – just during this $\delta^{13}C$ excursion indicating no significant reduction in annual precipitation. Thus, we interpret the large excursion in $\delta^{13}C$ values as a result of very dry conditions during the growth period of vegetation (spring to summer). Autumn to winter precipitation, in contrast, probably increased as reflected by the high speleothem growth rates preventing PCP in the aquifer. This interpretation of the $\delta^{13}C$ data is supported by the crystal fabric. Elongated columnar fabric, as observed at the bottom of the flowstone (Figure 4.4), forms in case of constant drip rates and high Mg/Ca ratios (Frisia, 2015). Open columnar fabric, in contrast, forms as a result of lower drip rates and lower Mg/Ca ratios (Frisia, 2015). The synchronous occurrence of an open columnar fabric and the large peak in the $\delta^{13}C$ values (Figure 4.4), thus, suggests drier conditions in the catchment of the cave in agreement with our interpretation of the $\delta^{13}C$ record. The formation of the open columnar fabric may further be related to the progressive decrease of the Mg/Ca ratio from the Late Glacial to the Early Holocene (Figure 4.4). We emphasise that the change in crystal fabrics and crystal growth effects are unlikely to be the cause of the large $\delta^{13}C$ excursion. Frisia (2015) compared $\delta^{13}C$ and $\delta^{18}O$ values for different speleothem crystal fabrics, and columnar, open columnar and elongated columnar fabrics show identical $\delta^{13}C$ and $\delta^{18}O$ values within uncertainty. Therefore, we interpret the large excursion in $\delta^{13}C$ values to result from a reduction in meteoric spring/summer precipitation, which also invoked the change in crystal fabrics. In summary, our $\delta^{13}C$ record indicates dry spring/summer conditions and

probably increased seasonality (drier spring/summer conditions and more humid autumn/winter conditions) in south-eastern Spain between 9.7 ± 0.3 and 7.8 ± 0.2 ka. Subsequently, the $\delta^{13}C$ values decrease to approximately -10 ‰ indicating a return to a dense vegetation cover above the cave.

### 4.6.3 Speleothem $\delta^{18}O$ values

Speleothem $\delta^{18}O$ values are affected by cave air temperature, drip rate and the $\delta^{18}O$ value of the drip water. The $\delta^{18}O$ values of the drip water are influenced by the $\delta^{18}O$ values of meteoric precipitation, which are strongly related to the source of precipitation, the temperature and humidity during evaporation in the moisture source region (Lachniet, 2009), the $\delta^{18}O$ value of the ocean (Rozanski et al., 1993; LeGrande and Schmidt, 2006), the duration of moisture transport, the pathway of the storm tracks, rainfall amount and air temperature (McDermott, 2004).

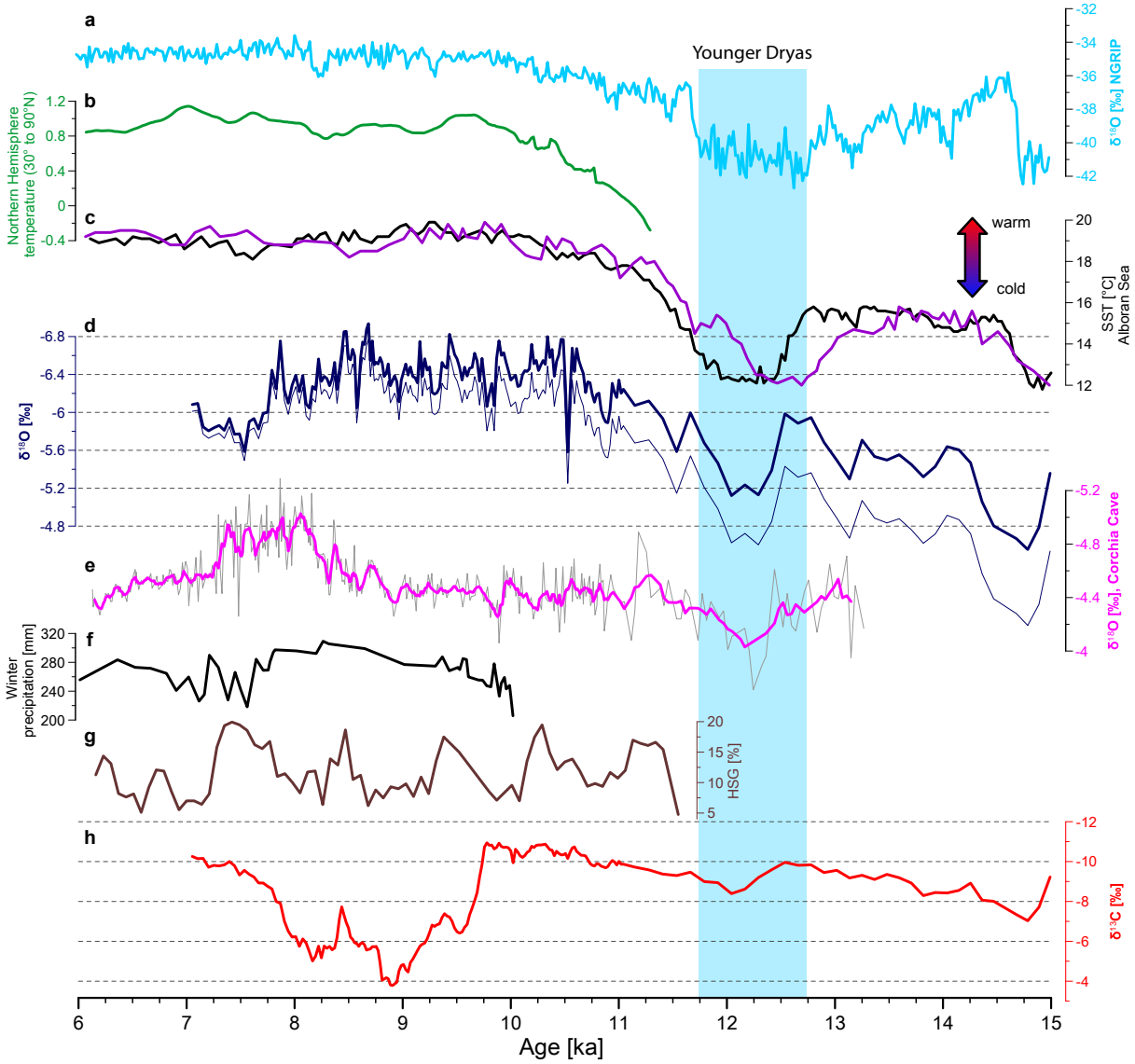


Figure 4.7: Comparison of the $\delta^{18}$O (d, lower curve is not corrected for ice volume) and $\delta^{13}$C (h) values (both axes are inverted) of the CV flowstone with other records: $\delta^{18}$O values from the NGRIP ice core (a, Rasmussen et al., 2006); speleothem $\delta^{18}$O record from Corchia Cave (e, Zanchetta et al., 2007); SST reconstructions from the Alboran Sea (c, violet Cacho et al., 1999, black Martrat et al., 2014); winter precipitation reconstruction from Lake Accesa (f, Peyron et al., 2011); Northern Hemisphere temperature between 30°and 90°N (b, Marcott et al., 2013) and the hematite-stained grain (HSG, g, Bond et al., 2001) record, which is an indicator for iceberg discharge in the North Atlantic.

In the Mediterranean, modern $\delta^{18}$O values can vary by $\approx 10$ ‰ for a single precipitation event depending on the air masses and the source region of the moisture (Celle-Jeanton et al., 2001; Moreno et al., 2014a; Sodemann and Stohl, 2009; Baldini et al., 2010). Whereas moisture uptake for rainfall in the area of CV during the dry summer season almost exclusively occurs over the Western Mediterranean Sea, a substantial fraction of precipitation is derived from the Atlantic

Ocean during the more humid winter season (Figure 4.5). Speleothem $\delta^{18}O$ values at CV should thus reflect both local and more distant changes in the North Atlantic. This leads to strong variability of the $\delta^{18}O$ values over the year, which is visible in the GNIP data (Figure 4.9). The local climate is characterised by a strong seasonality (Figure 4.10). Considering that the vegetation period in the area lasts from spring to summer (see section 5.3), a substantial amount of spring and summer rainfall will be used up by the vegetation. Thus, recharge of the aquifer is most effective during winter times, whereas the contribution of summer rainfall is insignificant (Carrasco et al., 2006), and the $\delta^{18}O$ values recorded by the flowstone should mainly reflect October to March rainfall. Ice-volume corrected flowstone $\delta^{18}O$ values progressively decrease from the onset of the Bølling (15 ka) towards the Early Holocene (10 ka), interrupted by higher values during the Younger Dryas (YD; Figure 4.7). The timing of the YD in our record is in good agreement with the NGRIP $\delta^{18}O$ record and SST reconstructions from the Alboran Sea (Cacho et al., 1999; Martrat et al., 2014; Figure 7). The general decreasing trend in the $\delta^{18}O$ values of the CV flowstone from the Late Glacial to the mid-Holocene shows a similar evolution as the NGRIP $\delta^{18}O$ values, which are interpreted to reflect temperature changes in the North Atlantic realm (North Greenland Ice Core Project members, 2004), and SST in the Alboran Sea (Cacho et al., 1999; Martrat et al., 2014; Figure 4.7a, d and e). A potential explanation for the observed negative relationship may be the effect of cave air temperature on the oxygen isotope fractionation between water and calcite of between -0.18 ‰/°C (Tremaine et al., 2011) and -0.24 ‰/°C (Kim and O'Neil, 1997), which is even imprinted on speleothem calcite if precipitation occurs under conditions of disequilibrium isotope fractionation (Mühlinghaus et al., 2009). The increase in SST from the Late Glacial to the Early Holocene is approximately 7 °C (Figure 4.7d). The corresponding decrease in speleothem $\delta^{18}O$ values related to SST changes from the YD to 10.5 ± 0.35 ka is -1.5 ‰ is about ≈0.21 ‰/°C, which is in good agreement with the theoretical (equilibrium) values. This suggests that changes in the $\delta^{18}O$ values of the CV flowstone on millennial and orbital timescales could be explained by temperature changes. However, if the speleothem $\delta^{18}O$ signal was only related to temperature, the $\delta^{18}O$ values of the drip water would have remained constant from the Late Glacial to the Holocene, which is very unlikely. Thus, we cannot exclude that changes in atmospheric circulation patterns or moisture source, in particular from the Late Glacial to the mid Holocene, played a role as well. The general complexity of processes controlling speleothem $\delta^{18}O$ values is also highlighted by detailed cave monitoring studies performed in northern Spain, where individual processes affecting the $\delta^{18}O$ signal could not be disentangled although these sites mainly receive moisture from the Atlantic Ocean (Bartolomé et al., 2015). High flowstone growth rates between 10.5 ± 0.35 and 7.0 ± 0.5 ka (compared to the older section of the flowstone) may be related to increased rainfall and recharge, which can cause increasing drip rates and – as a result – decreasing speleothem $\delta^{18}O$ values (Stoll et al., 2015; Mühlinghaus et al., 2009; Scholz et al., 2009). In addition, rainfall $\delta^{18}O$ values in the Mediterranean may also be related to the amount effect (Lachniet, 2009; Bar-Matthews et al., 2003; Ayalon et al., 1998). Thus, periods of reduced rainfall could be reflected by higher $\delta^{18}O$ values and vice versa. Although modern precipitation $\delta^{18}O$ data do not show a

significant relation to rainfall amount on inter-annual timescales, we cannot exclude that rainfall amount may have affected our speleothem $\delta^{18}O$ record on decadal and longer timescales. In summary, although we cannot disentangle the processes affecting the flowstone $\delta^{18}O$ values and the interpretation of the $\delta^{18}O$ record of the CV flowstone remains challenging, we assume that the $\delta^{18}O$ values of the CV flowstone on orbital timescales and during the Late Glacial might be related to temperature changes on the North Atlantic, which is supported by the good agreement with the SST records. However, the influence of other parameters, such as seasonality of rainfall, rainfall amount and changes in moisture source(s), cannot be excluded. For the period from $10.5 \pm 0.35$ to $7.8 \pm 0.2$ ka, higher growth rates coincide with lower $\delta^{18}O$ values, which suggest an additional influence of changes in the amount of autumn/winter precipitation on millennial timescales.

### 4.6.4 Implications for Western Mediterranean climate between 15 and 7 ka

#### 15 – 11.7 ka

The warming trend from the Late Glacial to the Early Holocene is reflected in the evolution towards lower $\delta^{18}O$ values in the CV flowstone, which parallels the evolution in the NGRIP ice core and SST in the Alboran Sea (Figure 4.7). This trend is also observed in several other terrestrial records (speleothems, pollen) from Europe and the Mediterranean south of 45°N (Moreno et al., 2014b; García-Alix et al., 2014). In addition, other speleothem data from the Western Mediterranean region and the Iberian Peninsula exhibit hiatuses during the cold interval prior to the B/A (Moreno et al., 2010; Moreno et al., 2017; Genty et al., 2006; Constantin et al., 2007; Frisia et al., 2005) suggesting limited recharge as a result of reduced rainfall. The onset of growth of the CV flowstone during the B/A coincides with the recovery of vegetation in the Mediterranean (Fletcher et al., 2010; Fletcher and Sánchez Goñi, 2008; Allen et al., 2002; Tzedakis, 2005), as a consequence of rising temperatures and humidity levels. This is also reflected in the $\delta^{13}C$ values of the CV flowstone, which are approximately -10 ‰ prior to the YD, suggesting relatively humid conditions and a well-developed vegetation above the cave during the B/A. Decreasing aridity towards the Early Holocene is also recorded in the sediments of Lake Salines (Burjachs et al., 2016).

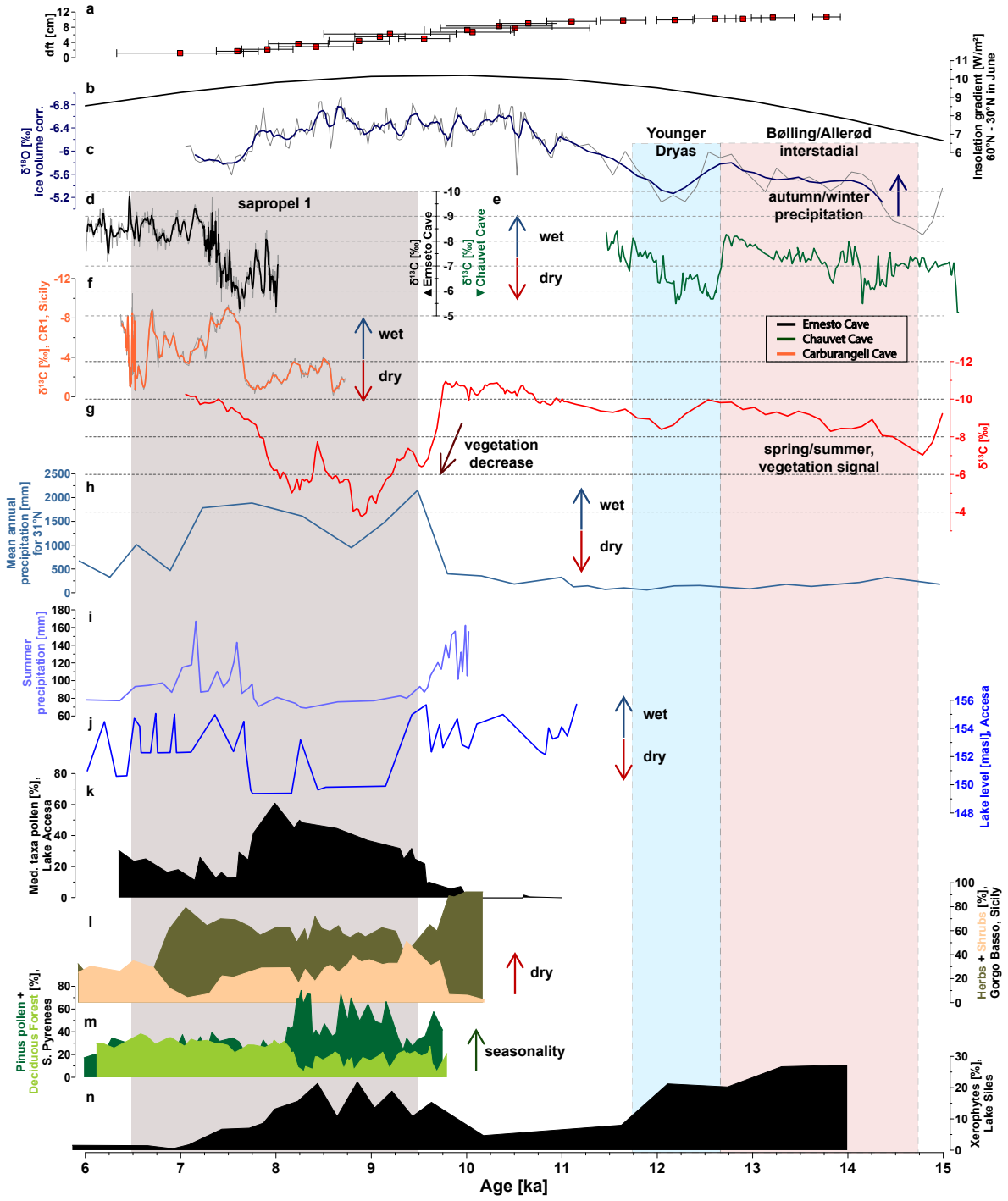


Figure 4.8: Continued.

▲ Figure 4.8 (continued): $\delta^{18}$O (c) and $\delta^{13}$C (g) records of the CV flowstone compared with speleothem $\delta^{13}$C records from Ernesto Cave (d, Scholz et al., 2012), Chauvet Cave (e, Genty et al., 2006) and Grotta di Carburangeli (f, Frisia et al., 2006). Mean annual precipitation of N Africa at 31°N displays the timing of the northernmost extent of the African monsoon (h, Tierney et al., 2017). Furthermore, pollen-inferred reconstructions of summer precipitation (i, Peyron et al., 2011) and lake levels (j, Finsinger et al., 2010) and a pollen record from Lake Accesa, Italy (k, Drescher-Schneider et al., 2007) are shown. Finally, three pollen records (l, herbs and shrubs from Gorgo Basso, Sicily (Tinner et al., 2009); m, Pinus (dark green) and deciduous forest (light green) pollen from Basa de la Mora, NE Spain (Pérez-Sanz et al., 2013), and n the amount of xerophytes in Siles Lake, S Spain (Carrión, 2002)), are plotted. Ages with adjacent uncertainties are plotted on top (a) and June insolation gradient between 60° and 30°N is plotted below (b, Berger, 1978). For the locations of the individual records, see Figure 4.1. The y-axes for records c to g are inverted.

The YD is clearly visible in the CV flowstone record by an increase in both the $\delta^{13}$C and the $\delta^{18}$O values, forming a trough with less negative values (Figures 4.7 and 4.8). This suggests both colder and drier conditions in south-eastern Spain during the YD, which is confirmed by the decrease in SST by approximately 4 °C and the decline in pollen of woody taxa in Italian lake sediments by about 20 % (Allen et al., 2002). Drier conditions during the YD were also observed in other speleothem $\delta^{13}$C records from southern Europe (e.g., Genty et al., 2006; Moreno et al., 2010; Figure 8e). Due to the relatively low temporal resolution of our record, we do not observe two phases of the YD, as has been reported for northern Spain (Baldini et al., 2015).

### 11.7 – 9.7 ka

The $\delta^{18}$O values of the CV flowstone progressively decrease from the YD to the maximum June insolation gradient (Figure 4.8a). This trend towards more negative $\delta^{18}$O values coincides with a positive trend in the NGRIP ice core $\delta^{18}$O record (Rasmussen et al., 2006) and SST in the Alboran Sea (Cacho et al., 1999; Martrat et al., 2014; Figure 4.7a and e). This decreasing trend in $\delta^{18}$O values is accompanied by a trend towards lower $\delta^{13}$C values, suggesting a further increase in vegetation density and spring/summer precipitation until the Holocene climate optimum. These trends can be observed in several records from the Mediterranean. For instance, the substantial decrease of xerophytes (Figure 4.8n) and the shift to 70 % of Pinus pollen in south-eastern Spain during this period indicates warmer and wetter conditions (Carrión, 2002; Carrión et al., 2010). A similar trend in pollen assemblages was found in the Alboran Sea with increasing woody pollen taxa from the YD to 9.7 ± 0.3 ka (Combourieu Nebout et al., 2009) and total pollen amount (Fletcher et al., 2013).

### 9.7 – 7 ka

Many climate records from the Iberian Peninsula are available for the time period between 9.7 and 7 ka. We first present a comparison with records from the cave region, followed by a comparison with records across the Iberian Peninsula and finally discuss the circum-Western Mediterranean. The CV speleothem $\delta^{13}$C values show a large positive excursion between 9.7 ± 0.3 and 7.8 ± 0.2 ka, while the $\delta^{18}$O record reaches a plateau at -6.6 ‰ around 10.5 ± 0.35 ka. As discussed above, we interpret this excursion in the $\delta^{13}$C values as a result of reduced vegetation density due to very dry conditions during the growth period of vegetation in spring and summer. Autumn/winter precipitation, in contrast, must have remained on a similar level or even increased, preventing PCP in the aquifer and resulting in a similar speleothem growth rate as for the previous section. This interval of strong spring and summer droughts was also observed in several other terrestrial records from the eastern and south-eastern Iberian Peninsula. For instance, a pollen record from Lake Siles, in the mountains to the west near CV, shows an increase of the proportion of xerophytes (Jalut et al., 2000; Carrión, 2002) during the $\delta^{13}$C excursion (Figure 4.8n), suggesting drier conditions during the vegetation season (spring/summer). Similarly, pollen records from fluvial deposits in the region of Almeria indicate a decrease of vegetation and microbiological activity in the soil due to less precipitation (Pantaléon-Cano et al., 2003). Further west, a speleothem record from Refugio Cave (Walczak et al., 2015) indicates temperate climate with rainfall throughout the year until 7 ka. However, it cannot be ruled out that this record predominantly represents winter precipitation. In addition, the speleothem records from Refugio Cave and CV both show a growth interruption subsequent to 7 ka, which is evidence for a dry regional climate. However, high speleothem growth rates between 6.9 and 6.4 ka observed at Nerja Cave (McMillan, 2006) demonstrate the complexity of the climate system in this region and may - as the Refugio cave site - also have been under the predominant influence of the NAO pattern (Comas-Bru and McDermott, 2014). Further north of CV and more inland, the eastern part of the Iberian Peninsula is still under the same precipitation regime as CV, which is strongly influenced by the WeMO in the present-day climate (Martin-Vide and Lopez-Bustins, 2006). Salines Lake documents sharp aridity events at 10 and 9.5 ka (Burjachs et al., 2016), although the occurrence of ostracods indicates a permanent lake level between 10 and 8 ka. The adjacent Villena Lake shows long-term aridity events at around 10 ka and from approx. 9 to 7 ka (Jones et al., 2018), which coincide very well with the large $\delta^{13}$C excursion in our speleothem record. Although the behaviour of Salines lake level appears contradictive to our speleothem $\delta^{13}$C record, this can be explained by the constant feed of groundwater to Lake Salines, as observed during the present-day situation (Burjachs et al., 2016). Lake Villarquemado shows pronounced abundance of xerophyte taxa from 10 to 9.3 ka, indicating a dry period (Aranbarri et al., 2014). This dry period might be shorter due to the high elevation and the less efficient evapotranspiration at this altitude (≈ 1000 m a.s.l.; Aranbarri et al., 2014). Close to this lake, a late winter/early spring aridity has been observed in a speleothem record from central Spain (Molinos Cave, Moreno et al., 2017) showing increased $\delta^{13}$C values (9.5 – 7.1 ka) and even an interruption of speleothem

growth (between 9.4 and 8.4 ka). In summary, several records suggest a consistently dry period (with enhanced seasonality) during the $\delta^{13}$C excursion of the CV record in south-eastern Spain. In northern Spain, a short and pronounced stalagmite growth phase between 10 and ca. 7 ka ending no later than at 4 ka suggests unfavourable conditions for stalagmite growth due to a regional drought (Stoll et al., 2013). This is in agreement with our record, since the positive WeMO index correlates positively with precipitation in this region, but negatively in eastern Spain and at CV, especially at the end of winter/early spring (Martin-Vide and Lopez-Bustins, 2006). In the eastern range of the Cantabrian Mountains, high $\delta^{13}$C values in the Kaite Cave record (9.5 – 8.2 ka, Domínguez-Villar et al., 2017) might reflect low vegetation density. This period coincides with high $\delta^{13}$C values and a hiatus in the speleothem record from Molinos Cave between 9.4 and 8.4 ka, which indicates the end of winter/early spring aridity (Moreno et al., 2017), although this record indicates dry conditions lasting until 4.8 ka. In the Pyrenees, a sharp increase of Pinus and deciduous forest pollen in the lake record at Basa de la Mora (Pérez-Sanz et al., 2013; Figure 4.8m) also indicates strong seasonality with dry summers and humid winters. This is supported by sediments in the Ebro basin suggesting a thin vegetation cover and semiarid conditions with extensive erosion (Bastida et al., 2013). Arid conditions with pronounced rainfall seasonality are indicated by tufa deposits from Marcelino (South Pyrenees, Pellicer et al., 2016) and are also reflected by a high percentage of non-arboreal pollen until 8 ka at La Garrotxa (NE Spain, Piqué et al., 2018). Although lake-level reconstructions from this region suggest high rainfall, these may again be biased by seasonal precipitation and enhanced melting of ice and snow in the Pyrenees, which also supply the lowlands, leading to the formation of riparian environments (González-Sampériz et al., 2017). In summary, despite a seemingly contrasting signal to the lake-level records from the Iberian Peninsula (Morellón et al., 2018), we conclude pronounced spring and summer drought and more humid autumn/winter conditions for Iberian Peninsula between approximately 10 and 7 ka. The apparent disagreement with some lake-level records may be related to a seasonal bias in the lake-level reconstructions (González-Sampériz et al., 2017), different altitudes of the catchment areas and/or continuous feeding groundwater (e.g., Lake Salines; Burjachs et al., 2016). We therefore suggest that the lake-level records presented by Morellón et al., (2018) predominantly reflect an autumn/winter rainfall signal (i.e., the main period of precipitation in south-eastern Spain), but did not record the dry spring/summer conditions reflected in our $\delta^{13}$C record. In a larger circum-West Mediterranean context, in northern Italy, higher $\delta^{13}$C values at Ernesto Cave between 8 and 7.5 ka indicate relatively dry conditions (Scholz et al., 2012; Figure 4.8d). A coeval speleothem record from Corchia Cave (Zanchetta et al., 2007; Figure 4.7b) shows low $\delta^{18}$O values, reflecting increased seasonality with drier summers and wetter winters. Lake-level reconstructions (Finsinger et al., 2010) based on pollen assemblages from Lake Accesa (Drescher-Schneider et al., 2007) in central Italy indicate a low lake level (Figure 4.8j; Peyron et al., 2011) due to reduced summer precipitation, but enhanced winter precipitation during the period of high CV flowstone $\delta^{13}$C values. In addition, the increase of Mediterranean pollen taxa at the same site (Drescher-Schneider et al., 2007) indicates summer drought (Figure 4.8k). Thus, the dry period recorded in the CV flowstone is also observed in

several archives from the north-eastern part of the Western Mediterranean (Ligurian Sea). In Sicily, herb and shrub pollen are abundant (Gorgo Basso; Tinner et al., 2009, Figure 4.8l), and the adjacent Lago Preola shows a similar pattern from dominant shrub to tree pollen assemblages at around 7 ka (Curry et al., 2016; Magny et al., 2011; Calò et al., 2012). A strong seasonality with high winter precipitation has also been suggested for northern Sicily based on high $\delta^{13}$C values in a speleothem from Grotta di Carburangeli (Frisia et al., 2006; Figure 4.8f). These records document a humid winter and dry summer interval in the south-eastern part of the Western Mediterranean (Tyrrhenian Sea). However, at higher elevations in Sicily, Lake Pergusa sediments record similar dry climate conditions with a rapid shift at already 8.9 ka towards a wetter climate and the establishment of a forest vegetation (Sadori and Narcisi, 2001). Whereas in the Western Mediterranean the spring/summer climate was drier and winters were wetter during 9.7 ± 0.3 – 7.8 ± 0.2 ka, climate records from Morocco (Wassenburg et al., 2016; Zielhofer et al., 2017) and Tunisia (Genty et al., 2006) show a different pattern. On multi-millennial timescales, the Lake Sidi Ali $\delta^{18}$O record shows a drying trend from the Early to Late Holocene, lacking evidence of a dry phase between 9.7 ± 0.3 and 7.8 ± 0.2 ka. This difference to the climate at CV can be explained by the strong influence of the NAO in North Morocco, as opposed to south-eastern Spain, where the relation to NAO is insignificant (Table 4.3). The Alboran Sea pollen records that are located between south to south-eastern Spain and Morocco (Combourieu Nebout et al., 2009; Cacho et al., 2001) likely reflect a mixture of both regions. Nevertheless, the increase in the abundance of pollen from plants adapted to dry conditions is strong evidence for several dry periods interrupted by short humid phases during the early to mid-Holocene. At the same time, in the Eastern Mediterranean, the deposition of a sapropel below 1000 m water depth indicates increased precipitation, but mainly during winter (Emeis et al., 2000; Rohling et al., 2015). Evidence for anoxic conditions in the Western Mediterranean due to increased river runoff were reported as well (Jimenez-Espejo et al., 2007). This might be related to increased autumn/winter precipitation as shown by the compilation of climate records in this study.

### The Implications for large-scale atmospheric circulation

The dry spring/summer conditions in the Western Mediterranean realm between 9.7 ± 0.3 and 7.8 ± 0.2 ka occurred when the North African monsoon reached its northernmost position, i.e., the so-called African humid period (deMenocal et al., 2000). Pollen records from the Sahara and the Sahel zone show high abundances of grass and trees (Tjallingii et al., 2008; Hély et al., 2014) indicating enhanced precipitation in northern Africa (Tierney et al., 2017). Especially the northernmost oceanic core off the Moroccan coast (31°N, Figure 4.1) shows a well defined wet period between 10 and 7.5 ka (Figure 4.8h; Tierney et al., 2017). The North African Monsoon is strongly related to the position of the Intertropical Convergence Zone (ITCZ), which together with the Azores Subtropical High is part of the Northern Hemisphere Hadley cell circulation. A change in either the strength or the position of the ITCZ will thus also affect the Azores Subtropical High. However, western Mediterranean precipitation is not only controlled by the summer

season, and we suggest that the seemingly contrasting precipitation patterns derived from the climate records discussed in this paper can only be explained by taking into account all seasons. The timing and evolution of the June insolation gradient between 60°and 30°N is in good agreement with long-term variation of the $\delta^{18}O$ values of the CV flowstone. Low winter insolation versus high summer insolation induced a high seasonality in precipitation, with enhanced winter precipitation (Kutzbach et al., 2014). Pollen-based climate reconstructions (Davis et al., 2003; Davis and Brewer, 2009; Mauri et al., 2015; Fletcher et al., 2010) suggest lower summer and lower winter temperatures (ca. 2 °C) between 10 and 7 ka in the Western Mediterranean/SW Europe and a reduced positive temperature anomaly in the Northern Hemisphere (Marcott et al., 2013; Figure 4.7c). In contrast, SSTs in the Alboran Sea record peak values (≈20 °C, Figure 4.7d; Cacho et al., 1999; Martrat et al., 2014). Lower summer temperatures may suppress convection and therefore precipitation during summer. However, annual precipitation at CV was higher from 9.7 ± 0.3 to 7.8 ± 0.2 ka (Mauri et al., 2015), which might be explained by enhanced seasonality. In combination with high SSTs, cold low pressure systems in autumn and winter (Figure 4.1a and d) enter the Western Mediterranean and force enhanced convection. This should be especially pronounced in the coastal region as modelled by Mauri et al. (2015). Figure 4.1 shows sea-level pressure patterns for different seasons for today and for the time period between 9.7 ± 0.3 and 7.8 ± 0.2 ka, interpreted from the climate records discussed in the text. During the time when the North African Monsoon reached its northernmost position, the Azores High has been shown to be weaker during the winter season (Tierney et al., 2017) associated with a southward shift of the Westerlies. We propose that this not only results in more negative NAO-like conditions during the Early Holocene as suggested by Deininger et al. (2016), but also in more frequent shifts of a weakened Icelandic Low towards the Iberian Peninsula extending into the Mediterranean (Kutzbach et al., 2014; Figure 1a). According to the southward shifted low, an intensified WeMO-type pattern (Martin-Vide and Lopez-Bustins, 2006) might become an increasingly important factor for precipitation in the eastern Iberian Peninsula due to elevated SSTs at this time. Precipitation patterns between northern Italy and the eastern Iberian Peninsula confirm the importance of the WeMO as a dominant pattern in the Early Holocene. Due to the southerly displacement of the Westerlies, Icelandic Lows predominantly entered the Western Mediterranean, inducing a WeMO structure in autumn/winter with elevated precipitation. During the boreal spring season, Northern Hemisphere insolation increases. We argue that during the spring season, the ITCZ and the Azores Subtropical High were (analogically to the summer situation) located north compared to the present day, which explains the shortened growth season for vegetation and dry spring conditions in the Western Mediterranean. The Subtropical High moved roughly to the present-day summer position. Riparian forest sites might benefit from high river discharge and high lake levels due to high winter precipitation and snowmelt during spring. During the summer season, Northern Hemisphere insolation was higher than today, which led to a more northern position of the ITCZ (Chiang and Friedman, 2012; Tierney et al., 2017) and the adjacent Subtropical High (Schneider et al., 2014). A recent modelling study shows a stable low pressure over northwest Africa during the time of maximum northward extent of the North

African Monsoon (Figure 4.1c, Pausata et al., 2016). Therefore, the Western Mediterranean is under a high pressure cell with dry north-easterly winds, which might suppress local convection (Walczak et al., 2015). During autumn, insolation decreases, and the ITCZ and the adjacent subtropical high move south. Hence, the Westerlies can enter the Western Mediterranean, and their relatively cold air in combination with high SSTs leads to strong convection and intense rainfall during autumn. This intense rainfall leads to aquifer recharge at CV. Many models focus on winter and summer precipitation (Mauri et al., 2015), but spring and autumn are not discussed. We propose that changes in precipitation during autumn and spring are most important for the annual precipitation budget in the eastern part of the Iberian Peninsula between 9.7 ± 0.3 and 7.8 ± 0.2 ka, although we cannot exclude a slight decrease in winter precipitation (Jin et al., 2012) as reported from Molinos Cave (Moreno et al., 2017).

## 4.7 Conclusions

We present a stable isotope and trace element records from flowstones of Cueva Victoria, south-eastern Spain, and based on several Holocene climate records from the Western Mediterranean, we present an estimation on atmospheric conditions for the time between 9.7 ± 0.3 and 7.8 ± 0.2 ka. On shorter timescale, we cannot disentangle the different processes influencing the speleothem $\delta^{18}O$ signal. However, on multi-millennial to orbital timescales, $\delta^{18}O$ values are mainly influenced by North Atlantic temperature changes and seasonality. In general, they represent autumn/winter precipitation $\delta^{18}O$ values, whereas $\delta^{13}C$ values reflect the vegetation density and microbiological activity in the soil and are therefore a spring to summer signal. Between the onset of the B/A and the Early Holocene, $\delta^{18}O$ values progressively decrease, suggesting an influence by increasing temperature and precipitation in south-eastern Spain in accordance with SSTs in the Alboran Sea. At the same time, decreasing $\delta^{13}C$ values indicate progressively increasing precipitation and vegetation density. This trend is interrupted by colder and drier conditions during the YD. Between 9.7 ± 0.3 and 7.8 ± 0.2 ka, the $\delta^{13}C$ values show a large positive excursion indicating a strong reduction in vegetation density and, thus, very dry spring/summer conditions. At the same time, autumn/winter precipitation probably increased indicating enhanced seasonality. This dry period with enhanced seasonality is also observed in several other climate records from the Western Mediterranean region, showing that the entire Western Mediterranean realm (Spain, Italy) experienced spring/summer droughts during this period. We suggest that this was related to a more northward positioned and/or stronger Azores Subtropical High. This occurred at the same time when the North African Monsoon reached its northernmost position, which suggests that this is a teleconnection pattern related to the Hadley cell circulation. The increase in autumn/winter precipitation was also observed in the Eastern Mediterranean, which has been suggested as a cause of anoxic conditions and the formation of sapropels.

## 4.8 Acknowledgements

We thank Andrés Ros, the team of CENM-naturaleza and the city of Cartagena for the support of the sampling and opportunity to work in Cueva Victoria. The assistance of Beate Schwager in the geochemistry lab (Max Planck Institute for Chemistry, Mainz) and Manuela Wimmer in the isotope laboratory (University of Innsbruck) is highly appreciated. The authors gratefully acknowledge the NOAA Air Resources Laboratory (ARL) for the provision of the HYSPLIT transport and dispersion model and/or READY website (http://www.ready.noaa.gov) used in this publication. This work was funded by the German Research Foundation (ME3761/2-1 to R. Mertz-Kraus and SCHO 1274/9-1 to D. Scholz). Constructive and detailed comments by the editor, Giles Young, and two anonymous reviewers were very helpful to improve the manuscript.

### References

Agencia Estatal de Meteorología (2011) Atlas climático ibérico: Temperatura del aire y precipitación (1971-2000) [Iberian climate atlas air temperature and precipitation (1971-2000)]. Madrid: Instituto Nacional de Meteorología.

Allan R, Ansell T (2006) A new globally complete monthly historical gridded mean sea level pressure dataset (HadSLP2): 1850–2004. *Journal of Climate* 19(22): 5816–5842.

Allen JRM, Brandt U, Brauer A, Huntley B, Keller J, Kraml M, Mackensen A, Mingram J, Negendank JFW, Nowaczyk NR, Oberhänsli H, Watts WA, Wulf S, Zolitschka B (1999) Rapid environmental changes in southern Europe during the last glacial period. *Nature* 400: 740–743.

Allen JRM, Watts WA, McGee E, Huntley B (2002) Holocene environmental variability—the record from Lago Grande di Monticchio, Italy. *Quaternary International* 88(1): 69–80.

Araguas-Araguas LJ, Diaz Teijeiro MF (2005) Isotope composition of precipitation and water vapour in the Iberian Peninsula: First results of the Spanish Network of Isotopes in Precipitation. In: Isotopic composition of precipitation in the Mediterranean Basin in relation to air circulation patterns and climate: Final report of a coordinated research project, 2000-2004. IAEA-TECDOC 1453. Vienna: International Atomic Energy Agency, 173–190.

Aranbarri J, González-Sampériz P, Valero-Garcés B, Moreno A, Gil-Romera G, Sevilla-Callejo M, García-Prieto E, Di Rita F, Mata MP, Morellón M, Magri D, Rodríguez-Lázaro J, Carrión JS (2014) Rapid climatic changes and resilient vegetation during the Lateglacial and Holocene in a continental region of south-western Europe. *Global and Planetary Change* 114: 50–65.

Ayalon A, Bar-Matthews M, Kaufman A (2002) Climatic conditions during marine oxygen isotope stage 6 in the eastern Mediterranean region from the isotopic composition of speleothems of Soreq Cave, Israel. *Geology* 30(4): 303–306.

Ayalon A, Bar-Matthews M, Sass E (1998) Rainfall-recharge relationships within a karstic terrain in the Eastern Mediterranean semi-arid region, Israel: $\delta^{18}$Oand ?D characteristics. *Journal of Hydrology* 207(1-2): 18–31.

Bajo P, Hellstrom J, Frisia S, Drysdale R, Black J, Woodhead J, Borsato A, Zanchetta G, Wallace MW, Regattieri E, Haese R (2016) "Cryptic" diagenesis and its implications for speleothem

geochronologies. *Quaternary Science Reviews* 148: 17–28.

Baldini LM, McDermott F, Baldini JUL, Arias P, Cueto M, Fairchild IJ, Hoffmann DL, Mattey DP, Müller W, Nita DC, Ontañón R, Garciá-Moncó C, Richards DA (2015) Regional temperature, atmospheric circulation, and sea-ice variability within the Younger Dryas Event constrained using a speleothem from northern Iberia. *Earth and Planetary Science Letters* 419(0): 101–110.

Baldini LM, McDermott F, Baldini JUL, Fischer MJ, Möllhoff M (2010) An investigation of the controls on Irish precipitation $\delta^{18}$Ovalues on monthly and event timescales. *Climate Dynamics* 35(6): 977–993.

Bard E, Delaygue G, Rostek F, Antonioli F, Silenzi S, Schrag DP (2002) Hydrological conditions over the western Mediterranean basin during the deposition of the cold Sapropel 6 (ca. 175 kyr BP). *Earth and Planetary Science Letters* 202(2): 481–494.

Bardají T, Goy JL, Zazo C, Hillaire-Marcel C, Dabrio CJ, Cabero A, Ghaleb B, Silva PG, Lario J (2009) Sea level and climate changes during OIS 5e in the Western Mediterranean. *Geomorphology* 104(1-2): 22–37.

Bar-Matthews M, Ayalon A, Gilmour M, Matthews A, Hawkesworth CJ (2003) Sea–land oxygen isotopic relationships from planktonic foraminifera and speleothems in the Eastern Mediterranean region and their implication for paleorainfall during interglacial intervals. *Geochimica et Cosmochimica Acta* 67(17): 3181–3199.

Barnston AG, Livezey RE (1987) Classification, Seasonality and Persistence of Low-Frequency Atmospheric Circulation Patterns. *Monthly Weather Review* 115(6): 1083–1126.

Bartolomé M, Moreno A, Sancho C, Stoll HM, Cacho I, Spötl C, Belmonte Á, Edwards RL, Cheng H, Hellstrom JC (2015) Hydrological change in Southern Europe responding to increasing North Atlantic overturning during Greenland Stadial 1. *Proceedings of the National Academy of Sciences* 112(21): 6568–6572.

Bastida J, Osácar MC, Sancho C, Muñoz A (2013) Environmental changes during the Upper Pleistocene–Holocene in Mediterranean NE Spain as recorded by the mineralogy and geochemistry of alluvial records. *Quaternary International* 302: 3–19.

Berger AL (1978) Long-term variations of daily insolation and Quaternary climatic changes. *Journal of the Atmospheric Sciences* 35(12): 2362–2367.

Boch R, Spötl C, Kramers J (2009) High-resolution isotope records of early Holocene rapid climate change from two coeval stalagmites of Katerloch Cave, Austria. *Quaternary Science Reviews* 28(23-24): 2527–2538.

Bond G, Kromer B, Beer J, Muscheler R, Evans M, Showers W, Hoffmann S, Lotti-Bond R, Hajdas I, Bonani G (2001) Persistent solar influence on North Atlantic climate during the Holocene. *Science* 294(5549): 2130–2136.

Brauer A, Allen JRM, Mingram J, Dulski P, Wulf S, Huntley B (2007) Evidence for last interglacial chronology and environmental change from Southern Europe. *Proceedings of the National Academy of Sciences* 104(2): 450–455.

Breecker DO, Payne AE, Quade J, Banner JL, Ball CE, Meyer KW, Cowan BD (2012) The sources and

sinks of $CO_2$ in caves under mixed woodland and grassland vegetation. Geochimica et Cosmochimica Acta 96: 230–246.

Budsky A, Scholz D, Gibert L, Mertz-Kraus R (2015) $^{230}$Th/U-dating of the Cueva Victoria flowstone sequence: Preliminary results and paleoclimate implications: Datación mediante $^{230}$Th/U de la secuencia de espeleotemas de Cueva Victoria: Resultados preliminares e implicaciones paleoclimáticas. In: Gibert L, Ferràndez-Canadell C (eds.) Geología y Paleontología de Cueva Victoria: Geology and Paleontology of Cueva Victoria. *Mastia* 11-13. Cartagena, 101–109.

Burjachs F, Jones SE, Giralt S, Fernández-López De Pablo J, Fernández-López De Pablo J (2016) Lateglacial to Early Holocene recursive aridity events in the SE Mediterranean Iberian Peninsula: The Salines playa lake case study. *Quaternary International* 403: 187–200.

Cacho I, Grimalt JO, Canals M, Sbaffi L, Shackleton NJ, Schönfeld J, Zahn R (2001) Variability of the western Mediterranean Sea surface temperature during the last 25,000 years and its connection with the Northern Hemisphere climatic changes. *Paleoceanography* 16(1): 40–52.

Cacho I, Grimalt JO, Pelejero C, Canals M, Sierro FJ, Flores JA, Shackleton N (1999) Dansgaard-Oeschger and Heinrich event imprints in Alboran Sea paleotemperatures. Paleoceanography 14(6): 698–705.

Calò C, Henne PD, Curry B, Magny M, Vescovi E, La Mantia T, Pasta S, Vannière B, Tinner W (2012) Spatio-temporal patterns of Holocene environmental change in southern Sicily. *Palaeogeography, Palaeoclimatology, Palaeoecology* 323-325: 110–122.

Calvo FR, Sánchez J, Acosta A, Wolf D, Faust D (2016) Granulometrical, mineralogical and geochemical characterization of loess deposits in the Tajo Basin. *Quaternary International* 407: 14–28. doi:10.1016/j.quaint.2015.11.122.

Camarero JJ, Gazol A, Tardif JC, Conciatori F (2015) Attributing forest responses to global-change drivers: Limited evidence of a $CO_2$ -fertilization effect in Iberian pine growth. *Journal of Biogeography* 42(11): 2220–2233.

Carrasco F, Andreo B, Liñán C, Mudry J (2006) Contribution of stable isotopes to the understanding of the unsaturated zone of a carbonate aquifer (Nerja Cave, southern Spain). *Comptes Rendus Geoscience* 338(16): 1203–1212.

Carrión JS (2002) Patterns and processes of Late Quaternary environmental change in a montane region of southwestern Europe. *Quaternary Science Reviews* 21(18-19): 2047–2066.

Carrión JS, Fernández S, González-Sampériz P, Gil-Romera G, Badal E, Carrión-Marco Y, López-Merino L, López-Sáez JA, Fierro E, Burjachs F (2010) Expected trends and surprises in the Lateglacial and Holocene vegetation history of the Iberian Peninsula and Balearic Islands. *Review of Palaeobotany and Palynology* 162(3): 458–475.

Celle-Jeanton H, Travi Y, Blavoux B (2001) Isotopic typology of the precipitation in the Western Mediterranean Region at three different time scales. *Geophysical Research Letters* 28(7): 1215–1218.

Cerling TE, Wang Y, Quade J (1993) Expansion of C4 ecosystems as an indicator of global ecological change in the late Miocene. *Nature* 361: 344–345.

Cheng H, Edwards RL, Hoff J, Gallup CD, Richards DA, Asmerom Y (2000) The half-lives of uranium-234 and thorium-230. *Chemical Geology* 169(1–2): 17–33.

Chiang JCH, Friedman AR (2012) Extratropical cooling, interhemispheric thermal gradients, and tropical climate change. *Annual Review of Earth and Planetary Sciences* 40(1): 383–412.

Comas-Bru L, McDermott F (2014) Impacts of the EA and SCA patterns on the European twentieth century NAO-winter climate relationship. *Quarterly Journal of the Royal Meteorological Society* 140(679): 354–363.

Combourieu Nebout N, Peyron O, Dormoy I, Desprat S, Beaudouin C, Kotthoff U, Marret F (2009) Rapid climatic variability in the west Mediterranean during the last 25 000 years from high resolution pollen data. *Climate of the Past* 5(3): 503–521.

Constantin S, Bojar A-V, Lauritzen S-E, Lundberg J (2007) Holocene and Late Pleistocene climate in the sub-Mediterranean continental environment: A speleothem record from Poleva Cave (Southern Carpathians, Romania). *Palaeogeography, Palaeoclimatology, Palaeoecology* 243(3-4): 322–338.

Coudé-Gaussen G (1990) The loess and loess-like deposits along the sides of the western Mediterranean Sea: Genetic and palaeoclimatic significance. *Quaternary International* 5: 1–8.

Curry B, Henne PD, Mesquita-Joanes F, Marrone F, Pieri V, La Mantia T, Calò C, Tinner W (2016) Holocene paleoclimate inferred from salinity histories of adjacent lakes in southwestern Sicily (Italy). *Quaternary Science Reviews* 150: 67–83.

Dansgaard W (1964) Stable isotopes in precipitation. *Tellus* 16(4): 436–468.

Davis BAS, Brewer S (2009) Orbital forcing and role of the latitudinal insolation/temperature gradient. *Climate Dynamics* 32(2): 143–165.

Davis BAS, Brewer S, Stevenson AC, Guiot J (2003) The temperature of Europe during the Holocene reconstructed from pollen data. *Quaternary Science Reviews* 22(15-17): 1701–1716.

Deininger M, Werner M, McDermott F (2016) North Atlantic Oscillation controls on oxygen and hydrogen isotope gradients in winter precipitation across Europe; implications for palaeoclimate studies. *Climate of the Past* 12(11): 2127–2143.

Denniston RF, González LA, Asmerom Y, Reagan MK, Recelli-Snyder H (2000) Speleothem carbon isotopic records of Holocene environments in the Ozark Highlands, USA. *Quaternary International* 67(1): 21–27.

Domínguez-Villar D, Wang X, Krklec K, Cheng H, Edwards RL (2017) The control of the tropical North Atlantic on Holocene millennial climate oscillations. *Geology* 45(4): 303–306.

Dorale JA, Edwards RL, Ito E, González LA (1998) Climate and vegetation history of the midcontinent from 75 to 25 ka: A speleothem record from Crevice Cave, Missouri, USA. *Science* 282(5395): 1871–1874.

Drescher-Schneider R, Beaulieu J-L de, Magny M, Walter-Simonnet A-V, Bossuet G, Millet L, Brugiapaglia E, Drescher A (2007) Vegetation history, climate and human impact over the last 15,000 years at Lago dell'Accesa (Tuscany, Central Italy). *Vegetation History and Archaeobotany* 16(4): 279–299.

Dreybrodt W, Scholz D (2011) Climatic dependence of stable carbon and oxygen isotope signals recorded in speleothems: From soil water to speleothem calcite. *Geochimica et Cosmochimica Acta* 75(3): 734–752.

Drysdale R, Zanchetta G, Hellstrom J, Maas R, Fallick A, Pickett M, Cartwright I, Piccini L (2006) Late Holocene drought responsible for the collapse of Old World civilizations is recorded in an Italian cave flowstone. *Geology* 34(2): 101.

Emeis K-C, Struck U, Schulz H-M, Rosenberg R, Bernasconi S, Erlenkeuser H, Sakamoto T, Martinez-Ruiz F (2000) Temperature and salinity variations of Mediterranean Sea surface waters over the last 16,000 years from records of planktonic stable oxygen isotopes and alkenone unsaturation ratios. *Palaeogeography, Palaeoclimatology, Palaeoecology* 158(3–4): 259–280.

Espinosa-Godoy J, Martin Vivaldi JM, Pérez Rojas A (1972) Mapa geologico de Espana: Llano del Beal, 978. Madrid: Instituto geologgico y minero de Espana.

Fairchild IJ, Baker A (2012) Speleothem science: From process to past environments. Oxford, U.K, Hoboken, N.J: Wiley.

Fairchild IJ, Borsato A, Tooth AF, Frisia S, Hawkesworth CJ, Huang Y, McDermott F, Spiro B (2000) Controls on trace element (Sr–Mg) compositions of carbonate cave waters: implications for speleothem climatic records. *Chemical Geology* 166(3-4): 255–269.

Fairchild IJ, Treble PC (2009) Trace elements in speleothems as recorders of environmental change. *Quaternary Science Reviews* 28(5-6): 449–468.

Fensterer C, Scholz D, Hoffmann D, Mangini A, Pajón JM (2010) $^{230}$Th/U-dating of a late Holocene low uranium speleothem from Cuba. *IOP Conference Series: Earth and Environmental Science* 9: 12015.

Ferràndez-Cañadell C, Ribot F, Gibert L (2014) New fossil teeth of Theropithecus oswaldi (Cercopithecoidea) from the Early Pleistocene at Cueva Victoria (SE Spain). *Journal of Human Evolution* 74: 55–66.

Finsinger W, Colombaroli D, Beaulieu J-L de, Valsecchi V, Vannière B, Vescovi E, Chapron E, Lotter AF, Magny M, Tinner W (2010) Early to mid-Holocene climate change at Lago dell'Accesa (central Italy): Climate signal or anthropogenic bias? *Journal of Quaternary Science* 25(8): 1239–1247.

Fletcher WJ, Debret M, Sanchez Goñi MF (2013) Mid-Holocene emergence of a low-frequency millennial oscillation in western Mediterranean climate: Implications for past dynamics of the North Atlantic atmospheric westerlies. *The Holocene* 23(2): 153–166.

Fletcher WJ, Sanchez Goñi MF, Peyron O, Dormoy I (2010) Abrupt climate changes of the last deglaciation detected in a Western Mediterranean forest record. *Climate of the Past* 6(2): 245–264.

Fletcher WJ, Sánchez Goñi MF (2008) Orbital- and sub-orbital-scale climate impacts on vegetation of the western Mediterranean basin over the last 48,000 yr. *Quaternary Research* 70(3): 451–464.

Fohlmeister J, Scholz D, Kromer B, Mangini A (2011) Modelling carbon isotopes of carbonates in cave drip water. *Geochimica et Cosmochimica Acta* 75(18): 5219–5228.

Fohlmeister J, Schröder-Ritzrau A, Scholz D, Spötl C, Riechelmann DFC, Mudelsee M, Wackerbarth A, Gerdes A, Riechelmann S, Immenhauser A, Richter DK, Mangini A (2012) Bunker Cave stalagmites: an archive for central European Holocene climate variability. *Climate of the Past* 8(5): 1751–1764.

Frisia S (2015) Microstratigraphic logging of calcite fabrics in speleothems as tool for palaeoclimate studies. *International Journal of Speleology* 44(1): 1–16.

Frisia S, Borsato A, Mangini A, Spötl C, Madonia G, Sauro U (2006) Holocene climate variability in Sicily from a discontinuous stalagmite record and the Mesolithic to Neolithic transition. *Quaternary Research* 66(3): 388–400.

Frisia S, Borsato A, Spötl C, Villa IM, Cucchi F (2005) Climate variability in the SE Alps of Italy over the past 17 000 years reconstructed from a stalagmite record. *Boreas* 34(4): 445–455.

García-Alix A, Jiménez-Moreno G, Jiménez-Espejo FJ, García-García F, Delgado Huertas A (2014) An environmental snapshot of the Bølling interstadial in Southern Iberia. *Quaternary Research* 81(2): 284–294.

Gazol A, Ribas M, Gutiérrez E, Camarero JJ (2017) Aleppo pine forests from across Spain show drought-induced growth decline and partial recovery. *Agricultural and Forest Meteorology* 232: 186–194.

Genty D, Blamart D, Ghaleb B, Plagnes V, Causse C, Bakalowicz M, Zouari K, Chkir N, Hellstrom J, Wainer K (2006) Timing and dynamics of the last deglaciation from European and North African $\delta^{13}$Cstalagmite profiles—comparison with Chinese and South Hemisphere stalagmites. *Quaternary Science Reviews* 25(17-18): 2118–2142.

Genty D, Combourieu Nebout N, Hatté C, Blamart D, Ghaleb B, Isabello L (2005) Rapid climatic changes of the last 90 kyr recorded on the European continent. *Comptes Rendus Geoscience* 337(10-11): 970–982.

Genty D, Blamart D, Ouahdi R, Gilmour M, Baker A, Jouzel J, Van-Exter S (2003) Precise dating of Dansgaard–Oeschger climate oscillations in western Europe from stalagmite data. *Nature* 421: 833–837.

Gibert L, Scott GR, Scholz D, Budsky A, Ferràndez C, Ribot F, Martin RA, Lería M, Ferrandez C, Leria M (2016) Chronology for the Cueva Victoria fossil site (SE Spain): Evidence for Early Pleistocene Afro-Iberian dispersals. *Journal of Human Evolution* 90: 183–197.

Gibert L, Ferràndez-Canadell C (eds.) (2015) Geología y Paleontología de Cueva Victoria: Geology and Paleontology of Cueva Victoria. *Mastia* 11-13. Cartagena.

Gibert J, Gibert L, Ribot F, Ferràndez-Canadell C, Sánchez F, Iglesias A, Walker MJ (2008) CV-0, an early Pleistocene human phalanx from Cueva Victoria (Cartagena, Spain). *Journal of Human Evolution* 54(1): 150–156.

Gimeno L, Nieto R, Trigo RM, Vicente-Serrano SM, López-Moreno JI (2010) Where Does the Iberian Peninsula Moisture Come From?: An Answer Based on a Lagrangian Approach. *Journal of Hydrometeorology* 11(2): 421–436.

González-Sampériz P, Aranbarri J, Pérez-Sanz A, Gil-Romera G, Moreno A, Leunda M, Sevilla-Callejo

M, Corella JP, Morellón M, Oliva B, Valero-Garcés B (2017) Environmental and climate change in the southern Central Pyrenees since the Last Glacial Maximum: A view from the lake records. *CATENA* 149: 668–688.

Grant KM, Rohling EJ, Bar-Matthews M, Ayalon A, Medina-Elizalde M, Ramsey CB, Satow C, Roberts AP (2012) Rapid coupling between ice volume and polar temperature over the past 150,000 years. *Nature* 491: 744–747.

Günster N, Eck P, Skowronek A, Zöller L (2001) Late Pleistocene loess and their paleosols in the Granada Basin, Southern Spain. *Quaternary International* 76-77(1): 241–245.

Hansen M, Scholz D, Froeschmann M-L, Schöne BR, Spötl C (2017) Carbon isotope exchange between gaseous $CO_2$ and thin solution films: Artificial cave experiments and a complete diffusion-reaction model. *Geochimica et Cosmochimica Acta* 211: 28–47.

Harris I, Jones PD, Osborn TJ, Lister DH (2014) Updated high?resolution grids of monthly climatic observations – the CRU TS3.10 Dataset. *International Journal of Climatology* 34(3): 623–642. doi:10.1002/joc.3711.

Hellstrom J (2006) U–Th dating of speleothems with high initial $^{230}$Th using stratigraphical constraint. *Quaternary Geochronology* 1(4): 289–295.

Hély C, Lézine A-M, contributors APD (2014) Holocene changes in African vegetation: Tradeoff between climate and water availability. *Climate of the Past* 10(2): 681–686.

Hodge EJ, Richards DA, Smart PL, Andreo B, Hoffmann DL, Mattey DP, González-Ramón A (2008) Effective precipitation in southern Spain ( 266 to 46 ka) based on a speleothem stable carbon isotope record. *Quaternary Research* 69(3): 447–457.

Hoffmann DL, Beck JW, Richards DA, Smart PL, Singarayer JS, Ketchmark T, Hawkesworth CJ (2010) Towards radiocarbon calibration beyond 28ka using speleothems from the Bahamas. *Earth and Planetary Science Letters* 289(1-2): 1–10.

Hurrell JW, Loon HV (1997) Decadal Variations in climate associated with the North Atlantic Oscillation. *Climatic Change* 36(3): 301–326.

Jaffey AH, Flynn KF, Glendenin LE, Bentley WC, Essling AM (1971) Precision measurement of half-lives and specific activities of 235U and $^{238}$U. *Physical Review C* 4(5): 1889.

Jalut G, Esteban Amat A, Bonnet L, Gauquelin T, Fontugne M (2000) Holocene climatic changes in the Western Mediterranean, from south-east France to south-east Spain. *Palaeogeography, Palaeoclimatology, Palaeoecology* 160(3-4): 255–290.

Jimenez-Espejo FJ, Martinez-Ruiz F, Sakamoto T, Iijima K, Gallego-Torres D, Harada N (2007) Paleoenvironmental changes in the western Mediterranean since the last glacial maximum: High resolution multiproxy record from the Algero–Balearic basin. *Palaeogeography, Palaeoclimatology, Palaeoecology* 246(2-4): 292–306.

Jin L, Chen F, Morrill C, Otto-Bliesner BL, Rosenbloom N (2012) Causes of early Holocene desertification in arid central Asia. *Climate Dynamics* 38(7): 1577–1591.

Jochum KP, Scholz D, Stoll B, Weis U, Wilson SA, Yang Q, Schwalb A, Börner N, Jacob DE, Andreae MO (2012) Accurate trace element analysis of speleothems and biogenic calcium carbonates by

LA-ICP-MS. *Chemical Geology* 318-319: 31–44.

Jochum KP, Weis U, Stoll B, Kuzmin D, Yang Q, Raczek I, Jacob DE, Stracke A, Birbaum K, Frick DA, Günther D, Enzweiler J (2011) Determination of reference values for NIST SRM 610-617 glasses following ISO guidelines. *Geostandards and Geoanalytical Research* 35(4): 397–429.

Jochum KP, Stoll B, Herwig K, Willbold M (2007) Validation of LA-ICP-MS trace element analysis of geological glasses using a new solid-state 193 nm Nd:YAG laser and matrix-matched calibration. *Journal of Analytical Atomic Spectrometry* 22(2): 112–121.

Jochum KP, Nohl U, Herwig K, Lammel E, Stoll B, Hofmann AW (2005) GeoReM: A new geochemical database for reference materials and isotopic standards. *Geostandards and Geoanalytical Research* 29(3): 333–338.

Johnson K, Hu C, Belshaw N, Henderson G (2006) Seasonal trace-element and stable-isotope variations in a Chinese speleothem: The potential for high-resolution paleomonsoon reconstruction. *Earth and Planetary Science Letters* 244(1-2): 394–407.

Jones PD, Jonsson T, Wheeler D (1997) Extension to the North Atlantic oscillation using early instrumental pressure observations from Gibraltar and south?west Iceland. *International Journal of Climatology* 17(13): 1433–1450.

Jones SE, Burjachs F, Ferrer-García C, Giralt S, Schulte L, Fernández-López De Pablo J (2018) A multi-proxy approach to understanding complex responses of salt-lake catchments to climate variability and human pressure: A Late Quaternary case study from south-eastern, Spain. *Quaternary Science Reviews* 184: 201–223.

Kaiser H, Specker H (1956) Bewertung und Vergleich von Analysenverfahren. Fresenius' *Zeitschrift für Analytische Chemie* 149(1-2): 46–66.

Kim S-T, O'Neil JR (1997) Equilibrium and nonequilibrium oxygen isotope effects in synthetic carbonates. *Geochimica et Cosmochimica Acta* 61(16): 3461–3475.

Klein Tank AMG, Wijngaard JB, Können GP, Böhm R, Demarée G, Gocheva A, Mileta M, Pashiardis S, Hejkrlik L, Kern-Hansen C, Heino R, Bessemoulin P, Müller-Westermeier G, Tzanakou M, Szalai S, Pálsdóttir T, Fitzgerald D, Rubin S, Capaldo M, Maugeri M, Leitass A, Bukantis A, Aberfeld R, van Engelen AFV, Forland E, Mietus M, Coelho F, Mares C, Razuvaev V, Nieplova E, Cegnar T, Antonio López J, Dahlström B, Moberg A, Kirchhofer W, Ceylan A, Pachaliuk O, Alexander LV, Petrovic P (2002) Daily dataset of 20th-century surface air temperature and precipitation series for the European Climate Assessment. *International Journal of Climatology* 22(12): 1441–1453.

Kottek M, Grieser J, Beck C, Rudolf B, Rubel F (2006) World Map of the Köppen-Geiger climate classification updated. *Meteorologische Zeitschrift* 15(3): 259–263.

Krklec K, Domínguez-Villar D (2014) Quantification of the impact of moisture source regions on the oxygen isotope composition of precipitation over Eagle Cave, central Spain. *Geochimica et Cosmochimica Acta* 134: 39–54.

Kutzbach JE, Chen G, Cheng H, Edwards RL, Liu Z (2014) Potential role of winter rainfall in explaining increased moisture in the Mediterranean and Middle East during periods of maximum orbitally-forced insolation seasonality. *Climate Dynamics* 42(3): 1079–1095

Lachniet MS (2009) Climatic and environmental controls on speleothem oxygen-isotope values. Quaternary Science Reviews 28(5-6): 412–432. doi:10.1016/j.quascirev.2008.10.021.

Lambeck K, Rouby H, Purcell A, Sun Y, Sambridge M (2014) Sea level and global ice volumes from the Last Glacial Maximum to the Holocene. *Proceedings of the National Academy of Sciences of the United States of America* 111(43): 15296–15303.

Le Roux LJ, Glendenin LE (1963) Half-life of $^{232}$Th. In: South Africa. Atomic Energy Board (ed.) National Conference on Nuclear Energy, Application of Isotopes and Radiation: Proceedings of the National Conference on Nuclear Energy held in Pretoria, April 5-8 1963. Pelindaba, 83–94.

LeGrande AN, Schmidt GA (2006) Global gridded data set of the oxygen isotopic composition in seawater. *Geophysical Research Letters* 33(12).

Linares JC, Delgado-Huertas A, Carreira JA (2011) Climatic trends and different drought adaptive capacity and vulnerability in a mixed Abies pinsapo–Pinus halepensis forest. *Climatic Change* 105(1): 67–90.

Longerich HP, Jackson SE, Günther D (1996) Inter-laboratory note. Laser ablation inductively coupled plasma mass spectrometric transient signal data acquisition and analyte concentration calculation. *Journal of Analytical Atomic Spectrometry* 11(9): 899–904.

Magny M, Joannin S, Galop D, Vannière B, Haas JN, Bassetti M, Bellintani P, Scandolari R, Desmet M (2012) Holocene palaeohydrological changes in the northern Mediterranean borderlands as reflected by the lake-level record of lake ledro, northeastern Italy. *Quaternary Research* 77(03): 382–396.

Magny M, Vannière B, Calo C, Millet L, Leroux A, Peyron O, Zanchetta G, La Mantia T, Tinner W (2011) Holocene hydrological changes in south-western Mediterranean as recorded by lake-level fluctuations at Lago Preola, a coastal lake in southern Sicily, Italy. *Quaternary Science Reviews* 30(19–20): 2459–2475.

Manteca Martínez JI, Pina R (2015) Las mineralizaciones ferro-manganesíferas de la mina-cueva Victoria y su contexto geológico: Fe-Mn mineralizations of the mine-cave Victoria and their geological context. In: Gibert L, Ferràndez-Canadell C (eds.) Geología y Paleontología de Cueva Victoria: Geology and Paleontology of Cueva Victoria. *Mastia* 11-13. Cartagena, 59–74.

Marcott SA, Shakun JD, Clark PU, Mix AC (2013) A reconstruction of regional and global temperature for the past 11,300 years. *Science* 339(6124): 1198–1201.

Martin-Vide J, Lopez-Bustins J-A (2006) The Western Mediterranean Oscillation and rainfall in the Iberian Peninsula. *International Journal of Climatology* 26(11): 1455–1475.

Martrat B, Jimenez-Amat P, Zahn R, Grimalt JO (2014) Similarities and dissimilarities between the last two deglaciations and interglaciations in the North Atlantic region. *Quaternary Science Reviews* 99: 122–134.

Mattey DP, Fairchild IJ, Atkinson TC, Latin J-P, Ainsworth M, Durell R (2010) Seasonal microclimate control of calcite fabrics, stable isotopes and trace elements in modern speleothem from St Michaels Cave, Gibraltar. Geological Society, London, *Special Publications* 336(1): 323–344.

Mauri A, Davis BAS, Collins PM, Kaplan JO (2015) The climate of Europe during the Holocene: A

gridded pollen-based reconstruction and its multi-proxy evaluation. *Quaternary Science Reviews* 112: 109–127.

Mauz B, Fanelli F, Elmejdoub N, Barbieri R (2012) Coastal response to climate change: Mediterranean shorelines during the Last Interglacial (MIS 5). *Quaternary Science Reviews* 54: 89–98.

McDermott F (2004) Palaeo-climate reconstruction from stable isotope variations in speleothems: a review. *Quaternary Science Reviews* 23(7-8): 901–918.

McDermott F, Atkinson TC, Fairchild IJ, Baldini LM, Mattey DP (2011) A first evaluation of the spatial gradients in $\delta^{18}$Orecorded by European Holocene speleothems. *Global and Planetary Change* 79(3-4): 275–287.

McMillan EA (2006) Tests for palaeoaridity in Holocene stalagmites from SW Europe: Ph.D, University of Keele, 314.

Mertz-Kraus R, Brachert TC, Jochum KP, Reuter M, Stoll B (2009) LA-ICP-MS analyses on coral growth increments reveal heavy winter rain in the Eastern Mediterranean at 9 Ma. *Palaeogeography, Palaeoclimatology, Palaeoecology* 273(1-2): 25–40.

Meyer KW, Feng W, Breecker DO, Banner JL, Guilfoyle A (2014) Interpretation of speleothem calcite $\delta^{13}$Cvariations: Evidence from monitoring soil $CO_2$, drip water, and modern speleothem calcite in central Texas. *Geochimica et Cosmochimica Acta* 142: 281–298.

Mischel SA, Mertz-Kraus R, Jochum KP, Scholz D (2017a) TERMITE: An R script for fast reduction of laser ablation inductively coupled plasma mass spectrometry data and its application to trace element measurements. *Rapid Communications in Mass Spectrometry* 31(13): 1079–1087.

Mischel SA, Scholz D, Spötl C, Jochum KP, Schröder-Ritzrau A, Fiedler S (2017b) Holocene climate variability in Central Germany and a potential link to the polar North Atlantic: A replicated record from three coeval speleothems. *The Holocene* 27(4): 509–525.

Morellón M, Aranbarri J, Moreno A, González-Sampériz P, Valero-Garcés BL (2018) Early Holocene humidity patterns in the Iberian Peninsula reconstructed from lake, pollen and speleothem records. *Quaternary Science Reviews* 181: 1–18.

Moreno A, Pérez-Mejías C, Bartolomé M, Sancho C, Cacho I, Stoll H, Delgado-Huertas A, Hellstrom J, Edwards RL, Cheng H (2017) New speleothem data from Molinos and Ejulve caves reveal Holocene hydrological variability in northeast Iberia. *Quaternary Research* 88(02): 223–233.

Moreno A, Sancho C, Bartolomé M, Oliva-Urcia B, Delgado-Huertas A, Estrela MJ, Corell D, López-Moreno JI, Cacho I (2014a) Climate controls on rainfall isotopes and their effects on cave drip water and speleothem growth: the case of Molinos cave (Teruel, NE Spain). *Climate Dynamics* 43(1-2): 221–241.

Moreno A, Svensson A, Brooks SJ, Connor S, Engels S, Fletcher W, Genty D, Heiri O, Labuhn I, Per?oiu A, Peyron O, Sadori L, Valero-Garcés B, Wulf S, Zanchetta G (2014b) A compilation of Western European terrestrial records 60–8 ka BP: towards an understanding of latitudinal climatic gradients. *Quaternary Science Reviews* 106: 167–185.

Moreno A, Stoll H, Jiménez-Sánchez M, Cacho I, Valero-Garcés B, Ito E, Edwards RL (2010) A speleothem record of glacial (25–11.6kyr BP) rapid climatic changes from northern Iberian

Peninsula. *Global and Planetary Change* 71(3-4): 218–231.

Mühlinghaus C, Scholz D, Mangini A (2009) Modelling fractionation of stable isotopes in stalagmites. *Geochimica et Cosmochimica Acta* 73(24): 7275–7289.

North Greenland Ice Core Project members (2004) High-resolution record of Northern Hemisphere climate extending into the last interglacial period. *Nature* 431: 147–151.

Obert JC, Scholz D, Felis T, Brocas WM, Jochum KP, Andreae MO (2016) $^{230}$Th/U dating of Last Interglacial brain corals from Bonaire (southern Caribbean) using bulk and theca wall material. *Geochimica et Cosmochimica Acta* 178: 20–40.

Pantaléon-Cano J, Yll E-I, Pérez-Obiol R, Roure JM (2003) Palynological evidence for vegetational history in semi-arid areas of the western Mediterranean (Almería, Spain). *The Holocene* 13(1): 109–119.

Pasho E, Camarero JJ, Luis M de, Vicente-Serrano SM (2011) Impacts of drought at different time scales on forest growth across a wide climatic gradient in north-eastern Spain. *Agricultural and Forest Meteorology* 151(12): 1800–1811.

Pausata FSR, Messori G, Zhang Q (2016) Impacts of dust reduction on the northward expansion of the African monsoon during the Green Sahara period. *Earth and Planetary Science Letters* 434: 298–307.

Pellicer XM, Corella JP, Gutiérrez F, Roqué C, Linares R, Carbonel D, Zarroca M, Guerrero J, Comas X (2016) Sedimentological and palaeohydrological characterization of Late Pleistocene and Holocene tufa mound palaeolakes using trenching methods in the Spanish Pyrenees. *Sedimentology* 63(6): 1786–1819.

Pérez-Sanz A, González-Sampériz P, Moreno A, Valero-Garcés B, Gil-Romera G, Rieradevall M, Tarrats P, Lasheras-Álvarez L, Morellón M, Belmonte A, Sancho C, Sevilla-Callejo M, Navas A (2013) Holocene climate variability, vegetation dynamics and fire regime in the central Pyrenees: the Basa de la Mora sequence (NE Spain). *Quaternary Science Reviews* 73: 149–169.

Peyron O, Magny M, Goring S, Joannin S, Beaulieu J-Ld, Brugiapaglia E, Sadori L, Garfi G, Kouli K, Ioakim C, Combourieu-Nebout N (2013) Contrasting patterns of climatic changes during the Holocene across the Italian Peninsula reconstructed from pollen data. *Climate of the Past* 9(3): 1233–1252.

Peyron O, Goring S, Dormoy I, Kotthoff U, Pross J, Beaulieu J-L de, Drescher-Schneider R, Vannière B, Magny M (2011) Holocene seasonality changes in the central Mediterranean region reconstructed from the pollen sequences of Lake Accesa (Italy) and Tenaghi Philippon (Greece). *The Holocene* 21(1): 131–146.

Piqué R, Revelles J, Burjachs F, Caruso Fermé L, Pérez-Obiol R (2018) Interdisciplinary approach to the landscape and firewood exploitation during the Holocene at La Garrotxa (Girona, NE Iberia). *Quaternary International* 463: 401–413.

Rasmussen SO, Andersen KK, Svensson AM, Steffensen JP, Vinther BM, Clausen HB, Siggaard-Andersen M-L, Johnsen SJ, Larsen LB, Dahl-Jensen D, Bigler M, Röthlisberger R, Fischer H, Goto-Azuma K, Hansson ME, Ruth U (2006) A new Greenland ice core chronology for the last glacial termination. *Journal of Geophysical Research: Atmospheres* 111(D6).

Ribot F, Ferràndez-Canadell C, Gibert L (2015) Los primates de Cueva Victoria: Primates from Cueva Victoria. In: Gibert L, Ferràndez-Canadell C (eds.) Geología y Paleontología de Cueva Victoria: Geology and Paleontology of Cueva Victoria. *Mastia* 11-13. Cartagena, 433–452.

Richards DA, Dorale JA (2003) Uranium-series Chronology and Environmental Applications of Speleothems. *Reviews in Mineralogy and Geochemistry* 52(1): 407–460.

Ridley HE, Asmerom Y, Baldini JUL, Breitenbach SFM, Aquino VV, Prufer KM, Culleton BJ, Polyak V, Lechleitner FA, Kennett DJ, Zhang M, Marwan N, Macpherson CG, Baldini LM, Xiao T, Peterkin JL, Awe J, Haug GH (2015) Aerosol forcing of the position of the intertropical convergence zone since ad 1550. *Nature Geoscience* 8(3): 195–200.

Ríos-Cornejo D, Penas Á, Álvarez-Esteban R, del Río S (2015) Links between teleconnection patterns and mean temperature in Spain: *Theoretical and Applied Climatology* 122(1-2): 1–18.

Rivera-Collazo I, Winter A, Scholz D, Mangini A, Miller T, Kushnir Y, Black D (2015) Human adaptation strategies to abrupt climate change in Puerto Rico ca. 3.5 ka. *The Holocene* 25(4): 627–640.

Rodriguez-Puebla C, Encinas AH, Nieto S, Garmendia J (1998) Spatial and temporal patterns of annual precipitation variability over the Iberian Peninsula. *International Journal of Climatology* 18(3): 299–316.

Rohling EJ, Marino G, Grant KM (2015) Mediterranean climate and oceanography, and the periodic development of anoxic events (sapropels). *Earth-Science Reviews* 143: 62–97.

Ros A, Llamusí JL (2015) Reconsrucción y génesis del karst de Cueva Victoria: Reconstruction and genesis of the Cueva Victoria karst. In: Gibert L, Ferràndez-Canadell C (eds.) Geología y Paleontología de Cueva Victoria: Geology and Paleontology of Cueva Victoria. *Mastia* 11-13. Cartagena, 111–125.

Roy-Barman M, Pons-Branchu E (2016) Improved U–Th dating of carbonates with high initial $^{230}$Th using stratigraphical and coevality constraints. *Quaternary Geochronology* 32: 29–39.

Rozanski K, Araguás-Araguás L, Gonfiantini R (1992) Relation between long-term trends of oxygen-18 isotope composition of precipitation and climate. *Science* 258(5084): 981–985.

Rozanski K, Araguás-Araguás L, Gonfiantini R (1993) Isotopic Patterns in Modern Global Precipitation. In: Swart PK, Lohmann KC, McKenzie J, Savin S (eds.) Climate Change in Continental Isotopic Records: American Geophysical Union, 1–36.

Rudzka D, McDermott F, Baldini LM, Fleitmann D, Moreno A, Stoll H (2011) The coupled $\delta^{13}$C-radiocarbon systematics of three Late Glacial/early Holocene speleothems; insights into soil and cave processes at climatic transitions. *Geochimica et Cosmochimica Acta* 75(15): 4321–4339.

Sadori L, Narcisi B (2001) The Postglacial record of environmental history from Lago di Pergusa, Sicily. *The Holocene* 11(6): 655–671.

Schneider T, Bischoff T, Haug GH (2014) Migrations and dynamics of the intertropical convergence zone. *Nature* 513: 45.

Scholz D, Tolzmann J, Hoffmann DL, Jochum KP, Spötl C, Riechelmann DFC (2014) Diagenesis of speleothems and its effect on the accuracy of $^{230}$Th/U-ages. *Chemical Geology* 387: 74–86.

Scholz D, Frisia S, Borsato A, Spötl C, Fohlmeister J, Mudelsee M, Miorandi R, Mangini A (2012) Holocene climate variability in north-eastern Italy: Potential influence of the NAO and solar activity recorded by speleothem data. *Climate of the Past* 8(4): 1367–1383.

Scholz D, Hoffmann D (2008) $^{230}$Th/U-dating fossil corals and speleothems. *Eiszeitalter und Gegenwart* 57(1/2): 52–76.

Scholz D, Hoffmann DL (2011) StalAge – An algorithm designed for construction of speleothem age models. *Quaternary Geochronology* 6(3-4): 369–382.

Scholz D, Mühlinghaus C, Mangini A (2009) Modelling $\delta^{13}$Cand $\delta^{18}$Oin the solution layer on stalagmite surfaces. *Geochimica et Cosmochimica Acta* 73(9): 2592–2602.

Siddall M, Rohling EJ, Almogi-Labin A, Hemleben C, Meischner D, Schmelzer I, Smeed DA (2003) Sea-level fluctuations during the last glacial cycle. *Nature* 423: 853–858.

Sinclair DJ, Banner JL, Taylor FW, Partin J, Jenson J, Mylroie J, Goddard E, Quinn T, Jocson J, Miklavi? B (2012) Magnesium and strontium systematics in tropical speleothems from the Western Pacific. *Chemical Geology* 294–295(0): 1–17. doi:10.1016/j.chemgeo.2011.10.008.

Sodemann H, Schwierz C, Wernli H (2008) Interannual variability of Greenland winter precipitation sources: Lagrangian moisture diagnostic and North Atlantic Oscillation influence. Journal of Geophysical Research: Atmospheres 113(D3).

Sodemann H, Stohl A (2009) Asymmetries in the moisture origin of Antarctic precipitation. *Geophysical Research Letters* 36(22).

Spötl C (2011) Long-term performance of the Gasbench isotope ratio mass spectrometry system for the stable isotope analysis of carbonate microsamples. *Rapid Communications in Mass Spectrometry* 25(11): 1683–1685.

Spötl C, Fairchild IJ, Tooth AF (2005) Cave air control on dripwater geochemistry, Obir Caves (Austria): Implications for speleothem deposition in dynamically ventilated caves. *Geochimica et Cosmochimica Acta* 69(10): 2451–2468.

Spötl C, Vennemann TW (2003) Continuous-flow isotope ratio mass spectrometric analysis of carbonate minerals. *Rapid Communications in Mass Spectrometry* 17(9): 1004–1006.

Stein AF, Draxler RR, Rolph GD, Stunder BJB, Cohen MD, Ngan F (2015) NOAA's HYSPLIT atmospheric transport and dispersion modeling system. *Bulletin of the American Meteorological Society* 96(12): 2059–2077.

Stoll H, Mendez-Vicente A, Gonzalez-Lemos S, Moreno A, Cacho I, Cheng H, Edwards RL (2015) Interpretation of orbital scale variability in mid-latitude speleothem $\delta^{18}$O: Significance of growth rate controlled kinetic fractionation effects. *Novel approaches to and new insights from speleothem-based climate reconstructions* 127: 215–228.

Stoll HM, Moreno A, Mendez-Vicente A, Gonzalez-Lemos S, Jimenez-Sanchez M, Dominguez-Cuesta MJ, Edwards RL, Cheng H, Wang X (2013) Paleoclimate and growth rates of speleothems in the northwestern Iberian Peninsula over the last two glacial cycles. *Quaternary Research* 80(2): 284–290.

Stoll HM, Müller W, Prieto M (2012) I-STAL, a model for interpretation of Mg/Ca, Sr/Ca and Ba/Ca

variations in speleothems and its forward and inverse application on seasonal to millennial scales. *Geochemistry, Geophysics, Geosystems* 13(9).

Tierney JE, Pausata FSR, deMenocal PB (2017) Rainfall regimes of the Green Sahara. *Science Advances* 3(1): e1601503.

Tinner W, van Leeuwen JFN, Colombaroli D, Vescovi E, van der Knaap WO, Henne PD, Pasta S, D'Angelo S, La Mantia T (2009) Holocene environmental and climatic changes at Gorgo Basso, a coastal lake in southern Sicily, Italy. *Quaternary Science Reviews* 28(15-16): 1498–1510.

Tjallingii R, Claussen M, Stuut J-BW, Fohlmeister J, Jahn A, Bickert T, Lamy F, Röhl U (2008) Coherent high- and low-latitude control of the northwest African hydrological balance. *Nature Geoscience* 1(10): 670–675.

Treble PC, Fairchild IJ, Griffiths A, Baker A, Meredith KT, Wood A, McGuire E (2015) Impacts of cave air ventilation and in-cave prior calcite precipitation on Golgotha Cave dripwater chemistry, southwest Australia: Novel approaches to and new insights from speleothem-based climate reconstructions. *Quaternary Science Reviews* 127: 61–72.

Tremaine DM, Froelich PN, Wang Y (2011) Speleothem calcite farmed in situ: Modern calibration of $\delta^{18}$Oand $\delta^{13}$Cpaleoclimate proxies in a continuously-monitored natural cave system. *Geochimica et Cosmochimica Acta* 75(17): 4929–4950.

Tzedakis PC (2005) Towards an understanding of the response of southern European vegetation to orbital and suborbital climate variability. *Quaternary Science Reviews* 24(14-15): 1585–1599.

Tzedakis PC, Hooghiemstra H, Pälike H (2006) The last 1.35 million years at Tenaghi Philippon: revised chronostratigraphy and long-term vegetation trends. *Quaternary Science Reviews* 25(23-24): 3416–3430.

Tzedakis PC, Roucoux KH, Abreu L de, Shackleton NJ (2004) The duration of forest stages in Southern Europe and interglacial climate variability. *Science* 306: 2231–2235.

Waelbroeck C, Labeyrie L, Michel E, Duplessy JC, McManus JF, Lambeck K, Balbon E, Labracherie M (2002) Sea-level and deep water temperature changes derived from benthic foraminifera isotopic records. *Quaternary Science Reviews* 21: 295–305.

Walczak IW, Baldini JUL, Baldini LM, McDermott F, Marsden S, Standish CD, Richards DA, Andreo B, Slater J (2015) Reconstructing high-resolution climate using CT scanning of unsectioned stalagmites: A case study identifying the mid-Holocene onset of the Mediterranean climate in southern Iberia. *Quaternary Science Reviews* 127: 117–128.

Wassenburg JA, Dietrich S, Fietzke J, Fohlmeister J, Jochum KP, Scholz D, Richter DK, Sabaoui A, Spötl C, Lohmann G, Andreae MO, Immenhauser A (2016) Reorganization of the North Atlantic Oscillation during early Holocene deglaciation. *Nature Geoscience* 9(8): 602–605.

Wedepohl HK (1995) The composition of the continental crust. *Geochimica et Cosmochimica Acta* 59(7): 1217–1232.

Yang Q, Scholz D, Jochum KP, Hoffmann DL, Stoll B, Weis U, Schwager B, Andreae MO (2015) Lead isotope variability in speleothems—A promising new proxy for hydrological change? First results from a stalagmite from western Germany. *Chemical Geology* 396: 143–151.

Zanchetta G, Drysdale RN, Hellstrom JC, Fallick AE, Isola I, Gagan MK, Pareschi MT (2007) Enhanced rainfall in the Western Mediterranean during deposition of sapropel S1: stalagmite evidence from Corchia cave (Central Italy). *Quaternary Science Reviews* 26(3-4): 279–286.

Zazo C, Goy JL, Dabrio CJ, Lario J, González-Delgado JA, Bardají T, Hillaire-Marcel C, Cabero A, Ghaleb B, Borja F, Silva PG, Roquero E, Soler V (2013) Retracing the Quaternary history of sea-level changes in the Spanish Mediterranean–Atlantic coasts: Geomorphological and sedimentological approach. *Geomorphology* 196: 36–49.

Zielhofer C, Fletcher WJ, Mischke S, Batist M de, Campbell JFE, Joannin S, Tjallingii R, El Hamouti N, Junginger A, Stele A, Bussmann J, Schneider B, Lauer T, Spitzer K, Strupler M, Brachert T, Mikdad A (2017) Atlantic forcing of Western Mediterranean winter rain minima during the last 12,000 years. *Quaternary Science Reviews* 157: 29–51.

## 4.9 Supplemental material

Table 4.1: Average concentrations (µg/g) of reference materials USGS BCR-2G (n = 6) and USGS MACS-3 (n = 6) with associated reference values and limit of detection (LOD, µg/g) for each element.

| | BCR-2G | | | MACS-3 | | | LOD |
|---|---|---|---|---|---|---|---|
| | Mean | 1 SD | GeoReM[a] | Mean | 1 SD | published values[b] | |
| Mg | 23500 | 700 | 21500 | 1730 | 50 | 1880 | 0.017 |
| Sr | 319 | 17 | 342 | 6550 | 240 | 6570 | 0.0002 |
| Ba | 704 | 47 | 683 | 58.6 | 2.1 | 58.9 | 0.002 |

[a] Preferred values from GeoReM database (http://georem.mpch-mainz.gwdg.de/, Application Version 18, January 2015, Jochum et al., 2005; Jochum et al., 2011).
[b] Mean values for MACS-3 (Jochum et al., 2012) and * personal communication by S. Wilson, USGS, therein.

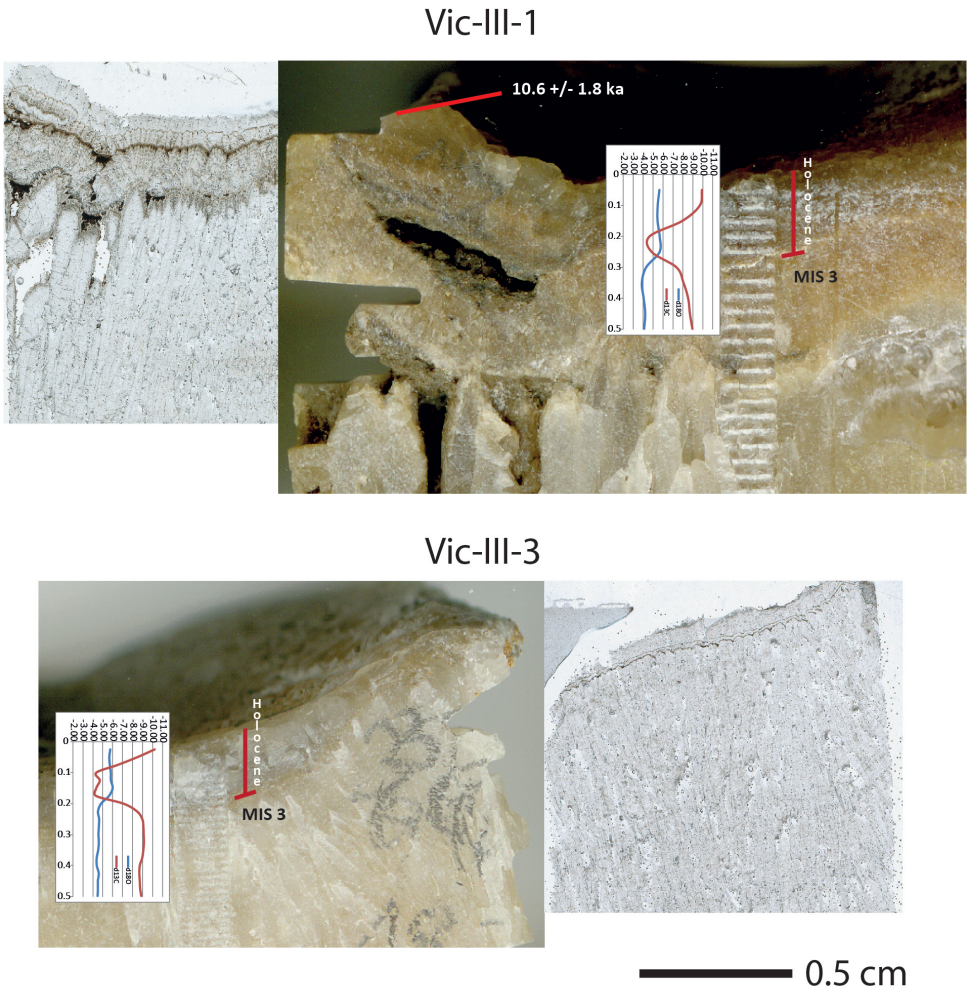


Figure 4.9: Flowstones Vic-III-1 and -3. The top sections of both cores correspond to the Holocene and display the same large excursion in $\delta^{13}C$. Establishing an age-depth model is unfortunately not possible due to the short transect of few millimeters only.

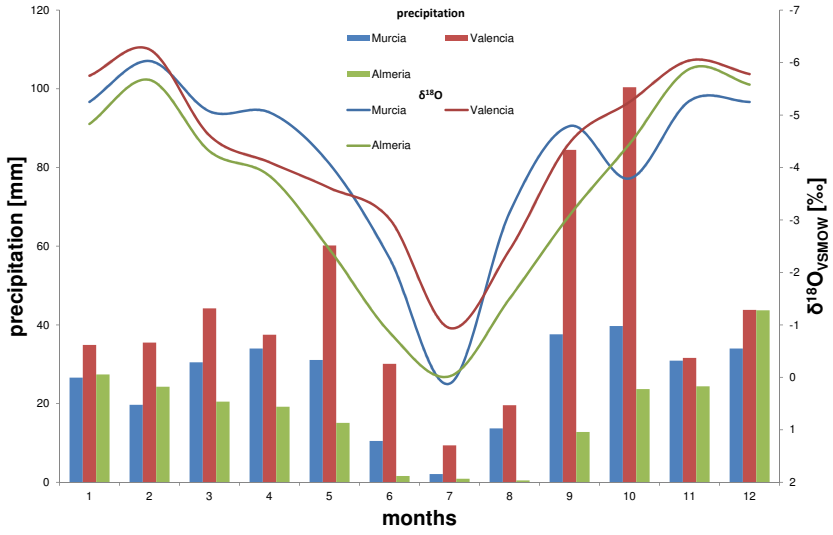


Figure 4.10: Annual evolution of precipitation amount and $\delta^{18}$Ovalues (axis is inverted) for three GNIP stations close to Cueva Victoria: Murcia, Valencia and Almeria (all 2000 - 2010).

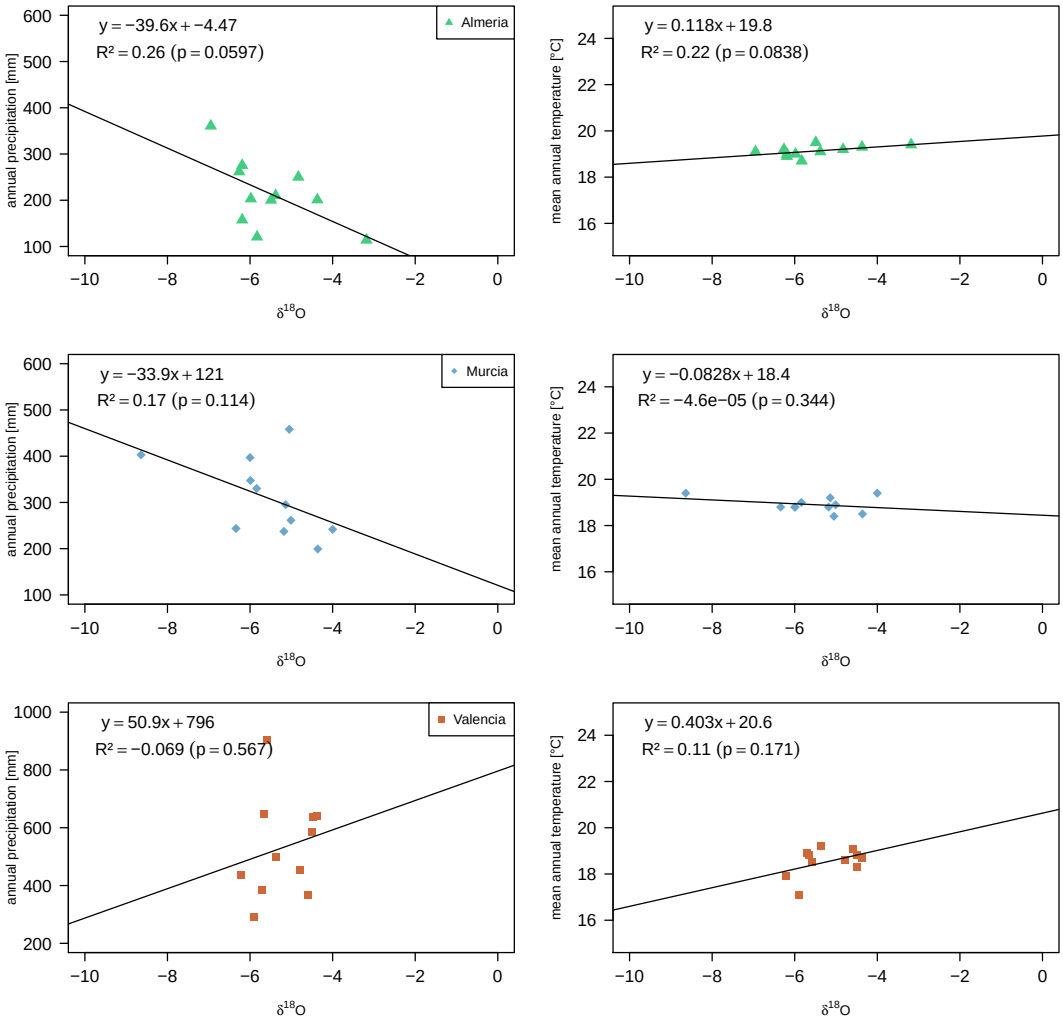


Figure 4.11: Plot of annual precipitation (left) and mean annual temperature (right) against mean annual $\delta^{18}$Ovalues of precipitation (same time interval same as in Figure S4.10). The correlation coefficients and the corresponding p-values are shown. The correlations are insignificant for all stations.

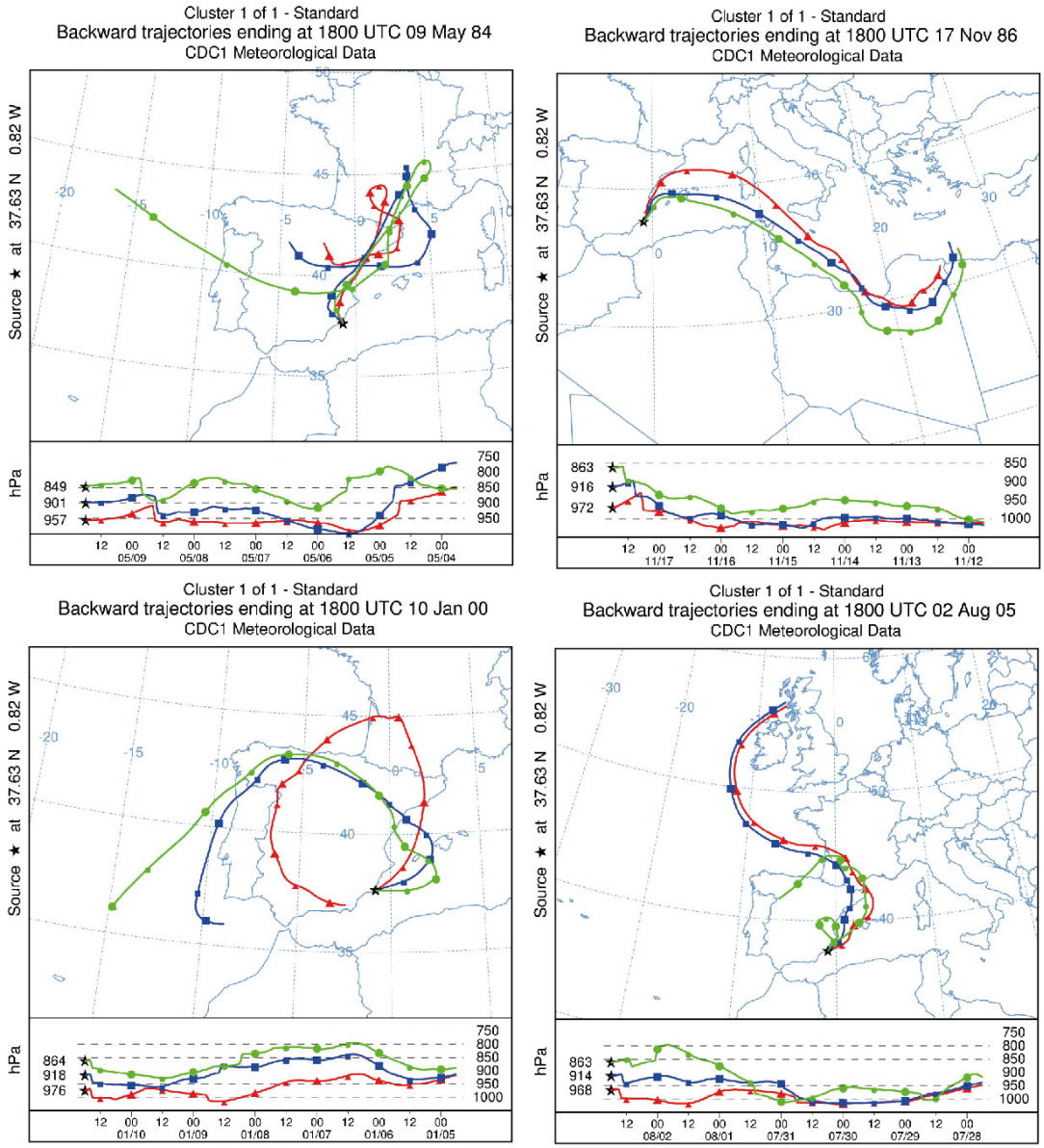


Figure 4.12: Air mass back-trajectories calculated using HYSPLIT to reconstruct the moisture pathways for important precipitation events at the San Javier meteorological station with the pressure history over the investigated 120 hours (direct HYSPLIT output).

Table 4.2: Results of $^{230}$Th/U-dating

| Sample | $^{238}$U (µg/g) | ± | ($^{230}$Th/$^{232}$Th) | ± | ($^{234}$U/$^{238}$U) | ± | ($^{230}$Th/$^{238}$U) | ± | age uncorrected (ka) | ± | age conventionally corrected (ka) | ± | age corrected (ka) | ± | dft (cm) |
|---|---|---|---|---|---|---|---|---|---|---|---|---|---|---|---|
| **Vic-III-4-15** | 0.055 | 0.0004 | 185.7 | 22.0 | 1.246 | 0.005 | 0.032 | 0.002 | 2.83 | 0.20 | 2.82 | 0.19 | 2.78 | 0.20 | 0.0 |
| **Vic-III-4-01** | 0.099 | 0.0006 | 18.8 | 0.3 | 1.253 | 0.002 | 0.089 | 0.002 | 8.32 | 0.12 | 7.99 | 0.20 | 6.90 | 0.71 | 1.0 |
| **Vic-III-4-20** | 0.128 | 0.0009 | 79.1 | 1.5 | 1.208 | 0.004 | 0.085 | 0.001 | 7.97 | 0.13 | 7.89 | 0.13 | 7.64 | 0.19 | 1.7 |
| **Vic-III-4-23** | 0.121 | 0.0008 | 62.5 | 0.9 | 1.228 | 0.003 | 0.091 | 0.001 | 8.40 | 0.12 | 8.30 | 0.12 | 7.97 | 0.24 | 2.1 |
| **Vic-III-4-05** | 0.115 | 0.0007 | 49.9 | 1.4 | 1.211 | 0.003 | 0.097 | 0.002 | 9.09 | 0.22 | 8.95 | 0.23 | 8.50 | 0.35 | 2.6 |
| **Vic-III-4-24** | 0.137 | 0.0010 | 55.8 | 0.8 | 1.202 | 0.005 | 0.093 | 0.001 | 8.81 | 0.11 | 8.69 | 0.13 | 8.31 | 0.27 | 3.4 |
| **Vic-III-4-21** | 0.129 | 0.0009 | 60.4 | 1.2 | 1.198 | 0.004 | 0.100 | 0.001 | 9.45 | 0.14 | 9.33 | 0.16 | 8.95 | 0.28 | 4.1 |
| **Vic-III-4-26** | 0.147 | 0.0011 | 82.5 | 1.4 | 1.199 | 0.005 | 0.105 | 0.002 | 10.00 | 0.15 | 9.90 | 0.16 | 9.61 | 0.24 | 4.8 |
| **Vic-III-4-06** | 0.143 | 0.0009 | 80.7 | 2.1 | 1.217 | 0.002 | 0.102 | 0.002 | 9.52 | 0.15 | 9.43 | 0.15 | 9.15 | 0.23 | 5.1 |
| **Vic-III-4-27** | 0.148 | 0.0011 | 28.3 | 0.4 | 1.215 | 0.005 | 0.112 | 0.001 | 10.56 | 0.13 | 10.27 | 0.19 | 9.37 | 0.58 | 5.8 |
| **Vic-III-4-16** | 0.160 | 0.0011 | 46.1 | 0.6 | 1.204 | 0.005 | 0.115 | 0.002 | 10.92 | 0.14 | 10.74 | 0.16 | 10.17 | 0.38 | 6.3 |
| **Vic-III-4-28** | 0.160 | 0.0029 | 55.1 | 0.8 | 1.224 | 0.021 | 0.115 | 0.002 | 10.72 | 0.31 | 10.57 | 0.30 | 10.10 | 0.42 | 6.9 |
| **Vic-III-4-22** | 0.165 | 0.0011 | 27.8 | 0.3 | 1.204 | 0.004 | 0.126 | 0.002 | 12.09 | 0.12 | 11.76 | 0.20 | 10.71 | 0.68 | 7.5 |
| **Vic-III-4-25** | 0.170 | 0.0012 | 37.0 | 0.5 | 1.232 | 0.005 | 0.123 | 0.001 | 11.47 | 0.14 | 11.23 | 0.18 | 10.48 | 0.50 | 8.0 |
| **Vic-III-4-07** | 0.175 | 0.0011 | 71.6 | 1.0 | 1.258 | 0.003 | 0.123 | 0.002 | 11.22 | 0.14 | 11.10 | 0.15 | 10.72 | 0.27 | 8.7 |
| **Vic-III-4-17** | 0.202 | 0.0015 | 86.0 | 0.9 | 1.249 | 0.005 | 0.126 | 0.001 | 11.59 | 0.10 | 11.49 | 0.11 | 11.16 | 0.23 | 9.2 |
| **Vic-III-4-32** | 0.244 | 0.0016 | 105.1 | 1.4 | 1.241 | 0.002 | 0.130 | 0.001 | 12.06 | 0.14 | 11.97 | 0.14 | 11.69 | 0.22 | 9.4 |
| **Vic-III-4-13** | 0.297 | 0.0113 | 168.3 | 2.0 | 1.225 | 0.005 | 0.132 | 0.001 | 12.45 | 0.14 | 12.39 | 0.14 | 12.22 | 0.17 | 9.5 |
| **Vic-III-4-18** | 0.246 | 0.0018 | 162.8 | 1.8 | 1.232 | 0.005 | 0.141 | 0.001 | 13.19 | 0.12 | 12.87 | 0.15 | 12.65 | 0.20 | 9.7 |
| **Vic-III-4-19** | 0.260 | 0.0017 | 142.3 | 2.0 | 1.240 | 0.003 | 0.139 | 0.002 | 12.93 | 0.15 | 13.13 | 0.13 | 12.94 | 0.17 | 9.9 |
| **Vic-III-4-33** | 0.230 | 0.0015 | 129.5 | 1.6 | 1.241 | 0.002 | 0.146 | 0.001 | 13.59 | 0.13 | 13.51 | 0.13 | 13.26 | 0.20 | 10.0 |
| **Vic-III-4-02** | 0.229 | 0.0014 | 164.7 | 1.9 | 1.259 | 0.002 | 0.151 | 0.001 | 13.96 | 0.12 | 13.90 | 0.12 | 13.70 | 0.16 | 10.3 |

All uncertainties are reported as 2$\sigma$ standard errors. Activity ratios were calculated using the half-lives given by Cheng et al. (2000) for $^{230}$Th and Jaffey et al. (1971) for $^{238}$U. Uncorrected ages are calculated without correction for Th from detritus. Conventionally detritus corrected ages (($^{232}$Th/$^{238}$U) = 1.25) and finally used corrected ages (($^{232}$Th/$^{238}$U) = 0.3 ± 0.15) following the method outlined in the text in the section 4.6.1, Chronology.

Table 4.3: Correlation coefficients (R, blue) and p-values (green) for the sum of precipitation between October and March from 1950 to 2010 at the meteorological station in San Javier and different climate indices. Bold values indicate significant correlations.

| | **R** | **precip** | **WeMO** | **SCA** | **NAO** | **EA** |
|---|---|---|---|---|---|---|
| **p** | | | | | | |
| **precip** | | | **-0.26** | -0.04 | -0.09 | **-0.18** |
| **WeMO** | | 0 | | -0.03 | **0.26** | 0.02 |
| **SCA** | | 0.45 | 0.59 | | **-0.16** | -0.01 |
| **NAO** | | 0.07 | 0 | 0 | | **0.3** |
| **EA** | | 0 | 0.75 | 0.81 | 0 | |

## References

Cheng H, Edwards RL, Hoff J, Gallup CD, Richards DA, Asmerom Y (2000) The half-lives of uranium-234 and thorium-230. Chemical Geology 169(1–2): 17–33. doi:10.1016/S0009-2541(99)00157-6.

Jaffey AH, Flynn KF, Glendenin LE, Bentley WC, Essling AM (1971) Precision Measurement of Half-Lives and Specific Activities of 235U and 238U. Physical Review C 4(5): 1889. doi:10.1103/PhysRevC.4.1889.

Jochum KP, Scholz D, Stoll B, Weis U, Wilson SA, Yang Q, Schwalb A, Börner N, Jacob DE, Andreae MO (2012) Accurate trace element analysis of speleothems and biogenic calcium carbonates by LA-ICP-MS. Chemical Geology 318-319: 31–44. doi:10.1016/j.chemgeo.2012.05.009.

Jochum KP, Weis U, Stoll B, Kuzmin D, Yang Q, Raczek I, Jacob DE, Stracke A, Birbaum K, Frick DA, Günther D, Enzweiler J (2011) Determination of Reference Values for NIST SRM 610-617 Glasses Following ISO Guidelines. Geostandards and Geoanalytical Research 35(4): 397–429. doi:10.1111/j.1751-908X.2011.00120.x.

Jochum, K.P., Nohl, U., Herwig, K., Lammel, E., Stoll, B., Hofmann, A.W., 2005. GeoReM: a new geochemical database for reference materials and isotopic standards, Geostandards and Geoanalytical Research, 29, 333-338.

# 5 Western Mediterranean climate response to Dansgaard/Oeschger events - new insights from speleothem records

Alexander Budsky[1], Jasper A. Wassenburg[2], Regina Mertz-Kraus[1], Christoph Spötl[3], Klaus Peter Jochum[2], Luis Gibert[4] and Denis Scholz[1]

[1]Institute for Geosciences, Johannes Gutenberg University, Johann-Joachim-Becher-Weg 21, 55128 Mainz, Germany
[2]Max Planck Institute for Chemistry, Department of Climate Geochemistry, P.O. Box 3060, 55020 Mainz, Germany
[3]Institute of Geology, Innsbruck University, Innrain 52, Innsbruck 6020, Austria
[4]Departament de Mineralogia, Petrologia i Geologia Aplicada, Universitat de Barcelona, C/Martí i Franqués s/n, 08028 Barcelona, Spain

Corresponding author: Alexander Budsky (albudsky@students.uni-mainz.de)

**Key Points:**

- Western Mediterranean precipitation responded to Greenland interstadials and stadials in a coherent manner
- Dansgaard/Oeschger interstadials were accompanied by humid climate conditions over the Western Mediterranean
- Atmospheric circulation patterns did not induce spatial differences in precipitation during the last glacial as they did during the Holocene

**Abstract** The climate of the western Mediterranean was characterized by a strong precipitation gradient during the Holocene driven by atmospheric circulation patterns. The scarcity of terrestrial paleoclimate archives has precluded exploring this hydroclimate pattern during Marine Isotope Stages 5 to 3. Here we present stable carbon and oxygen isotope records from three flowstones from southeast Iberia, which show that Dansgaard/Oeschger (D/O) events were as-

sociated with more humid conditions. This is in agreement with other records from the Iberian Peninsula, the Mediterranean and western Europe, which all responded in a similar way to millennial-scale climate variability in Greenland. This general increase in precipitation during D/O events cannot be explained by any present-day or Holocene winter atmospheric circulation pattern. Instead, we suggest that changes in sea surface temperature played a dominant role in determining precipitation amounts in the western Mediterranean.

**Plain Language Summary** Climate events characterized by a sudden temperature increase of up to 10 °C occurring in less than a few decades during the last glacial are recorded in Greenland ice cores. These abrupt warmings, the Dansgaard/Oeschger events, affected large regions of the Northern Hemisphere. The understanding of the regional response in precipitation during these climate shifts is limited for the western Mediterranean, due to the restricted number of terrestrial climate records that cover the last glacial period at sufficient resolution. Speleothems and their stable isotope compositions allow to trace changes in climate and vegetation based on an accurate chronological framework. Here we present a speleothem stable isotope record that shows that the Dansgaard/Oeschger events were associated with increased rainfall and a denser vegetation in the western Mediterranean. As a similar pattern was observed for Western Europe and other parts of the Mediterranean, and we propose that this was related to generally higher sea surface temperatures of the surrounding oceans rather than a reorganization of atmospheric circulation.

## 5.1 Introduction

During the last glacial period, global climate underwent a series of rapid changes superimposed on a long-term cooling trend (Deplazes et al., 2013; Martrat et al., 2007; North Greenland Ice Core Project members, 2004; Wang et al., 2008). In particular, Greenland ice core records show large, rapid changes in $\delta^{18}O$ values interpreted as changes in temperature (Johnsen et al., 2001; Wolff et al., 2010). This climate variability on millennial timescales with warm Dansgaard/Oeschger (D/O) events - also referred to as Greenland Interstadials (Dansgaard et al., 1993) - and Greenland stadials (Hemming, 2004) is reflected in marine sediment cores from the North Atlantic (Heinrich, 1988; Hemming, 2004; Martrat et al., 2007) as well as the Mediterranean Sea (Cacho et al., 1999; Frigola et al., 2012; Incarbona et al., 2013; Martrat et al., 2004). These millennial-scale fluctuations are assumed to have been linked to the Atlantic Meridional Overturning Circulation (AMOC), which strongly affected climate variability in the Northern Hemisphere during Marine Isotope Stage (MIS) 5b to 3 (96-29 ka; Henry et al., 2016; Li and Born, 2019). The strength of the AMOC controls oceanic heat transport to high northern latitudes (Böhm et al., 2015; Menviel et al., 2014). Concomitantly, the AMOC has a large impact on sea surface temperatures (SST) in the North Atlantic (Pailler and Bard, 2002) as well as the western Mediterranean Sea (Martrat et al., 2004; Bagniewski et al., 2017). Changes in SST and the position and topography of the ice sheets, in turn, have an impact on the atmospheric

circulation (Cacho et al., 2000; Merz et al., 2015; Moreno et al., 2005; Naughton et al., 2009) by influencing the pathways of North Atlantic storm tracks and the position of the intertropical convergence zone (ITCZ; Naughton et al., 2009; Stríkis et al., 2018) and, as a consequence, on effective precipitation in the Mediterranean (Hodge et al., 2008a, 2008b). A decrease or even shutdown of the AMOC is coupled to lower SSTs in the North Atlantic and a southward shifted oceanic thermal front, which results in a more southerly route of the Atlantic jet stream and its associated westerlies (Naughton et al., 2009). Climate models suggest that on orbital timescales, this mechanism causes an increase in precipitation during cold phases over the western Iberian Peninsula (Hofer et al., 2012b; Merz et al., 2015). However, biome data reflect increased dryness, especially during winter (Hofer et al., 2012a; Wu et al., 2007), which is in agreement with paleoclimate records from SW Europe (Cortina et al., 2016; Denniston et al., 2018; Moreno et al., 2002, 2005). The rapid climate changes during MIS 5b and 3 are also reflected in marine and terrestrial pollen records (Allen et al., 1999; Pons and Reille, 1988; Sánchez Goñi et al., 2008; Tzedakis et al., 2006) and proxy records of precisely dated speleothems (Denniston et al., 2018; Genty et al., 2010). The present-day climate of the Iberian Peninsula is dominated by several regional atmospheric circulation patterns. For instance, the Western Mediterranean Oscillation (WeMO) and the North Atlantic Oscillation (NAO) lead to strong spatial differences in precipitation (Comas-Bru and McDermott, 2014; Hurrell and Loon, 1997; Martin-Vide and Lopez-Bustins, 2006). Pollen records from offshore sediments provide a wealth of information on last interglacial to glacial vegetation and climate changes, but these data reflect a large region encompassing sub-regions dominated by different atmospheric circulation patterns. Thus, in order to understand the importance of regional atmospheric circulation patterns, precisely dated terrestrial climate records are needed. However, so far, only very few terrestrial records from the Iberian Peninsula covering MIS 5b to 3 are available. Here we present carbon and oxygen isotope records from three precisely dated flowstones from Cueva Victoria (CV, SE Spain), covering the period from 96 to 45 ka (MIS 5b – 3, including D/O events 22 to 12). These records allow to examine how climate variability in the western Mediterranean was related to abrupt climate change in the North Atlantic during the last glacial.

## 5.2 Sample Site and Methods

Cueva Victoria (37.63°N, 0.82°W, 40 m asl., Figure 5.1) is located in SE Spain and developed in Triassic lime- and dolostones of the Inner Betic Cordillera (Manteca Martínez and Pina, 2015). The cave system consists of more than 3 km of galleries that were artificially widened by mining activities during the early 20th century. The climate of the region shows a strong seasonality with warm and dry summers and precipitation maxima in spring and autumn (up to 300 mm/a, mean annual temperature $\approx 17$°C, Figure 5.1c). This seasonality is also reflected by the monthly $\delta^{18}$O values of local precipitation, which show an inverse correlation with rainfall and temperature (Araguas-Araguas and Diaz Teijeiro, 2005). On the inter-annual timescale, the $\delta^{18}$O values of precipitation do not show a significant correlation to temperature or precipitation (Budsky et

al., 2019). Climate is classified as a BSk climate according to the Köppen-Geiger classification (Kottek et al., 2006). The vegetation period lasts from spring to summer and highly depends on rainfall during these seasons (Camarero et al., 2015; Pasho et al., 2011). Precipitation is prevalent during periods characterized by a negative WeMO (Cortesi et al., 2014; Martin-Vide and Lopez-Bustins, 2006; Moreno et al., 2014) index (Figure 5.1a). The main moisture sources of precipitation are the surrounding Mediterranean and Alboran Sea as well as the North Atlantic (Budsky et al., 2019). There is no direct influence of the NAO (Figure 5.1b, Hurrell and Loon, 1997) or the ITCZ (Broccoli et al., 2006). Similarly the main modern European winter circulation patterns, such as the Eastern Atlantic (EA) or the Scandinavian pattern (SCA, Barnston and Livezey, 1987), have almost no impact on precipitation in SE Spain (Comas-Bru and McDermott, 2014).

Flowstone SR01t (6 cm thick) was sampled from the center of "Sala de las Reuniones", while cores Vic-III-1 and Vic-III-3 were drilled in thick (> 50 cm) flowstones in room "Victoria 3" (Ros and Llamusí, 2015). For Vic-III-1 (42 cm) and -3 (40.5 cm), we focus on the upper 23 and 8 cm here (Figure 5.4), which correspond to the last 96 ka (MIS 5b/c transition). Cave monitoring at CV is not possible due to the lack of active drip sites and the artificial widening of the cave, which strongly altered the natural cave system. For $^{230}$Th/U dating, small pieces (0.05 – 0.3 g) were cut from the flowstone, prepared by column chemistry (Gibert et al., 2016; Yang et al., 2015) and analyzed using multi-collector inductively coupled plasma mass spectrometry (MC-ICP-MS) at the Max Planck Institute for Chemistry in Mainz (Obert et al., 2016). Samples for stable isotope analysis were milled at an equidistant spacing of 500 µm (Vic-III-1, SR01t) and 250 µm (Vic-III-3), respectively. The obtained powders were analyzed at the University of Innsbruck with a DeltaplusXL isotope ratio mass spectrometer linked to a Gasbench II (Spötl, 2011; Spötl and Vennemann, 2003).

## 5.3 Results

For all samples used for $^{230}$Th/U dating, $^{232}$Th was below 10 ng/g. Nevertheless, some samples have a ($^{230}$Th/$^{232}$Th) $< 200$, and detrital contamination may have a significant effect on the $^{230}$Th/U-ages (Richards and Dorale, 2003). Thus, $^{230}$Th/U ages were corrected for detrital contamination. The ($^{232}$Th/$^{238}$U) activity ratio of the detrital material was calculated for each flowstone following the approach of Budsky et al. (2019) by minimizing the total sum of all age inversions. This resulted in a ($^{232}$Th/$^{238}$U) activity ratio of 0.24 ± 0.12 for Vic-III-1 and 0.37 ± 0.19 for Vic-III-3, respectively, which are in agreement within uncertainty. For sample SR01t, the correction is negligible due its low content of detrital material (($^{230}$Th/$^{232}$Th) » 200 (Richards and Dorale, 2003)). An exception is sub-sample SR01t-11 (($^{230}$Th/$^{232}$Th) = 49.01). Therefore, we used the mean ($^{232}$Th/$^{238}$U) activity ratio of samples Vic-III-1 and Vic-III-3 for detrital correction (($^{232}$Th/$^{238}$U) = 0.31 ± 0.16) for SR01t. The corrected ages range from 95.7 ± 4.7 to 46.2 ± 0.6 ka (Vic-III-1), excluding the uppermost age, which corresponds to the Holocene (Budsky et al., 2019), 92.8 ± 1.8 to 49.9 ± 0.4 ka (Vic-III-3) and 85.4 ± 1.2 to 49.5 ± 1.3 ka

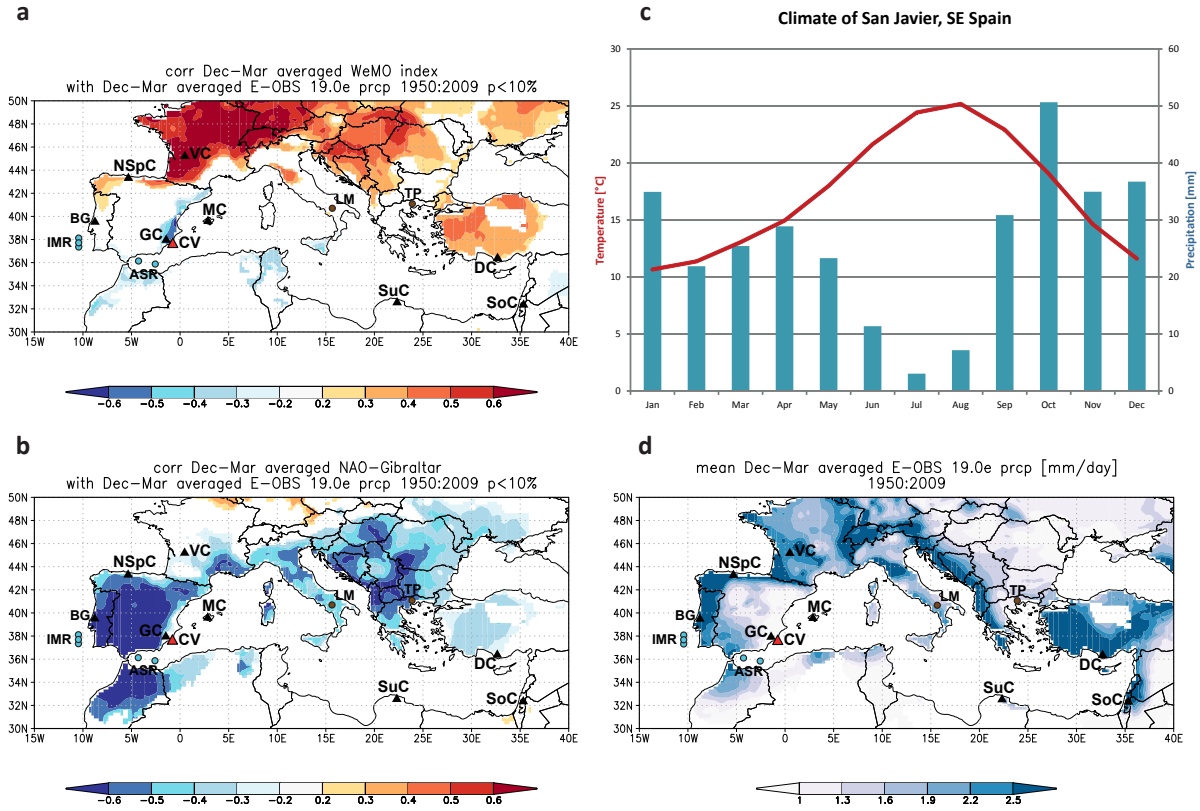


Figure 5.1: (a) Correlation of observed precipitation (E-OBS 19.0, Cornes et al., 2018) from December to March (1950-2009) with the WeMO (Martin-Vide and Lopez-Bustins, 2006) and (b) the NAO index (Jones et al., 1997). (c) Climate diagram for San Javier with temperature (red) and precipitation (blue) displaying strong seasonality. (d) Mean precipitation (1950-2010) for December to March in mm/day (Cornes et al., 2018). The correlation (a, b) and precipitation (d) maps were created with the KNMI Climate Explorer (http://climexp.knmi.nl). Speleothem records are indicated by triangles (CV: Cueva Victoria (this study, red triangle), GC: Gitana Cave (Hodge et al., 2008a), BG: Buraca Gloriosa (Denniston et al., 2018), NSpC: Caves in North Spain (Muñoz-García et al., 2007; Stoll et al., 2013), VC: Villars Cave (Genty et al., 2010), MC: Mallorcan Caves (Dumitru et al., 2018; Hodge et al., 2008b), SuC: Susah Cave (Hoffmann et al., 2016), DC: Dim Cave (Ünal-Ímer et al., 2015), SoC: Soreq Cave (Bar-Matthews et al., 2003)). Marine sediment cores are indicated by blue circles (ASR: Alboran Sea (ODP161-977, MD95-2043, Martrat et al., 2004; Cacho et al., 1999), IMR: Iberian Margin (MD01-2443/4, MD95-2042, Martrat et al., 2007; Daniau et al., 2007; Shackleton et al., 2000). The lake Monticchio (LM, Allen et al., 1999) and Tenaghi Philippon (TP, Tzedakis et al., 2003) records are indicated by brown circles.

(SR01t). The final age models for all flowstones were constructed using the corrected ages and the StalAge algorithm (Scholz and Hoffmann, 2011, Figure 5.5). Visible hiatuses were included manually into the StalAge age model by fitting the corresponding flowstone sections separately (see supplementary material). For very short growth phases consisting of only one $^{230}$Th/U-age, we used a mean growth rate of the corresponding longer growth intervals to establish an age-depth model. These short growth intervals were stratigraphically identified by dark layers in thin sections. There is no evidence of dissolution or diagenesis at these growth stops. Thin sections show a pristine elongated/open columnar fabric (cf; Frisia, 2015). The stable isotope values show a large variability on millennial timescales (Figures 5.2 and 5.3). $\delta^{18}$O values range from -6.0 to -3.5 ‰ (Vic-III-1) and -6 to -3 ‰ (Vic-III-3), whereas the $\delta^{18}$O values of SR01t are slightly less negative (-5.5 to -3.0 ‰). The $\delta^{13}$C values of Vic-III-1 and Vic-III-3 range from -11.0 to -9.5 ‰, whereas SR01t shows ca. 3 ‰ higher $\delta^{13}$C values. In all samples, the lowest $\delta^{13}$C and $\delta^{18}$O values occur around 85 ka (D/O 21). $\delta^{18}$O and $\delta^{13}$C values correlate positively with r = 0.67 for SR01t, 0.55 for Vic-III-1, and 0.7 for Vic-III-3.

## 5.4 Discussion

### 5.4.1 Interpretation of the Cueva Victoria speleothem record

The three flowstone records from CV cover a long period between the last interglacial and the Last Glacial Maximum, which is only sparsely covered by other paleoclimate archives from SE Spain. The typical D/O pattern as recorded by the NGRIP ice core (North Greenland Ice Core Project members, 2004; Obrochta et al., 2014; Svensson et al., 2013) is reflected in both the carbon and oxygen isotope records of the CV flowstones with lower values occurring during D/O events and vice versa. This indicates a strong link between climate in the North Atlantic region and SE Spain on millennial timescales. In the overlapping sections, all three flowstones show consistent $\delta^{13}$C and $\delta^{18}$O values (Figures 5.2 and 5.3). This replication of the proxy signals confirms that the observed variability is related to climate change above the cave rather than processes within the cave or the karst aquifer. Temporal discrepancies are likely largely due to uncertainties in the chronology of our flowstones, in particular for a few short growth periods that cannot be constrained by more than one $^{230}$Th/U-age, and probably to a smaller extent due to the uncertainties of the chronology of NGRIP (up to 1.5 ka, Svensson et al., 2008, Figure 5.2). Budsky et al. (2019) demonstrated a strong influence of effective precipitation on vegetation density and microbiological activity in the soil above CV during the Holocene. Higher $\delta^{13}$C values were interpreted as decreased precipitation during the season of vegetation growth (spring to summer). This interpretation is in agreement with other studies using $\delta^{13}$C values as a proxy for vegetation density (Cerling et al., 1993; Fohlmeister et al., 2011) and soil microbiological activity (Genty et al., 2003; Meyer et al., 2014), which in turn are related to effective precipitation during the growing season (Denniston et al., 2018; Hodge et al., 2008a, 2008b). In addition to these processes occurring in the soil zone, several processes within the aquifer and the cave can

result in carbon isotope fractionation, such as prior calcite precipitation (PCP), cave ventilation and the distance of flow on flowstones (Hansen et al., 2017; Johnson et al., 2006; Mühlinghaus et al., 2009; Spötl et al., 2005). Stronger cave ventilation and increased distances of flow lead to enhanced degassing of $CO_2$ from the solution and precipitation of calcite prior to the sampling site. This may be particularly relevant for sample SR01t, which is associated with the longest distance of flow due to its position in the middle of the cave chamber, and may explain the elevated $\delta^{13}C$ values compared to the other flowstones. In general, despite their complexity, all processes result in higher $\delta^{13}C$ values during drier conditions above the cave. Thus, we interpret higher $\delta^{13}C$ values in the CV flowstones as reflecting periods of reduced precipitation/infiltration.

Lower $\delta^{13}C$ values during D/O events thus suggest increased precipitation in the western Mediterranean during these warm events in the North Atlantic region (Budsky et al., 2019; Genty et al., 2003). This is in agreement with other climate archives from the Mediterranean, such as pollen records from the western Mediterranean (Burjachs et al., 2012; Camuera et al., 2019; Combourieu Nebout et al., 2002; Sánchez Goñi et al., 2008) and Italy (Allen et al., 1999).

The interpretation of $\delta^{18}O$ values in the CV flowstone records is more complex (Budsky et al., 2019). Modern precipitation $\delta^{18}O$ values on a monthly timescale are related to precipitation amount between October and April. Low $\delta^{18}O$ values of monthly precipitation correlate with high rainfall amount and vice versa (Araguas-Araguas and Diaz Teijeiro, 2005). Since summer precipitation with elevated $\delta^{18}O$ values does not infiltrate into the karst rock, the CV flowstones mainly record the more negative $\delta^{18}O$ signal of winter precipitation (Budsky et al., 2019; Carrasco et al., 2006). On the inter-annual timescale, we thus expect lower $\delta^{18}O$ values for years with increased October-April precipitation, consistent with the interpretation for other Mediterranean speleothem $\delta^{18}O$ records (Ayalon et al., 1998; Ayalon et al., 2002; Bard et al., 2002). However, during D/O events, SSTs on the Iberian Margin and in the Alboran Sea were higher (Figure 5.3) and the continent was warmer (Genty et al., 2010; Martrat et al., 2007), which may have resulted in higher rainfall $\delta^{18}O$ values (Rozanski et al., 1993) even if Budsky et al. (2019) did not find a significant correlation between temperature and rainfall $\delta^{18}O$ values on inter-annual timescales. At the same time, warmer cave air results in lower calcite $\delta^{18}O$ values due to the temperature-dependent isotope fractionation between water and calcite (Hansen et al., 2019; Kim and O'Neil, 1997; Tremaine et al., 2011). The interpretation is further complicated because the $\delta^{18}O$ values of precipitation are not directly related to changes in the moisture source (Moreno et al., 2014) preventing to disentangled precipitation originating in the Atlantic from that coming from the Mediterranean. This also implies that the transport distance of the water vapor and potential rain-out effects (McDermott, 2004; Mook, 2001) are not dominant because the Mediterranean is the more local moisture source compared to the more distant Atlantic. In addition, temporal changes in the $\delta^{18}O$ value of surface ocean water have to be taken into account, but unfortunately, there is no seawater $\delta^{18}O$ reconstruction available from the region. $\delta^{18}O$ values of planktonic foraminifera in sediment cores from the Iberian margin and the Alboran Sea (Vautravers and Shackleton, 2006), a proxy for both SST and the $\delta^{18}O$ value of seawater, reflect all D/O events (Figure 5.3b). However, considering the temperature dependence of the $\delta^{18}O$ values of planktonic

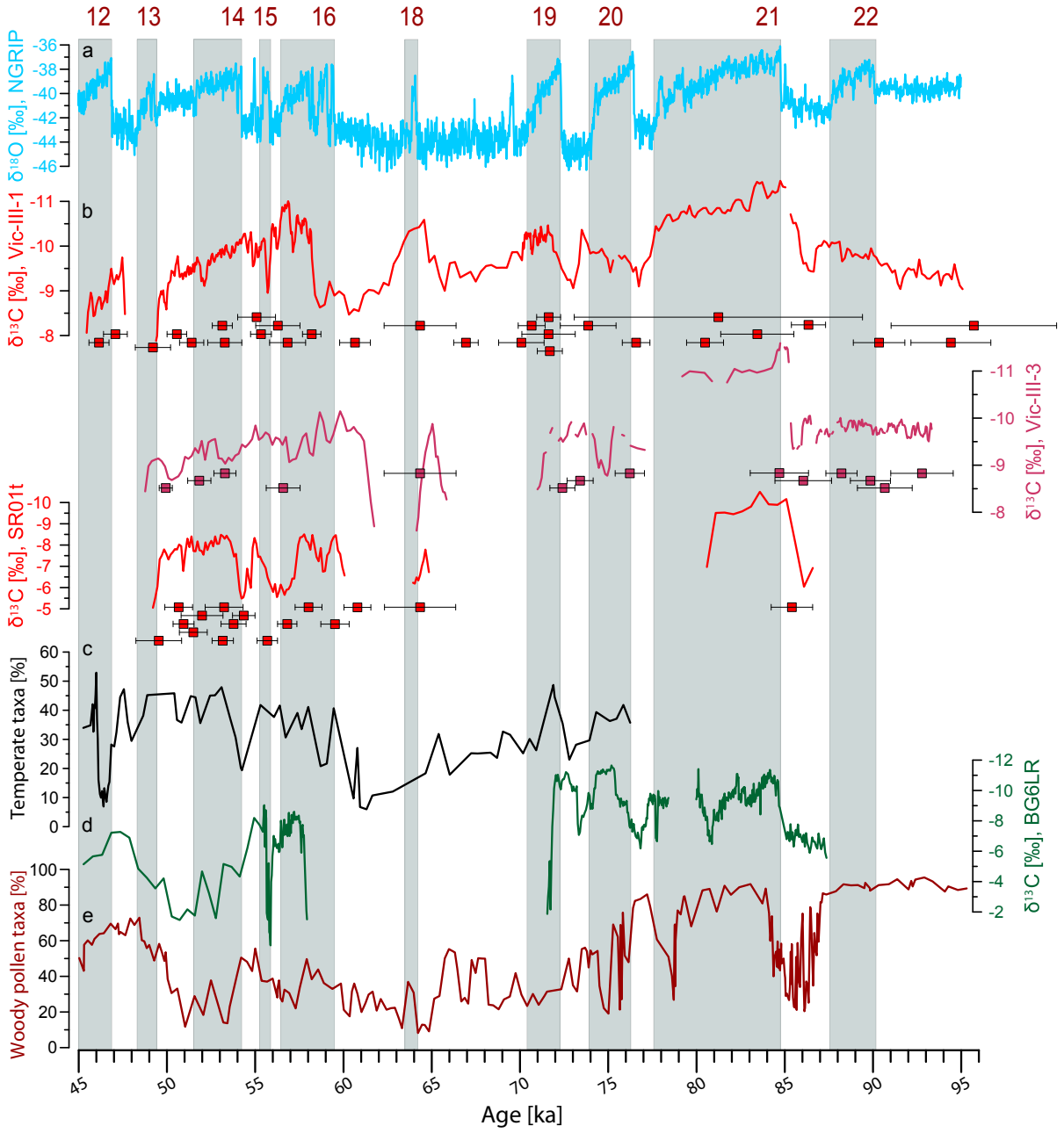


Figure 5.2: $\delta^{13}$C values of the three CV flowstones with corresponding $^{230}$Th/U ages (b), which reflect vegetation density above the cave. Also shown are the NGRIP $\delta^{18}$O record (a, Obrochta et al., 2014), which shows North Greenland temperature variations, temperate taxa pollen from the Alboran Sea (c, ODP 976, Combourieu Nebout et al., 2002), and the $\delta^{13}$C values of a speleothem record from Portugal (d, Denniston et al., 2018). In addition, we show the percentage of woody pollen taxa from Lake Monticchio in Italy (e, Allen et al., 1999), which reflect vegetation density. The gray bars indicate the D/O events.

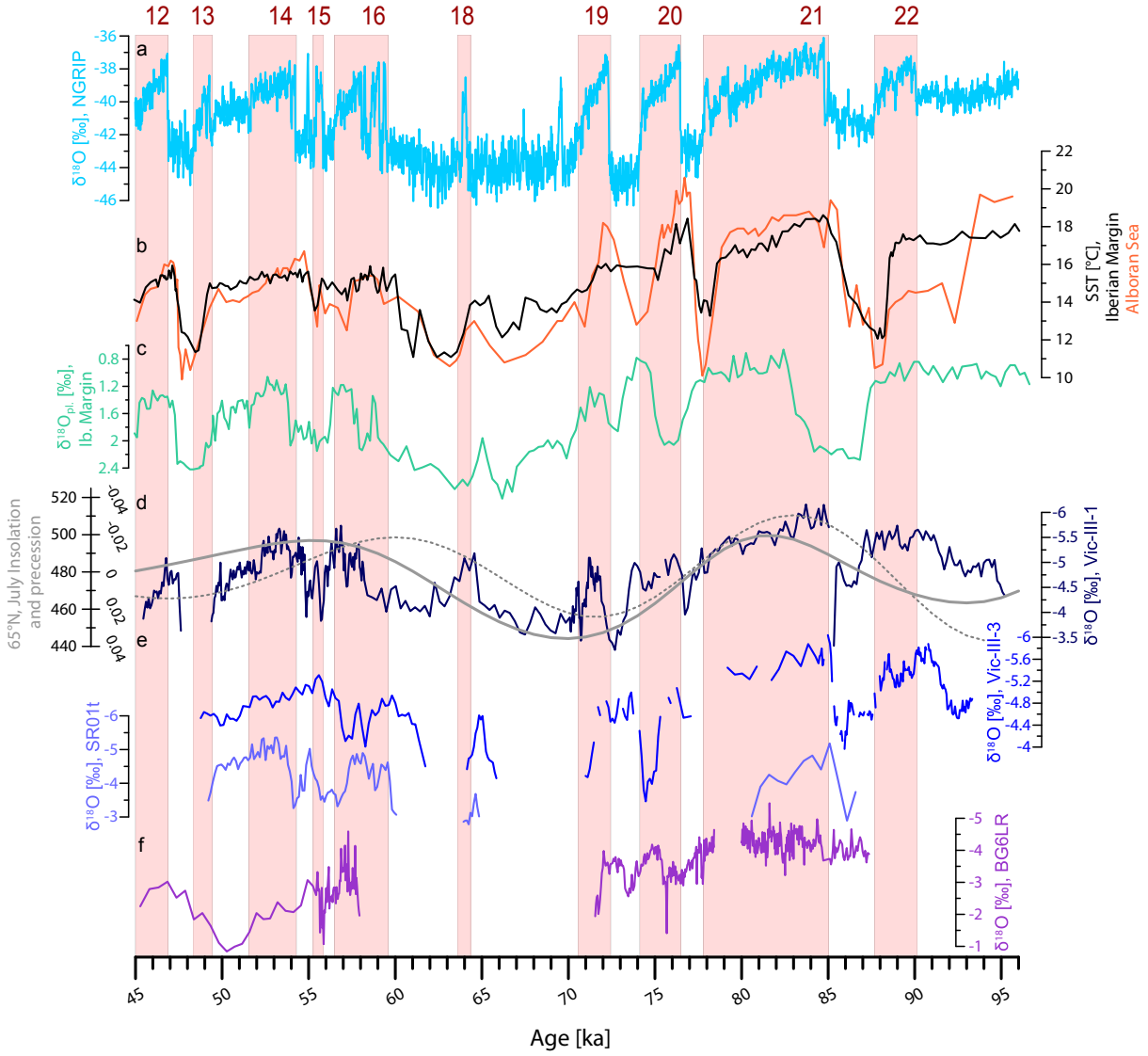


Figure 5.3: $\delta^{18}$O values of the three CV flowstones (e) in comparison with NGRIP (a, Obrochta et al., 2014, indicating warm D/O events) as well as SST from the Iberian Margin and the Alboran Sea (b, Martrat et al., 2004; Martrat et al., 2007). Also shown are $\delta^{18}$O values of planktonic foraminifera (*G. bulloides*) from the Iberian Margin (c, Vautravers and Shackleton, 2006; Hodell et al., 2013), which reflect changes in both temperature and the $\delta^{18}$O values of the source for moisture uptake. Long-term changes in flowstone $\delta^{18}$O values (e) track the 65°N July insolation (d, Laskar et al., 2004) and precession (d, dashed line, Berger, 1978). (f) $\delta^{18}$O values of a speleothem record from Portugal (Denniston et al., 2018). The reddish bars indicate the D/O events.

foraminifera of ca. -0.21 ‰/°C (Bemis et al., 1998), suggests only minor changes in the $\delta^{18}O$ value of seawater during the D/O events (Figure 5.3b, c). Therefore, we interpret our flowstone $\delta^{18}O$ record as reflecting a combination of the amount of winter precipitation and cave air temperature, with more negative flowstone $\delta^{18}O$ values corresponding to warmer and more humid conditions. This relationship is potentially weakened by the positive relationship between surface air temperature and rainfall $\delta^{18}O$ values.

### 5.4.2 Climate variability on orbital timescales

On orbital timescales, the flowstone $\delta^{18}O$ record follows 65°N July insolation, whereby high insolation is associated with low $\delta^{18}O$ and $\delta^{13}C$ values (warm and humid) and vice versa (Figure 5.3d, e; Berger, 1978). Only few terrestrial climate archives in southern Europe and the western Mediterranean cover MIS 5 to 3. For MIS 5c-a, coastal sediments suggest more humid conditions in SE Spain (Mauz et al., 2012). Enhanced precipitation during interglacials is also corroborated by stalagmite growth in northern Iberia (Muñoz-García et al., 2007; Stoll et al., 2013). Located close to CV, the low resolution Gitana Cave record (Figure 5.1) is in good agreement with our records on orbital timescales, with higher effective precipitation during interglacials and a cessation of speleothem growth during Heinrich stadial 5 ($\approx$ 46 ka, Hodge et al., 2008a). This coincides with a prominent sea level drop at ca. 45 ka (Siddall et al., 2008) and the termination of calcite deposition in CV. Speleothem $\delta^{13}C$ values from Portugal also suggest that high 65°N summer insolation is associated with higher precipitation (Denniston et al., 2018). In summary, on orbital timescales, precipitation on both the western and the eastern Iberian Peninsula responds to 65°N July insolation. 65°N July insolation depends on the interplay between obliquity and precession (Davis and Brewer, 2009). Both lead to a varying latitudinal insolation gradient, which in turn drives the latitudinal temperature gradient and thus climate in higher and lower latitudes by a latitudinal displacement and varying intensity of the mid-latitude storm tracks and the tropical Hadley Cell/ITCZ (Schneider et al., 2014; Stríkis et al., 2018). In particular, precession minima are associated with stronger latitudinal shifts of the ITCZ and the mid latitude storm tracks on seasonal timescales, and are thus associated with higher seasonality and enhanced autumn/winter precipitation due to higher storm activity in the Mediterranean (Kutzbach et al., 2014; Bosmans et al., 2015; Toucanne et al., 2015). This phenomenon may explain the wetter conditions observed around 80-85 ka in our record, but not those at 50-60 ka (Figure 5.3). This suggests that the combined signal of 65°N July insolation is more important than precession alone. Higher 65°N July insolation during interglacials is associated with a weaker latitudinal temperature gradient. A higher temperature gradient during glacial periods was associated with a weakened AMOC (Böhm et al., 2015) and leads to stronger and southward shifted westerlies (Merz et al., 2015). Consequently, this should lead to more precipitation on the Iberian Peninsula during glacial periods (Hofer et al., 2012b). Interestingly, this is not observed in the western Iberian Peninsula, where glacial periods were characterized by drier conditions, whereas interglacials were relatively wet (Denniston et al., 2018). This apparent controversy may be explained

by the fact that the glacials (interglacials) were associated with a reduced (stronger) AMOC and lower (higher) 65°N July insolation, which lead to lower (higher) SST's. On orbital timescales, SSTs at the Iberian margin are correlated with precipitation at both the western (Denniston et al., 2018) and the eastern Iberian Peninsula (CV; this study). This strongly suggests that SST controlled precipitation on the Iberian Peninsula on orbital timescales although it remains difficult to assess whether this is related to an increase in winter or summer precipitation or both (Kutzbach et al. 2014).

### 5.4.3 Climate variability on millennial timescales

On millennial timescales, we observe that the D/O events are associated with warm and humid conditions, which is even the case for the short-lived D/O events 15 (≈55 ka) and 18 (≈64 ka). In contrast, Greenland stadials are associated with cold and dry conditions at CV (Figure 5.3). The same pattern is observed across the Iberian Peninsula (Denniston et al., 2018; Hodge et al., 2008a; Sánchez Goñi et al., 2008; Combourieu Nebout et al., 2002) and in other regions of western Europe (Genty et al., 2003, 2010; Hofer et al., 2012a; Wu et al., 2007; Sanchez Goni et al., 2013) and the Mediterranean (Allen et al., 1999; Brauer et al., 2007; Dumitru et al., 2018; Fletcher et al., 2010; Hodge et al., 2008b). Warming of the North Atlantic during D/O events is associated with an enhanced AMOC, which results in a decreased temperature gradient. In general, a weakened AMOC during stadials reduces the heat transport to the North concomitant with reduced SSTs (Bagniewski et al., 2017). In combination with the presence of the Laurentide ice sheet, this induces a southward shift of the Hadley Cell, associated with stronger and southward shifted westerlies (Menviel et al., 2014). Stronger and southward shifted westerlies during stadials lead to decreased precipitation over the Iberian Peninsula and vice versa (Menviel et al., 2014; Bagniewski et al., 2017). Nevertheless, from a sediment core off the northwest Iberian coast, a more complex response of precipitation to Heinrich events 4, 2 and 1 was observed (Naughton et al., 2009). Naughton et al. (2009) suggested that the 1st phase of the Heinrich events was associated with relatively wet and cold conditions, whereas the 2nd phase was characterized by dry and cold conditions following the displacement of the ocean polar front. However, since the CV-record does not cover Heinrich events 4, 2 and 1, this cannot be verified for the Eastern Iberian Peninsula. Moreover, the CV record shows drier conditions during stadials and wetter conditions during D/O events.

## 5.5 Precipitation patterns: present-day versus last glacial period

The present-day precipitation distribution on the Iberian Peninsula is strongly influenced by several atmospheric circulation patterns including the WeMO and the NAO (Comas-Bru and McDermott, 2014; Cortesi et al., 2014). A negative WeMO index leads to enhanced precipitation in SE Spain, whereas the northern parts remain dry and vice versa (Martin-Vide and Lopez-Bustins, 2006, Figure 5.1a and d). This bipolar precipitation pattern has also been dis-

cussed in detail for the Holocene (Budsky et al., 2019). In contrast, the NAO particularly affects precipitation in the regions of the Iberian Peninsula that are not affected by the WeMO (Figure 5.1b). During the last glacial D/O events, it is well documented that many regions in addition to south-eastern Spain, such as western Europe (Genty et al., 2003; Wainer et al., 2009) and the eastern Mediterranean (Grant et al., 2012; Ünal-Ímer et al., 2015), also experienced increased precipitation. This is in agreement with higher tree pollen percentages in Greece (Tenaghi Philippon, Tzedakis et al., 2003) and Italy (Lake Monticchio, Allen et al., 1999) and speleothem $\delta^{18}O$ values and growth phases in northern Libya (Hoffmann et al., 2016). Thus, it was more humid during the D/O events in the whole Mediterranean area and western Europe. This simultaneous increase in precipitation associated with the D/O events in this large region cannot be explained by changes in modern winter atmospheric circulation pattern, such as the NAO, the EA, the SCA or the WeMO (Comas-Bru & McDermott, 2014; Martin-Vide & Lopez-Bustins, 2006). Instead, we suggest that changes in North Atlantic and Mediterranean SSTs controlled the water vapor content of the atmosphere and regulated changes in precipitation. We emphasize that this general increase in precipitation does neither exclude changes in atmospheric circulation during D/O events nor that it is related to increases in both winter and summer precipitation. Such a strong link between SST and precipitation has also been suggested for the last glacial (Denniston et al., 2018; Hodge et al., 2008b), primarily for the Mediterranean due to instabilities in winter associated with high SSTs during D/O events (Bosmans et al., 2015). In particular, it is well known that the water vapor content of the air over the North Atlantic increased during warmer periods, and these warm and moist air masses were then transported to the western Mediterranean causing an increase in precipitation (Bosmans et al., 2015; Kutzbach and Liu, 1997; Trenberth et al., 1998). During glacials, cool SSTs in the North Atlantic decreased the energy budget over the ocean and the moisture uptake in winter. This resulted in drier conditions in the western Mediterranean (Daniau et al., 2007; Dumitru et al., 2018; Hodge et al., 2008b; Moreno et al., 2005).

## 5.6 Conclusions

Three overlapping flowstone $\delta^{13}C$ and $\delta^{18}O$ records from CV demonstrate that precipitation in SE Spain between MIS 5b to MIS 3 (96-45 ka) was related to the North Atlantic climate variability. Warm D/O events were associated with higher precipitation and an expansion of vegetation, even during short D/O events, such as D/O 15 and 18. Cold stadials were associated with lower precipitation and reduced vegetation cover. Warm and humid conditions during D/O events are also recorded by pollen and were associated with an expansion of forests in the Mediterranean region. Climate of the Iberian Peninsula during the Holocene and the present-day shows strong regional differences due to different controlling factors, such as the NAO and the WeMO. However, vast regions in the Mediterranean and western Europe show coherently more humid conditions during D/O events and drier conditions during Greenland stadials. We conclude that this coherent large-scale climate response cannot be explained by present-day

winter atmospheric circulation patterns alone. Instead, the SST of the North Atlantic and the Mediterranean Sea played a key role in determining the water vapor content of the atmosphere that controlled precipitation in the western Mediterranean and western Europe.

**Acknowledgements, Samples, and Data** This work was funded by the German Research Foundation (ME3761/2-1 to R. Mertz-Kraus and SCHO 1274/9-1 and SCHO 1274/11-1 to D. Scholz). We thank Andrés Ros and the team of CENM-naturaleza as well as the city of Cartagena for the opportunity to work in Cueva Victoria and the support during field campaigns. The assistance of Beate Schwager in the geochemistry lab of the Max Planck Institute for Chemistry, Mainz, and Manuela Wimmer in the isotope laboratory of the University of Innsbruck is highly appreciated. Marie Froeschmann is thanked for taking isotope samples. The authors gratefully acknowledge the KNMI for providing the online tool "Climate Explorer" (http://climexp.knmi.nl/start.cgi) used in Figure 1 of this publication. Data access will be available at the database of the NOAA website. We thank two anonymous reviewers for their thorough and constructive reviews.

## References

Allen, J. R. M., Brandt, U., Brauer, A., Huntley, B., Keller, J., Kraml, M., et al. (1999). Rapid environmental changes in southern Europe during the last glacial period. *Nature, 400*(6746), 740–743.

Araguas-Araguas, L.J., & Diaz Teijeiro, M.F. (2005). Isotope composition of precipitation and water vapour in the Iberian Peninsula: First results of the Spanish Network of Isotopes in Precipitation. In *IAEA-TECDOC: Vol. 1453. Isotopic composition of precipitation in the Mediterranean Basin in relation to air circulation patterns and climate: Final report of a coordinated research project, 2000-2004* (pp. 173–190). Vienna: International Atomic Energy Agency.

Ayalon, A., Bar-Matthews, M., & Kaufman, A. (2002). Climatic conditions during marine oxygen isotope stage 6 in the eastern Mediterranean region from the isotopic composition of speleothems of Soreq Cave, Israel. *Geology, 30*(4), 303–306. https://doi.org/10.1130/0091-7613(2002)030<0303:CCDMOI>2.0.CO;2

Ayalon, A., Bar-Matthews, M., & Sass, E. (1998). Rainfall-recharge relationships within a karstic terrain in the Eastern Mediterranean semi-arid region, Israel: $\delta^{18}$Oand $\delta$D characteristics. *Journal of Hydrology, 207*(1-2), 18–31. https://doi.org/10.1016/S0022-1694(98)00119-X

Bagniewski, W., Meissner, K. J., & Menviel, L. (2017). Exploring the oxygen isotope fingerprint of Dansgaard-Oeschger variability and Heinrich events. *Quaternary Science Reviews, 159*, 1–14. https://doi.org/10.1016/j.quascirev.2017.01.007

Bard, E., Delaygue, G., Rostek, F., Antonioli, F., Silenzi, S., & Schrag, D. P. (2002). Hydrological conditions over the western Mediterranean basin during the deposition of the cold Sapropel 6 (ca. 175 kyr BP). *Earth and Planetary Science Letters, 202*(2), 481–494. https://doi.org/10.1016/S0012-821X(02)00788-4

Bar-Matthews, M., Ayalon, A., Gilmour, M., Matthews, A., & Hawkesworth, C. J. (2003). Sea–land oxygen isotopic relationships from planktonic foraminifera and speleothems in the Eastern

Mediterranean region and their implication for paleorainfall during interglacial intervals. *Geochimica et Cosmochimica Acta, 67*(17), 3181–3199. https://doi.org/10.1016/S0016-7037(02)01031-1

Barnston, A. G., & Livezey, R. E. (1987). Classification, Seasonality and Persistence of Low-Frequency Atmospheric Circulation Patterns. *Monthly Weather Review, 115*(6), 1083–1126. https://doi.org/10.1175/1520-0493(1987)115<1083:CSAPOL>2.0.CO;2

Bemis, B. E., Spero, H. J., Bijma, J., & Lea, D. W. (1998). Reevaluation of the oxygen isotopic composition of planktonic foraminifera: Experimental results and revised paleotemperature equations. *Paleoceanography, 13*(2), 150–160. https://doi.org/10.1029/98PA00070

Berger, A. L. (1978). Long-term variations of daily insolation and Quaternary climatic changes. *Journal of the Atmospheric Sciences, 35*(12), 2362–2367. https://doi.org/10.1175/1520-0469(1978)035<2362:LTVODI>2.0.CO;2

Böhm, E., Lippold, J., Gutjahr, M., Frank, M., Blaser, P., Antz, B., et al. (2015). Strong and deep Atlantic meridional overturning circulation during the last glacial cycle. *Nature, 517*, 73. https://doi.org/10.1038/nature14059

Bosmans, J.H.C., Drijfhout, S. S., Tuenter, E., Hilgen, F. J., Lourens, L. J., & Rohling, E. J. (2015). Precession and obliquity forcing of the freshwater budget over the Mediterranean. *Quaternary Science Reviews, 123*, 16–30. https://doi.org/10.1016/j.quascirev.2015.06.008

Brauer, A., Allen, J. R. M., Mingram, J., Dulski, P., Wulf, S., & Huntley, B. (2007). Evidence for last interglacial chronology and environmental change from Southern Europe. *Proceedings of the National Academy of Sciences, 104*(2), 450–455. https://doi.org/10.1073/pnas.0603321104

Broccoli, A. J., Dahl, K. A., & Stouffer, R. J. (2006). Response of the ITCZ to Northern Hemisphere cooling. *Geophysical Research Letters, 33*, L01702. https://doi.org/10.1029/2005GL024546

Budsky, A., Scholz, D., Wassenburg, J. A., Mertz-Kraus, R., Spötl, C., Riechelmann, D. F.C., et al. (2019). Speleothem $\delta^{13}$Crecord suggests enhanced spring/summer drought in south-eastern Spain between 9.7 and 7.8 ka – A circum-Western Mediterranean anomaly? *The Holocene, 44*(1), 095968361983802. https://doi.org/10.1177/0959683619838021

Burjachs, F., López-García, J. M., Allué, E., Blain, H.-A., Rivals, F., Bennàsar, M., & Expósito, I. (2012). Palaeoecology of Neanderthals during Dansgaard–Oeschger cycles in northeastern Iberia (Abric Romaní): From regional to global scale. *Quaternary International, 247*, 26–37. https://doi.org/10.1016/j.quaint.2011.01.035

Cacho, I., Grimalt, J. O., Pelejero, C., Canals, M., Sierro, F. J., Flores, J. A., & Shackleton, N. (1999). Dansgaard-Oeschger and Heinrich event imprints in Alboran Sea paleotemperatures. *Paleoceanography, 14*(6), 698–705. https://doi.org/10.1029/1999PA900044

Cacho, I., Grimalt, J. O., Sierro, F. J., Shackleton, N., & Canals, M. (2000). Evidence for enhanced Mediterranean thermohaline circulation during rapid climatic coolings. *Earth and Planetary Science Letters, 183*(3-4), 417–429. https://doi.org/10.1016/S0012-821X(00)00296-X

Camarero, J. J., Gazol, A., Tardif, J. C., & Conciatori, F. (2015). Attributing forest responses to global-change drivers: Limited evidence of a CO2 -fertilization effect in Iberian pine growth. *Journal of Biogeography, 42*(11), 2220–2233. https://doi.org/10.1111/jbi.12590

Camuera, J., Jiménez-Moreno, G., Ramos-Román, M. J., García-Alix, A., Toney, J. L., Anderson, R. S., et al. (2019). Vegetation and climate changes during the last two glacial-interglacial cycles in the western Mediterranean: A new long pollen record from Padul (southern Iberian Peninsula). *Quaternary Science Reviews, 205*, 86–105. https://doi.org/10.1016/j.quascirev.2018.12.013

Carrasco, F., Andreo, B., Liñán, C., & Mudry, J. (2006). Contribution of stable isotopes to the understanding of the unsaturated zone of a carbonate aquifer (Nerja Cave, southern Spain). *Comptes Rendus Geoscience, 338*(16), 1203–1212. https://doi.org/10.1016/j.crte.2006.09.009

Cerling, T. E., Wang, Y., & Quade, J. (1993). Expansion of C4 ecosystems as an indicator of global ecological change in the late Miocene. *Nature, 361*, 344–345. https://doi.org/10.1038/361344a0

Comas-Bru, L., & McDermott, F. (2014). Impacts of the EA and SCA patterns on the European twentieth century NAO-winter climate relationship. *Quarterly Journal of the Royal Meteorological Society, 140*(679), 354–363. https://doi.org/10.1002/qj.2158

Combourieu Nebout, N., Turon, J.L., Zahn, R., Capotondi, L., Londeix, L., & Pahnke, K. (2002). Enhanced aridity and atmospheric high-pressure stability over the western Mediterranean during the North Atlantic cold events of the past 50 k.y. *Geology, 30*(10), 863-866. https://doi.org/10.1130/0091-7613(2002)030<0863:EAAAHP>2.0.CO;2

Cornes, R. C., van der Schrier, G., Besselaar, Else J. M. van den, & Jones, P. D. (2018). An ensemble version of the E-OBS temperature and precipitation data sets. *Journal of Geophysical Research: Atmospheres, 123*(17), 9391–9409. https://doi.org/10.1029/2017JD028200

Cortesi, N., Gonzalez?Hidalgo, J. C., Trigo, R. M., & Ramos, A. M. (2014). Weather types and spatial variability of precipitation in the Iberian Peninsula. *International Journal of Climatology, 34*(8), 2661–2677. https://doi.org/10.1002/joc.3866

Cortina, A., Grimalt, J. O., Rigual-Hernández, A., Ballegeer, A.-M., Martrat, B., Sierro, F. J., & Flores, J. A. (2016). The impact of ice-sheet dynamics in western Mediterranean environmental conditions during Terminations. An approach based on terrestrial long chain n-alkanes deposited in the upper slope of the Gulf of Lions. *Chemical Geology, 430*, 21–33. https://doi.org/10.1016/j.chemgeo.2016.03.015

Daniau, A.-L., Sánchez-Goñi, M.F., Beaufort, L., Laggoun-Défarge, F., Loutre, M.-F., & Duprat, J. (2007). Dansgaard–Oeschger climatic variability revealed by fire emissions in southwestern Iberia. *Quaternary Science Reviews, 26*(9-10), 1369–1383. https://doi.org/10.1016/j.quascirev.2007.02.005

Dansgaard, W., Johnsen, S. J., Clausen, H. B., Dahl-Jensen, D., Gundestrup, N. S., Hammer, C. U., et al. (1993). Evidence for general instability of past climate from a 250-kyr ice-core record. *Nature, 364*, 218–220. https://doi.org/10.1038/364218a0

Davis, B. A. S., & Brewer, S. (2009). Orbital forcing and role of the latitudinal insolation/temperature gradient. *Climate Dynamics, 32*(2), 143–165. https://doi.org/10.1007/s00382-008-0480-9

Del Valle, L., Gómez-Pujol, L., Fornós, J. J., Timar-Gabor, A., Anechitei–Deacu, V., & Pomar, F. (2016). Middle to Late Pleistocene dunefields in rocky coast settings at Cala Xuclar (Eivissa, Western Mediterranean): Recognition, architecture and luminescence chronology. *Quaternary International, 407*, 4–13. https://doi.org/10.1016/j.quaint.2016.01.050

Denniston, R. F., Houts, A. N., Asmerom, Y., Wanamaker Jr., A. D., Haws, J. A., Polyak, V. J., et al. (2018). A stalagmite test of North Atlantic SST and Iberian hydroclimate linkages over the last two glacial cycles. *Climate of the Past, 14*(12), 1893–1913. https://doi.org/10.5194/cp-14-1893-2018

Deplazes, G., Lückge, A., Peterson, L. C., Timmermann, A., Hamann, Y., Hughen, K. A., et al. (2013). Links between tropical rainfall and North Atlantic climate during the last glacial period. *Nature Geoscience, 6*(3), 213. https://doi.org/10.1038/ngeo1712

Dumitru, O. A., Onac, B. P., Polyak, V. J., Wynn, J. G., Asmerom, Y., & Fornós, J. J. (2018). Climate variability in the western Mediterranean between 121 and 67 ka derived from a Mallorcan speleothem record. *Palaeogeography, Palaeoclimatology, Palaeoecology, 506*, 128–138. https://doi.org/10.1016/j.palaeo.2018.06.028

Fletcher, W. J., Sánchez Goñi, M. F., Allen, J. R.M., Cheddadi, R., Combourieu-Nebout, N., Huntley, B., et al. (2010). Millennial-scale variability during the last glacial in vegetation records from Europe. *Quaternary Science Reviews, 29*(21-22), 2839–2864. https://doi.org/10.1016/j.quascirev.2009.11.015

Fohlmeister, J., Scholz, D., Kromer, B., & Mangini, A. (2011). Modelling carbon isotopes of carbonates in cave drip water. *Geochimica et Cosmochimica Acta, 75*(18), 5219–5228. https://doi.org/10.1016/j.gca.2011.06.023

Fornós, J. J., Clemmensen, L. B., Gómez-Pujol, L., & Murray, A. S. (2009). Late Pleistocene carbonate aeolianites on Mallorca, Western Mediterranean: A luminescence chronology. *Quaternary Science Reviews, 28*(25-26), 2697–2709. https://doi.org/10.1016/j.quascirev.2009.06.008

Frigola, J., Canals, M., Cacho, I., Moreno, A., Sierro, F. J., Flores, J. A., et al. (2012). A 500 kyr record of global sea-level oscillations in the Gulf of Lion, Mediterranean Sea: new insights into MIS 3 sea-level variability. *Climate of the Past, 8*(3), 1067–1077. https://doi.org/10.5194/cp-8-1067-2012

Frisia, S. (2015). Microstratigraphic logging of calcite fabrics in speleothems as tool for palaeoclimate studies. *International Journal of Speleology, 44*(1), 1–16. https://doi.org/10.5038/1827-806X.44.1.1

Genty, D., Blamart, D., Ouahdi, R., Gilmour, M., Baker, A., Jouzel, J., & Van-Exter, S. (2003). Precise dating of Dansgaard–Oeschger climate oscillations in western Europe from stalagmite data. *Nature, 421*, 833–837. https://doi.org/10.1038/nature01391

Genty, D., Combourieu-Nebout, N., Peyron, O., Blamart, D., Wainer, K., Mansuri, F., et al. (2010). Isotopic characterization of rapid climatic events during OIS3 and OIS4 in Villars Cave stalagmites (SW-France) and correlation with Atlantic and Mediterranean pollen records. *Quaternary Science Reviews, 29*(19-20), 2799–2820. https://doi.org/10.1016/j.quascirev.2010.06.035

Gibert, L., Scott, G. R., Scholz, D., Budsky, A., Ferràndez, C., Ribot, F., et al. (2016). Chronology for the Cueva Victoria fossil site (SE Spain): Evidence for Early Pleistocene Afro-Iberian dispersals. *Journal of Human Evolution, 90*, 183–197. https://doi.org/10.1016/j.jhevol.2015.08.002

Grant, K. M., Rohling, E. J., Bar-Matthews, M., Ayalon, A., Medina-Elizalde, M., Ramsey, C. B., et al.

(2012). Rapid coupling between ice volume and polar temperature over the past 150,000 years. *Nature, 491*, 744–747. https://doi.org/10.1038/nature11593

Hansen, M., Scholz, D., Froeschmann, M.-L., Schöne, B. R., & Spötl, C. (2017). Carbon isotope exchange between gaseous $CO_2$ and thin solution films: Artificial cave experiments and a complete diffusion-reaction model. *Geochimica et Cosmochimica Acta, 211*, 28–47. https://doi.org/10.1016/j.gca.2017.05.005

Hansen, M., Scholz, D., Schöne, B. R., & Spötl, C. (2019). Simulating speleothem growth in the laboratory: Determination of the stable isotope fractionation ($\delta^{13}$Cand $\delta^{18}$O) between $H_2O$, DIC and $CaCO_3$. *Chemical Geology, 509*, 20–44. https://doi.org/10.1016/j.chemgeo.2018.12.012

Heinrich, H. (1988). Origin and consequences of cyclic ice rafting in the Northeast Atlantic Ocean during the past 130,000 years. *Quaternary Research, 29*(2), 142–152. https://doi.org/10.1016/0033-5894(88)90057-9

Hemming, S. R. (2004). Heinrich events: Massive late Pleistocene detritus layers of the North Atlantic and their global climate imprint. *Reviews of Geophysics, 42*(1). https://doi.org/10.1029/2003RG000128

Henry, L. G., McManus, J. F., Curry, W. B., Roberts, N. L., Piotrowski, A. M., & Keigwin, L. D. (2016). North Atlantic ocean circulation and abrupt climate change during the last glaciation. *Science, 353*(6298), 470–474. https://doi.org/10.1126/science.aaf5529

Hodell, D., Crowhurst, S., Skinner, L., Tzedakis, P. C., Margari, V., Channell, J. E.T., et al. (2013). Response of Iberian Margin sediments to orbital and suborbital forcing over the past 420?ka. *Paleoceanography, 28*(1), 185–199. https://doi.org/10.1002/palo.20017

Hodge, E. J., Richards, D. A., Smart, P. L., Andreo, B., Hoffmann, D. L., Mattey, D. P., & González-Ramón, A. (2008a). Effective precipitation in southern Spain ( 266 to 46 ka) based on a speleothem stable carbon isotope record. *Quaternary Research, 69*(3), 447–457. https://doi.org/10.1016/j.yqres.2008.02.013

Hodge, E. J., Richards, D. A., Smart, P. L., Ginés, A., & Mattey, D. P. (2008b). Sub-millennial climate shifts in the western Mediterranean during the last glacial period recorded in a speleothem from Mallorca, Spain. *Journal of Quaternary Science, 23*(8), 713–718. https://doi.org/10.1002/jqs.1198

Hofer, D., Raible, C. C., Dehnert, A., & Kuhlemann, J. (2012a). The impact of different glacial boundary conditions on atmospheric dynamics and precipitation in the North Atlantic region. *Climate of the Past, 8*(3), 935–949. https://doi.org/10.5194/cp-8-935-2012

Hofer, D., Raible, C. C., Merz, N., Dehnert, A., & Kuhlemann, J. (2012b). Simulated winter circulation types in the North Atlantic and European region for preindustrial and glacial conditions. *Geophysical Research Letters, 39*. https://doi.org/10.1029/2012GL052296

Hoffmann, D. L., Rogerson, M., Spötl, C., Luetscher, M., Vance, D., Osborne, A. H., et al. (2016). Timing and causes of North African wet phases during the last glacial period and implications for modern human migration. *Scientific Reports, 6*, 36367. https://doi.org/10.1038/srep36367

Hurrell, J. W., & Loon, H. V. (1997). Decadal Variations in climate associated with the North Atlantic Oscillation. Climatic Change, 36(3), 301–326. https://doi.org/10.1023/A:1005314315270

Incarbona, A., Sprovieri, M., Di Stefano, A., Di Stefano, E., Salvagio Manta, D., Pelosi, N., et al. (2013). Productivity modes in the Mediterranean Sea during Dansgaard–Oeschger (20,000–70,000 yr ago) oscillations. *Palaeogeography, Palaeoclimatology, Palaeoecology, 392*, 128–137. https://doi.org/10.1016/j.palaeo.2013.09.023

Johnsen, S. J., Dahl-Jensen, D., Gundestrup, N., Steffensen, J. P., Clausen, H. B., Miller, H., et al. (2001). Oxygen isotope and palaeotemperature records from six Greenland ice-core stations: Camp Century, Dye-3, GRIP, GISP2, Renland and NorthGRIP. *Journal of Quaternary Science, 16*(4), 299–307. https://doi.org/10.1002/jqs.622

Johnson, K., Hu, C., Belshaw, N., & Henderson, G. (2006). Seasonal trace-element and stable-isotope variations in a Chinese speleothem: The potential for high-resolution paleomonsoon reconstruction. *Earth and Planetary Science Letters, 244*(1-2), 394–407. https://doi.org/10.1016/j.epsl.2006.01.064

Jones, P. D., Jonsson, T., & Wheeler, D. (1997). Extension to the North Atlantic oscillation using early instrumental pressure observations from Gibraltar and south?west Iceland. *International Journal of Climatology, 17*(13), 1433–1450. https://doi.org/10.1002/(SICI)1097-0088(19971115)17:13<1433::AID-JOC203>3.0.CO;2-P

Kim, S.-T., & O'Neil, J. R. (1997). Equilibrium and nonequilibrium oxygen isotope effects in synthetic carbonates. *Geochimica et Cosmochimica Acta, 61*(16), 3461–3475. https://doi.org/10.1016/S0016-7037(97)00169-5

Kottek, M., Grieser, J., Beck, C., Rudolf, B., & Rubel, F. (2006). World Map of the Köppen-Geiger climate classification updated. *Meteorologische Zeitschrift, 15*(3), 259–263. https://doi.org/10.1127/0941-2948/2006/0130

Kutzbach, J. E., & Liu, Z. (1997). Response of the African Monsoon to Orbital Forcing and Ocean Feedbacks in the Middle Holocene. *Science, 278*, 440–443.

Kutzbach, J. E., Chen, G., Cheng, H., Edwards, R. L., & Liu, Z. (2014). Potential role of winter rainfall in explaining increased moisture in the Mediterranean and Middle East during periods of maximum orbitally-forced insolation seasonality. *Climate Dynamics, 42*(3), 1079–1095. https://doi.org/10.1007/s00382-013-1692-1

Lachniet, M. S. (2009). Climatic and environmental controls on speleothem oxygen-isotope values. *Quaternary Science Reviews, 28*(5-6), 412–432. https://doi.org/10.1016/j.quascirev.2008.10.021

Laskar, J., Robutel, P., Joutel, F., Gastineau, M., Correia, A. C. M., & Levrard, B. (2004). A long-term numerical solution for the insolation quantities of the Earth. *Astronomy and Astrophysics, 428*(1), 261–285. https://doi.org/10.1051/0004-6361:20041335

Li, C., & Born, A. (2019). Coupled atmosphere-ice-ocean dynamics in Dansgaard-Oeschger events. *Quaternary Science Reviews, 203*, 1–20. https://doi.org/10.1016/j.quascirev.2018.10.031

Manteca Martínez, J. I., & Pina, R. (2015). Las mineralizaciones ferro-manganesíferas de la mina-cueva Victoria y su contexto geológico: Fe-Mn mineralizations of the mine-cave Victoria and their geological context. In L. Gibert & C. Ferràndez?Canadell (Eds.), *Geología y Paleontología de Cueva Victoria: Geology and Paleontology of Cueva Victoria Mastia* (Vol. 11–13, pp. 59–74). Cartagena: Revista del Museo Arqueolgico Municipal de Cartagena. Retrieved from

http://dialnet.unirioja.es/servlet/articulo?codigo=5093320

Martin-Vide, J., & Lopez-Bustins, J.-A. (2006). The Western Mediterranean Oscillation and rainfall in the Iberian Peninsula. *International Journal of Climatology, 26*(11), 1455–1475. https://doi.org/10.1002/joc.1388

Martrat, B., Grimalt, J. O., Lopez-Martinez, C., Cacho, I., Sierro, F. J., Flores, J. A., et al. (2004). Abrupt Temperature Changes in the Western Mediterranean over the Past 250,000 Years. *Science, 306*, 1762–1765. https://doi.org/10.1126/science.1101706

Martrat, B., Grimalt, J. O., Shackleton, N. J., Abreu, L. de, Hutterli, M. A., & Stocker, T. F. (2007). Four climate cycles of recurring deep and surface water destabilizations on the Iberian Margin. *Science, 317*, 502–507. https://doi.org/10.1126/science.1139994

Mauz, B., Fanelli, F., Elmejdoub, N., & Barbieri, R. (2012). Coastal response to climate change: Mediterranean shorelines during the Last Interglacial (MIS 5). *Quaternary Science Reviews, 54*, 89–98. https://doi.org/10.1016/j.quascirev.2012.02.021

McDermott, F. (2004). Palaeo-climate reconstruction from stable isotope variations in speleothems: a review. *Quaternary Science Reviews, 23*(7-8), 901–918. https://doi.org/10.1016/j.quascirev.2003.06.021

Menviel, L., Timmermann, A., Friedrich, T., & England, M. H. (2014). Hindcasting the continuum of Dansgaard/Oeschger variability: mechanisms, patterns and timing. *Climate of the Past, 10*(1), 63–77. https://doi.org/10.5194/cp-10-63-2014

Merz, N., Raible, C. C., & Woollings, T. (2015). North Atlantic Eddy-Driven Jet in Interglacial and Glacial Winter Climates. *Journal of Climate, 28*(10), 3977–3997. https://doi.org/10.1175/JCLI-D-14-00525.1

Meyer, K. W., Feng, W., Breecker, D. O., Banner, J. L., & Guilfoyle, A. (2014). Interpretation of speleothem calcite $\delta^{13}$Cvariations: Evidence from monitoring soil $CO_2$, drip water, and modern speleothem calcite in central Texas. *Geochimica et Cosmochimica Acta, 142*, 281–298. https://doi.org/10.1016/j.gca.2014.07.027

Mook, W. G. (Ed.). (2001). *Environmental isotopes in the hydrological cycle: Principles and applications. Technical documents in hydrology:* Vol. 39. Paris: UNESCO International Hydrological Programme.

Moreno, A., Cacho, I., Canals, M., Grimalt, J. O., Sánchez-Goñi, M. F., Shackleton, N., & Sierro, F. J. (2005). Links between marine and atmospheric processes oscillating on a millennial time-scale. A multi-proxy study of the last 50,000 yr from the Alboran Sea (Western Mediterranean Sea). *Quaternary Land-ocean Correlation Quaternary Land-ocean Correlation, 24*(14–15), 1623–1636. https://doi.org/10.1016/j.quascirev.2004.06.018

Moreno, A., Cacho, I., Canals, M., Prins, M. A., & Moreno, A. (2002). Saharan Dust Transport and High-Latitude Glacial Climatic Variability: The Alboran Sea Record. *Quaternary Research, 58*(3), 318–328. https://doi.org/10.1006/qres.2002.2383

Moreno, A., Sancho, C., Bartolomé, M., Oliva-Urcia, B., Delgado-Huertas, A., Estrela, M. J., et al. (2014). Climate controls on rainfall isotopes and their effects on cave drip water and speleothem growth: the case of Molinos cave (Teruel, NE Spain). *Climate Dynamics, 43*(1-2), 221–241.

https://doi.org/10.1007/s00382-014-2140-6

Mühlinghaus, C., Scholz, D., & Mangini, A. (2009). Modelling fractionation of stable isotopes in stalagmites. *Geochimica et Cosmochimica Acta, 73*(24), 7275–7289. https://doi.org/10.1016/j.gca.2009.09.010

Muñoz-García, M.B., Martín-Chivelet, J., Rossi, C., Ford, D. C., & Schwarcz, H.P. (2007). Chronology of Termination II and the Last Interglacial Period in North Spain based on stable isotope records of stalagmites from Cueva del Cobre (Palencia). *Journal of Iberian Geology, 33*(1), 17–30.

Naughton, F., Sánchez Goñi, M. F., Kageyama, M., Bard, E., Duprat, J., Cortijo, E., et al. (2009). Wet to dry climatic trend in north-western Iberia within Heinrich events. *Earth and Planetary Science Letters, 284*(3-4), 329–342. https://doi.org/10.1016/j.epsl.2009.05.001

North Greenland Ice Core Project members. (2004). High-resolution record of Northern Hemisphere climate extending into the last interglacial period. *Nature, 431*, 147–151. https://doi.org/10.1038/nature02805

Obert, J. C., Scholz, D., Felis, T., Brocas, W. M., Jochum, K. P., & Andreae, M. O. (2016). $^{230}$Th/U dating of Last Interglacial brain corals from Bonaire (southern Caribbean) using bulk and theca wall material. *Geochimica et Cosmochimica Acta, 178*, 20–40. https://doi.org/10.1016/j.gca.2016.01.011

Obrochta, S. P., Yokoyama, Y., Morén, J., & Crowley, T. J. (2014). Conversion of GISP2-based sediment core age models to the GICC05 extended chronology. *Quaternary Geochronology, 20*, 1–7. https://doi.org/10.1016/j.quageo.2013.09.001

Pailler, D., & Bard, E. (2002). High frequency palaeoceanographic changes during the past 140 000 yr recorded by the organic matter in sediments of the Iberian Margin. *Palaeogeography, Palaeoclimatology, Palaeoecology, 181*(4), 431–452. https://doi.org/10.1016/S0031-0182(01)00444-8

Pasho, E., Camarero, J. J., Luis, M. de, & Vicente-Serrano, S. M. (2011). Impacts of drought at different time scales on forest growth across a wide climatic gradient in north-eastern Spain. *Agricultural and Forest Meteorology, 151*(12), 1800–1811. https://doi.org/10.1016/j.agrformet.2011.07.018

Pons, A., & Reille, M. (1988). The Holocene- and upper Pleistocene pollen record from Padul (Granada, Spain): A new study. *Palaeogeography, Palaeoclimatology, Palaeoecology, 66*(3-4), 243–263. https://doi.org/10.1016/0031-0182(88)90202-7

Richards, D. A., & Dorale, J. A. (2003). Uranium-series Chronology and Environmental Applications of Speleothems. *Reviews in Mineralogy and Geochemistry, 52*(1), 407–460. https://doi.org/10.2113/0520407

Ros, A., & Llamusí, J. L. (2015). Reconsrucción y génesis del karst de Cueva Victoria: Reconstruction and genesis of the Cueva Victoria karst. In L. Gibert & C. Ferràndez?Canadell (Eds.), *Geología y Paleontología de Cueva Victoria: Geology and Paleontology of Cueva Victoria Mastia* (Vol. 11–13, pp. 111–125). Cartagena: Revista del Museo Arqueológico Municipal de Cartagena. Retrieved from https://dialnet.unirioja.es/servlet/articulo?codigo=5093425

Rozanski, K., Araguás-Araguás, L., & Gonfiantini, R. (1993). Isotopic Patterns in Modern Global

Precipitation. In P. K. Swart, K. C. Lohmann, J. McKenzie, and S. Savin (Eds.), *Climate Change in Continental Isotopic Records* (pp. 1–36). American Geophysical Union. https://doi.org/10.1029/GM078p0001

Sánchez Goñi, M. F., Landais, A., Fletcher, W. J., Naughton, F., Desprat, S., & Duprat, J. (2008). Contrasting impacts of Dansgaard–Oeschger events over a western European latitudinal transect modulated by orbital parameters. *Quaternary Science Reviews, 27*(11–12), 1136–1151. https://doi.org/10.1016/j.quascirev.2008.03.003

Sánchez Goñi, M. F., Bard, E., Landais, A., Rossignol, L., & D'Errico, F. (2013). Air-sea temperature decoupling in western Europe during the last interglacial-glacial transition. *Nature Geoscience, 6*(10), 837–841. https://doi.org/10.1038/ngeo1924

Schneider, T., Bischoff, T., & Haug, G. H. (2014). Migrations and dynamics of the intertropical convergence zone. *Nature, 513*, 45. https://doi.org/10.1038/nature13636

Scholz, D., & Hoffmann, D. L. (2011). StalAge – An algorithm designed for construction of speleothem age models. *Quaternary Geochronology, 6*(3-4), 369–382. https://doi.org/10.1016/j.quageo.2011.02.002

Shackleton, N. J., Hall, M. A., & Vincent, E. (2000). Phase relationships between millennial-scale events 64,000-24,000 years ago. *Paleoceanography, 15*(6), 565–569. https://doi.org/10.1029/2000PA000513

Siddall, M., Rohling, E. J., Thompson, W. G., & Waelbroeck, C. (2008). Marine isotope stage 3 sea level fluctuations: Data synthesis and new outlook. *Reviews of Geophysics, 46*(4), 109. https://doi.org/10.1029/2007RG000226

Spötl, C. (2011). Long-term performance of the Gasbench isotope ratio mass spectrometry system for the stable isotope analysis of carbonate microsamples. *Rapid Communications in Mass Spectrometry, 25*(11), 1683–1685. https://doi.org/10.1002/rcm.5037

Spötl, C., Fairchild, I. J., & Tooth, A. F. (2005). Cave air control on dripwater geochemistry, Obir Caves (Austria): Implications for speleothem deposition in dynamically ventilated caves. *Geochimica et Cosmochimica Acta, 69*(10), 2451–2468. https://doi.org/10.1016/j.gca.2004.12.009

Spötl, C., & Vennemann, T. W. (2003). Continuous-flow isotope ratio mass spectrometric analysis of carbonate minerals. *Rapid Communications in Mass Spectrometry, 17*(9), 1004–1006. https://doi.org/10.1002/rcm.1010

Stoll, H. M., Moreno, A., Mendez-Vicente, A., Gonzalez-Lemos, S., Jimenez-Sanchez, M., Dominguez-Cuesta, M. J., et al. (2013). Paleoclimate and growth rates of speleothems in the northwestern Iberian Peninsula over the last two glacial cycles. *Quaternary Research, 80*(2), 284–290. https://doi.org/10.1016/j.yqres.2013.05.002

Stríkis, N. M., Cruz, F. W., Barreto, E. A. S., Naughton, F., Vuille, M., Cheng, H., et al. (2018). South American monsoon response to iceberg discharge in the North Atlantic. *Proceedings of the National Academy of Sciences, 115*(15), 3788–3793. https://doi.org/10.1073/pnas.1717784115

Svensson, A., Andersen, K. K., Bigler, M., Clausen, H. B., Dahl-Jensen, D., Davies, S. M., et al. (2008). A 60 000 year Greenland stratigraphic ice core chronology. *Climate of the Past, 4*(1), 47–57. https://doi.org/10.5194/cp-4-47-2008

Svensson, A., Bigler, M., Blunier, T., Clausen, H. B., Dahl-Jensen, D., Fischer, H., et al. (2013). Direct linking of Greenland and Antarctic ice cores at the Toba eruption (74 ka BP). *Climate of the Past, 9*(2), 749–766. https://doi.org/10.5194/cp-9-749-2013

Toucanne, S., Angue Minto'o, C. M., Fontanier, C., Bassetti, M.-A., Jorry, S. J., & Jouet, G. (2015). Tracking rainfall in the northern Mediterranean borderlands during sapropel deposition. *Quaternary Science Reviews, 129*, 178–195. https://doi.org/10.1016/j.quascirev.2015.10.016

Tremaine, D. M., Froelich, P. N., & Wang, Y. (2011). Speleothem calcite farmed in situ: Modern calibration of $\delta^{18}$Oand $\delta^{13}$Cpaleoclimate proxies in a continuously-monitored natural cave system. *Geochimica et Cosmochimica Acta, 75*(17), 4929–4950. https://doi.org/10.1016/j.gca.2011.06.005

Trenberth, K. E., Branstator, G. W., Karoly, D., Kumar, A., Lau, N.?C., & Ropelewski, C. (1998). Progress during TOGA in understanding and modeling global teleconnections associated with tropical sea surface temperatures. *Journal of Geophysical Research: Oceans, 103*(C7), 14291–14324. https://doi.org/10.1029/97JC01444

Tzedakis, P.C., Hooghiemstra, H., & Pälike, H. (2006). The last 1.35 million years at Tenaghi Philippon: revised chronostratigraphy and long-term vegetation trends. *Quaternary Science Reviews, 25*(23-24), 3416–3430. https://doi.org/10.1016/j.quascirev.2006.09.002

Tzedakis, P.C., McManus, J.F., Hooghiemstra, H., Oppo, D.W., & Wijmstra, T.A. (2003). Comparison of changes in vegetation in northeast Greece with records of climate variability on orbital and suborbital frequencies over the last 450 000 years. *Earth and Planetary Science Letters, 212*(1-2), 197–212. https://doi.org/10.1016/S0012-821X(03)00233-4

Ünal-Ímer, E., Shulmeister, J., Zhao, J.-x., Uysal, I. T., Feng, Y.-X., Nguyen, A. D., & Yüce, G. (2015). An 80 kyr-long continuous speleothem record from Dim Cave, SW Turkey with paleoclimatic implications for the Eastern Mediterranean. *Scientific Reports, 5*, 13560. https://doi.org/10.1038/srep13560

Vautravers, M. J., & Shackleton, N. J. (2006). Centennial?scale surface hydrology off Portugal during marine isotope stage 3: Insights from planktonic foraminiferal fauna variability. *Paleoceanography, 21*(3). https://doi.org/10.1029/2005PA001144

Wainer, K., Genty, D., Blamart, D., Hoffmann, D., & Couchoud, I. (2009). A new stage 3 millennial climatic variability record from a SW France speleothem. *Palaeogeography, Palaeoclimatology, Palaeoecology, 271*(1–2), 130–139. https://doi.org/10.1016/j.palaeo.2008.10.009

Wang, Y., Cheng, H., Edwards, R. L., Kong, X., Shao, X., Chen, S., et al. (2008). Millennial- and orbital-scale changes in the East Asian monsoon over the past 224,000 years. *Nature, 451*, 1090–1093. https://doi.org/10.1038/nature06692

Wolff, E.W., Chappellaz, J., Blunier, T., Rasmussen, S.O., & Svensson, A. (2010). Millennial-scale variability during the last glacial: The ice core record. *Quaternary Science Reviews, 29*(21-22), 2828–2838. https://doi.org/10.1016/j.quascirev.2009.10.013

Wu, H., Guiot, J., Brewer, S., & Guo, Z. (2007). Climatic changes in Eurasia and Africa at the last glacial maximum and mid-Holocene: reconstruction from pollen data using inverse vegetation modelling. *Climate Dynamics, 29*(2-3), 211–229. https://doi.org/10.1007/s00382-007-0231-3

Yang, Q., Scholz, D., Jochum, K. P., Hoffmann, D. L., Stoll, B., Weis, U., et al. (2015). Lead isotope

variability in speleothems—A promising new proxy for hydrological change? First results from a stalagmite from western Germany. *Chemical Geology, 396*, 143–151.
https://doi.org/10.1016/j.chemgeo.2014.12.028

## 5.7 Supplemental material

**Age modelling** The presented CV flowstones (Figure 5.4) display several hiatuses and changes in growth rate (Table 5.7, Figure 5.5). In case of more than two ages for a single segment, we used StalAge (Scholz & Hoffmann, 2011) to construct an age-depth model. However, some CV flowstones show very short growth phases, which are constrained by less than three ages. In case of two ages, we linearly interpolated the age-depth model between the two ages (Vic-III-3). In case of a single age, we assumed a distinct growth rate (approx. average growth rate over the whole sample) for the corresponding growth interval (Vic-III-1, 3). For D/O 18, we used another approach to eliminate age discrepancies between the records. Since we have a single age for each record, we calculated the weighted mean age of all three records ($64.34 \pm 2.04$ ka) with a subsequently enlarged age uncertainty (Figure 5.6). This age is then used to construct the StalAge model (Vic-III-1) or as the initial value for an assumed growth rate (0.05 µm/a for SR01t and 0.025 µm/a for Vic-III-3).

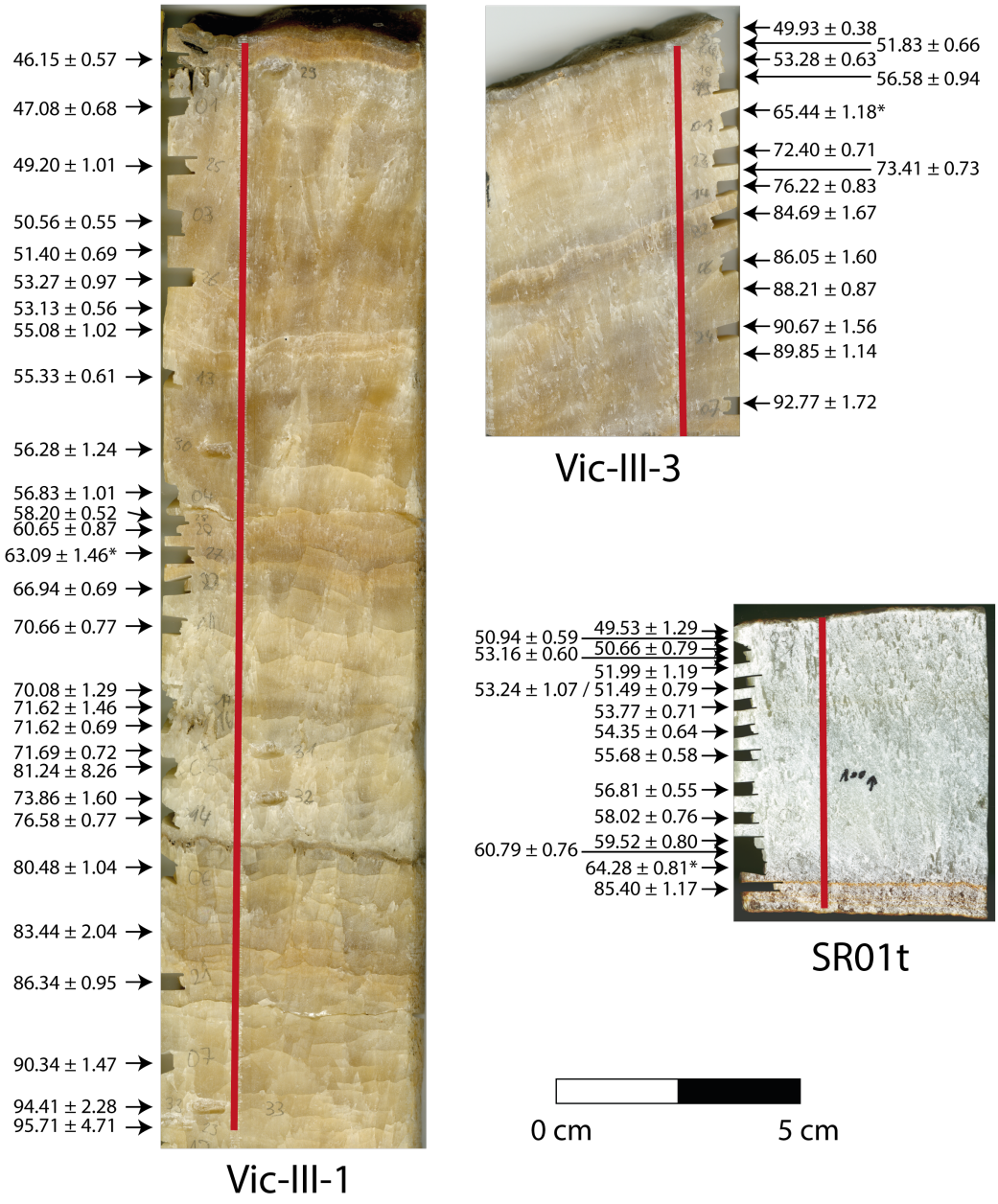


Figure 5.4: Pictures of the investigated sample material. The locations of sampling for $^{230}$Th/U-dating are indicated with an arrow and the corresponding age in ka. The age with an asterisk has been modified for the age model (see text). The track of the stable isotope measurements is indicated by the red line.

$^{230}$Th/U dating results for flowstones Vic-III-1, Vic-III-3 and SR01t.

| Sample | $^{238}$U [µg/g] | ± | ($^{230}$Th/$^{232}$Th) | ± | ($^{234}$U/$^{238}$U) | ± | ($^{230}$Th/$^{238}$U) | ± | age corr.[ka] | error [ka] | age uncorr. [ka] | error [ka] | dft [cm] |
|---|---|---|---|---|---|---|---|---|---|---|---|---|---|
| Vic-III-1-29 | 0.216 | 0.001 | 240.8 | 3.0 | 1.194 | 0.002 | 0.421 | 0.004 | 46.15 | 0.57 | 46.80 | 0.57 | 0.8 |
| Vic-III-1-01 | 0.225 | 0.002 | 149.4 | 1.5 | 1.201 | 0.004 | 0.435 | 0.003 | 47.08 | 0.68 | 48.16 | 0.67 | 1.4 |
| Vic-III-1-37 | 0.256 | 0.003 | 130.1 | 1.1 | 1.189 | 0.011 | 0.445 | 0.004 | 49.20 | 1.01 | 50.49 | 1.00 | 1.8 |
| Vic-III-1-25 | 0.282 | 0.002 | 196.9 | 2.3 | 1.180 | 0.002 | 0.448 | 0.003 | 50.56 | 0.55 | 51.42 | 0.55 | 2.7 |
| Vic-III-1-03 | 0.242 | 0.001 | 140.2 | 1.5 | 1.181 | 0.002 | 0.458 | 0.003 | 51.40 | 0.69 | 52.63 | 0.69 | 3.85 |
| Vic-III-1-38 | 0.259 | 0.003 | 171.0 | 1.8 | 1.169 | 0.009 | 0.463 | 0.005 | 53.27 | 0.97 | 54.31 | 0.97 | 4.4 |
| Vic-III-1-26 | 0.274 | 0.002 | 259.9 | 3.1 | 1.174 | 0.002 | 0.462 | 0.003 | 53.13 | 0.56 | 53.81 | 0.57 | 5.4 |
| Vic-III-1-39 | 0.355 | 0.004 | 255.2 | 2.6 | 1.169 | 0.011 | 0.473 | 0.005 | 55.08 | 1.02 | 55.78 | 1.07 | 6.4 |
| Vic-III-1-40 | 0.318 | 0.004 | 160.1 | 1.5 | 1.163 | 0.012 | 0.481 | 0.005 | 55.33 | 0.61 | 56.07 | 0.59 | 7.2 |
| Vic-III-1-13 | 0.289 | 0.002 | 244.7 | 2.3 | 1.169 | 0.004 | 0.475 | 0.003 | 56.28 | 1.24 | 57.43 | 1.25 | 7.3 |
| Vic-III-1-30 | 0.248 | 0.002 | 97.7 | 1.0 | 1.171 | 0.003 | 0.493 | 0.004 | 56.83 | 1.01 | 58.76 | 1.02 | 8.6 |
| Vic-III-1-04 | 0.291 | 0.002 | 312.9 | 3.2 | 1.182 | 0.002 | 0.499 | 0.003 | 58.20 | 0.52 | 58.80 | 0.52 | 9.6 |
| Vic-III-1-20 | 0.359 | 0.002 | 106.9 | 0.9 | 1.183 | 0.002 | 0.522 | 0.002 | 60.65 | 0.87 | 62.49 | 0.87 | 10.2 |
| Vic-III-1-27 | 0.228 | 0.001 | 65.9 | 0.8 | 1.182 | 0.002 | 0.545 | 0.004 | 63.09* | 1.46* | 66.22 | 1.43 | 10.7 |
| Vic-III-1-22 | 0.264 | 0.002 | 207.2 | 1.9 | 1.165 | 0.003 | 0.547 | 0.003 | 66.94 | 0.69 | 67.94 | 0.69 | 11.2 |
| Vic-III-1-11 | 0.233 | 0.002 | 429.9 | 4.2 | 1.144 | 0.004 | 0.555 | 0.004 | 70.66 | 0.77 | 71.16 | 0.76 | 12.3 |
| Vic-III-1-41 | 0.248 | 0.003 | 295.8 | 2.7 | 1.156 | 0.010 | 0.559 | 0.005 | 70.08 | 1.29 | 70.80 | 1.29 | 13 |
| Vic-III-1-17 | 0.214 | 0.001 | 69.7 | 0.6 | 1.156 | 0.002 | 0.581 | 0.003 | 71.62 | 1.46 | 74.85 | 1.51 | 13.9 |
| Vic-III-1-16 | 0.214 | 0.001 | 248.1 | 2.4 | 1.158 | 0.002 | 0.569 | 0.003 | 71.62 | 0.69 | 72.50 | 0.68 | 14.2 |
| Vic-III-1-31 | 0.274 | 0.002 | 534.0 | 5.7 | 1.152 | 0.002 | 0.564 | 0.004 | 71.69 | 0.72 | 72.09 | 0.71 | 14.7 |
| Vic-III-1-05 | 0.148 | 0.001 | 257.6 | 23.5 | 1.156 | 0.003 | 0.621 | 0.043 | 81.24 | 8.26 | 82.16 | 8.17 | 15.05 |
| Vic-III-1-32 | 0.075 | 0.000 | 222.0 | 5.6 | 1.149 | 0.003 | 0.578 | 0.008 | 73.86 | 1.60 | 74.87 | 1.58 | 15.6 |
| Vic-III-1-14 | 0.208 | 0.001 | 320.5 | 2.9 | 1.148 | 0.004 | 0.591 | 0.003 | 76.58 | 0.77 | 77.29 | 0.78 | 16.3 |
| Vic-III-1-06 | 0.168 | 0.001 | 165.5 | 1.6 | 1.126 | 0.004 | 0.603 | 0.004 | 80.48 | 1.04 | 81.92 | 1.05 | 17.3 |
| Vic-III-1-42 | 0.118 | 0.001 | 66.8 | 0.6 | 1.121 | 0.006 | 0.625 | 0.005 | 83.44 | 2.04 | 87.19 | 2.07 | 18.5 |
| Vic-III-1-21 | 0.185 | 0.001 | 342.4 | 3.7 | 1.151 | 0.002 | 0.642 | 0.004 | 86.34 | 0.95 | 87.06 | 0.97 | 19.4 |
| Vic-III-1-07 | 0.074 | 0.000 | 295.6 | 4.5 | 1.178 | 0.004 | 0.680 | 0.007 | 90.34 | 1.47 | 91.20 | 1.46 | 21 |
| Vic-III-1-33 | 0.105 | 0.001 | 236.2 | 6.2 | 1.159 | 0.003 | 0.687 | 0.010 | 94.41 | 2.28 | 95.51 | 2.26 | 22 |
| Vic-III-1-23 | 0.109 | 0.001 | 197.3 | 10.3 | 1.202 | 0.010 | 0.723 | 0.022 | 95.71 | 4.71 | 97.04 | 4.69 | 22.4 |

| Sample | $^{238}$U [µg/g] | ± | ($^{230}$Th/$^{232}$Th) | ± | ($^{234}$U/$^{238}$U) | ± | ($^{230}$Th/$^{238}$U) | ± | age corr.[ka] | error [ka] | age uncorr. [ka] | error [ka] | dft [cm] |
|---|---|---|---|---|---|---|---|---|---|---|---|---|---|
| Vic-III-3-33 | 0.238 | 0.001 | 251.3 | 2.4 | 1.177 | 0.002 | 0.440 | 0.002 | 49.93 | 0.38 | 50.36 | 0.37 | 0.4 |
| Vic-III-3-04 | 0.194 | 0.001 | 222.0 | 2.6 | 1.174 | 0.005 | 0.452 | 0.004 | 51.83 | 0.66 | 52.33 | 0.66 | 0.6 |
| Vic-III-3-18 | 0.225 | 0.001 | 145.9 | 2.0 | 1.170 | 0.002 | 0.462 | 0.003 | 53.28 | 0.63 | 54.07 | 0.62 | 0.9 |
| Vic-III-3-19 | 0.267 | 0.002 | 134.6 | 2.2 | 1.169 | 0.003 | 0.484 | 0.006 | 56.58 | 0.94 | 57.47 | 0.96 | 1.2 |
| Vic-III-3-01 | 0.172 | 0.002 | 317.4 | 3.5 | 1.166 | 0.009 | 0.535 | 0.005 | 65.44* | 1.18* | 65.85 | 1.16 | 2 |
| Vic-III-3-23 | 0.208 | 0.001 | 437.1 | 4.3 | 1.143 | 0.003 | 0.562 | 0.003 | 72.40 | 0.71 | 72.72 | 0.71 | 2.7 |
| Vic-III-3-41 | 0.259 | 0.002 | 393.3 | 4.8 | 1.145 | 0.001 | 0.570 | 0.004 | 73.41 | 0.73 | 73.77 | 0.74 | 2.9 |
| Vic-III-3-14 | 0.166 | 0.001 | 412.8 | 4.2 | 1.136 | 0.004 | 0.580 | 0.004 | 76.22 | 0.83 | 76.58 | 0.83 | 3.5 |
| Vic-III-3-32 | 0.105 | 0.001 | 52.0 | 0.5 | 1.132 | 0.005 | 0.634 | 0.004 | 84.69 | 1.67 | 87.81 | 1.65 | 4 |
| Vic-III-3-06 | 0.207 | 0.002 | 383.8 | 4.0 | 1.143 | 0.009 | 0.634 | 0.006 | 86.05 | 1.60 | 86.46 | 1.60 | 5 |
| Vic-III-3-42 | 0.184 | 0.001 | 285.0 | 3.1 | 1.134 | 0.002 | 0.640 | 0.004 | 88.21 | 0.87 | 88.78 | 0.88 | 5.5 |
| Vic-III-3-24 | 0.160 | 0.001 | 173.1 | 1.7 | 1.121 | 0.007 | 0.645 | 0.006 | 90.67 | 1.56 | 91.62 | 1.55 | 6.4 |
| Vic-III-3-43 | 0.154 | 0.001 | 122.9 | 1.4 | 1.138 | 0.002 | 0.654 | 0.005 | 89.85 | 1.14 | 91.19 | 1.13 | 6.5 |
| Vic-III-3-07 | 0.161 | 0.002 | 238.9 | 2.3 | 1.148 | 0.009 | 0.670 | 0.006 | 92.77 | 1.72 | 93.47 | 1.77 | 7.6 |
| SR01t-13 | 0.348 | 0.002 | 6710.0 | 308.1 | 2.049 | 0.003 | 0.773 | 0.017 | 49.53 | 1.29 | 49.54 | 1.31 | 0.2 |
| SR01t-09 | 0.350 | 0.003 | 86873.8 | 8444.8 | 1.882 | 0.007 | 0.724 | 0.006 | 50.94 | 0.59 | 50.94 | 0.58 | 0.5 |
| SR01t-15 | 0.362 | 0.002 | 811324.2 | 419545.4 | 1.899 | 0.005 | 0.728 | 0.009 | 50.66 | 0.79 | 50.66 | 0.78 | 0.65 |
| SR01t-01 | 0.300 | 0.011 | 29390.2 | 1637.1 | 1.833 | 0.008 | 0.730 | 0.006 | 53.16 | 0.60 | 53.16 | 0.61 | 0.9 |
| SR01t-14 | 0.314 | 0.002 | 89755.0 | 13065.1 | 1.921 | 0.004 | 0.752 | 0.014 | 51.99 | 1.19 | 51.99 | 1.21 | 1.1 |
| SR01t-06 | 0.360 | 0.003 | 7300.6 | 214.3 | 1.815 | 0.007 | 0.723 | 0.012 | 53.24 | 1.07 | 53.24 | 1.09 | 1.3 |
| SR01t-06re | 0.361 | 0.003 | 7107.2 | 143.4 | 1.839 | 0.009 | 0.714 | 0.008 | 51.49 | 0.79 | 51.50 | 0.82 | 1.3 |
| SR01t-03 | 0.336 | 0.002 | 9614.8 | 165.1 | 1.757 | 0.007 | 0.705 | 0.007 | 53.77 | 0.71 | 53.78 | 0.71 | 1.8 |
| SR01t-04 | 0.346 | 0.003 | 8530.9 | 117.8 | 1.888 | 0.008 | 0.766 | 0.006 | 54.35 | 0.64 | 54.35 | 0.63 | 2.3 |
| SR01t-07 | 0.335 | 0.002 | 54212.9 | 2504.2 | 1.795 | 0.007 | 0.741 | 0.005 | 55.68 | 0.58 | 55.68 | 0.57 | 2.8 |
| SR01t-05 | 0.378 | 0.003 | 38931.4 | 604.6 | 1.882 | 0.007 | 0.791 | 0.005 | 56.81 | 0.55 | 56.81 | 0.54 | 3.5 |
| SR01t-08 | 0.290 | 0.002 | 8061.3 | 144.5 | 1.884 | 0.008 | 0.805 | 0.008 | 58.02 | 0.76 | 58.02 | 0.78 | 4.1 |
| SR01t-10 | 0.335 | 0.002 | 38364.7 | 1169.5 | 1.776 | 0.008 | 0.773 | 0.008 | 59.52 | 0.80 | 59.52 | 0.81 | 4.55 |
| SR01t-12 | 0.270 | 0.002 | 3152.6 | 66.9 | 1.960 | 0.003 | 0.871 | 0.009 | 60.79 | 0.76 | 60.80 | 0.78 | 4.8 |
| SR01t-02 | 0.312 | 0.012 | 28484.1 | 791.3 | 1.897 | 0.009 | 0.879 | 0.008 | 64.28* | 0.81* | 64.28 | 0.85 | 5.1 |
| SR01t-11 | 0.134 | 0.001 | 49.0 | 0.5 | 1.894 | 0.007 | 1.091 | 0.008 | 85.40 | 1.17 | 86.32 | 1.06 | 5.55 |

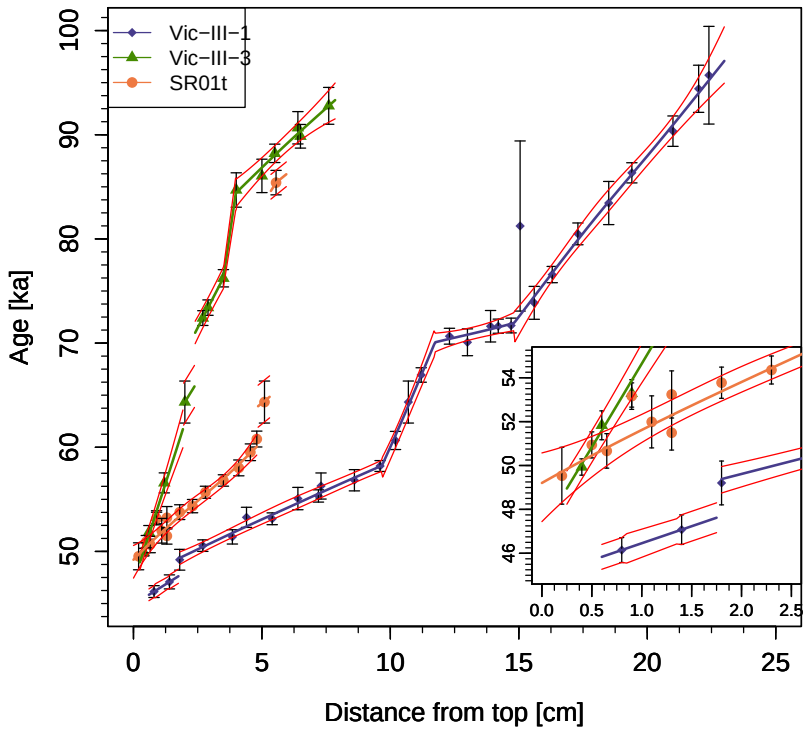


Figure 5.5: StalAge models (Scholz & Hoffmann, 2011) for the three flowstone records (Vic-III-1, -3, SR01t) with the $^{230}$Th/U ages (Table 5.7).

## References

Budsky, A., Scholz, D., Wassenburg, J. A., Mertz-Kraus, R., Spötl, C., Riechelmann, D. F. C., et al. (2019). Speleothem $\delta^{13}$C record suggests enhanced spring/summer drought in south-eastern Spain between 9.7 and 7.8 ka – A circum-Western Mediterranean anomaly? The Holocene, 44(1), 095968361983802. https://doi.org/10.1177/0959683619838021

Cheng, H., Edwards, R.L., Hoff, J., Gallup, C.D., Richards, D.A., & Asmerom, Y. (2000). The half-lives of uranium-234 and thorium-230. Chemical Geology, 169(1–2), 17–33. https://doi.org/10.1016/S0009-2541(99)00157-6

Jaffey, A. H., Flynn, K. F., Glendenin, L. E., Bentley, W. C., & Essling, A. M. (1971). Precision measurement of half-lives and specific activities of $^{235}$U and $^{238}$U. Physical Review C, 4(5), 1889. https://doi.org/10.1103/PhysRevC.4.1889

Scholz, D., & Hoffmann, D. L. (2011). StalAge – An algorithm designed for construction of speleothem age models. Quaternary Geochronology, 6(3-4), 369–382. https://doi.org/10.1016/j.quageo.2011.02.002

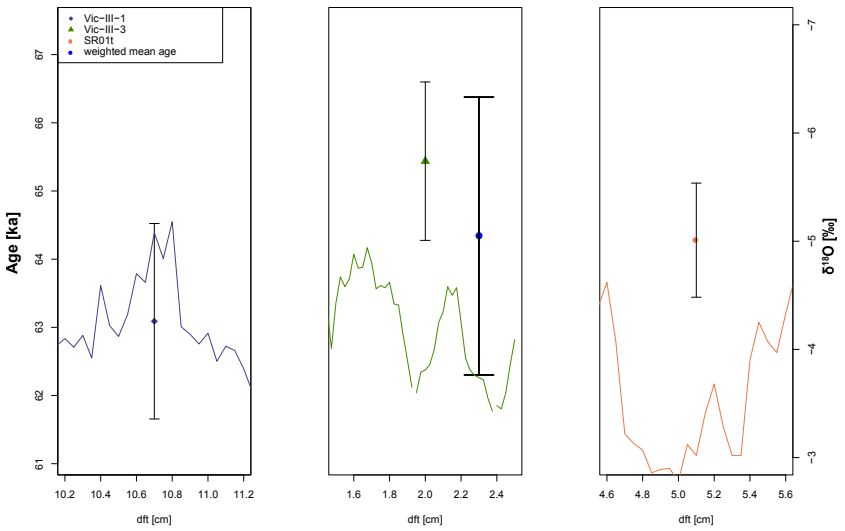


Figure 5.6: Ages and $\delta^{18}$O values (inverted y-axes) for D/O 18 in Vic-III-1, -3, and SR01t vs. distance from top. The blue dot shows the weighted mean age, which is used for D/O 18 in three all samples for further calculations of the age models.

# 6 Climate variability during the Last Interglacial revealed by a speleothem record from south-eastern Spain covering the last 190 ka

Budsky, Alexander[1]; Mertz-Kraus, Regina[1]; Spötl, Christoph[2]; Jochum, Klaus Peter[3]; Scholz, Denis[1]

[1]Institute for Geosciences, Johannes Gutenberg University, Johann-Joachim-Becher-Weg 21, 55128 Mainz, Germany
[2]Institute of Geology, Innsbruck University, Innrain 52, Innsbruck 6020, Austria
[3]Max Planck Institute for Chemistry, Department of Climate Geochemistry, P.O. Box 3060, 55020 Mainz, Germany

Corresponding author:
Alexander Budsky, Institute for Geosciences, Johannes Gutenberg University Mainz, Johann-Joachim-Becher-Weg 21, 55128 Mainz, Germany
Phone: 0049 (0)6131-39-23173
Email: albudsky@students.uni-mainz.de

**Abstract** Modern Western Mediterranean interglacial climate is characterised by strong seasonality, and especially south-eastern Spain is strongly influenced by limited rainfall. Significant climate variability during the Last Interglacial observed in terrestrial archives from the Mediterranean suggests to revise the assumption of rather stable climate similar to Holocene climate. Last interglacial climate in south -eastern Spain was strongly influenced by arid events introduced by cold freshwater outburst in the North Atlantic influencing climate in the Western Mediterranean. We present speleothem stable isotope records from Cueva Victoria in south-eastern Spain covering the periods from marine isotope stages 6.5 to 5c (190 – 100 ka). The records document several climate instabilities of the hydrological system during the penultimate glacial, the last interglacial and the last glacial inception. Combining previous studies, we further conclude climatic variability on orbital time scale. In addition to sea-surface temperature of the

North Atlantic and the Western Mediterranean Sea, solar insolation is an important driver of precipitation variability in south-eastern Spain. ?

## 6.1 Introduction

Temperature and sea-level of the Last Interglacial (LIG, 129 – 116 ka) have often been compared with the Holocene (< 11.7 ka), although orbital parameters were different (Martrat et al., 2014). In general, at the beginning of an interglacial, the deglaciation, which was accompanied by increasing temperatures and a sea level rise, and an intensified Atlantic Meridional Overturning Circulation (AMOC, Böhm et al., 2015) resulted in increased temperature and humidity on the continent (Demény et al., 2017; Genty et al., 2003; Sirocko et al., 2005; Vansteenberge et al., 2016). In addition, as a result of high solar summer insolation during interglacials, the Intertropical Convergence Zone (ITCZ) arrived at its most northern position over Africa (Pausata et al., 2016; Rohling et al., 2002; Tierney et al., 2017), influencing the southern borderlands of the Mediterranean by increased freshwater input (Rohling et al., 2015; Rossignol-Strick and Paterne, 1999; Weldeab et al., 2002). Subsequently, ocean circulation in the Mediterranean changed into stratiform and anoxic conditions forming sapropels in the Eastern Mediterranean (Emeis et al., 2000; Rohling et al., 2015). At the same time, lower winter insolation lead to a shift of the Atlantic jet to a more southern position enabling depressions to enter the Mediterranean (Kutzbach et al., 2014). Hence, (winter) conditions in the Mediterranean were more humid during interglacials as documented by various pollen (Allen et al., 1999; Allen and Huntley, 2009; Camuera et al., 2019; Roucoux et al., 2008; Tzedakis, 2005) and speleothem records (Bar-Matthews et al., 2003; Drysdale et al., 2007; Hodge et al., 2008; Regattieri et al., 2014). Apart from these general similarities, there are also differences between the LIG and the Holocene. LIG sea level exceeded those during the Holocene climate optimum of about 2 to 4 m (Bardají et al., 2009; Rovere et al., 2016) and peaked at 6 to 9 m above present sea level (Dutton and Lambeck, 2012; Grant et al., 2014; Hearty et al., 2007). In addition, global mean temperature (CAPE-Last Interglacial Project Members, 2006; Pedersen et al., 2017) and SST (Leduc et al., 2010; Martrat et al., 2014) were warmer due to the higher summer insolation (Berger, 1978). As a result, the monsoon strength (Rossignol-Strick and Paterne, 1999) and precipitation in the Eastern Mediterranean (Bar-Matthews et al., 2003; Grant et al., 2016) exceeded the Holocene levels as revealed by a minimized dust input (Ehrmann et al., 2017). Several incursions of ice rafted debris (IRD, Bond et al., 1999) into the North Atlantic recorded during the LIG (Galaasen et al., 2014; Mokeddem et al., 2014; Tzedakis et al., 2018) lead to increased climate instability compared to the Holocene (Bond et al., 2001). High temporal resolution terrestrial records enable to reconstruct the climatic transition from the penultimate glacial into the LIG (Regattieri et al., 2016; Regattieri et al., 2017; Tzedakis et al., 2018; Vansteenberge et al., 2019). The penultimate glacial (MIS 6, 190 – 130 ka) is known for its deposition of sapropel S6 (Emeis et al., 2000; Rossignol-Strick and Paterne, 1999), which indicates unusually humid climate conditions at the beginning of MIS 6 (185 – 170 ka, MIS 6.5) in the Mediterranean (Bard et al., 2002; Hodge et

al., 2008; Toucanne et al., 2015) and Europe (Wainer et al., 2011). Although sea level MIS during 6.5 was reduced by about -50 m compared to the present (Grant et al., 2014; Scholz et al., 2007), insolation reached its maximum (≈ 174 ka, Berger, 1978) inducing strong seasonality by strong African (Tisserand et al., 2009) and Asian monsoon (Wang et al., 2008) despite of reduced SST, which were on a similar level as during MIS 3 (Martrat et al., 2004; Martrat et al., 2007). Here we present new speleothem records from south-eastern Spain covering parts of the penultimate glacial (175 – 160 ka) and the LIG (133 – 100 ka) displaying large hydrological shifts and climate instability during the LIG. In combination with previous studies from the same cave reconstructing hydrological and vegetational changes during the Holocene (Budsky et al., 2019a) and MIS 3 (Budsky et al., 2019b), we elaborate the two main drivers favouring speleothem growth in south-eastern Spain. These are primarily the sea surface temperatures (SST) from the surrounding oceans providing moisture in combination with summer insolation as an indicator for high summer temperatures enabling moisture uptake.

## 6.2 Regional setting

Cueva Victoria (CV) is located in south-eastern Spain (37.6°N, 0.82°W, 40 m asl, Figure 6.1) and located at one of the driest regions in Europe with an annual precipitation between 200 and 300 mm and a strong seasonality (Agencia Estatal de Meteorología, 2011; Araguas-Araguas and Diaz Teijeiro, 2005; Budsky et al., 2019a). According to the Köppen-Geiger classification, climate can be classified as BSk climate, which reflects arid cold steppe climate with a mean annual temperature (MAT) below 18 °C (Kottek et al., 2006). The most important atmospheric setting leading to precipitation is the Western Mediterranean Oscillation (WeMO, Martin-Vide and Lopez-Bustins, 2006), whereas annual temperature is more strongly influenced by the East Atlantic pattern (EA, Ríos-Cornejo et al., 2015). The North Atlantic Oscillation (NAO, Comas-Bru and McDermott, 2014), which has a strong influence in many other parts of Europe (Deininger et al., 2016; Hurrell and Loon, 1997) shows no significant influence on precipitation.

Cueva Victoria formed in Triassic limestones and dolostones of the Inner Betic System. These partly karstified rocks belong to the Alpujarride metamorphic complex (San Ginés unit, Manteca Martínez and Pina, 2015). The cave system extends over 3 km laterally and 155 m vertically and consists of several chambers (Ros and Llamusí, 2015). Until the last century, the manganese ore linked to fault systems was mined, and the original cave system was widened and, thus, strongly modified. This is, for instance, evident by high present-day ventilation (cave $pCO_2$ <500 ppmV, data provided by the local caving group, CENM-naturaleza). Therefore, cave monitoring makes not much sense at CV. The flowstone cores were recovered in a less ventilated part of the cave (reflected by high relative humidity > 90 %). The approximate mean annual cave air temperature at the sampling site of the flowstones is 17 °C (CENM-naturaleza). Previous studies (Budsky et al., 2015; Budsky et al., 2019a; b) showed preferential speleothem growth during more humid interglacials and interstadials. Associated with that, increased vegetation and the refilling of the aquifer reactivated the karst system for flowstone deposition.

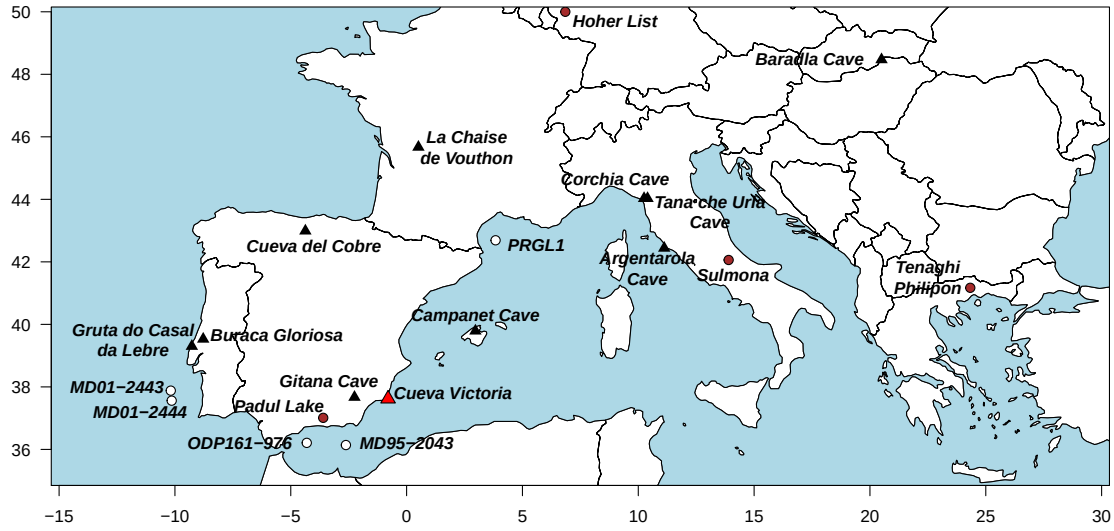


Figure 6.1: Map showing the location of Cueva Victoria, which is displayed by a red triangle. Important sites discussed in the text are also shown. Sediment records (Hoher List, Sirocko et al., 2005; Padul Lake, Camuera et al., 2019; Sulmona Basin, Regattieri et al., 2015; Tenaghi Philippon, Tzedakis et al., 2006) are indicated by brown circles, whereas triangles display speleothem records (Bradla Cave, Demény et al., 2017; La Chaise de Vouthon, Couchoud et al., 2009; Corchia Cave, Drysdale et al., 2005; Tana che Urla Cave, Regattieri et al., 2014; Cueva del Cobre, Rossi et al., 2014; Argentarola Cave, Bard et al., 2002b; Campanet Cave, Dumitru et al., 2018; Buraca Gloriosa and Gruta do Casal da Lebre, Denniston et al., 2018 and Gitana Cave, Hodge et al., 2008). Open white circles show marine records (PRGL1, Cortina et al., 2011; MD01-2443/4, Martrat et al., 2007; ODP161-976, Martrat et al., 2014 and MD95-2043, Cacho et al., 1999).

## 6.3 Material and methods

Two flowstone cores were collected from chamber Victoria III (Ros and Llamusí, 2015) using a mobile core drilling device with a diameter of 5 cm. Vic-III-1 (Vic-III-3) has a length of 41.5 cm (40.5 cm) and the preparation has already been described by Budsky et al. (2019a). Here, we focus on the section covering MIS 5 to MIS 6, corresponding to 23 to 29.5 cm distance from top (dft) for Vic-III-1 and 7.85 to 37.5 cm dft for Vic-III-3, respectively. Both flowstone cores are generally composed of calcite with a columnar fabric (Frisia, 2015). Vic-III-3 shows partly open columnar fabric from 11 to 18 cm dft. In addition, this core shows a distinct dark layer at 34.4 cm dft. We took nine samples for U-series dating from Vic-III-1 and 33 samples from Vic-III-3, respectively. The sample mass varied between 100 and 300 mg. The sample preparation is described in (Budsky et al., 2019a) and details for spike preparation and separation of U and Th can be found in (Gibert et al., 2016; Yang et al., 2015). Mass spectrometric analyses of U

and Th isotopes were performed with a Nu instruments MC-ICP-MS (multi-collector inductively coupled plasma mass spectrometer) at the Max Planck Institute for Chemistry, Mainz. Details are provided by Obert et al. (2016). To determine ages and activity ratios, the half-lives of (Cheng et al., 2000) for $^{230}$Th and $^{234}$U, (Le Roux and Glendenin, 1963) for $^{232}$Th, and (Jaffey et al., 1971) for $^{238}$U were used. The detrital correction factor was adjusted in order to minimize age inversions in each flowstone (see Budsky et al., 2019a, for details). This resulted in activity ratios of ($^{232}$Th/$^{238}$U) = 0.24 (Vic-III-1) and 0.37 (Vic-III-3), respectively. The resulting ages were then used for calculation of an age model using the StalAge algorithm (Scholz and Hoffmann, 2011). In case of only two ages for a growth period, we linearly interpolated an age depth model with appropriate uncertainties (Figure 6.2). Samples for stable isotope measurement were taken at a spatial resolution of 500 µm in Vic-III-1 and 250 µm in Vic-III-3, respectively, using a NWR MicroMill. Measurements were performed at the Institute of Geology, University of Innsbruck, using a Thermo Fisher DeltaplusXL isotope ratio mass spectrometer. This is linked to a Gasbench II as described in (Spötl and Vennemann, 2003) and (Spötl, 2011). The long-term analytical precision ($1\sigma$) of the $\delta^{18}$O measurements is 0.08 ($\delta^{13}$C: 0.06 ‰). Both values are displayed relative to the V-PDB standard.

## 6.4 Results and Discussion

The bottom sections of both samples (Vic-III-1 and Vic-III-3) show pale white calcite below a distinct brown layer (Figure 6.7). Maximum ages for this section are 186.3 ± 4.9 at 29.5 cm dft for Vic-III-1 and 175.6 ± 4.4 for Vic-III-3 at 36.7 cm dft, respectively. Above the hiatus, sample Vic-III-1 shows two growth phases from 113 – 107 ka and 103 – 100 ka. Vic-III-3 records several short growth periods at approx. 132 and 126 ka and a main growth phase between 117.5 ka and 102 ka (Figure 6.2).

The few, only preliminary stable isotope values for MIS 6.5 (Figure 6.7) show strongly increasing $\delta^{18}$O values with decreasing age (Figure 6.3). $\delta^{18}$O values are in good agreement between the two speleothem records from Cueva Victoria and vary between ca. -6.75 ‰ at 105 and 127 ka and -4.25 ‰ at the onset of DO 24 (≈ 109 ka) in Vic-III-3. The $\delta^{13}$C values in Vic-III-3 show two plateaus with more negative values around -11.25 ‰ between 102 to 109 ka and 116 to 133 ka and higher values of ca. -10.25 ‰ in between. The $\delta^{13}$C values of Vic-III-1 show the same magnitude. According to Budsky et al. (2019a; b) the $\delta^{13}$C values of CV flowstones display changes in vegetation density based on precipitation changes during the growth period of vegetation. The interpretation of $\delta^{18}$O values is more difficult (Budsky et al., 2019a; b) due to a combined influence of temperature, moisture source and rainfall amount (Lachniet, 2009; McDermott, 2004; Bar-Matthews et al., 2003). However, the generally good agreement between both the CV flowstone $\delta^{18}$O and $\delta^{13}$C values with Greenland ice core $\delta^{18}$O values (NGRIP, North Greenland Ice Core Project members, 2004) shows the link of the CV climate records with Northern Hemisphere temperature changes.

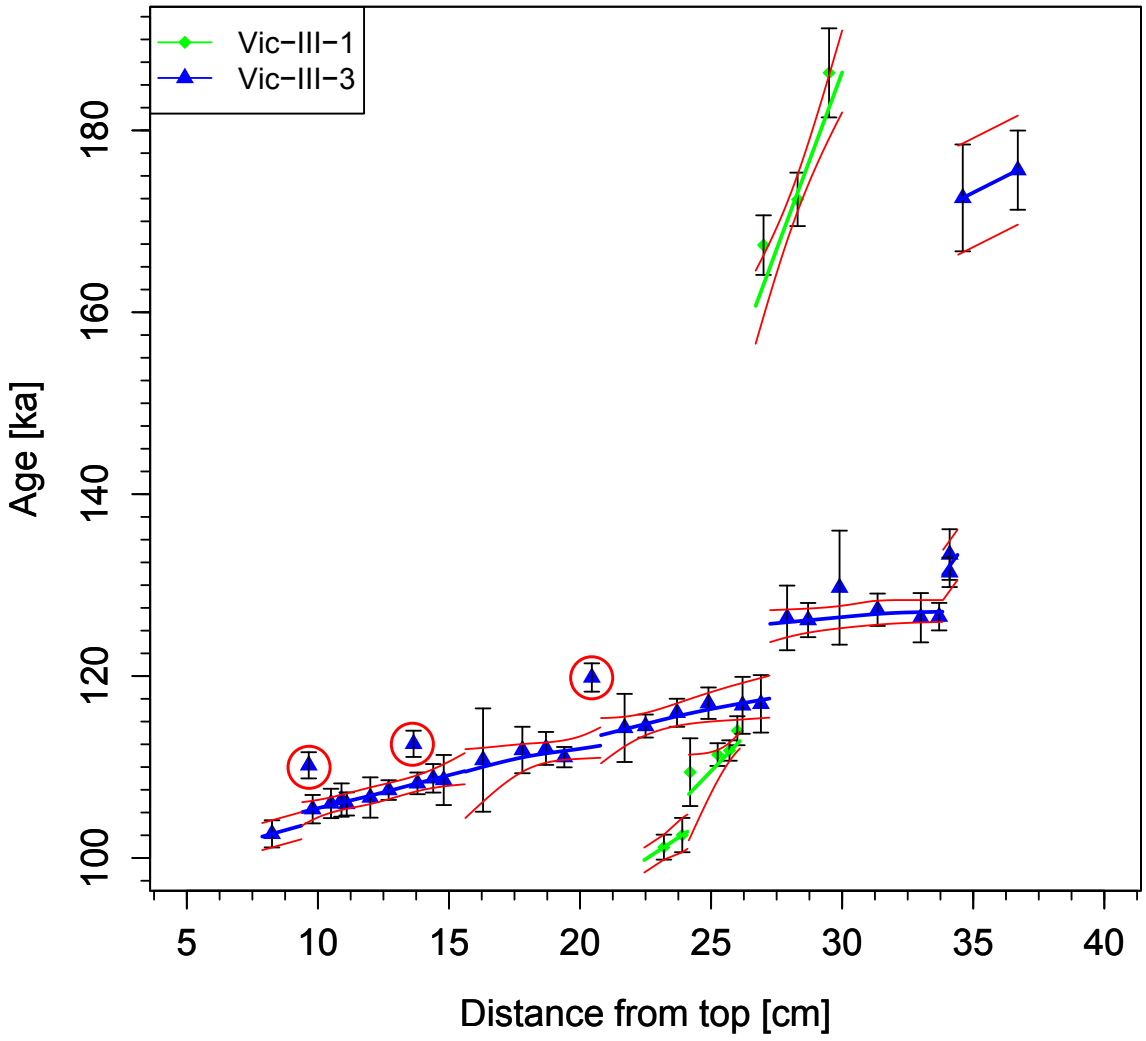


Figure 6.2: $^{230}$Th/U-ages and age models of Vic-III-1 (green) and Vic-III-3 (blue) calculated for the individual growth phases using the StalAge algorithm (Scholz and Hoffmann, 2011). The circled ages were not used for the age model calculation.

### 6.4.1 MIS 6.5

Although MIS 6 is a glacial phase, it was characterised by a maximum in northern summer insolation (Berger, 1978), a sea level highstand of ca. -50 m (Scholz et al., 2007) and unusually wet climate conditions in the entire Mediterranean region (Toucanne et al., 2015), which is also supported by the deposition of sapropel S6 (Emeis et al., 2003; Gallego-Torres et al., 2010) and low $\delta^{18}$O values recorded in Soreq Cave speleothems (Ayalon et al., 2002). The exceptionally humid conditions of MIS 6.5 are also reflected in a speleothem record from the coastal Argentarola cave (central Italy, Bard et al., 2002a; b). Elevated arboreal pollen amounts in terrestrial pollen records from central Italy (Valle di Castiglione, Follieri et al., 1989), southern France (Velay stack, Cheddadi et al., 2005) and north-western Greece (Ioannina, Tzedakis, 1993) indicate humid climate conditions. These are are less pronounced compared to full interglacials in northern Greece (Tenaghi Phillipon, Tzedakis et al., 2006) and southern Spain (Padul, Camuera et al., 2019). SSTs at the Iberian Margin (Martrat et al., 2007) and the Alboran Sea (Martrat et al., 2004) were similar to MIS 3 ($\approx$15 °C). In contrast, SSTs in the Gulf of Lions (north Western Mediterranean) were similar to interglacial conditions (Cortina et al., 2016). High river runoff is also reflected by very low $\delta^{18}$O values of planktonic foraminifera in the northern part of the Western Mediterranean (Corse, Toucanne et al., 2015).

Despite of the low temporal resolution of our records and the relatively large uncertainties of the speleothem age models (only two ages for Vic-III-3, Figures 6.2 and 6.3), the $\delta^{18}$O values are in good agreement with the $\delta^{18}$O values of the speleothem from Argentarola Cave (Bard et al., 2002b) and show multiple humid phases (multiple negative peaks in $\delta^{18}$O values), which are common for sapropel deposition (Ayalon et al., 2002). This is interesting because both locations show large differences in annual precipitation amount and in modern $\delta^{18}$O values of both seawater (LeGrande and Schmidt, 2006) and precipitation (Bard et al., 2002b; Bowen and Wilkinson, 2002; Budsky et al., 2019a). This may indicate similar $\delta^{18}$O configurations of sea water or and precipitation at both locations. In addition, we can investigate speleothem $\delta^{13}$C values, they reflect the type of vegetation (Cerling et al., 1993), microbiological activity in the soil (Genty et al., 2003) and can be indicative for precipitation (Ridley et al., 2015) influencing the vegetation density (Budsky et al., 2019a; Budsky et al., 2019b). Values of about -11 ‰ (Figure 6.3b) suggest a well-developed, dense vegetation similar to interglacial conditions. This is not completely supported by the Padul pollen record (Camuera et al., 2019), but several speleothems show prominent negative $\delta^{13}$C excursions during MIS 6.5 (Gitana Cave, S Spain, Hodge et al., 2008, Villar Cave, SW France, Wainer et al., 2011; Wainer et al., 2013). In addition, the pollen record of southern France (Velay) suggest an increase in annual precipitation (Cheddadi et al., 2005) and support humid conditions in the Western Mediterranean. In contrast to the $\delta^{18}$O values, the $\delta^{13}$C values show no gradually increasing trend, which would be indicative of decreasing vegetation density. Either precipitation remained relatively high despite of the cooling climate, or vegetation feedbacks retained favourable conditions for soil and plant development as suggested for sapropel 1 (S1, Krinner et al., 2012). Evidence for similar multiple phases of humid conditions

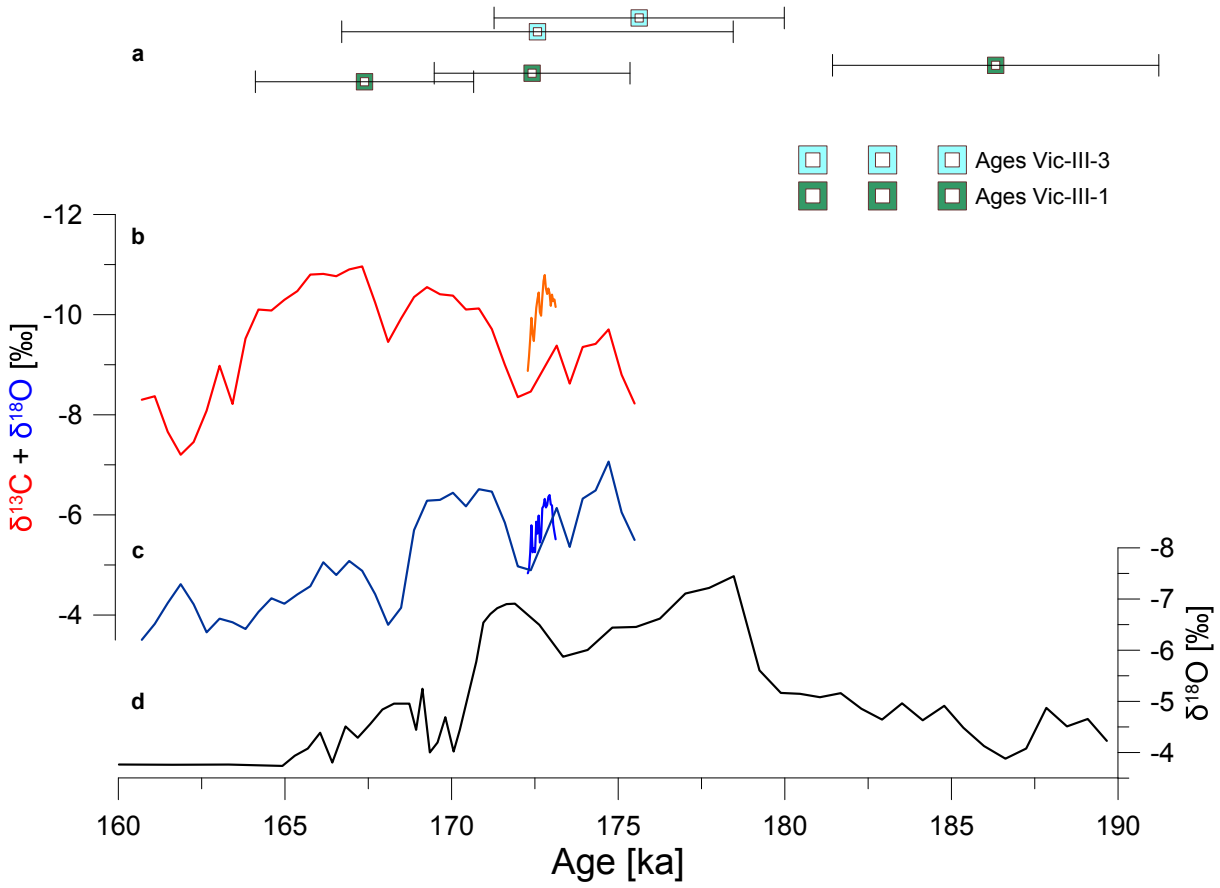


Figure 6.3: $\delta^{13}$C (b) and $\delta^{18}$O (c) values of the two CV flowstone records (Vic-III-1 and Vic-III-3) with the corresponding ages shown on top (a). Also shown are the $\delta^{18}$O values (d) of a stalagmite from Argentarola Cave, Italy (Bard et al., 2002b), showing similar $\delta^{18}$O values during MIS 6.5.

were recorded in pollen records from central Italy (Valle di Castiglione, Follieri et al., 1989) and southern Spain (Padul, Camuera et al., 2019). This is in agreement with the CV record indicating a humid phase. Similarly, as during the Holocene or the Last Interglacial, the African summer monsoon was increased and in its northernmost position (Dupont and Hooghiemstra, 1989) during MIS 6.5 (Tisserand et al., 2009). This is also in agreement with an intensified Asian monsoon in MIS 6.5 (Wang et al., 2008), although the global climate was different from real interglacial conditions as highlighted by reduced sea level (Grant et al., 2014) and SSTs (Emeis et al., 2003; Martrat et al., 2007). Climate was probably comparable to MIS 3 (Wainer et al., 2013) or to the deposition of sapropels 3 and 4 (Bard et al., 2002b). As a result, we would expect a strong seasonality for the times of sapropel deposition with a strong northernmost African monsoon in summer and southward shifted westerlies during winter time (Toucanne et al., 2015). However, potential spring/summer drought as observed during the Holocene by Budsky et al. (2019a) might be reduced, as indicated by the very negative speleothem $\delta^{13}$C values recorded at CV, which are similar to those during DO events (Budsky et al., 2019b). This

suggests SST-driven precipitation changes (Budsky et al., 2019b; Denniston et al., 2018) and is also in agreement with the Villars Cave record suggesting humid and/or warm DO events during MIS 6 (Wainer et al., 2013). Distinctly lower speleothem $\delta^{18}O$ values for CV and Argentarola Cave compared to the Atlantic sites (Villars Cave, SW France, Wainer et al., 2013, and Lebre Cave, Portugal, Denniston et al., 2018) might result from a combination of the amount effect (Bard et al., 2002b) in the Western Mediterranean and more negative $\delta^{18}O$ values of the seawater in the basin due to higher runoff (Toucanne et al., 2015) and potential meltwater (Emeis et al., 2003).

### 6.4.2 The Last Interglacial, MIS 5e

The last interglacial can be divided into five substages (a to e) with alternating warm and cold phases and high and low sea-level, respectively (Grant et al., 2014; Siddall et al., 2003). The timing of the onset of MIS 5 is still under debate and seems to vary by about a few thousand years between different locations and archives (Govin et al., 2015). From Mediterranean speleothems, the onset of MIS 5 occurred at $\approx$ 129 ka (Drysdale et al., 2005; Drysdale et al., 2009) and was preceded by a postglacial warming, similar to the Bølling/Allerød for the Holocene (Moseley et al., 2015) and a distinct increase in precipitation at ca. 132 ka (Tana che Urla Cave, north Italy, Regattieri et al., 2016). An early warming is also recorded in marine sediment cores (Martrat et al., 2007; Martrat et al., 2014) with low $\delta^{18}O$ values of both benthic (Skinner and Shackleton, 2006) and planktonic foraminifera (Mokeddem et al., 2014) in the North Atlantic prior to Heinrich event 11. In contrast, such a precursor warming is not present in speleothem records from China representing the Asian monsoon (Cheng et al., 2009; Wang et al., 2008). The first growth phase of Vic-III-3 above the hiatus at 34.2 cm dft (133.4 $\pm$ 2.8 ka and 131.4 $\pm$ 1.6 ka at 34.1 cm dft) indicates an early onset of the LIG for the Western Mediterranean. The precursor warming might be recorded in flowstone Vic-III-3 subsequent to H11.2 (Figures 6.4 and 6.5). Even if the corresponding growth period is short and not well constrained, it is contemporaneous with the increase in precipitation reflected by decreasing speleothem $\delta^{18}O$ values in speleothems from Tana che Urla Cave (Regattieri et al., 2016, Figure 6.4d) and Portugal (Denniston et al., 2018). A subsequent growth interruption seems to be related to the third phase of the dry and cold Heinrich event 11.3 (Drysdale et al., 2009; Tzedakis et al., 2018). This is supported by the results of Budsky et al. (2019b), who found dry climate conditions in the Western Mediterranean during cold Heinrich events.

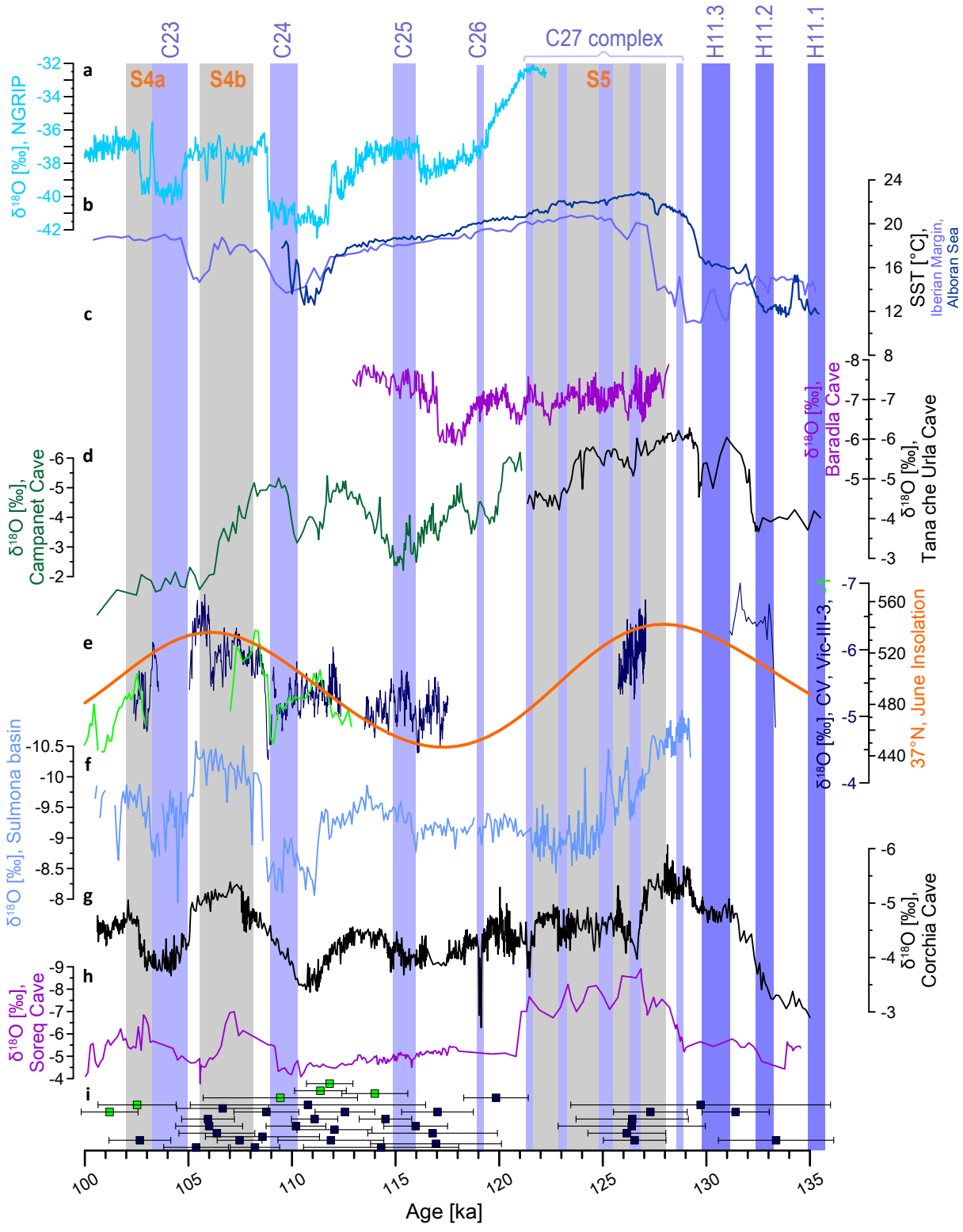


Figure 6.4: Continued.

▲ Figure 6.4 (continued): CV speleothem $\delta^{18}$O values and corresponding ages (i). Also shown are 37° N June insolation (e, Laskar et al., 2004) and the $\delta^{18}$O values of NRGIP (a) indicating Northern Hemisphere temperature changes (North Greenland Ice Core Project members, 2004) with a chronology suggested by (Rossi et al., 2014) based on the Corchia Cave speleothem record (Drysdale et al., 2007). In addition, we compare with SST records (b) from the Iberian Margin (Martrat et al., 2007) and Alboran Sea (Martrat et al., 2014) and speleothem records Bradla Cave (c, Demény et al., 2017), Campanet Cave (Dumitru et al., 2018) and Tana che Urla Cave (Regattieri et al., 2014, both d), Soreq Cave (h, Bar-Matthews et al., 2003; Grant et al., 2012), Corchia Cave (g, Drysdale et al., 2007; Tzedakis et al., 2018) and $\delta^{18}$O values of carbonate sediments from Sulmona basin (f, Regattieri et al., 2015; Regattieri et al., 2017). Grey bars indicate the deposition of sapropels in the Eastern Mediterranean (Grant et al., 2016) and blue bars represent dry cold events (timing: C23 + C24: Regattieri et al., 2017, C25 – C27 and H11.1 – H11.3 defined by Corchia Cave stack Tzedakis et al., 2018 and North Atlantic marine record Mokeddem et al., 2014).

Contemporaneously with the highest relative sea-level (RSL, Grant et al., 2014) and peak SSTs in the Alboran Sea at ca. 126 ± 1.5 ka (Martrat et al., 2004; Martrat et al., 2014, Figures 6.4 and 6.5) and the North Atlantic (Galaasen et al., 2014; Irvalıet al., 2016), CV flowstone Vic-III-3 restarted to growth with high growth rates of up to 80 µm/a (127.2 ± 1.3 ka to 125.6 ± 1.8 ka, Figure 6.3). Highest SSTs in the North Atlantic indicate a reduced temperature gradient between the tropics and the polar zones. A reduced temperature gradient and a strong Atlantic Meridional Overturning Circulation (AMOC, Böhm et al., 2015) weakens the westerlies and shifts the ITCZ further north leading to higher annual precipitation in the Mediterranean, which is in good agreement with the highest river input close to Corsica (Toucanne et al., 2015), an African Humid Period (Ehrmann et al., 2017) and the formation of sapropel S5 in the Eastern Mediterranean (Grant et al., 2016; Rossignol-Strick and Paterne, 1999). The $\delta^{18}$O values continuously increase (+0.67 ‰/1ka) during this short growth period (small peak ($\delta^{18}$O ≈-5.25 ‰) at 126.6 ka) following the insolation curve (Figure 6.4e, Laskar et al., 2004) and the decreasing SSTs (Martrat et al., 2014), which is in agreement with the $\delta^{18}$O values of a speleothem record from SW France (Bourgeois–Delaunay Cave, Couchoud et al., 2009) and a carbonate sediment record from central Italy (Sulmona Basin, Figure 6.4f, Regattieri et al., 2017). Due to the short growth phase in the CV speleothems, the strong shift to higher $\delta^{18}$O values at 125.5 ka of the speleothem stack from northern Italy (Corchia Cave, Figure 6.4g, Tzedakis et al., 2018), which is related to the central cold event of the C27 complex in the North Atlantic (Irvalıet al., 2012) is not visible in the CV speleothem record. Although almost no trend, but higher variability is observed further east in Hungary (Figure 6.4c, Baradla Cave), $\delta$D values of speleothem fluid inclusions record cold and wet winters between 127 and 126 ka (Demény et al., 2017). In the eastern Mediterranean, the

lowest $\delta^{18}$O values of the Soreq Cave record (Figure 6.4h and 6.6i, Grant et al., 2012) indicate high rainfall during the time of sapropel (S5) deposition (Grant et al., 2016; Rohling et al., 2015) supported by a high stand of Lake Lisan in the Levant (Torfstein et al., 2015). Stable carbon isotope values ($\delta^{13}$C) display a strong double peak during this short growth phase with overall slightly increasing values (Figure 5e). This double peak is also recorded in a speleothem from central Italy (Tana che Urla Cave, Regattieri et al., 2016, Figure 6.5h) and at the Sulmona Basin (Regattieri et al., 2017, Figure 6.5f) and a single peak plateau in western France (Couchoud et al., 2009). Corchia Cave, in contrast, shows the highest $\delta^{13}$C values during this phase indicating rather dry climate conditions, which has been related to several cold and arid events of the C27 complex (Drysdale et al., 2005; Tzedakis et al., 2018). Within dating uncertainties, the CV $\delta^{13}$C values also agree with the $\delta^{13}$C values of the Baradla Cave stalagmite indicating fully interglacial conditions (Hungary, Demény et al., 2017, Figure 6.5d). More negative $\delta^{13}$C values of stalagmites typically reflect a higher microbial activity in the soil combined with dense vegetation due to enhanced precipitation (Genty et al., 2003). These records are all in good agreement with marine pollen records from the Iberian Margin, which show peak Mediterranean forest and Atlantic forest conditions further north in the Gulf of Biscay (Sánchez Goñi et al., 2008) during this phase. In contrast, pollen in lake records from southern Italy, Albania and Greece show a stepwise increase of tree pollen and a plateau at 128 – 126 ka (Brauer et al., 2007; Milner et al., 2016; Roucoux et al., 2008; Sinopoli et al., 2018), which is lower than under full interglacial climate conditions (125 – 115 ka).

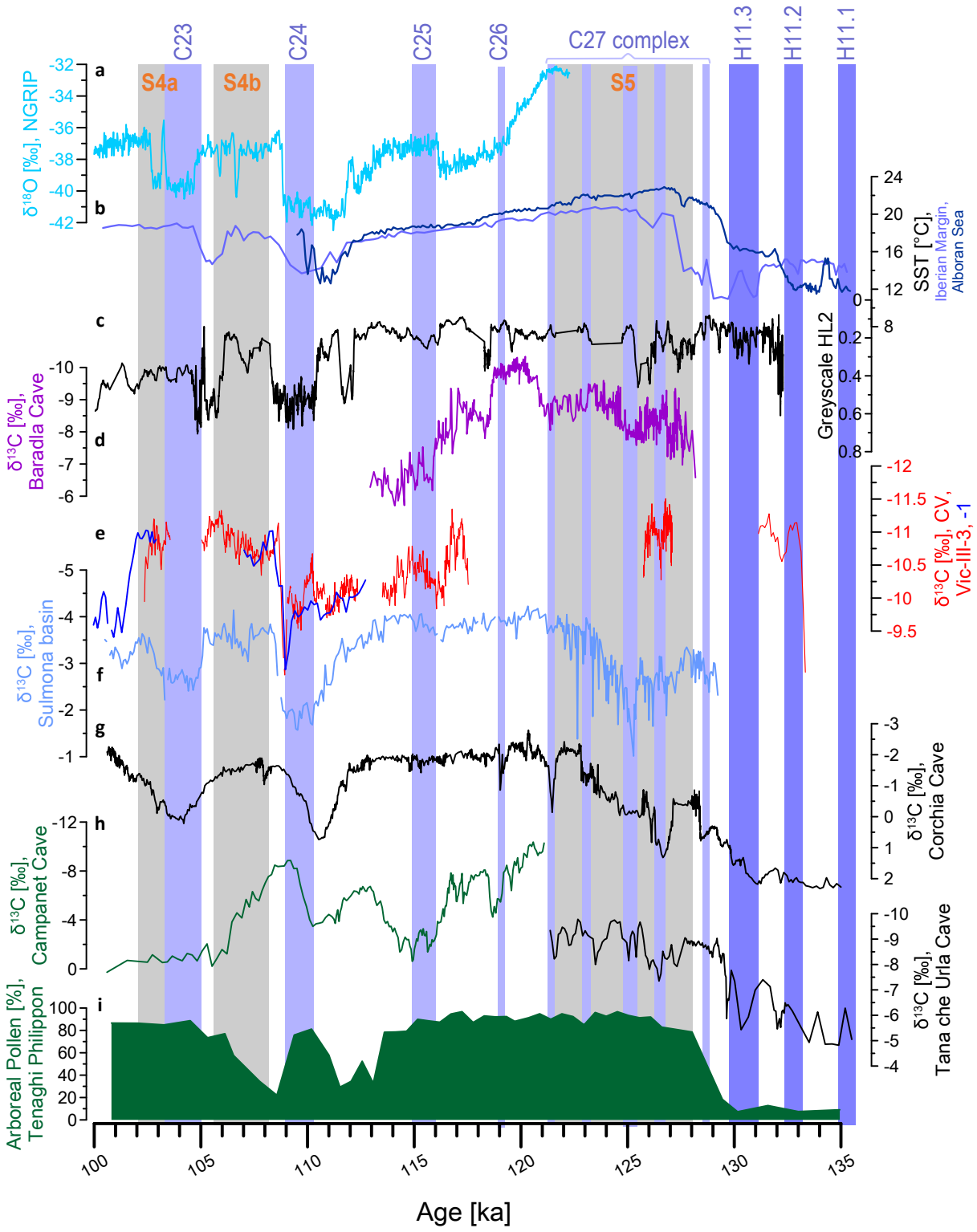


Figure 6.5: Continued.

▲ Figure 6.5 (continued): CV speleothem $\delta^{13}$C values (e) with $\delta^{18}$O values of NRGIP (a) indicating Northern Hemisphere temperature changes (North Greenland Ice Core Project members, 2004) with a chronology suggested by (Rossi et al., 2014) based on the Corchia Cave speleothem record (Drysdale et al., 2007). Local temperatures are reflected by SST records (b) from the Iberian Margin (Martrat et al., 2007) and the Alboran Sea (Martrat et al., 2014). Also shown are the speleothem $\delta^{13}$C records from Bradla Cave (d, Demény et al., 2017), Campanet Cave (Dumitru et al., 2018) and Tana che Urla Cave (Regattieri et al., 2014, both h), and Corchia Cave (g, Drysdale et al., 2007; Tzedakis et al., 2018) as well as the $\delta^{13}$C values of carbonate sediments from the Sulmona basin (f, Regattieri et al., 2015; Regattieri et al., 2017) indicating increased soil microbiological activity and vegetation density by lower $\delta^{13}$C values and vice versa. In addition, we show the HL2 greyscale record from western Germany (c, Sirocko et al., 2005) and the arboreal pollen percentage from Greece (i, Tzedakis et al., 2006). Vertical bars equivalent to Figure 6.4.

---

The cessation of the second short MIS 5e speleothem growth phase at 127.2 ± 1.3 ka is synchronous to the central C27 cold event at ≈ 125 ka in the North Atlantic (Figures 6.4e and 6.5e, Irvalıet al., 2012) that is also visible in the central Mediterranean (Incarbona et al., 2011) and interpreted as a freshwater outburst into the North Atlantic, similar to the "8.2 ka-event" (Alley and Agustsdottir, 2005; Galaasen et al., 2014; Nicholl et al., 2012). While earlier studies considered the C27 event as one single event, more recent high temporal resolution records (Mokeddem et al., 2014; Tzedakis et al., 2018) enable to distinguish between several cold events, summarized as the C27 complex (Figures 6.4 and 6.5), with different regional repercussions, such as C27' at 125 ka (Tzedakis et al., 2018), which is visible at the Iberian Margin (Martrat et al., 2014) and distinct at the Sulmaona Basin (Regattieri et al., 2017, Figure 5f), but is absent in the Eastern Mediterranean (Soreq Cave, Bar-Matthews et al., 2003). This regional event may be related to the cessation of CV speleothem growth at 125 ka (Figures 6.4e and 6.5e). The multiple cold events of C27 led to SST reductions with different extent over the North Atlantic Ocean (Irvalıet al., 2016) and changes in the circulation of the subpolar gyre (Irvalıet al., 2016; Mokeddem et al., 2014). A corresponding reduction in vegetation was recorded in the $\delta^{13}$C values of speleothems from the Western Mediterranean, which show a recovery after ≈ 1 ka (Couchoud et al., 2009; Drysdale et al., 2009; Regattieri et al., 2014), carbonate sediments (Regattieri et al., 2017) and pollen records (Brauer et al., 2007). The decrease in vegetation density is also recorded in the percentage of tree pollen in Padul lake during the progressive decrease in lake level to MIS 5c (Camuera et al., 2019). This could indicate persistently dry climate conditions in southern Iberia related to multiple phases of the C27 complex and a negative precipitation-evaporation balance due to high temperatures within fully interglacial conditions (Kutzbach et al., 2014). A potential breakdown of vegetation is also reflected by a prominent cooling at 125 ka in the Sulmona basin

by the highest carbonate $\delta^{13}$C values (Figure 6.5f, Regattieri et al., 2017). Modern annual rainfall is three times higher in the Sulmona Basin (Regattieri et al., 2015) than in south-eastern Spain (Budsky et al., 2019a). This may explain why speleothem growth did not restart subsequent to the central C27 event ($\approx$ 125 ka).

### 6.4.3 MIS 5d-c

Subsequent to the end of MIS 5e, a prominent cooling initiated the Weichselian glaciation. Although the timing of the onset and the impact of the cooling is regionally different, the CV speleothem restarts to grow at 117.5 $\pm$ 2 ka within the uncertainties of the age model subsequent to the cooling of C27b in Irvalıet al. (2016) and an unnamed aridity event in the Corchia Cave stack (Tzedakis et al., 2018). This is in temporal agreement with the onset of stalagmite growth in northern Italy (Vanghi et al., 2018) and north-eastern Spain (Pérez-Mejías et al., 2019). A prominent cooling is neither recorded in the SST reconstructions from the Iberian Margin nor the Alboran Sea (Cacho et al., 1999; Martrat et al., 2014), but is remarkable with a drop of several degrees at higher latitudes in the North Atlantic (Mokeddem et al., 2014; Oppo et al., 2006). An impact on lower latitude terrestrial climate is observed in several records from central and eastern Europe as a cold and particularly dry period at approximately 118 ka (Late Eemian Aridity Pulse, LEAP, Sirocko et al., 2005; Vansteenberge et al., 2019; arid pulse, Demény et al., 2017). At the same time, a strong shift towards more negative $\delta^{18}$O values in speleothems from the Alps (Meyer et al., 2008; Moseley et al., 2015) and the Mediterranean (Grant et al., 2012; Rossi et al., 2014; Tzedakis et al., 2018) indicates major changes in atmospheric circulation. In the following, climate shifted from the interglacial mode to the ice-sheet and AMOC dominated state with millennial scale DO variability as observed during MIS 3 (Bagniewski et al., 2017; Menviel et al., 2014). As already elaborated by Budsky et al. (2019b), CV speleothems record warm and humid DO events in MIS 3 to 5b. This climate interpretation of DO patterns subsequent to the last interglacial seems to be valid also for MIS 5d to c and is in good agreement with climate records from Italy (Sulmona basin, Regattieri et al., 2017; Corchia Cave, Drysdale et al., 2007), Portuguese speleothems (Denniston et al., 2018), NGRIP (North Greenland Ice Core Project members, 2004) as well as pollen records from Italy (Allen and Huntley, 2009; Follieri et al., 1989) and Spain (Camuera et al., 2019). In detail, after the LEAP, the CV flowstone restarts to grow at 117.5 $\pm$ 2ka, followed by a short interruption between 112.35 and 113.5 ka potentially corresponding to a strong reduction in SST in the polar North Atlantic, which may coincide with multiple cold events (Irvalıet al., 2016) at the end of DO 25 (111 – 113 ka). Although CV speleothem $\delta^{18}$O values are generally difficult to interpret, on the orbital to millennial scale, more negative values correspond to warmer and wetter climate (Budsky et al., 2019a; b). In this context, the onset of DO 25 (116 ka) in NGRIP (North Greenland Ice Core Project members, 2004) on the timescale (Rossi et al., 2014) based on Corchia Cave speleothems (Drysdale et al., 2007) can be recognized (Figures 6.4a and 6.5a). Speleothem records from the Alps display an increase in temperature (decreasing $\delta^{18}$O values) during DO 25 (Boch et al., 2011; Moseley

et al., 2015). Western Mediterranean speleothem and sediment records also clearly reflect the onset of DO 25 by decreasing $\delta^{18}$O values (Corchia Cave, Drysdale et al., 2007; Tzedakis et al., 2018, Sulmona basin, Regattieri et al., 2017) indicating increased precipitation. This is also in agreement with a speleothem record from the Balearic Islands indicating progressively increasing precipitation over the DO event (Dumitru et al., 2018) as well as increasing tree pollen taxa in Italy (Lake Monticchio, Brauer et al., 2007) and northern Greece (Tenaghi Philippon, Milner et al., 2016). However, the impact of DO 25 seems to be restricted to the region surrounding the North Atlantic. More distant regions, such as the eastern Mediterranean (Soreq Cave, Grant et al., 2012) and the Middle East (Qal'e Kord, Mehterian et al., 2017), show a less prominent DO 25. In addition, a weak Asian monsoon during DO 25 associated with low insolation has been suggested by speleothem records from China (Kelly et al., 2006; Wang et al., 2008). Rossi et al. (2014) suggest drier conditions for central Spain during the second phase of the magnetic Blake excursion ($\approx$ 113 ka, Osete et al., 2012). Within uncertainty, this is in agreement with a short growth interruption in the CV speleothem record between 112.35 and 113.5 ka and coincides with a short cold event in the North Atlantic (Irvalıet al., 2016) as well as a short vegetation decline in Europe (Sirocko et al., 2005, Figure 6.5c). However, a continuous trend with increasing $\delta^{13}$C values (Rossi et al., 2014) is not observed in the CV record. This implies a rather constant vegetation cover. Remarkably, the CV flowstones also grew during the much more prominent C24 ($\approx$ 111 – 109 ka) and do not show a significant increase in $\delta^{18}$O and $\delta^{13}$C values indicating favorable conditions for speleothem growth and thus a relatively high vegetation density. This is in contrast to a pollen record from Italy indicating a drop of 50 % in tree pollen during C24 at 109 ka (Brauer et al., 2007). In the Corchia Cave speleothem record (Drysdale et al., 2007) and in sedimentary carbonates from Italy (Regattieri et al., 2015), C24 is also more pronounced. Surprisingly, the CV $\delta^{13}$C values indicate a short humid phase at the onset of the stadial, which might reflect an early phase of Heinrich events with humid and cold conditions during the last glacial, as assumed by (Naughton et al., 2009). However, more recent studies from the Mediterranean (Sardinia, (Columbu et al., 2017), northern Italy (Frasassi Cave, Vanghi et al., 2018) and north-eastern Spain (Ejulve cave, Pérez-Mejías et al., 2019) also indicate the DO pattern, with less humid and cold climate conditions during C24. The onset of the subsequent DO24 ($\approx$ 108.5 ka) is documented by decreasing stable isotope values indicating an increase in precipitation and vegetation density (Budsky et al., 2019b; Denniston et al., 2018; Genty et al., 2010) and coincides with the deposition of sapropel S4b during the phase of highest summer insolation (Figures 6.4 and 6.5). Increased SSTs at the Iberian Margin ($\approx$ 19 °C, Martrat et al., 2007) and in the Western Mediterranean (Gulf of Lions, $\approx$ 14 °C, Cortina et al., 2016) suggest enhanced moisture availability, which promoted increased precipitation over the Western Mediterranean basin. This is coherent to other paleoclimate archives (Figures 6.4 and 6.5) from Iberia (Camuera et al., 2019; Pérez-Mejías et al., 2019; Stoll et al., 2015) and Italy (Allen and Huntley, 2009; Drysdale et al., 2007; Regattieri et al., 2015) indicating a humid phase during sapropel deposition. Between DO 24 and DO 23, a prominent cold incursion (C23 $\approx$ 104 ka, Figures 6.4 and 6.5) caused a pause of the African monsoon and interrupted the sapropel deposition (Grant

et al., 2016). The incursion ends with a precursor warming prior to DO 23, which is visible in the CV speleothem $\delta^{18}O$ values (Figure 6.4e). This indicates that changes in the North Atlantic were immediately transferred to atmospheric circulation, resulting in increased precipitation in south-eastern Spain in turn reactivating speleothem growth during warming events. This coincides with a previous study of CV speleothems showing a strong relationship between DO variability and Atlantic SST during MIS 5b to 3 (Budsky et al. 2019b).

### 6.4.4 Interpretation of past climate variability in south-eastern Spain on the orbital timescale

A combination of all CV speleothem records (this study, Budsky et al., 2019a; b) suggests differences between orbital and millennial climate variability in south-eastern Spain. Speleothem growth mainly occurred during interglacials and terminated during full glacial conditions (MIS 2 and 6, Budsky et al., 2015). This pattern is superimposed by increased precipitation in south-eastern Spain during insolation maxima and periods of high SST (Figure 6.6). Increased precipitation and vegetation density are in agreement with other speleothem records from Portugal (Denniston et al., 2018), Italy (Tzedakis et al., 2018) and Israel (Bar-Matthews et al., 2003) and expressed by more negative speleothem $\delta^{18}O$ and $\delta^{13}C$ values. Pollen records from southern Spain (Camuera et al., 2019), southern Italy (Allen et al., 1999) and Greece (Tzedakis et al., 2006) support the orbital variability reflected by high pollen amount within humid interglacials and sparse vegetation cover during dry glacials. According to the variation of solar insolation, the strength of the African (Tierney et al., 2017; Tjallingii et al., 2008; Toucanne et al., 2015) and Asian (Cheng et al., 2016; Wang et al., 2005; Wang et al., 2008) monsoons intensified with high boreal summer insolation, and the ITCZ was dislocated further north. In detail, for the LIG, pronounced seasonality during phases of high precession with a negative precipitation minus evaporation balance has been calculated for large parts of the Mediterranean (Kutzbach et al., 2014). The high summer insolation in combination with low winter insolation shifts the westerlies further south during winter and the African summer monsoon further north in summer (Toucanne et al., 2015). It also intensifies the East Asian monsoon as reflected by low speleothem $\delta^{18}O$ values in China (Wang et al., 2008). However, even though increased seasonality shifts the westerlies further south in winter, a positive precipitation minus evaporation balance is particularly required during spring for vegetation development. For CV, this was limited during the Holocene climate optimum (Budsky et al., 2019a). Surprisingly, CV speleothems did not grow during large parts of the LIG (MIS 5e). The most straightforward reason for this observation is owed to the behaviour of flowstone deposition itself when thin water films using different pathways during descend on the sinter deposits. Subsequent growth interruptions may have occurred due to the generally slow growth rates of flowstones. Another option would be continuous cave flooding, which would also inhibit speleothem growth. However, this seems to be unlikely for about 9 ka. Similarly, high cave $pCO_2$ suppressing speleothem growth (Banner et al., 2007; Meyer et al., 2014) is not reasonable for the Holocene Climate Optimum. Budsky

et al. (2019a) already pointed out the limitation of precipitation during the vegetation period (spring and summer) during peak insolation for the Holocene and the subsequent decrease in vegetation density, which was a result of strong seasonality during the sapropel deposition. Since LIG global (CAPE-Last Interglacial Project Members, 2006; Pedersen et al., 2017) and regional (Merz et al., 2016) temperatures exceeded the Holocene maximum by about 1 to 2°C, spring and summer drought might be even prolonged and increased. Suggesting enhanced seasonality and warmer temperatures in MIS 5e, this might induce a crossing of a certain threshold of annual precipitation required for the development of vegetation in southern Spain ($\approx$200 mm/a). Such a reduction in vegetation and increased drought stress may also have been occurred for parts of MIS 5e as indicated by a certain amount of sclerophyllous pollen (Camuera et al., 2019; Milner et al., 2012) introduced by several arid phases (Tzedakis et al., 2018) in between the cold IRD events in the North Atlantic during the C27 complex (Figure 6.4 and 6.5). The short growth period during MIS 5e seems to be related to a short time with reduced summer aridity and a pause of the African monsoon (Toucanne et al., 2015).

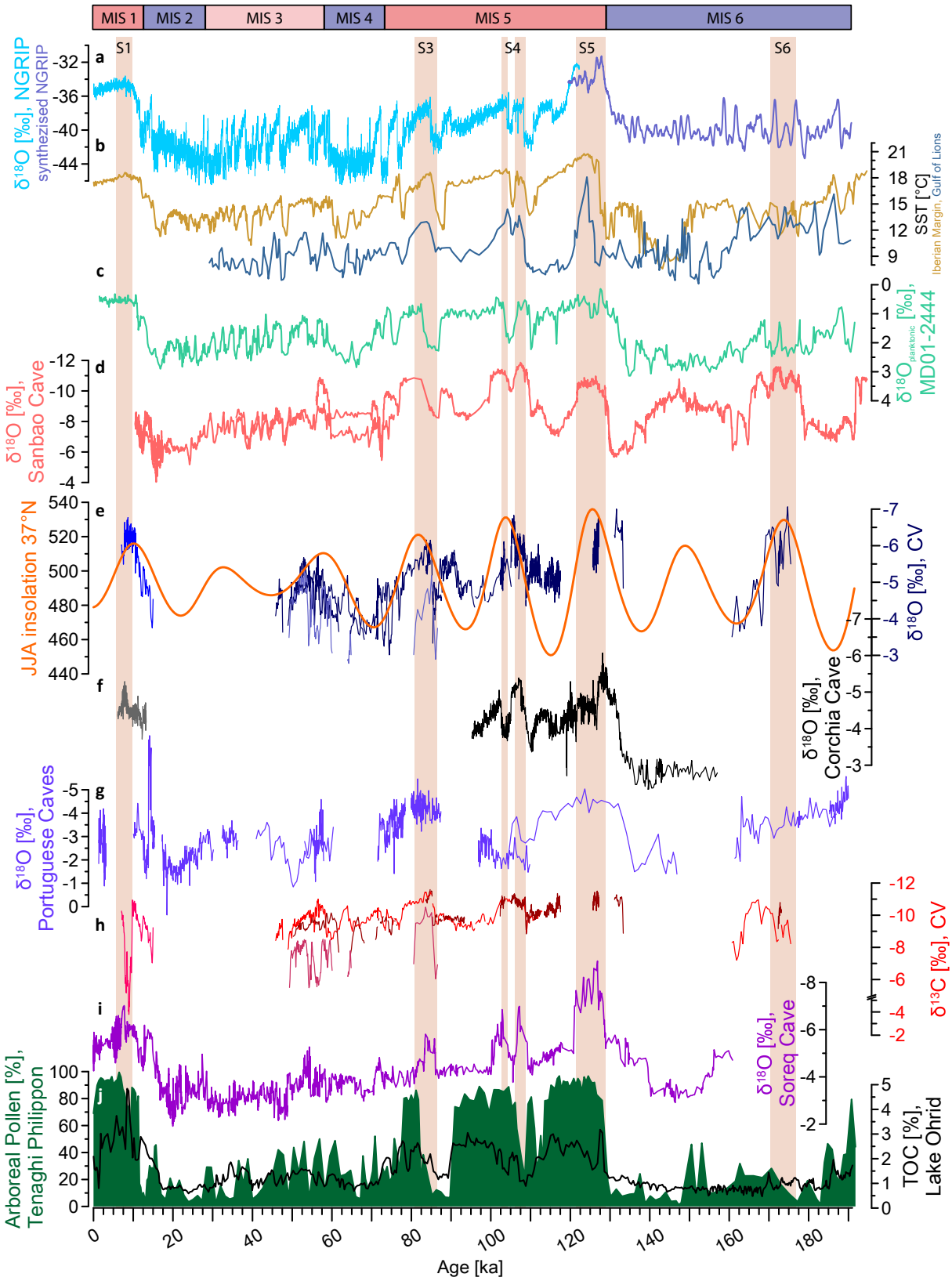


Figure 6.6: Continued.

▲ Figure 6.6 (continued): CV speleothem $\delta^{18}$O (e) and $\delta^{13}$C (h) values on orbital time scale including previous studies (Budsky et al., 2019a; b). (a) NGRIP record (Obrochta et al., 2014) and synthetic NGRIP (Barker et al., 2011). (b) SST from Iberian Margin (Martrat et al., 2007) and Gulf of Lions (Cortina et al., 2016) indicates a potential for moisture uptake and the source is displayed as $\delta^{18}$O values of planktonic foraminifera (*Globigerina bulloides*) from the Iberian Margin (c, Hodell et al., 2013; Vautravers and Shackleton, 2006). Sanbao Cave speleothem $\delta^{18}$O values indicate the strength of the East Asian monsoon (d, Wang et al., 2001; Wang et al., 2008) prevalent influenced by summer insolation (e, Laskar et al., 2004). (f) Corchia Cave $\delta^{18}$O record (Drysdale et al., 2007; Drysdale et al., 2009; Tzedakis et al., 2018; Zanchetta et al., 2007) show hydrological changes in the northern Western Mediterranean and Soreq Cave record (i, Bar-Matthews et al., 2003; Grant et al., 2012) for the Eastern Mediterranean. (g) Portuguese Caves (Figure 6.1, Denniston et al., 2018) indicate humid phases on Western Iberian Peninsula, which depends on SST of the Iberian Margin. (j) Pollen record from Tenaghi Philippon (Tzedakis et al., 2006) and total organic carbon (TOC) from Lake Ohrid (Wagner et al., 2019). The vertical red bars denote the sapropel formation in the Eastern Mediterranean (Bard et al., 2002b; Grant et al., 2016).

Even speleothems from North Spain do not cover part of this time interval ($\approx$ 126 – 122 ka, Stoll et al., 2015), and speleothem growth in Portugal is also reduced (Figure 6.6g, Denniston et al., 2018). Figure 6.6 displays preferred speleothem growth in south-eastern Spain with the formation of the sapropel, which indicates high seasonality. Sapropel formation within glacial conditions enhances net annual precipitation significantly, which cannot be significantly diminished by potentially extended summer aridity due to less evaporation by lower temperature (Figure 6.6, S3, S4 and S6). In contrast, interglacial sapropel deposition during warm climate conditions, with high evaporation rates was strongly influenced by climate instability in the North Atlantic, such as cold IRD events enhancing the even strong seasonality during MIS 5e (Irvalıet al., 2016; Mokeddem et al., 2014) or Bond events within the Holocene (Alley and Agustsdottir, 2005; Bond et al., 2001; Denton et al., 2005). We can point out that vegetation in south-eastern Spain, close to the required today's annual net precipitation, is highly sensitive within interglacial and glacial conditions, whereas warm interglacial conditions are in general more favourable for vegetation as recorded by pollen records (Allen et al., 1999; Allen and Huntley, 2009; Camuera et al., 2019; Tzedakis et al., 2006; Wagner et al., 2019).

## 6.5 Conclusions

CV speleothems and their $\delta^{18}O$ and $\delta^{13}C$ values provide new insights into past climate variability on millennial and orbital scale for the last 190 ka. We conclude the following major points from the new speleothem records:

1. During full glacial phases, such as MIS 2 and 6, speleothem growth was absent at CV. Speleothem growth conditions were more favourable during warm interglacials and interstadials.

2. On the millennial scale, $\delta^{18}O$ and $\delta^{13}C$ values mainly resemble the pattern of the NGRIP ice core, indicating more humid conditions during warm interstadials and slow growth rates or even hiatuses during stadials.

3. CV speleothem $\delta^{18}O$ values are in very good agreement with other terrestrial carbonate archives from Italy. This implies similarities in climate change on the millennial scale both during interglacials (MIS 5c and d) and glacials (MIS 6.5), despite of generally different annual amounts of present-day precipitation.

4. Even during interglacials, climate in south-eastern Spain was strongly influenced by changes in SST and North Atlantic freshwater outbursts, and CV speleothems record the resulting instabilities during the LIG as more arid conditions.

5. Besides millennial scale temperature variability, orbital parameters were the main drivers of regional seasonality and the length and intensity of summer drought in the Western Mediterranean. Although seasonality was pronounced during periods of high summer and low winter insolation, speleothem deposition during these periods was very common. This suggests that even during these phases, enough water for speleothem growth was available.

**Acknowledgments** [redacted]

## References

Agencia Estatal de Meteorología. 2011. Atlas climático ibérico: Temperatura del aire y precipitación (1971-2000) = Atlas climático ibérico temperatura do ar e precipitação (1971-2000) = Iberian climate atlas air temperature ... Instituto Nacional de Meteorología: Madrid.

Allen JRM, Brandt U, Brauer A, Huntley B, Keller J, Kraml M, Mackensen A, Mingram J, Negendank JFW, Nowaczyk NR, Oberhänsli H, Watts WA, Wulf S, Zolitschka B. 1999. Rapid environmental changes in southern Europe during the last glacial period. Nature 400 (6746): 740–743.

Allen JRM, Huntley B. 2009. Last Interglacial palaeovegetation, palaeoenvironments and chronology: A new record from Lago Grande di Monticchio, southern Italy. Quaternary Science Reviews 28 (15-16): 1521–1538. 10.1016/j.quascirev.2009.02.013.

Alley R, Agustsdottir A. 2005. The 8k event: cause and consequences of a major Holocene abrupt climate change. Quaternary Science Reviews 24 (10-11): 1123–1149. 10.1016/j.quascirev.2004.12.004.

Araguas-Araguas LJ, Diaz Teijeiro MF. 2005. Isotope composition of precipitation and water vapour in the Iberian Peninsula: First results of the Spanish Network of Isotopes in Precipitation. In Isotopic composition of precipitation in the Mediterranean Basin in relation to air circulation patterns and climate. Final report of a coordinated research project, 2000-2004. International Atomic Energy Agency: Vienna; 173–190.

Ayalon A, Bar-Matthews M, Kaufman A. 2002. Climatic conditions during marine oxygen isotope stage 6 in the eastern Mediterranean region from the isotopic composition of speleothems of Soreq Cave, Israel. Geol 30 (4): 303–306. 10.1130/0091-7613(2002)030<0303:CCDMOI>2.0.CO;2.

Bagniewski W, Meissner KJ, Menviel L. 2017. Exploring the oxygen isotope fingerprint of Dansgaard-Oeschger variability and Heinrich events. Quaternary Science Reviews 159: 1–14. 10.1016/j.quascirev.2017.01.007.

Banner JL, Guilfoyle A, James EW, Stern LA, Musgrove M. 2007. Seasonal Variations in Modern Speleothem Calcite Growth in Central Texas, U.S.A. SEPM JSR 77 (8): 615–622. 10.2110/jsr.2007.065.

Bard E, Antonioli F, Silenzi S. 2002a. Sea-level during the penultimate interglacial period based on a submerged stalagmite from Argentarola Cave (Italy). Earth and Planetary Science Letters 196 (3-4): 135–146. 10.1016/S0012-821X(01)00600-8.

Bard E, Delaygue G, Rostek F, Antonioli F, Silenzi S, Schrag DP. 2002b. Hydrological conditions over the western Mediterranean basin during the deposition of the cold Sapropel 6 (ca. 175 kyr BP). Earth and Planetary Science Letters 202 (2): 481–494. 10.1016/S0012-821X(02)00788-4.

Bardají T, Goy JL, Zazo C, Hillaire-Marcel C, Dabrio CJ, Cabero A, Ghaleb B, Silva PG, Lario J. 2009. Sea level and climate changes during OIS 5e in the Western Mediterranean. Geomorphology 104 (1-2): 22–37. 10.1016/j.geomorph.2008.05.027.Barker S, Knorr G, Edwards RL, Parrenin F, Putnam AE, Skinner LC, Wolff E, Ziegler M. 2011. 800,000 Years of Abrupt Climate Variability. Science 334 (6054): 347–351. 10.1126/science.1203580.

Bar-Matthews M, Ayalon A, Gilmour M, Matthews A, Hawkesworth CJ. 2003. Sea–land oxygen isotopic relationships from planktonic foraminifera and speleothems in the Eastern

Mediterranean region and their implication for paleorainfall during interglacial intervals. Geochimica et Cosmochimica Acta 67 (17): 3181–3199. 10.1016/S0016-7037(02)01031-1.

Berger AL. 1978. Long-term variations of caloric insolation resulting from the earth's orbital elements. Quaternary Research 9 (2): 139–167. 10.1016/0033-5894(78)90064-9.

Boch R, Cheng H, Spötl C, Edwards RL, Wang X, Häuselmann P. 2011. NALPS: a precisely dated European climate record 120–60 ka. Climate of the Past 7 (4): 1247–1259. 10.5194/cp-7-1247-2011.

Böhm E, Lippold J, Gutjahr M, Frank M, Blaser P, Antz B, Fohlmeister J, Frank N, Andersen MB, Deininger M. 2015. Strong and deep Atlantic meridional overturning circulation during the last glacial cycle. Nature 517 (7532): 73. 10.1038/nature14059.

Bond G, Kromer B, Beer J, Muscheler R, Evans M, Showers W, Hoffmann S, Lotti-Bond R, Hajdas I, Bonani G. 2001. Persistent Solar Influence on North Atlantic Climate During the Holocene. Science 294 (5549): 2130–2136. 10.1126/science.1065680.

Bond GC, Showers W, Elliot M, Evans M, Lotti R, Hajdas I, Bonani G, Johnson S. 1999. The North Atlantic's 1–2 kyr climate rhythm: Relation to Heinrich events, Dansgaard/Oeschger cycles and the Little Ice Age. In Mechanisms of Global Climate Change at Millennial Time Scales, Clark U, Webb S, Keigwin D (eds). American Geophysical Union: Washington, D. C; 35–58.

Bowen GJ, Wilkinson B. 2002. Spatial distribution of $\delta^{18}$Oin meteoric precipitation. Geology 30 (4): 315. 10.1130/0091-7613(2002)030<0315:SDOOIM>2.0.CO;2.

Brauer A, Allen JRM, Mingram J, Dulski P, Wulf S, Huntley B. 2007. Evidence for last interglacial chronology and environmental change from Southern Europe. Proceedings of the National Academy of Sciences 104 (2): 450–455. 10.1073/pnas.0603321104.

Budsky A, Scholz D, Gibert L, Mertz-Kraus R. 2015. 230Th/U-dating of the Cueva Victoria flowstone sequence: Preliminary results and paleoclimate implications: Datación mediante 230Th/U de la secuencia de espeleotemas de Cueva Victoria: Resultados preliminares e implicaciones paleoclimáticas. In Geología y Paleontología de Cueva Victoria. Geology and Paleontology of Cueva Victoria, Gibert L, Ferràndez-Canadell C (eds): Cartagena; 101–109.

Budsky A, Scholz D, Wassenburg JA, Mertz-Kraus R, Spötl C, Riechelmann DFC, Gibert L, Jochum KP, Andreae MO. 2019a. Speleothem $\delta^{13}$Crecord suggests enhanced spring/summer drought in south-eastern Spain between 9.7 and 7.8 ka – A circum-Western Mediterranean anomaly? The Holocene 29 (7): 1113–1133. 10.1177/0959683619838021.

Budsky A, Wassenburg JA, Mertz?Kraus R, Spötl C, Jochum KP, Gibert L, Scholz D. 2019b. Western Mediterranean Climate Response to Dansgaard/Oeschger Events: New Insights From Speleothem Records. Geophys. Res. Lett. 46 (15): 9042–9053. 10.1029/2019GL084009.

Cacho I, Grimalt JO, Pelejero C, Canals M, Sierro FJ, Flores JA, Shackleton N. 1999. Dansgaard-Oeschger and Heinrich event imprints in Alboran Sea paleotemperatures. Paleoceanography 14 (6): 698–705. 10.1029/1999PA900044.

Camuera J, Jiménez-Moreno G, Ramos-Román MJ, García-Alix A, Toney JL, Anderson RS, Jiménez-Espejo F, Bright J, Webster C, Yanes Y, Carrión JS. 2019. Vegetation and climate changes during the last two glacial-interglacial cycles in the western Mediterranean: A new long

pollen record from Padul (southern Iberian Peninsula). Quaternary Science Reviews 205: 86–105. 10.1016/j.quascirev.2018.12.013.

CAPE-Last Interglacial Project Members. 2006. Last Interglacial Arctic warmth confirms polar amplification of climate change. Dating, Synthesis, and Interpretation of Palaeoclimatic Records and Model-data Integration: Advances of the INTIMATE project(INTegration of Ice core, Marine and TErrestrial records, COST Action ES0907) 25 (13-14): 1383–1400. 10.1016/j.quascirev.2006.01.033.

Cerling TE, Wang Y, Quade J. 1993. Expansion of C4 ecosystems as an indicator of global ecological change in the late Miocene. Nature 361 (6410): 344–345. 10.1038/361344a0.

Cheddadi R, Beaulieu J-L de, Jouzel J, Andrieu-Ponel V, Laurent J-M, Reille M, Raynaud D, Bar-Hen A. 2005. Similarity of vegetation dynamics during interglacial periods. Proceedings of the National Academy of Sciences 102 (39): 13939–13943. 10.1073/pnas.0501752102.

Cheng H, Edwards RL, Sinha A, Spötl C, Yi L, Chen S, Kelly M, kathayat G, Wang X, Li X, Kong X, Wang Y, Ning Y, Zhang H. 2016. The Asian monsoon over the past 640,000 years and ice age terminations. Nature 534 (7609): 640–646. 10.1038/nature18591.

Cheng H, Edwards RL, Broecker WS, Denton GH, Kong X, Wang Y, Zhang R, Wang X. 2009. Ice Age Terminations. Science 326 (5950): 248–252. 10.1126/science.1177840.

Cheng H, Edwards RL, Hoff J, Gallup CD, Richards DA, Asmerom Y. 2000. The half-lives of uranium-234 and thorium-230. Chemical Geology 169 (1–2): 17–33. 10.1016/S0009-2541(99)00157-6.

Columbu A, Drysdale R, Capron E, Woodhead J, Waele J de, Sanna L, Hellstrom J, Bajo P. 2017. Early last glacial intra-interstadial climate variability recorded in a Sardinian speleothem. Quaternary Science Reviews 169: 391–397. 10.1016/j.quascirev.2017.05.007.

Comas-Bru L, McDermott F. 2014. Impacts of the EA and SCA patterns on the European twentieth century NAO-winter climate relationship. Q.J.R. Meteorol. Soc. 140 (679): 354–363. 10.1002/qj.2158.

Cortina A, Grimalt JO, Rigual-Hernández A, Ballegeer A-M, Martrat B, Sierro FJ, Flores JA. 2016. The impact of ice-sheet dynamics in western Mediterranean environmental conditions during Terminations. An approach based on terrestrial long chain n-alkanes deposited in the upper slope of the Gulf of Lions. Chemical Geology 430: 21–33. 10.1016/j.chemgeo.2016.03.015.

Cortina A, Sierro FJ, González-Mora B, Asioli A, Flores JA. 2011. Impact of climate and sea level changes on the ventilation of intermediate water and benthic foraminifer assemblages in the Gulf of Lions, off South France, during MIS 6 and 7. Palaeogeography, Palaeoclimatology, Palaeoecology 309 (3-4): 215–228. 10.1016/j.palaeo.2011.06.005.

Couchoud I, Genty D, Hoffmann D, Drysdale R, Blamart D. 2009. Millennial-scale climate variability during the Last Interglacial recorded in a speleothem from south-western France. Quaternary Science Reviews 28 (27-28): 3263–3274. 10.1016/j.quascirev.2009.08.014.

Deininger M, Werner M, McDermott F. 2016. North Atlantic Oscillation controls on oxygen and hydrogen isotope gradients in winter precipitation across Europe; implications for palaeoclimate studies. Clim. Past 12 (11): 2127–2143. 10.5194/cp-12-2127-2016.

Demény A, Kern Z, Czuppon G, Németh A, Leél-?ssy S, Siklósy Z, Lin K, Hu H-M, Shen C-C, Vennemann TW, Haszpra L. 2017. Stable isotope compositions of speleothems from the last interglacial – Spatial patterns of climate fluctuations in Europe. Quaternary Science Reviews 161: 68–80. 10.1016/j.quascirev.2017.02.012.

Denniston RF, Houts AN, Asmerom Y, Wanamaker Jr. AD, Haws JA, Polyak VJ, Thatcher DL, Altan-Ochir S, Borowske AC, Breitenbach SFM, Ummenhofer CC, Regala FT, Benedetti MM, Bicho NF. 2018. A stalagmite test of North Atlantic SST and Iberian hydroclimate linkages over the last two glacial cycles. Climate of the Past 14 (12): 1893–1913. 10.5194/cp-14-1893-2018.

Denton GH, Alley RB, Comer GC, Broecker WS. 2005. The role of seasonality in abrupt climate change. Quaternary Science Reviews 24 (10-11): 1159–1182. 10.1016/j.quascirev.2004.12.002.

Drysdale RN, Hellstrom JC, Zanchetta G, Fallick AE, Sanchez Goni MF, Couchoud I, McDonald J, Maas R, Lohmann G, Isola I. 2009. Evidence for Obliquity Forcing of Glacial Termination II. Science 325 (5947): 1527–1531. 10.1126/science.1170371.

Drysdale RN, Zanchetta G, Hellstrom JC, Fallick AE, McDonald J, Cartwright I. 2007. Stalagmite evidence for the precise timing of North Atlantic cold events during the early last glacial. Geol 35 (1): 77. 10.1130/G23161A.1.

Drysdale RN, Zanchetta G, Hellstrom JC, Fallick AE, Zhao J-x. 2005. Stalagmite evidence for the onset of the Last Interglacial in southern Europe at 129 ± 1 ka. Geophys. Res. Lett. 32 (24). 10.1029/2005GL024658.

Dumitru OA, Onac BP, Polyak VJ, Wynn JG, Asmerom Y, Fornós JJ. 2018. Climate variability in the western Mediterranean between 121 and 67 ka derived from a Mallorcan speleothem record. Palaeogeography, Palaeoclimatology, Palaeoecology 506: 128–138. 10.1016/j.palaeo.2018.06.028.

Dupont LM, Hooghiemstra H. 1989. The Saharan-Sahelian boundary during the Brunhes chron. Acta Botanica Neerlandica 38 (4): 405–415. 10.1111/j.1438-8677.1989.tb01372.x.

Dutton A, Lambeck K. 2012. Ice volume and sea level during the last interglacial. Science (New York, N.Y.) 337 (6091): 216–219. 10.1126/science.1205749.

Ehrmann W, Schmiedl G, Beuscher S, Krüger S. 2017. Intensity of African Humid Periods Estimated from Saharan Dust Fluxes. PLOS ONE 12 (1): e0170989. 10.1371/journal.pone.0170989.

Emeis K-C, Sakamoto T, Wehausen R, Brumsack H-J. 2000. The sapropel record of the eastern Mediterranean Sea — results of Ocean Drilling Program Leg 160. Palaeogeography, Palaeoclimatology, Palaeoecology 158 (3-4): 371–395. 10.1016/S0031-0182(00)00059-6.

Emeis K-C, Schulz H, Struck U, Rossignol-Strick M, Erlenkeuser H, Howell MW, Kroon D, Mackensen A, Ishizuka S, Oba T, Sakamoto T, Koizumi I. 2003. Eastern Mediterranean surface water temperatures and $\delta^{18}$Ocomposition during deposition of sapropels in the late Quaternary. Paleoceanography 18 (1): n/a-n/a. 10.1029/2000PA000617.

Follieri M, Magri D, Sadori L. 1989. Pollen stratigraphical synthesis from Valle di Castiglione (Roma). Quaternary International 3-4: 81–84. 10.1016/1040-6182(89)90076-1.

Frisia S. 2015. Microstratigraphic logging of calcite fabrics in speleothems as tool for palaeoclimate studies. International Journal of Speleology 44 (1): 1–16. 10.5038/1827-806X.44.1.1.

Galaasen EV, Ninnemann US, IrvalıN, Kleiven HF, Rosenthal Y, Kissel C, Hodell DA. 2014. Rapid Reductions in North Atlantic Deep Water During the Peak of the Last Interglacial Period. Science 343 (6175): 1129–1132. 10.1126/science.1248667.

Gallego-Torres D, Martinez-Ruiz F, Lange GJ de, Jimenez-Espejo FJ, Ortega-Huertas M. 2010. Trace-elemental derived paleoceanographic and paleoclimatic conditions for Pleistocene Eastern Mediterranean sapropels. Palaeogeography, Palaeoclimatology, Palaeoecology 293 (1-2): 76–89. 10.1016/j.palaeo.2010.05.001.

Genty D, Blamart D, Ouahdi R, Gilmour M, Baker A, Jouzel J, Van-Exter S. 2003. Precise dating of Dansgaard–Oeschger climate oscillations in western Europe from stalagmite data. Nature 421 (6925): 833–837. 10.1038/nature01391.

Genty D, Combourieu-Nebout N, Peyron O, Blamart D, Wainer K, Mansuri F, Ghaleb B, Isabello L, Dormoy I, Grafenstein U von. 2010. Isotopic characterization of rapid climatic events during OIS3 and OIS4 in Villars Cave stalagmites (SW-France) and correlation with Atlantic and Mediterranean pollen records. Quaternary Science Reviews 29 (19-20): 2799–2820. 10.1016/j.quascirev.2010.06.035.

Gibert L, Scott GR, Scholz D, Budsky A, Ferràndez C, Ribot F, Martin RA, Lería M, Ferrandez C, Leria M. 2016. Chronology for the Cueva Victoria fossil site (SE Spain): Evidence for Early Pleistocene Afro-Iberian dispersals. Journal of Human Evolution 90: 183–197. 10.1016/j.jhevol.2015.08.002.

Govin A, Capron E, Tzedakis PC, Verheyden S, Ghaleb B, Hillaire-Marcel C, St-Onge G, Stoner JS, Bassinot F, Bazin L, Blunier T, Combourieu-Nebout N, El Ouahabi A, Genty D, Gersonde R, Jimenez-Amat P, Landais A, Martrat B, Masson-Delmotte V, Parrenin F, Seidenkrantz M-S, Veres D, Waelbroeck C, Zahn R. 2015. Sequence of events from the onset to the demise of the Last Interglacial: Evaluating strengths and limitations of chronologies used in climatic archives. Quaternary Science Reviews 129: 1–36. 10.1016/j.quascirev.2015.09.018.

Grant KM, Grimm R, Mikolajewicz U, Marino G, Ziegler M, Rohling EJ. 2016. The timing of Mediterranean sapropel deposition relative to insolation, sea-level and African monsoon changes. Quaternary Science Reviews 140: 125–141. 10.1016/j.quascirev.2016.03.026.

Grant KM, Rohling EJ, Bar-Matthews M, Ayalon A, Medina-Elizalde M, Ramsey CB, Satow C, Roberts AP. 2012. Rapid coupling between ice volume and polar temperature over the past 150,000 years. Nature 491: 744–747. 10.1038/nature11593.

Grant KM, Rohling EJ, Ramsey CB, Cheng H, Edwards RL, Florindo F, Heslop D, Marra F, Roberts AP, Tamisiea ME, Williams F. 2014. Sea-level variability over five glacial cycles. Nature Communications 5: 5076. 10.1038/ncomms6076.

Hearty PJ, Hollin JT, Neumann AC, O'Leary MJ, McCulloch M. 2007. Global sea-level fluctuations during the Last Interglaciation (MIS 5e). Quaternary Science Reviews 26 (17-18): 2090–2112. 10.1016/j.quascirev.2007.06.019.

Hodell D, Crowhurst S, Skinner L, Tzedakis PC, Margari V, Channell JET, Kamenov G, MacLachlan S, Rothwell G. 2013. Response of Iberian Margin sediments to orbital and suborbital forcing over the past 420?ka. Paleoceanography 28 (1): 185–199. 10.1002/palo.20017.

Hodge EJ, Richards DA, Smart PL, Andreo B, Hoffmann DL, Mattey DP, González-Ramón A. 2008. Effective precipitation in southern Spain (≈266 to 46 ka) based on a speleothem stable carbon isotope record. Quaternary Research 69 (3): 447–457. 10.1016/j.yqres.2008.02.013. Hurrell JW, Loon HV. 1997. Decadal Variations in climate associated with the North Atlantic Oscillation. Climatic Change 36 (3): 301–326. 10.1023/A:1005314315270.

Incarbona A, Sprovieri M, Lirer F, Sprovieri R. 2011. Surface and deep water conditions in the Sicily channel (central Mediterranean) at the time of sapropel S5 deposition. Palaeogeography, Palaeoclimatology, Palaeoecology 306 (3-4): 243–248. 10.1016/j.palaeo.2011.04.030.

IrvalıN, Ninnemann US, Galaasen EV, Rosenthal Y, Kroon D, Oppo DW, Kleiven HF, Darling KF, Kissel C. 2012. Rapid switches in subpolar North Atlantic hydrography and climate during the Last Interglacial (MIS 5e). Paleoceanography 27 (2). 10.1029/2011PA002244.

IrvalıN, Ninnemann US, Kleiven HF, Galaasen EV, Morley A, Rosenthal Y. 2016. Evidence for regional cooling, frontal advances, and East Greenland Ice Sheet changes during the demise of the last interglacial. Quaternary Science Reviews 150: 184–199. 10.1016/j.quascirev.2016.08.029.

Jaffey AH, Flynn KF, Glendenin LE, Bentley WC, Essling AM. 1971. Precision measurement of half-lives and specific activities of 235U and 238U. Phys. Rev. C 4 (5): 1889. 10.1103/PhysRevC.4.1889.

Kelly MJ, Edwards RL, Cheng H, Yuan D, Cai Y, Zhang M, Lin Y, An Z. 2006. High resolution characterization of the Asian Monsoon between 146,000 and 99,000 years B.P. from Dongge Cave, China and global correlation of events surrounding Termination II. Palaeogeography, Palaeoclimatology, Palaeoecology 236 (1-2): 20–38. 10.1016/j.palaeo.2005.11.042.

Kottek M, Grieser J, Beck C, Rudolf B, Rubel F. 2006. World Map of the Köppen-Geiger climate classification updated. Meteorologische Zeitschrift 15 (3): 259–263. 10.1127/0941-2948/2006/0130.

Krinner G, Lézine A-M, Braconnot P, Sepulchre P, Ramstein G, Grenier C, Gouttevin I. 2012. A reassessment of lake and wetland feedbacks on the North African Holocene climate. Geophys. Res. Lett. 39 (7): L07701. 10.1029/2012GL050992.

Kutzbach JE, Chen G, Cheng H, Edwards RL, Liu Z. 2014. Potential role of winter rainfall in explaining increased moisture in the Mediterranean and Middle East during periods of maximum orbitally-forced insolation seasonality. Climate Dynamics 42 (3): 1079–1095. 10.1007/s00382-013-1692-1.

Lachniet MS. 2009. Climatic and environmental controls on speleothem oxygen-isotope values. Quaternary Science Reviews 28 (5-6): 412–432. 10.1016/j.quascirev.2008.10.021.

Laskar J, Robutel P, Joutel F, Gastineau M, Correia ACM, Levrard B. 2004. A long-term numerical solution for the insolation quantities of the Earth. Astronomy & Astrophysics 428 (1): 261–285. 10.1051/0004-6361:20041335.

Le Roux LJ, Glendenin LE. 1963. Half-life of $^{232}$Th. In National Conference on Nuclear Energy, Application of Isotopes and Radiation: Proceedings of the National Conference on Nuclear Energy held in Pretoria, April 5-8 1963, South Africa. Atomic Energy Board (ed): Pelindaba; 83–94.

Leduc G, Schneider R, Kim J-H, Lohmann G. 2010. Holocene and Eemian sea surface temperature trends as revealed by alkenone and Mg/Ca paleothermometry. Quaternary Science Reviews 29 (7-8): 989–1004. 10.1016/j.quascirev.2010.01.004.

LeGrande AN, Schmidt GA. 2006. Global gridded data set of the oxygen isotopic composition in seawater. Geophys. Res. Lett. 33 (12): n/a. 10.1029/2006GL026011.

Manteca Martínez JI, Pina R. 2015. Las mineralizaciones ferro-manganesíferas de la mina-cueva Victoria y su contexto geológico: Fe-Mn mineralizations of the mine-cave Victoria and their geological context. In Geología y Paleontología de Cueva Victoria. Geology and Paleontology of Cueva Victoria, Gibert L, Ferràndez-Canadell C (eds): Cartagena; 59–74.

Martin-Vide J, Lopez-Bustins J-A. 2006. The Western Mediterranean Oscillation and rainfall in the Iberian Peninsula. Int. J. Climatol. 26 (11): 1455–1475. 10.1002/joc.1388.

Martrat B, Grimalt JO, Lopez-Martinez C, Cacho I, Sierro FJ, Flores JA, Zahn R, Canals M, Curtis JH, Hodell DA. 2004. Abrupt Temperature Changes in the Western Mediterranean over the Past 250,000 Years. Science 306 (5702): 1762–1765. 10.1126/science.1101706.

Martrat B, Grimalt JO, Shackleton NJ, Abreu L de, Hutterli MA, Stocker TF. 2007. Four Climate Cycles of Recurring Deep and Surface Water Destabilizations on the Iberian Margin. Science 317 (5837): 502–507. 10.1126/science.1139994.

Martrat B, Jimenez-Amat P, Zahn R, Grimalt JO. 2014. Similarities and dissimilarities between the last two deglaciations and interglaciations in the North Atlantic region. Quaternary Science Reviews 99: 122–134. 10.1016/j.quascirev.2014.06.016.

McDermott F. 2004. Palaeo-climate reconstruction from stable isotope variations in speleothems: a review. Quaternary Science Reviews 23 (7-8): 901–918. 10.1016/j.quascirev.2003.06.021.

Mehterian S, Pourmand A, Sharifi A, Lahijani HAK, Naderi M, Swart PK. 2017. Speleothem records of glacial/interglacial climate from Iran forewarn of future Water Availability in the interior of the Middle East. Quaternary Science Reviews 164: 187–198. 10.1016/j.quascirev.2017.03.028.

Menviel L, Timmermann A, Friedrich T, England MH. 2014. Hindcasting the continuum of Dansgaard/Oeschger variability: mechanisms, patterns and timing. Climate of the Past 10 (1): 63–77. 10.5194/cp-10-63-2014.

Merz N, Born A, Raible CC, Stocker TF. 2016. Warm Greenland during the last interglacial: The role of regional changes in sea ice cover. Climate of the Past 12 (10): 2011–2031. 10.5194/cp-12-2011-2016.

Meyer MC, Spötl C, Mangini A. 2008. The demise of the Last Interglacial recorded in isotopically dated speleothems from the Alps. Quaternary Science Reviews 27 (5-6): 476–496. 10.1016/j.quascirev.2007.11.005.

Meyer KW, Feng W, Breecker DO, Banner JL, Guilfoyle A. 2014. Interpretation of speleothem calcite $\delta^{13}$Cvariations: Evidence from monitoring soil $CO_2$, drip water, and modern speleothem calcite in central Texas. Geochimica et Cosmochimica Acta 142: 281–298. 10.1016/j.gca.2014.07.027.

Milner AM, Collier REL, Roucoux KH, Müller UC, Pross J, Kalaitzidis S, Christanis K, Tzedakis PC. 2012. Enhanced seasonality of precipitation in the Mediterranean during the early part of the

Last Interglacial. Geology 40 (10): 919–922. 10.1130/G33204.1.

Milner AM, Roucoux KH, Collier REL, Müller UC, Pross J, Tzedakis PC. 2016. Vegetation responses to abrupt climatic changes during the Last Interglacial Complex (Marine Isotope Stage 5) at Tenaghi Philippon, NE Greece. Quaternary Science Reviews 154: 169–181. 10.1016/j.quascirev.2016.10.016.

Mokeddem Z, McManus JF, Oppo DW. 2014. Oceanographic dynamics and the end of the last interglacial in the subpolar North Atlantic. Proceedings of the National Academy of Sciences of the United States of America 111 (31): 11263–11268. 10.1073/pnas.1322103111.

Moseley GE, Spötl C, Cheng H, Boch R, Min A, Edwards RL. 2015. Termination-II interstadial/stadial climate change recorded in two stalagmites from the north European Alps. Quaternary Science Reviews 127: 229–239. 10.1016/j.quascirev.2015.07.012.

Naughton F, Sánchez Goñi MF, Kageyama M, Bard E, Duprat J, Cortijo E, Desprat S, Malaizé B, Joly C, Rostek F, Turon J-L. 2009. Wet to dry climatic trend in north-western Iberia within Heinrich events. Earth and Planetary Science Letters 284 (3-4): 329–342. 10.1016/j.epsl.2009.05.001.

Nicholl JAL, Hodell DA, Naafs BDA, Hillaire-Marcel C, Channell JET, Romero OE. 2012. A Laurentide outburst flooding event during the last interglacial period. Nature Geoscience 5 (12): 901. 10.1038/ngeo1622.

North Greenland Ice Core Project members. 2004. High-resolution record of Northern Hemisphere climate extending into the last interglacial period. Nature 431 (7005): 147–151. 10.1038/nature02805.

Obert JC, Scholz D, Felis T, Brocas WM, Jochum KP, Andreae MO. 2016. $^{230}$Th/U dating of Last Interglacial brain corals from Bonaire (southern Caribbean) using bulk and theca wall material. Geochimica et Cosmochimica Acta 178: 20–40. 10.1016/j.gca.2016.01.011.

Obrochta SP, Yokoyama Y, Morén J, Crowley TJ. 2014. Conversion of GISP2-based sediment core age models to the GICC05 extended chronology. Quaternary Geochronology 20: 1–7. 10.1016/j.quageo.2013.09.001.

Oppo DW, McManus JF, Cullen JL. 2006. Evolution and demise of the Last Interglacial warmth in the subpolar North Atlantic. Quaternary Science Reviews 25 (23-24): 3268–3277. 10.1016/j.quascirev.2006.07.006.

Osete M-L, Martín-Chivelet J, Rossi C, Edwards RL, Egli R, Muñoz-García MB, Wang X, Pavón-Carrasco FJ, Heller F. 2012. The Blake geomagnetic excursion recorded in a radiometrically dated speleothem. Earth and Planetary Science Letters 353-354: 173–181. 10.1016/j.epsl.2012.07.041.

Pausata FSR, Messori G, Zhang Q. 2016. Impacts of dust reduction on the northward expansion of the African monsoon during the Green Sahara period. Earth and Planetary Science Letters 434: 298–307. 10.1016/j.epsl.2015.11.049.

Pedersen RA, Langen PL, Vinther BM. 2017. The last interglacial climate: Comparing direct and indirect impacts of insolation changes. Climate Dynamics 48 (9): 3391–3407. 10.1007/s00382-016-3274-5.

Pérez-Mejías C, Moreno A, Sancho C, Martín-García R, Spötl C, Cacho I, Cheng H, Edwards RL. 2019. Orbital-to-millennial scale climate variability during Marine Isotope Stages 5 to 3 in northeast Iberia. Quaternary Science Reviews 224: 105946. 10.1016/j.quascirev.2019.105946.

Regattieri E, Giaccio B, Nomade S, Francke A, Vogel H, Drysdale RN, Perchiazzi N, Wagner B, Gemelli M, Mazzini I, Boschi C, Galli P, Peronace E. 2017. A Last Interglacial record of environmental changes from the Sulmona Basin (central Italy). Palaeogeography, Palaeoclimatology, Palaeoecology 472: 51–66. 10.1016/j.palaeo.2017.02.013.

Regattieri E, Giaccio B, Zanchetta G, Drysdale RN, Galli P, Nomade S, Peronace E, Wulf S. 2015. Hydrological variability over the Apennines during the Early Last Glacial precession minimum, as revealed by a stable isotope record from Sulmona basin, Central Italy. J. Quaternary Sci. 30 (1): 19–31. 10.1002/jqs.2755.

Regattieri E, Zanchetta G, Drysdale RN, Isola I, Hellstrom JC, Roncioni A. 2014. A continuous stable isotope record from the penultimate glacial maximum to the Last Interglacial (159–121 ka) from Tana Che Urla Cave (Apuan Alps, central Italy). Quaternary Research 82 (02): 450–461. 10.1016/j.yqres.2014.05.005.

Regattieri E, Zanchetta G, Drysdale RN, Isola I, Woodhead JD, Hellstrom JC, Giaccio B, Greig A, Baneschi I, Dotsika E. 2016. Environmental variability between the penultimate deglaciation and the mid Eemian: Insights from Tana che Urla (central Italy) speleothem trace element record. Quaternary Science Reviews 152: 80–92. 10.1016/j.quascirev.2016.09.027.

Ridley HE, Asmerom Y, Baldini JUL, Breitenbach SFM, Aquino VV, Prufer KM, Culleton BJ, Polyak V, Lechleitner FA, Kennett DJ, Zhang M, Marwan N, Macpherson CG, Baldini LM, Xiao T, Peterkin JL, Awe J, Haug GH. 2015. Aerosol forcing of the position of the intertropical convergence zone since ad 1550. Nature Geoscience (Nature Geoscience) 8 (3): 195–200. 10.1038/ngeo2353.

Ríos-Cornejo D, Penas á, álvarez-Esteban R, del Río S. 2015. Links between teleconnection patterns and mean temperature in Spain: Theoretical and Applied Climatology. Theor Appl Climatol 122 (1-2): 1–18. 10.1007/s00704-014-1256-2.

Rohling EJ, Cane TR, Cooke S, Sprovieri M, Bouloubassi I, Emeis KC, Schiebel R, Kroon D, Jorissen FJ, Lorre A, Kemp AES. 2002. African monsoon variability during the previous interglacial maximum. Earth and Planetary Science Letters 202 (1): 61–75. 10.1016/S0012-821X(02)00775-6.

Rohling EJ, Marino G, Grant KM. 2015. Mediterranean climate and oceanography, and the periodic development of anoxic events (sapropels). Earth-Science Reviews 143: 62–97. 10.1016/j.earscirev.2015.01.008.

Ros A, Llamusí JL. 2015. Reconsrucción y génesis del karst de Cueva Victoria: Reconstruction and genesis of the Cueva Victoria karst. In Geología y Paleontología de Cueva Victoria. Geology and Paleontology of Cueva Victoria, Gibert L, Ferràndez-Canadell C (eds): Cartagena; 111–125.

Rossi C, Mertz-Kraus R, Osete M-L. 2014. Paleoclimate variability during the Blake geomagnetic excursion (MIS 5d) deduced from a speleothem record. Quaternary Science Reviews 102: 166–180. 10.1016/j.quascirev.2014.08.007.

Rossignol-Strick M, Paterne M. 1999. A synthetic pollen record of the eastern Mediterranean sapropels

of the last 1 Ma: implications for the time-scale and formation of sapropels. Marine Geology 153 (1-4): 221–237. 10.1016/S0025-3227(98)00080-2.

Roucoux KH, Tzedakis PC, Frogley MR, Lawson IT, Preece RC. 2008. Vegetation history of the marine isotope stage 7 interglacial complex at Ioannina, NW Greece. Quaternary Science Reviews 27 (13-14): 1378–1395. 10.1016/j.quascirev.2008.04.002.

Rovere A, Raymo ME, Vacchi M, Lorscheid T, Stocchi P, Gómez-Pujol L, Harris DL, Casella E, O'Leary MJ, Hearty PJ, O'Leary MJ. 2016. The analysis of Last Interglacial (MIS 5e) relative sea-level indicators: Reconstructing sea-level in a warmer world. Earth-Science Reviews 159: 404–427. 10.1016/j.earscirev.2016.06.006.

Sánchez Goñi MF, Landais A, Fletcher WJ, Naughton F, Desprat S, Duprat J. 2008. Contrasting impacts of Dansgaard–Oeschger events over a western European latitudinal transect modulated by orbital parameters. Quaternary Science Reviews 27 (11–12): 1136–1151. 10.1016/j.quascirev.2008.03.003.

Scholz D, Hoffmann DL. 2011. StalAge – An algorithm designed for construction of speleothem age models. Quaternary Geochronology 6 (3-4): 369–382. 10.1016/j.quageo.2011.02.002.

Scholz D, Mangini A, Meischner D. 2007. 9. U-redistribution in fossil reef corals from Barbados, West Indies, and sea-level reconstruction for MIS 6.5. In The Climate of Past Interglacials, Sirocko F, Claussen M, Sánchez Goñi MF, Litt T (eds). Elsevier: Amsterdam; 119–139.

Siddall M, Rohling EJ, Almogi-Labin A, Hemleben C, Meischner D, Schmelzer I, Smeed DA. 2003. Sea-level fluctuations during the last glacial cycle. Nature 423 (6942): 853–858. 10.1038/nature01690.

Sinopoli G, Masi A, Regattieri E, Wagner B, Francke A, Peyron O, Sadori L. 2018. Palynology of the Last Interglacial Complex at Lake Ohrid: Palaeoenvironmental and palaeoclimatic inferences. Quaternary Science Reviews 180: 177–192. 10.1016/j.quascirev.2017.11.013.

Sirocko F, Seelos K, Schaber K, Rein B, Dreher F, Diehl M, Lehne R, Jäger K, Krbetschek M, Degering D. 2005. A late Eemian aridity pulse in central Europe during the last glacial inception. Nature 436 (7052): 833. 10.1038/nature03905.

Skinner LC, Shackleton NJ. 2006. Deconstructing Terminations I and II: Revisiting the glacioeustatic paradigm based on deep-water temperature estimates. Quaternary Science Reviews 25 (23-24): 3312–3321. 10.1016/j.quascirev.2006.07.005.

Spötl C. 2011. Long-term performance of the Gasbench isotope ratio mass spectrometry system for the stable isotope analysis of carbonate microsamples. Rapid Commun. Mass Spectrom. 25 (11): 1683–1685. 10.1002/rcm.5037.

Spötl C, Vennemann TW. 2003. Continuous-flow isotope ratio mass spectrometric analysis of carbonate minerals. Rapid Commun. Mass Spectrom. 17 (9): 1004–1006. 10.1002/rcm.1010.

Stoll H, Mendez-Vicente A, Gonzalez-Lemos S, Moreno A, Cacho I, Cheng H, Edwards RL. 2015. Interpretation of orbital scale variability in mid-latitude speleothem $\delta^{18}$O: Significance of growth rate controlled kinetic fractionation effects. Novel approaches to and new insights from speleothem-based climate reconstructions 127: 215–228. 10.1016/j.quascirev.2015.08.025.

Tierney JE, Pausata FSR, deMenocal PB. 2017. Rainfall regimes of the Green Sahara. Science Advances 3 (1): e1601503. 10.1126/sciadv.1601503.

Tisserand A, Malaizé B, Jullien E, Zaragosi S, Charlier K, Grousset F. 2009. African monsoon enhancement during the penultimate glacial period (MIS 6.5 ? 170 ka) and its atmospheric impact. Paleoceanography 24 (2): PA2220. 10.1029/2008PA001630.

Tjallingii R, Claussen M, Stuut J-BW, Fohlmeister J, Jahn A, Bickert T, Lamy F, Röhl U. 2008. Coherent high- and low-latitude control of the northwest African hydrological balance. Nature Geosci 1 (10): 670–675. 10.1038/ngeo289.

Torfstein A, Goldstein SL, Kushnir Y, Enzel Y, Haug G, Stein M. 2015. Dead Sea drawdown and monsoonal impacts in the Levant during the last interglacial. Earth and Planetary Science Letters 412: 235–244. 10.1016/j.epsl.2014.12.013.

Toucanne S, Angue Minto'o CM, Fontanier C, Bassetti M-A, Jorry SJ, Jouet G. 2015. Tracking rainfall in the northern Mediterranean borderlands during sapropel deposition. Quaternary Science Reviews 129: 178–195. 10.1016/j.quascirev.2015.10.016.

Tzedakis PC. 1993. Long-term tree populations in northwest Greece through multiple Quaternary climatic cycles. Nature 364 (6436): 437–440. 10.1038/364437a0.

Tzedakis PC. 2005. Towards an understanding of the response of southern European vegetation to orbital and suborbital climate variability. Quaternary Science Reviews 24 (14-15): 1585–1599. 10.1016/j.quascirev.2004.11.012.

Tzedakis PC, Drysdale RN, Margari V, Skinner LC, Menviel L, Rhodes RH, Taschetto AS, Hodell DA, Crowhurst SJ, Hellstrom JC, Fallick AE, Grimalt JO, McManus JF, Martrat B, Mokeddem Z, Parrenin F, Regattieri E, Roe K, Zanchetta G. 2018. Enhanced climate instability in the North Atlantic and southern Europe during the Last Interglacial. Nature Communications 9 (1): 4235. 10.1038/s41467-018-06683-3.

Tzedakis PC, Hooghiemstra H, Pälike H. 2006. The last 1.35 million years at Tenaghi Philippon: revised chronostratigraphy and long-term vegetation trends. Quaternary Science Reviews 25 (23-24): 3416–3430. 10.1016/j.quascirev.2006.09.002.

Vanghi V, Borsato A, Frisia S, Drysdale R, Hellstrom J, Bajo P. 2018. Climate variability on the Adriatic seaboard during the last glacial inception and MIS 5c from Frasassi Cave stalagmite record. Quaternary Science Reviews 201: 349–361. 10.1016/j.quascirev.2018.10.023.

Vansteenberge S, Verheyden S, Cheng H, Edwards RL, Keppens E, Claeys P. 2016. Paleoclimate in continental northwestern Europe during the Eemian and early Weichselian (125–97?ka): Insights from a Belgian speleothem. Climate of the Past 12 (7): 1445–1458. 10.5194/cp-12-1445-2016.

Vansteenberge S, Verheyden S, Genty D, Blamart D, Goderis S, van Malderen SJM, Vanhaecke F, Hodel F, Gillikin D, Ek C, Quinif Y, Cheng H, Edwards RL, Claeys P. 2019. Characterizing the Eemian-Weichselian transition in northwestern Europe with three multiproxy speleothem archives from the Belgian Han-sur-Lesse and Remouchamps cave systems. Quaternary Science Reviews 208: 21–37. 10.1016/j.quascirev.2019.01.011.

Vautravers MJ, Shackleton NJ. 2006. Centennial?scale surface hydrology off Portugal during marine isotope stage 3: Insights from planktonic foraminiferal fauna variability. Paleoceanography 21

(3). 10.1029/2005PA001144.

Waelbroeck C, Labeyrie L, Michel E, Duplessy JC, McManus JF, Lambeck K, Balbon E, Labracherie M. 2002. Sea-level and deep water temperature changes derived from benthic foraminifera isotopic records. Quaternary Science Reviews 21: 295–305. 10.1016/S0277-3791(01)00101-9.

Wagner B, Vogel H, Francke A, Friedrich T, Donders T, Lacey JH, Leng MJ, Regattieri E, Sadori L, Wilke T, Zanchetta G, Albrecht C, Bertini A, Combourieu-Nebout N, Cvetkoska A, Giaccio B, Grazhdani A, Hauffe T, Holtvoeth J, Joannin S, Jovanovska E, Just J, Kouli K, Kousis I, Koutsodendris A, Krastel S, Lagos M, Leicher N, Levkov Z, Lindhorst K, Masi A, Melles M, Mercuri AM, Nomade S, Nowaczyk N, Panagiotopoulos K, Peyron O, Reed JM, Sagnotti L, Sinopoli G, Stelbrink B, Sulpizio R, Timmermann A, Tofilovska S, Torri P, Wagner-Cremer F, Wonik T, Zhang X. 2019. Mediterranean winter rainfall in phase with African monsoons during the past 1.36 million years. Nature 573 (7773): 256–260. 10.1038/s41586-019-1529-0.

Wainer K, Genty D, Blamart D, Bar-Matthews M, Quinif Y, Plagnes V. 2013. Millennial climatic instability during penultimate glacial period recorded in a south-western France speleothem. Palaeogeography, Palaeoclimatology, Palaeoecology 376: 122–131. 10.1016/j.palaeo.2013.02.026.

Wainer K, Genty D, Blamart D, Daëron M, Bar-Matthews M, Vonhof H, Dublyansky Y, Pons-Branchu E, Thomas L, van Calsteren P, Quinif Y, Caillon N. 2011. Speleothem record of the last 180 ka in Villars cave (SW France): Investigation of a large $\delta^{18}$Oshift between MIS6 and MIS5. Quaternary Science Reviews 30 (1-2): 130–146. 10.1016/j.quascirev.2010.07.004.

Wang Y, Cheng H, Edwards RL, He Y, Kong X, An Z, Wu J, Kelly MJ, Dykoski CA, Li X. 2005. The Holocene Asian Monsoon: Links to Solar Changes and North Atlantic Climate. Science 308 (5723): 854–857. 10.1126/science.1106296.

Wang Y, Cheng H, Edwards RL, Kong X, Shao X, Chen S, Wu J, Jiang X, Wang X, An Z. 2008. Millennial- and orbital-scale changes in the East Asian monsoon over the past 224,000 years. Nature 451 (7182): 1090–1093. 10.1038/nature06692.

Wang YJ, Cheng H, Edwards RL, An ZS, Wu JY, Shen C-C, Dorale JA. 2001. A High-Resolution Absolute-Dated Late Pleistocene Monsoon Record from Hulu Cave, China. Science 294 (5550): 2345–2348. 10.1126/science.1064618.

Weldeab S, Emeis K-C, Hemleben C, Vennemann TW, Schulz H. 2002. Sr and Nd isotope composition of Late Pleistocene sapropels and nonsapropelic sediments from the Eastern Mediterranean Sea. Geochimica et Cosmochimica Acta 66 (20): 3585–3598. 10.1016/S0016-7037(02)00954-7.

Yang Q, Scholz D, Jochum KP, Hoffmann DL, Stoll B, Weis U, Schwager B, Andreae MO. 2015. Lead isotope variability in speleothems—A promising new proxy for hydrological change? First results from a stalagmite from western Germany. Chemical Geology 396: 143–151. 10.1016/j.chemgeo.2014.12.028.

Zanchetta G, Drysdale RN, Hellstrom JC, Fallick AE, Isola I, Gagan MK, Pareschi MT. 2007. Enhanced rainfall in the Western Mediterranean during deposition of sapropel S1: stalagmite evidence from Corchia cave (Central Italy). Quaternary Science Reviews 26 (3-4): 279–286. 10.1016/j.quascirev.2006.12.003.

## 6.6 Supplemental material

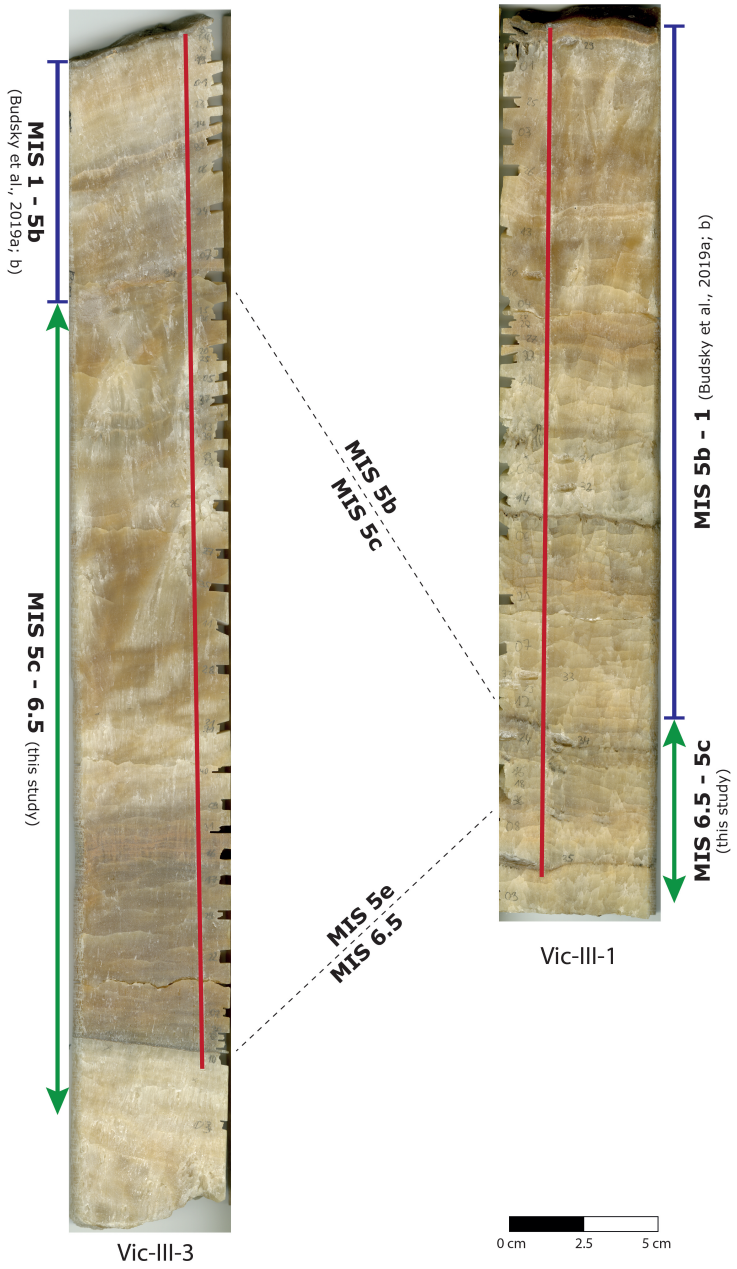


Figure 6.7: Samples Vic-III-1 (right) and Vic-III-3 (left). The top sections of the samples (violet bar, MIS 1 to 5b) was already published in Budsky et al. (2019a, b). The red bar indicates the profile for stable isotope milling.

Table 6.1: $^{230}$Th/U dating results for flowstones Vic-III-3 and Vic-III-1.

| Sample | $^{238}$U [µg/g] | ± | ($^{230}$Th/$^{232}$Th) | ± | ($^{234}$U/$^{238}$U) | ± | ($^{230}$Th/$^{238}$U) | ± | age corr.[ka] | error [ka] | age uncorr. [ka] | error [ka] | dft [cm] |
|---|---|---|---|---|---|---|---|---|---|---|---|---|---|
| Vic-III-3-34 | 0.150 | 0.001 | 73.49 | 0.76 | 1.141 | 0.003 | 0.717 | 0.005 | 102.66 | 1.49 | 105.11 | 1.18 | 8.25 |
| Vic-III-3-15 | 0.197 | 0.001 | 253.48 | 2.32 | 1.110 | 0.005 | 0.718 | 0.004 | 110.19 | 1.44 | 110.92 | 1.47 | 9.65 |
| Vic-III-3-36 | 0.190 | 0.001 | 249.78 | 2.49 | 1.126 | 0.005 | 0.711 | 0.005 | 105.37 | 1.56 | 106.09 | 1.53 | 9.8 |
| Vic-III-3-44 | 0.160 | 0.001 | 79.28 | 0.90 | 1.128 | 0.002 | 0.721 | 0.005 | 106.00 | 1.61 | 108.31 | 1.30 | 10.5 |
| Vic-III-3-20 | 0.142 | 0.001 | 102.46 | 1.38 | 1.129 | 0.003 | 0.721 | 0.007 | 106.37 | 1.83 | 108.15 | 1.74 | 10.9 |
| Vic-III-3-25 | 0.151 | 0.001 | 160.45 | 1.81 | 1.128 | 0.001 | 0.716 | 0.005 | 105.94 | 1.27 | 107.07 | 1.23 | 11.1 |
| Vic-III-3-05 | 0.161 | 0.001 | 170.95 | 1.91 | 1.131 | 0.008 | 0.721 | 0.007 | 106.65 | 2.22 | 107.71 | 2.17 | 12 |
| Vic-III-3-37 | 0.169 | 0.001 | 187.03 | 1.90 | 1.130 | 0.002 | 0.723 | 0.004 | 107.47 | 1.08 | 108.44 | 1.00 | 12.7 |
| Vic-III-3-13 | 0.201 | 0.002 | 366.20 | 3.42 | 1.110 | 0.005 | 0.726 | 0.004 | 112.56 | 1.44 | 113.07 | 1.48 | 13.65 |
| Vic-III-3-38 | 0.192 | 0.001 | 185.94 | 1.94 | 1.137 | 0.002 | 0.731 | 0.004 | 108.21 | 1.19 | 109.19 | 1.13 | 13.8 |
| Vic-III-3-39 | 0.145 | 0.001 | 258.88 | 3.21 | 1.143 | 0.002 | 0.736 | 0.006 | 108.76 | 1.57 | 109.47 | 1.54 | 14.4 |
| Vic-III-3-08 | 0.174 | 0.002 | 314.45 | 3.14 | 1.145 | 0.011 | 0.736 | 0.008 | 108.57 | 2.75 | 109.15 | 2.84 | 14.8 |
| Vic-III-3-26 | 0.252 | 0.005 | 353.01 | 3.04 | 1.119 | 0.022 | 0.726 | 0.015 | 110.77 | 5.68 | 111.29 | +6.29-5.31 | 16.3 |
| Vic-III-3-27 | 0.332 | 0.003 | 222.58 | 2.00 | 1.133 | 0.010 | 0.742 | 0.007 | 111.88 | 2.55 | 112.70 | 2.62 | 17.8 |
| Vic-III-3-35 | 0.304 | 0.002 | 410.44 | 3.93 | 1.139 | 0.006 | 0.745 | 0.006 | 112.05 | 1.81 | 112.50 | 1.83 | 18.7 |
| Vic-III-3-45 | 0.310 | 0.002 | 319.15 | 3.43 | 1.145 | 0.001 | 0.746 | 0.004 | 111.09 | 1.12 | 111.67 | 1.12 | 19.4 |
| Vic-III-3-11 | 0.338 | 0.002 | 629.44 | 5.70 | 1.114 | 0.005 | 0.755 | 0.004 | 119.85 | 1.56 | 120.15 | 1.60 | 20.45 |
| Vic-III-3-28 | 0.369 | 0.005 | 246.19 | 2.26 | 1.142 | 0.014 | 0.757 | 0.010 | 114.30 | 3.75 | 115.07 | 3.85 | 21.7 |
| Vic-III-3-46 | 0.291 | 0.002 | 401.70 | 4.42 | 1.139 | 0.001 | 0.755 | 0.005 | 114.51 | 1.26 | 114.98 | 1.27 | 22.5 |
| Vic-III-3-21 | 0.346 | 0.002 | 384.36 | 4.69 | 1.144 | 0.003 | 0.764 | 0.006 | 115.97 | 1.54 | 116.46 | 1.58 | 23.7 |
| Vic-III-3-40 | 0.319 | 0.002 | 639.55 | 6.45 | 1.140 | 0.005 | 0.765 | 0.005 | 117.02 | 1.73 | 117.32 | 1.77 | 24.9 |
| Vic-III-3-09 | 0.255 | 0.003 | 367.62 | 3.90 | 1.148 | 0.011 | 0.771 | 0.009 | 116.79 | 3.13 | 117.30 | 3.23 | 26.2 |
| Vic-III-3-31 | 0.198 | 0.001 | 28.97 | 0.28 | 1.154 | 0.005 | 0.799 | 0.005 | 116.95 | 3.16 | 123.86 | 1.93 | 26.9 |
| Vic-III-3-16 | 0.168 | 0.001 | 26.84 | 0.26 | 1.136 | 0.004 | 0.820 | 0.006 | 126.40 | 3.55 | 134.21 | 2.14 | 27.9 |
| Vic-III-3-17 | 0.267 | 0.002 | 149.60 | 1.37 | 1.133 | 0.005 | 0.795 | 0.005 | 126.16 | 1.88 | 127.49 | 1.84 | 28.7 |
| Vic-III-3-29 | 0.344 | 0.006 | 545.63 | 4.91 | 1.130 | 0.019 | 0.802 | 0.014 | 129.72 | 6.27 | 130.09 | +6.65-6.04 | 29.9 |
| Vic-III-3-22 | 0.317 | 0.002 | 124.19 | 1.18 | 1.139 | 0.004 | 0.805 | 0.005 | 127.30 | 1.78 | 128.90 | 1.74 | 31.35 |
| Vic-III-3-02 | 0.425 | 0.004 | 192.20 | 1.86 | 1.151 | 0.008 | 0.809 | 0.007 | 126.42 | 2.71 | 127.45 | 2.73 | 33 |
| Vic-III-3-30 | 0.455 | 0.003 | 313.85 | 3.34 | 1.151 | 0.002 | 0.809 | 0.005 | 126.54 | 1.51 | 127.17 | 1.54 | 33.7 |
| Vic-III-3-12 | 0.494 | 0.004 | 348.87 | 3.67 | 1.128 | 0.007 | 0.813 | 0.007 | 133.37 | 2.78 | 133.95 | 2.73 | 34.1 |
| Vic-III-3-12re | 0.468 | 0.003 | 376.94 | 3.26 | 1.133 | 0.004 | 0.810 | 0.004 | 131.41 | 1.62 | 131.95 | 1.64 | 34.1 |
| Vic-III-3-10 | 0.249 | 0.003 | 908.29 | 9.68 | 1.167 | 0.011 | 0.956 | 0.010 | 172.58 | 5.87 | 172.82 | +6,23-5,46 | 34.6 |
| Vic-III-3-03 | 0.267 | 0.002 | 499.57 | 4.93 | 1.162 | 0.007 | 0.958 | 0.008 | 175.63 | 4.35 | 176.08 | 4.49 | 36.7 |

| Sample | $^{238}$U [µg/g] | ± | ($^{230}$Th/$^{232}$Th) | ± | ($^{234}$U/$^{238}$U) | ± | ($^{230}$Th/$^{238}$U) | ± | age corr.[ka] | error [ka] | age uncorr. [ka] | error [ka] | dft [cm] |
|---|---|---|---|---|---|---|---|---|---|---|---|---|---|
| Vic-III-1-12 | 0.100 | 0.001 | 164.74 | 1.57 | 1.186 | 0.004 | 0.740 | 0.005 | 101.20 | 1.37 | 103.16 | 1.24 | 23.2 |
| Vic-III-1-34 | 0.107 | 0.001 | 104.81 | 1.31 | 1.153 | 0.003 | 0.726 | 0.007 | 102.52 | 1.89 | 105.17 | 1.55 | 23.9 |
| Vic-III-1-24 | 0.098 | 0.001 | 62.14 | 1.17 | 1.149 | 0.005 | 0.759 | 0.012 | 109.44 | 3.72 | 114.15 | 3.35 | 24.2 |
| Vic-III-1-15 | 0.179 | 0.001 | 530.98 | 5.09 | 1.155 | 0.004 | 0.755 | 0.004 | 111.37 | 1.25 | 112.01 | 1.28 | 25.25 |
| Vic-III-1-18 | 0.218 | 0.001 | 400.81 | 4.06 | 1.162 | 0.002 | 0.762 | 0.004 | 111.82 | 1.12 | 112.53 | 1.15 | 25.7 |
| Vic-III-1-36 | 0.107 | 0.001 | 248.57 | 2.88 | 1.169 | 0.002 | 0.778 | 0.006 | 113.99 | 1.59 | 115.16 | 1.53 | 26 |
| Vic-III-1-08 | 0.158 | 0.001 | 200.73 | 2.05 | 1.149 | 0.005 | 0.929 | 0.007 | 167.39 | 3.28 | 169.43 | 3.30 | 27 |
| Vic-III-1-35 | 0.180 | 0.001 | 431.44 | 4.85 | 1.147 | 0.002 | 0.936 | 0.007 | 172.42 | 2.94 | 173.22 | 3.00 | 28.3 |
| Vic-III-1-09 | 0.095 | 0.001 | 255.34 | 3.57 | 1.122 | 0.003 | 0.944 | 0.009 | 186.33 | 4.90 | 188.00 | 5.02 | 29.5 |

All uncertainties are reported as 2?-standard errors. Activity ratios were calculated using the half-lives given by Cheng et al. (2000) for $^{230}$Th and $^{234}$U and Jaffey et al. (1971) for $^{238}$U. Corrected ages were calculated using different correction factors for detrital contamination (($^{232}$Th/$^{238}$U) = 0.37 ± 0.19 (Vic-III-3) and 0.24 ± 0.12 (Vic-III-1), estimated following the method of Budsky et al. (2019).

## References

Budsky, A., Scholz, D., Wassenburg, J. A., Mertz-Kraus, R., Spötl, C., Riechelmann, D. F. C., et al. (2019). Speleothem $\delta^{13}$C record suggests enhanced spring/summer drought in south-eastern Spain between 9.7 and 7.8 ka – A circum-Western Mediterranean anomaly? The Holocene, 44(1), 095968361983802. https://doi.org/10.1177/0959683619838021

Cheng, H., Edwards, R.L., Hoff, J., Gallup, C.D., Richards, D.A., & Asmerom, Y. (2000). The half-lives of uranium-234 and thorium-230. Chemical Geology, 169(1–2), 17–33. https://doi.org/10.1016/S0009-2541(99)00157-6

Jaffey, A. H., Flynn, K. F., Glendenin, L. E., Bentley, W. C., & Essling, A. M. (1971). Precision measurement of half-lives and specific activities of $^{235}$U and $^{238}$U. Physical Review C, 4(5), 1889. https://doi.org/10.1103/PhysRevC.4.1889

Scholz, D., & Hoffmann, D. L. (2011). StalAge – An algorithm designed for construction of speleothem age models. Quaternary Geochronology, 6(3-4), 369–382. https://doi.org/10.1016/j.quageo.2011.02.002

# 7 Outlook

Additional to the extensive work on the timing of the last interglacial to the Holocene (Chapters 4 to 6), further age determinations beyond the last interglacial have been performed. $^{230}$Th/U-ages indicate a preferred speleothem growth during interglacials, as already investigated by one flowstone drill core (Chapter 3). Preliminary ages provide a huge potential for further palaeoclimate reconstructions on a deeper timescales towards the limitations of the $^{230}$Th/U dating method. As elaborated in chapter 5, the connection to Northern Hemisphere temperature changes could potentially be linked to rapidly changing speleothem $\delta^{18}$O values in CV. The interglacial–glacial sequence with several warm/humid cycles was proposed on the basis of a Chinese speleothem stack covering the last 640 ka (Cheng et al., 2016). For the Mediterranean and Iberian Margin, marine records provide palaeoclimate information and phytoplankton productivity for the last $\approx$ 400 ka (Cortina et al., 2016; Hodell et al., 2013; Martrat et al., 2007; Toucanne et al., 2015). However, accurate age-models and temporal resolution are limited, due to a missing comparable long-term local chronology and therefore these proxies of the marine records were often linked to orbital forcing (Girone et al., 2013) or the synthetic Greenland record (Barker et al., 2011). Only a few terrestrial pollen records in the Mediterranean cover several interglacial to glacial cycles (Camuera et al., 2019; Tzedakis et al., 2006). These records indicate humid conditions during interglacials. Consistent to them, the CV speleothems age distribution (Figure 7.1) shows a preferred speleothem growth during interglacials and insolation maxima (MIS 7, 9) reflecting humid conditions in south-eastern Spain.

The penultimate interglacial (MIS 7) can be traced in almost every CV speleothem sample (Vic-III-1 to Vic-III-5, ST02 and one stalagmite; Figure 7.1). In particular, the stalagmite sample provides a huge potential to study the penultimate interglacial MIS 7 in high temporal resolution of $\approx$7 µm/a (Figure 7.1) and the additional flowstone samples (e.g., ST02) may provide some replication of proxies for a robust interpretation. MIS 7 speleothem $^{230}$Th/U-ages match with periods with high arboreal pollen amount (7a, 7c) of a marine sediment core from the Iberian Margin (Roucoux et al., 2006) and one from Greece (Ioannina, Roucoux et al. 2008). However, the onset of the second termination (MIS 7e, $\approx$ 240 ka) with the sapropel (S9) deposition (Ziegler et al., 2010) seems to be absent in CV speleothems, which could probably related to similar reasons as for the last peak interglacial conditions (Chapter 6).

Although glacial conditions during MIS 8 predominate, contemporaneous to the insolation maxima, several speleothem growth phases might indicate more humid and vegetated conditions. This coincides with pollen from the Iberian Margin (Roucoux et al., 2006) and from Greece (Tenaghi Philippon, Tzedakis et al., 2006). It also coincides with the highest SSTs at the Iberian

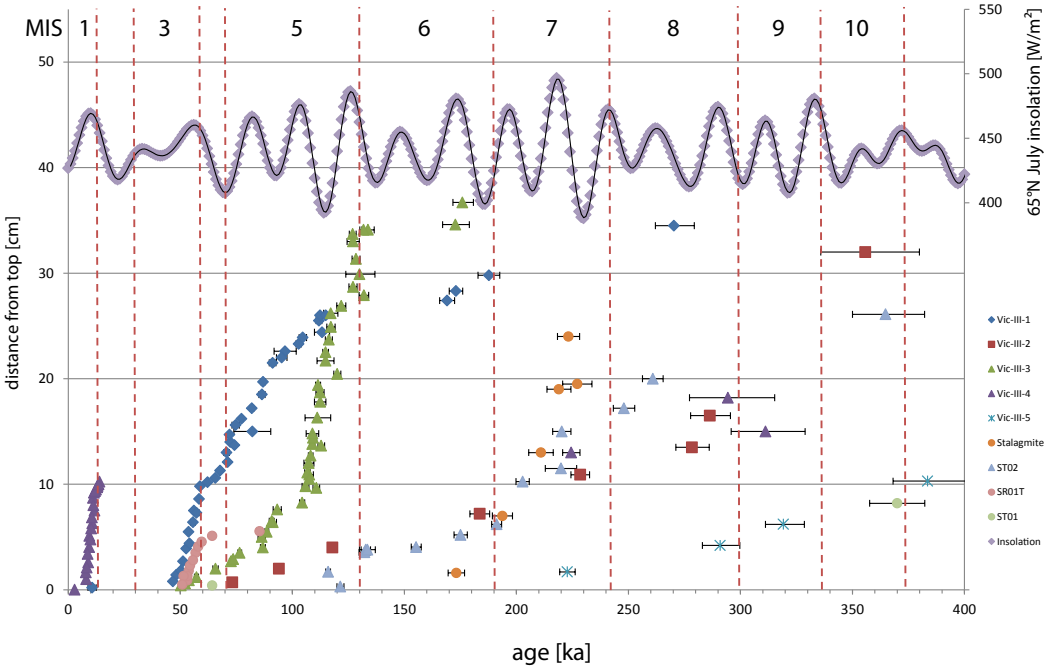


Figure 7.1: $^{230}$Th/U-ages of several CV samples vs. distance from top for the last 400 ka (MIS 1 – 11). High July 65° N insolation on top indicate interglacial and therewith potential humid phases.

Margin in MIS 8 (Martrat et al., 2007). Further back in time, during MIS 9, some periods of speleothem growth in CV occurred as well. Unfortunately, due to the analytical limitations, the precession of $^{230}$Th/U-ages is low at the moment. Improved analytical settings and a new generation of MC-ICP-MS potentially enables to date speleothems close to the secular equilibrium ($\approx$ 600 ka; Cheng et al., 2013; Scholz & Hoffmann, 2008) even with low radiogenic $^{230}$Th (Chiang et al., 2019). These advantages can be used for CV speleothems to reconstruct the palaeoclimate of the Middle Pleistocene with high temporal resolution and accuracy. Stacking Pleistocene CV speleothems could further provide a new broad reference record for future marine and terrestrial pollen records in respect to local Western Mediterranean climate signals.

In addition, new active drip sites in the cave may enable a future monitoring in CV, which is hitherto missing. Although the recent cave environment is not comparable to the former phases of speleothem growth, this may give new insights into the rainwater seeping into the karst and fractionation processes in general for this cave. $\delta^{18}$O and $\delta^{2}$H measurements of two drip water samples in September 2018 indicate strong evaporation effects (Table 7.1; Lachniet, 2009) according to low relative humidity at the drip sites ($<$ 90 %, measurements of CENM-naturaleza, September 2012). Also possible evaporation of summer rainfall may shift the $\delta^{18}$O and $\delta^{2}$H values off any Western Mediterranean or local meteoric water line (Moreno et al., 2014).

Post-mining calcite precipitation underneath an active drip site (September 2018) has $\delta^{18}$O

Table 7.1: $\delta^{18}$O and $\delta^{2}$H measurements of drip water sampled in September 2018. All values in ‰ are relative to VSMOW standard

| **Location** | $\delta^{18}$**O [‰]** | $\delta^{2}$**H [‰]** |
|---|---|---|
| El Tunel | -1.53 | -10.46 |
| Sala Redonda | -3.17 | -14.77 |

values of -3.88 ± 0.02 ‰ and for $\delta^{13}$C -6.37 ± 0.03 ‰, respectively. In particular, the $\delta^{18}$O value is surprisingly high compared to the average $\delta^{18}$O values of rainwater (≈-5 ‰; see chapter 4) and does not agree with observations of farmed cave calcites in central Spain (Pérez-Mejías et al., 2018). However, this might be a result of several cave-specific fractionation processes such as evaporation, PCP and continuous ventilation (section 2.3). Theses processes fractionate speleothem $\delta^{13}$C values even more efficiently (Hansen et al., 2019).

Although the cave environment is not pristine anymore, a monitoring setup is highly recommended for future work to measure the isotopic signature of rainwater and drip water of available drip sites related to recent calcite precipitation in the cave. This could help to understand stable isotopes of speleothems and cave/karst-inside processes in low altitude semi-arid regions.

# 8 Conclusions

Cueva Victoria speleothems provide, as one of the first records from this region, new insights into palaeoclimate variability over the past interglacial – glacial from south-eastern Spain. The region is one of the driest in Europe and very sensitive to hydrological changes. Nevertheless, the lack of terrestrial palaeoclimate records emphasizes the importance of precisely dated speleothem records covering an interglacial – glacial cycle. This thesis examined climate variability with focus on the last 190 ka. Although the CV speleothems do not cover the whole 190 ka, they were suitable for palaeoclimate reconstructions. On orbital timescale, $^{230}$Th/U-datings show preferential speleothem growth during interglacials, but almost no speleothem growth during glacial conditions. This indicates almost completely dry climate conditions in south-eastern Spain, which is in agreement with several other palaeoclimate records. However, there are some exceptions such as the MIS 6.5, which coincides with humid conditions in the Mediterranean resulting in strong seasonality with sapropel deposition in the Eastern Mediterranean. Apart from that, interglacials display favourable conditions for speleothem growth at CV and therewith humid and vegetated conditions in south-eastern Spain. These humid conditions can also be assumed on millennial timescale for warm and humid DO events during MIS 5 to 3.

High spatial resolution stable isotope measurements enable to reconstruct changes in vegetation, precipitation and, to a limited extend, in temperature on orbital and millennial timescales. As elaborated in this thesis, $\delta^{18}$O values were difficult to interpret, but could be disentangled with installing a monitoring site. On the one hand, CV speleothem $\delta^{18}$O values follow the pattern of latitudinal summer insolation, on the other hand they reflect a combination of SST, amount effect and, to certain extent, the composition of the proximate ocean water as a local source for moisture uptake (Chapter 4). Subsequent, fast changes of Northern Hemisphere temperature and hydrological cycle are immediately transferred into speleothem $\delta^{18}$O values, as can be seen by the pattern of DO events with strong shifts in $\delta^{18}$O values. Despite several possibilities of $\delta^{13}$C alteration en route to speleothem precipitation, $\delta^{13}$C values can be reproduced by several flowstone samples from the cave. Therewith, they are very indicative of vegetation and soil microbiological activity, which is influenced by precipitation and in total a positive annual net precipitation-evapotranspiration balance. Both, $\delta^{18}$O and $\delta^{13}$C values, are suitable to reconstruct palaeoclimate conditions in the Western Mediterranean, and react very sensitive to palaeoclimatic changes, or even to seasonality. Finally CV speleothems have the potential to fill the missing gap of palaeoclimate records between the North Atlantic and the terrestrial central to eastern Mediterranean, and thus grant new insights into one of the driest region of the European Mediterranean on one hand and the understanding of differences over the entire Mediterranean

basin, on the other. Contrary to Eastern Mediterranean sapropel deposition indicating enhanced winter-humid conditions in the northern borderlands, the impact on the Western Mediterranean is quite different. Depending on summer insolation and the position of the Hadley cell, it can lead to prolonged spring and summer drought by increased seasonality, causing a decline in vegetation and microbiological soil activity, if accompanied by high temperatures (Chapter 4). Albeit, associated with lower temperatures besides full interglacial conditions, precipitation is significantly increased during sapropel deposition (e.g., S4 and S6) as indicated by very negative stable isotope ($\delta^{13}$C, $\delta^{18}$O) values (Chapter 6).

To conclude, past CV speleothem growth always indicates humid climate conditions with a certain amount of vegetation cover during warm phases, while cold glacial phases are, in general, missing, indicating a negative precipitation-evapotranspiration balance. Therefore CV speleothems are ideal for studying the climate of past interglacial conditions.

# Bibliography


Barker, S., G. Knorr, R. L. Edwards, F. Parrenin, A. E. Putnam, L. C. Skinner, E. Wolff, & M. Ziegler (2011). 800,000 Years of Abrupt Climate Variability. *Science* **334** (6054), pp. 347–351.

Camuera, J., G. Jiménez-Moreno, M. J. Ramos-Román, A. García-Alix, J. L. Toney, R. S. Anderson, F. Jiménez-Espejo, J. Bright, C. Webster, Y. Yanes, & J. S. Carrión (2019). Vegetation and climate changes during the last two glacial-interglacial cycles in the western Mediterranean: A new long pollen record from Padul (southern Iberian Peninsula). *Quaternary Science Reviews* **205**, pp. 86–105.

Cheng, H., R. L. Edwards, A. Sinha, C. Spötl, L. Yi, S. Chen, M. Kelly, G. Kathayat, X. Wang, X. Li, X. Kong, Y. Wang, Y. Ning, & H. Zhang (2016). The Asian monsoon over the past 640,000 years and ice age terminations. *Nature* **534** (7609), pp. 640–646.

Cheng, H., R. Lawrence Edwards, C.-C. Shen, V. J. Polyak, Y. Asmerom, J. Woodhead, J. Hellstrom, Y. Wang, X. Kong, C. Spötl, X. Wang, & E. Calvin Alexander Jr. (2013). Improvements in 230Th dating, 230Th and 234U half-life values, and U–Th isotopic measurements by multi-collector inductively coupled plasma mass spectrometry. *Earth and Planetary Science Letters* **371–372**, pp. 82–91.

Chiang, H.-W., Y. Lu, X. Wang, K. Lin, & X. Liu (2019). Optimizing MC-ICP-MS with SEM protocols for determination of U and Th isotope ratios and 230Th ages in carbonates. *Quaternary Geochronology* **50**, pp. 75–90.

Cortina, A., J. O. Grimalt, A. Rigual-Hernández, A.-M. Ballegeer, B. Martrat, F. J. Sierro, & J. A. Flores (2016). The impact of ice-sheet dynamics in western Mediterranean environmental conditions during Terminations. An approach based on terrestrial long chain n-alkanes deposited in the upper slope of the Gulf of Lions. *Chemical Geology* **430**, pp. 21–33.

Girone, A., P. Maiorano, M. Marino, & M. Kucera (2013). Calcareous plankton response to orbital and millennial-scale climate changes across the Middle Pleistocene in the western Mediterranean. *Palaeogeography, Palaeoclimatology, Palaeoecology* **392**, pp. 105–116.

Hansen, M., D. Scholz, B. R. Schöne, & C. Spötl (2019). Simulating speleothem growth in the laboratory: Determination of the stable isotope fractionation (d13C and d18O) between H2O, DIC and CaCO3. *Chemical Geology* **509**, pp. 20–44.

Hodell, D., S. Crowhurst, L. Skinner, P. C. Tzedakis, V. Margari, J. E. Channell, G. Kamenov, S. MacLachlan, & G. Rothwell (2013). Response of Iberian Margin sediments to orbital and suborbital forcing over the past 4202009ka. *Paleoceanography* **28** (1), pp. 185–199.

Lachniet, M. S. (2009). Climatic and environmental controls on speleothem oxygen-isotope values. *Quaternary Science Reviews* **28** (5-6), pp. 412–432.

Martrat, B., J. O. Grimalt, N. J. Shackleton, L. de Abreu, M. A. Hutterli, & T. F. Stocker (2007). Four Climate Cycles of Recurring Deep and Surface Water Destabilizations on the Iberian Margin. *Science* **317** (5837), pp. 502–507.

Moreno, A., C. Sancho, M. Bartolomé, B. Oliva-Urcia, A. Delgado-Huertas, M. J. Estrela, D. Corell, J. I. López-Moreno, & I. Cacho (2014). Climate controls on rainfall isotopes and their effects on cave drip water and speleothem growth: the case of Molinos cave (Teruel, NE Spain). *Climate Dynamics* **43** (1-2), pp. 221–241.

Pérez-Mejías, C., A. Moreno, C. Sancho, M. Bartolomé, H. Stoll, M. C. Osácar, I. Cacho, & A. Delgado-Huertas (2018). Transference of isotopic signal from rainfall to dripwaters and farmed calcite in Mediterranean semi-arid karst. *Geochimica et Cosmochimica Acta* **243**, pp. 66–98.

Roucoux, K. H., P. C. Tzedakis, M. R. Frogley, I. T. Lawson, & R. C. Preece (2008). Vegetation history of the marine isotope stage 7 interglacial complex at Ioannina, NW Greece. *Quaternary Science Reviews* **27** (13-14), pp. 1378–1395.

Roucoux, K., P. Tzedakis, L. de Abreu, & N. Shackleton (2006). Climate and vegetation changes 180,000 to 345,000 years ago recorded in a deep-sea core off Portugal. *Earth and Planetary Science Letters* **249** (3-4), pp. 307–325.

Scholz, D. & D. Hoffmann (2008). 230Th/U-dating fossil corals and speleothems. *Eiszeitalter und Gegenwart Quaternary Science Journal* **57** (1/2), pp. 52–76.

Toucanne, S., C. M. Angue Minto'o, C. Fontanier, M.-A. Bassetti, S. J. Jorry, & G. Jouet (2015). Tracking rainfall in the northern Mediterranean borderlands during sapropel deposition. *Quaternary Science Reviews* **129**, pp. 178–195.

Tzedakis, P., H. Hooghiemstra, & H. Pälike (2006). The last 1.35 million years at Tenaghi Philippon: revised chronostratigraphy and long-term vegetation trends. *Quaternary Science Reviews* **25** (23-24), pp. 3416–3430.

Ziegler, M., E. Tuenter, & L. J. Lourens (2010). The precession phase of the boreal summer monsoon as viewed from the eastern Mediterranean (ODP Site 968). *Quaternary Science Reviews* **29** (11-12), pp. 1481–1490.